

Alma Mater Studiorum – Università di Bologna

DOTTORATO DI RICERCA IN

INGEGNERIA CIVILE, CHIMICA, AMBIENTALE E DEI MATERIALI

Ciclo XXXIII

**Settore Concorsuale:** 08/B3

**Settore Scientifico Disciplinare:** ICAR/09

TITOLO TESI

Seismic retrofit of existing RC and masonry buildings using external  
aluminium alloy exoskeleton

**Presentata da:** Stefani Francesca

**Coordinatore Dottorato**

**Prof. Luca Vittuari**

**Supervisore**

**Prof. Claudio Mazzotti**

**Esame finale anno 2021**



## Abstract

This thesis is the result of the industrial PhD carried out in collaboration with *Aliva S.r.l.* company, which has its headquarter in San Mauro Pascoli (FC), Italy and it develops customized solutions for ventilated facades. The ventilated façade is a multi-layer protective system for the building envelope consisting, from the inside to the outside, of a continuous insulation, a light bearing structure, a ventilation chamber and a modular cladding. The ventilated façade allows several benefits such as the thermo-hygrometric improvement, energy saving, acoustic insulation and the architectural renovation of the building. The light bearing structure is usually made of aluminium alloy for its property of lightness, durability, corrosion resistance, workability thanks to the extrusion process and eco-sustainability. The scope of this thesis is to investigate the use of aluminium alloys in application fields different from that of the ventilated façade. The use of aluminium alloys in structural engineering is a quite recent activity, because this family of materials is relatively new. In the 20<sup>th</sup> century the use of aluminium alloys spread in many fields, in the aeronautical, transport, automotive and shipping industry. In civil engineering structures, the use of aluminium alloys has been less widespread because they have to compete with steel, the most widely used metallic material in this field. Nowadays, after the several research carried out in order to characterize the design of aluminium alloys structures and the publication of Eurocode 9 *Design of Aluminium Structures*, there are many applications of aluminium alloys in structural engineering. The main fields of structural applications are the roofing systems, bridges and prefabricated systems. However, there is still a lack of information about the ductility of this material and its use in seismic zones. In fact to date there is no seismic regulations for aluminium alloys applications, only recently in the project for the development of the next generation of structural Eurocodes, it was decided to introduce the aluminium alloys

among the new emerging materials for anti-seismic structures. This thesis aims to make a contribution to the study of the possible use of aluminium alloys in seismic areas and intends to study if it can be a competitive solution in the seismic retrofit field. This study is part of the European research project Pro-GET-onE that means Proactive synergy of inteGrated Efficient Technologies on building's Envelope, in which the Aliva company is involved together with the university of Bologna and other members. The distinctive feature of the project is the integration between energy deep renovation techniques and seismic retrofitting actions. The project aims to combine in a same holistic and integrated system based on preassembled components the highest performance in terms of energy requirements, safety and social sustainability increasing the real estate value of the buildings. This incremented value will be obtained through the development and application of integrated efficient technologies (GETs) that introduce a metal structure with efficient stiffness applied externally to the existing building, with benefits in regarding the construction site, since it does not require operations inside the buildings. Different solutions of GET systems were proposed and analysed to provide the strengthening of the existing buildings and these are made of timber, aluminium alloys or steel. This thesis shows the study and the development of the design of an external structural frame, also called exoskeleton, made of aluminium alloys. The in-depth study of the wide range of aluminium alloys led to the choice of the most suitable one that combines high strength and ductility and the possibility of being extruded in order to obtain any type of desired sections. The 6000 series aluminium alloy is chosen, it is a magnesium-silicon alloy and it is the most used alloy in the extrusion process. The latter allows the designer to design the optimal section of the frame profiles considering the maximum extrusion sizes that are related to the billet diameter and the press load capacity. The study of the section has to avoid slender sections that have local instability in the elastic field, designed sections in class 1, 2 or 3 according to the classification of cross-sections present in Eurocode 9. Last but not least the design of the extruded sections allows the simplicity of connections

and the development of innovative solutions. To confirm the feasibility of the idea and the assembly efficiency in Aliva warehouse we realized a full scale visual mock-up. It is a plug and play solution where all components are preassembled in the factory and ready to be installed to reduce construction times. The evaluation of the seismic improvement achieved for the existing building with the addition of the aluminium alloy exoskeleton is performed using the structural analysis software Midas Gen. Considering the Italian case study taken into account in the European project, a social housing located in Reggio Emilia, the seismic vulnerability of the building before and after the intervention is assessed with linear and nonlinear analyses. Finally, a possible improvement of the exoskeleton is examined, nine solutions of the additional aluminium frames are proposed and analysed. The nine proposed solutions are compared in terms of pushover curve, behaviour factor, seismic risk index and costs.

**Keywords:** Seismic vulnerability; Seismic retrofitting; Aluminium alloys; External exoskeleton.



# Table of contents

Alma Mater Studiorum – Università di Bologna	i
Chapter 1	1
INTRODUCTION	1
1.1 GENERAL OVERVIEW	1
1.2 MOTIVATION AND RESEARCH OBJECTIVES	3
1.3 ORGANIZATION AND OUTLINE	5
1.4 PROGETONE	6
1.5 STATE OF THE ART OF EXOSKELETON APPLICATIONS	11
1.6 CASE STUDY	15
1.7 REFERENCES	22
Chapter 2	25
ALUMINIUM ALLOYS: CHARACTERISTICS AND APPLICATIONS	25
2.1 INTRODUCTION	25
2.2 CHARACTERISTICS AND CIVIL-ENGINEERING APPLICATIONS	28
2.3 ALUMINIUM ALLOYS	37
2.4 THE EXTRUSION PROCESS	44
2.5 DESIGN CRITERIA	51
2.5.1 Design resistance and material properties	52
2.5.2 Stress-strain relationship	57
2.5.3 Classification of cross-sections	61
2.5.4 Resistance of cross-sections	67
2.5.5 Buckling resistance of members	73
2.6 DURABILITY AND PROTECTION SYSTEMS	83
2.7 REFERENCES	88
Chapter 3	91
DESIGN OF THE ALUMINIUM ALLOY EXOSKELETON	91
3.1 INTRODUCTION	91
3.2 FEASIBILITY STUDY WITH A FULL SCALE MOCK-UP	93
3.3 ALUMINIUM ALLOYS SELECTED	101
3.4 DESIGN OF THE CUSTOMIZED SECTIONS OF THE EXTRUDED PROFILES	103

3.5 REFERENCES	107
Chapter 4	109
NUMERICAL ANALYSIS FOR CASE STUDY	109
4.1 NUMERICAL MODEL	109
4.2 SEISMIC VULNERABILITY WITH LINEAR STATIC ANALYSIS	114
4.3 SEISMIC VULNERABILITY WITH NONLINEAR STATIC ANALYSIS	120
4.3.1 Inelastic deformation capacity of reinforced concrete	121
4.3.2 Inelastic deformation capacity of masonry	126
4.3.3 Sensitivity of the pushover curve	129
4.4 RESULTS	138
4.5 REFERENCES	140
Chapter 5	141
SEISMIC IMPROVEMET ASSESSMENT	141
5.1 FIRST NUMERICAL MODEL OF EXTERNAL EXOSKELETON	141
5.1.1 Seismic vulnerability with linear static analysis	147
5.1.2 Seismic vulnerability with nonlinear static analysis	148
5.1.3 Results	157
5.2 SECOND NUMERICAL MODEL OF EXTERNAL EXOSKELETON	159
5.2.1 Seismic vulnerability with linear static analysis	162
5.2.2 Seismic vulnerability with nonlinear static analysis	163
5.2.3 Results	169
5.3 IMPROVEMENT TO THE EXOSKELETON	171
5.4 ECONOMIC EVALUATION	180
5.5 REFERENCES	183
Chapter 6	185
CONCLUSIONS	185
APPENDIX A	189
Case 3 of the exoskeleton EB-EX 3	189
Case 4 of the exoskeleton EB-EX 4	191
Case 5 of the exoskeleton EB-EX 5	193
Case 6 of the exoskeleton EB-EX 6	195
Case 7 of the exoskeleton EB-EX 7	197



Case 8 of the exoskeleton EB-EX 8	199
Case 9 of the exoskeleton EB-EX 9	201

## List of figures

Figure 1.1: Magneti Marelli factory seismic retrofit after seismic event of 2012 [6,7]. .....	8
Figure 1.2: Connection linking the existing building and the exoskeleton. ....	9
Figure 1.3: (a) Interaction between the existing façade and steel-aluminium structure; (b) the possible positioning of ducts/pipes/storage; (c) the same external structure in timber or X-Lam structure [5]. ....	10
Figure 1.4: Different options for the new envelope.....	10
Figure 1.5: Exoskeleton 2D with shear walls arranged perpendicular (2D $\perp$ ) or parallel (2D//) to the façade [11]. ....	11
Figure 1.6: Exoskeleton 3D with plane (3Dp) and curved (3Dc) structures [11]. ....	12
Figure 1.7: Retrofit intervention with 2D// steel exoskeleton of the Hospital Ángeles Clinica Londres in Mexico City [11].....	13
Figure 1.8: Retrofit intervention with 3Dp steel exoskeleton of the Hörsaalgebäude Physik building in Zurich [11]. ....	14
Figure 1.9: Case study of Bagnolo in Piano, Reggio Emilia. ....	15
Figure 1.10: Structural plan. (a) First storey plan; (b) Typical plan. ....	16
Figure 1.11: Vertical section. ....	17
Figure 1.12: Plan of the foundations. ....	17
Figure 1.13: Beam construction details. ....	21
Figure 2.1: Worldwide evolution of recycled and primary aluminium [2]. ....	26
Figure 2.2: Global end-use markets for finished aluminium products, 2007 [2]. ....	27
Figure 2.3: Comparison between typical stress-strain curves for aluminium alloy and steel [5]. ....	30
Figure 2.4: Comparison between the exponent $n$ of the Ramberg-Osgood law and the values of ratio $f_{0,2}/f_{0,1}$ , which are related to the Sutter classes [5].....	32
Figure 2.5: (a) The reticular space structure of the Interamerican Exhibition Center of Sao Paulo (Brazil); (b) the International Congress Center of Rio de Janeiro (Brazil) [4]. ....	33
Figure 2.6: (a) The Conference Center in Glasgow; (b) roof of the Millennium Stadium in Welfes [7]. ....	33
Figure 2.7: The “Dome of Discovery” in UK [7].....	34
Figure 2.8: The Geo-system and its application in the geodetic dome of the “Mercati Traianei” Museum, Rome, Italy [6].....	34

Figure 2.9: (a) Epoct Center in Florida; (b) the University of Connecticut in USA [7]. .....	34
Figure 2.10: (a) Arvida bridge, Quebec, Canada; (b) German military bridge: erection phases [6]. ....	35
Figure 2.11: The Real Ferdinando Bridge on the Garigliano River, Italy [8]. ....	36
Figure 2.12: (a) The Enel Tower, Naples, Italy; (b) the Information Tower, Naples, Italy [6]. ....	37
Figure 2.13: Wrought aluminium alloys by group [1]. ....	39
Figure 2.14: European aluminium alloy designation [1]. ....	39
Figure 2.15: Stress-strain curves of aluminium in comparison with various metals and alloys [1]. ....	44
Figure 2.16: Direct extrusion [1]. ....	44
Figure 2.17: Typical extrusion plant layout [1]. ....	46
Figure 2.18: 6050 tonnes extrusion press (picture Metra). ....	46
Figure 2.19: Cylindrical billet [1]. ....	47
Figure 2.20: Relative extrudability of aluminium alloys [1]. ....	47
Figure 2.21: Relationship between mechanical strength and extrudability of some extrusion alloys [1]. ....	48
Figure 2.22: Typical assembly of flat die [11]. ....	49
Figure 2.23: (a) Pothole die to realize a circular section tube [11]; (b) extrusion of hollow section [1]. ....	49
Figure 2.24: Typical assembly of porthole die [11]. ....	50
Figure 2.25: (a) Examples of open flat section extrusions; (b) examples of hollow section extrusions. ....	50
Figure 2.26: Examples of aluminium extrusions. (a) Doors and windows (Metra); (b) ventilated facades (Aliva); (c) automotive (Metra); (d) naval transport (Metra). ....	51
Figure 2.27: The extend of heat affected zones (HAZ) [12]. ....	54
Figure 2.28: Characteristic values of 0,2% proof strength $f_0$ , ultimate tensile strength $f_u$ , min. elongation A, reduction factors $\rho_{o,haz}$ and $\rho_{u,haz}$ in HAZ, buckling class and exponent $n_p$ for wrought aluminium alloys – Sheet, strip and plate. ....	55
Figure 2.29: Characteristic values of 0,2% proof strength $f_0$ , ultimate tensile strength $f_u$ , min. elongation A, reduction factors $\rho_{o,haz}$ and $\rho_{u,haz}$ in HAZ, buckling class and exponent $n_p$ for wrought aluminium alloys – Extruded profiles, extruded tube, extruded rod/bar and drawn tube [12]. ....	56
Figure 2.30: (a) Bi-linear model with hardening; (b) Elastic-perfectly plastic model [12]. ....	58
Figure 2.31: (a) Three-linear model with hardening; (b) Perfectly plastic model [12]. .....	59
Figure 2.32: Continuous models in the form $\varepsilon = \varepsilon(\sigma)$ [12]. ....	60

Figure 2.33: Classification of cross-sections [12].	61
Figure 2.34: Types of cross-section parts [12].	62
Figure 2.35: Flat internal parts under stress gradient, values of $\eta$ . For internal parts or outstands (peak compression at root) use curve A. For outstands (peak compression at toe) use line B [12].	63
Figure 2.36: Buckling modes for flat reinforced parts. (a) Mode 1; (b) mode 2; (c) mode 3; (d) sub-part buckles; (e) whole reinforced part buckles [12].	64
Figure 2.37: Values of $\eta$ for reinforced cross section parts [12].	65
Figure 2.38: Reduction factor $\chi$ for flexural buckling [12].	75
Figure 2.39: Reduction factor $\chi$ for torsional and torsional-flexural buckling [12].	76
Figure 2.40: Reduction factor for lateral-torsional buckling [12].	78
Figure 2.41: Buckling length $l_c$ and definition of $x_s$ ( $=x_A$ or $x_B$ ) [12].	82
Figure 3.1: Computer graphic drawing of existing RC buildings reinforced by SNE-Truss [1, 2].	92
Figure 3.2: Shape and material of SNE-Truss connection [2].	92
Figure 3.3: Loading tests of SNE-Truss [2].	93
Figure 3.4: Plan view of the full scale mock-up.	94
Figure 3.5: (a) Longitudinal section of the full scale mock-up; (b) transverse section.	94
Figure 3.6: Section of the vertical mullions of the mock-up.	95
Figure 3.7: Section of the beams of the mock-up.	96
Figure 3.8: Assembly phases of the prefabricated components of the mock-up.	97
Figure 3.9: Parallel beams pre-assembled with x-lam slabs.	98
Figure 3.10: Erection phases and installation of the mock-up.	99
Figure 3.11: Installation of wooden-framed walls, windows and parts of the technical building equipment.	100
Figure 3.12: Various possibilities of the additional spaces: sunspace, extra room and balcony.	100
Figure 3.13: Comparison between the experimental and theoretical $\sigma - \varepsilon$ curve of the 6082 T6 alloy.	102
Figure 3.14: Comparison between the experimental and theoretical $\sigma - \varepsilon$ curve of the 6060 T5 alloy.	102
Figure 3.15: Computer graphic drawing of the innovative connection system.	104
Figure 3.16: The study of the customized extruded section.	105
Figure 3.17: Geometrical properties of mullions type A and type B.	106
Figure 3.18: Geometrical properties of longitudinal beams and transverse beams and diagonals.	106
Figure 4.1: The finite element model of the case study developed with Midas Gen software.	109

Figure 4.2: Structural plan of the finite element model of the case study – Type plan. .....	110
Figure 4.3: Vertical section of the finite element model of the case study.....	110
Figure 4.4: Design response spectrum at the Life Safety limit state. ....	112
Figure 4.5: Design response spectrum at the Damage Limitation limit state. ....	112
Figure 4.6: Modal shapes of the existing building.....	113
Figure 4.7: Evaluation of the annual average expected loss parameter (PAM) for the existing building. ....	118
Figure 4.8: The finite element model for nonlinear analysis.....	121
Figure 4.9: Generalized Force-Deformation relations for concrete elements [6]....	123
Figure 4.10: Modelling parameters and numerical acceptance criteria for nonlinear analysis for reinforced concrete beams [6]. ....	124
Figure 4.11: Modelling parameters and numerical acceptance criteria for nonlinear analysis for reinforced concrete columns [6]. ....	125
Figure 4.12: Default moment-rotation hinge properties for RC beams and columns implemented in Midas Gen.....	126
Figure 4.13: Acceptance criteria for RC beams and columns in Midas Gen.....	126
Figure 4.14: Generalized force-deformation relation for masonry [6]. ....	127
Figure 4.15: Modelling parameters and numerical acceptance criteria for nonlinear analysis for unreinforced masonry walls [6]. ....	128
Figure 4.16: Masonry properties of the existing building for the nonlinear analysis. .....	128
Figure 4.17: Default hinge properties for masonry failing in shear in Midas Gen..	128
Figure 4.18: Default hinge properties for masonry failing in bending in Midas Gen. .....	129
Figure 4.19: Capacity curve in x direction for the existing building.....	129
Figure 4.20: Capacity curve in y direction for the existing building.....	130
Figure 4.21: (a) Inter-storey drift; (b) storey displacement for the existing bulding. .....	132
Figure 4.22: (a) Pushover curve in x direction and displacement target for the existing building; (b,c,d) development of plastic hinges in the corresponding points of the curve.....	133
Figure 4.23: (a) Pushover curve in y direction and displacement target for the existing building; (b,c,d) development of plastic hinges in the corresponding points of the curve.....	133
Figure 4.24: Curve of the SDOF system and bilinear equivalent curve for the existing building. (a) x direction; (b) y direction. ....	134
Figure 4.25: Capacity/demand ratio for the Life Safety limit state in x direction for the existing building. ....	135

Figure 4.26: Capacity/demand ratio for the Life Safety limit state in y direction for the existing building. ....	136
Figure 4.27: Capacity/demand ratio for the Damage Limitation limit state in x direction for the existing building.....	136
Figure 4.28: Capacity/demand ratio for the Damage Limitation limit state in y direction for the existing building.....	137
Figure 4.29: Evaluation of the annual average expected loss parameter (PAM) with nonlinear analysis for the existing building.....	138
Figure 4.30: Comparison between the risk class evaluated with linear and nonlinear analysis for the existing building.....	139
Figure 5.1: (a) Existing building. (b) Computer graphic drawing of the new envelope. ....	141
Figure 5.2: First numerical model of the external aluminium alloy exoskeleton.....	142
Figure 5.3: Structural scheme of the external exoskeleton. (a) Plan view; (b) Front view. ....	143
Figure 5.4: Modal shapes of the retrofitted building.....	145
Figure 5.5: Connection detail between the existing building and the exoskeleton. .	146
Figure 5.6: Evaluation of the annual average expected loss parameter (PAM) for the retrofitted building.....	147
Figure 5.7: User-defined hinge properties for aluminium alloy 6082 T6. ....	148
Figure 5.8: User-defined hinge properties for aluminium alloy 6060 T5. ....	148
Figure 5.9: Capacity curves of the existing building, the exoskeleton and the retrofitted building in x direction. ....	149
Figure 5.10: (a) Aluminium diagonals yielding at first floor at 12 cm. (b) Aluminium longitudinal beams start to yield at 24 cm. (c) RC columns failure at 30 cm. ....	150
Figure 5.11: Capacity curves of the existing building, the exoskeleton and the retrofitted building in y direction.....	150
Figure 5.12: (a) Inter-storey drift; (b) storey displacement in x direction; (c) storey displacement in y direction.....	152
Figure 5.13: (a) Pushover curve in x direction and displacement target; (b) plastic hinges on masonry and RC columns at displacement target; (c) plastic hinges on aluminium exoskeleton at displacement target.....	153
Figure 5.14: Evaluation of the increased strength and stiffness in both directions..	153
Figure 5.15: Curve of the SDOF system and bilinear equivalent curve in both directions for the retrofitted building. ....	153
Figure 5.16: Capacity/demand ratio for the Life Safety limit state in x direction for the retrofitted building.....	155
Figure 5.17: Capacity/demand ratio for the Life Safety limit state in y direction for the retrofitted building.....	155

Figure 5.18: Capacity/demand ratio for the Damage Limitation limit state in x direction for the retrofitted building.....	155
Figure 5.19: Capacity/demand ratio for the Damage Limitation limit state in y direction for the retrofitted building.....	156
Figure 5.20: Evaluation of the annual average expected loss parameter (PAM) with nonlinear analysis for the retrofitted building.....	157
Figure 5.21: Comparison between the risk class evaluated with linear and nonlinear analysis for the existing building retrofitted with the first model of exoskeleton...	158
Figure 5.22: Second numerical model of the external aluminium alloy exoskeleton. (a) South elevation; (b) North elevation.....	160
Figure 5.23: Vertical section and windows height from the landing.....	161
Figure 5.24: Modal shapes of the retrofitted building with the second model of the exoskeleton. ....	162
Figure 5.25: Evaluation of the annual average expected loss parameter (PAM) for the retrofitted building with the second model of exoskeleton.....	163
Figure 5.26: Capacity curves of the existing building EB, the retrofitted building with the first model of exoskeleton EB-EX 1 and the second model of the exoskeleton EB-EX 2 in x direction.....	164
Figure 5.27: Capacity curves of the existing building EB, the retrofitted building with the first model of exoskeleton EB-EX 1 and the second model of the exoskeleton EB-EX 2 in y direction.....	164
Figure 5.28: Evaluation of the increased strength and stiffness in x direction obtained with the second model of the exoskeleton.....	165
Figure 5.29: Curve of the SDOF system and bilinear equivalent curve in both directions for the retrofitted building with the second model of the exoskeleton. ..	166
Figure 5.30: Capacity/demand ratio for the Life Safety limit state in x direction for the retrofitted building with the second model of the exoskeleton.....	167
Figure 5.31: Capacity/demand ratio for the Life Safety limit state in y direction for the retrofitted building with the second model of the exoskeleton.....	167
Figure 5.32: Capacity/demand ratio for the Damage Limitation limit state in x direction for the retrofitted building with the second model of the exoskeleton. ....	167
Figure 5.33: Capacity/demand ratio for the Damage Limitation limit state in y direction for the retrofitted building with the second model of the exoskeleton. ....	168
Figure 5.34: Evaluation of the annual average expected loss parameter (PAM) with nonlinear analysis for the retrofitted building with the second model of the exoskeleton. ....	169
Figure 5.35: Comparison between the risk class evaluated with linear and nonlinear analysis for the existing building retrofitted with the second model of exoskeleton. ....	170

Figure 5.36: Geometrical properties of the diagonals considered in case 5 of the exoskeleton. ....	172
Figure 5.37: Sixth model of the exoskeleton with the addition of bracings at the four corners of the building. ....	173
Figure 5.38: Geometrical properties of the longitudinal beam considered in case 6 of the exoskeleton. ....	174
Figure 5.39: Summary table of the nine cases studied for the improvement of the exoskeleton. ....	175
Figure 5.40: Capacity curves in x direction for the nine solutions of the exoskeleton. ....	178
Figure 5.41: Capacity curves in y direction for the nine solutions of the exoskeleton. ....	179
Figure A.1: Curve of the SDOF system and bilinear equivalent curve in both directions for EB-EX 3. ....	189
Figure A.2: Evaluation of the increased strength in both directions for EB-EX 3. ....	189
Figure A.3: Curve of the SDOF system and bilinear equivalent curve in both directions for EB-EX 4. ....	191
Figure A.4: Evaluation of the increased strength in both directions for EB-EX 4. ....	191
Figure A.5: Curve of the SDOF system and bilinear equivalent curve in both directions for EB-EX 5. ....	193
Figure A.6: Evaluation of the increased strength in both directions for EB-EX 5. ....	193
Figure A.7: Curve of the SDOF system and bilinear equivalent curve in both directions for EB-EX 6. ....	195
Figure A.8: Evaluation of the increased strength in both directions for EB-EX 6. ....	195
Figure A.9: Curve of the SDOF system and bilinear equivalent curve in both directions for EB-EX 7. ....	197
Figure A.10: Evaluation of the increased strength in both directions for EB-EX 7. ....	197
Figure A.11: Curve of the SDOF system and bilinear equivalent curve in both directions for EB-EX 8. ....	199
Figure A.12: Evaluation of the increased strength in both directions for EB-EX 8. ....	199
Figure A.13: Curve of the SDOF system and bilinear equivalent curve in both directions for EB-EX 9. ....	201
Figure A.14: Evaluation of the increased strength in both directions for EB-EX 9. ....	201



## List of tables

Table 1.1: Table of reinforced concrete columns. ....	19
Table 1.2: Table of reinforced concrete beams.....	19
Table 1.3: Load patterns .....	21
Table 1.4: Parameters defining the spectral shape.....	21
Table 2.1: Comparison of properties among three aluminium alloys and the common mild steel [6]. ....	30
Table 2.2: Design value of material constants [12]. ....	52
Table 2.3: Partial safety factors for ultimate limit states .....	53
Table 2.4: Slenderness parameters $\beta_1 / \varepsilon$ , $\beta_2 / \varepsilon$ and $\beta_3 / \varepsilon$ [12]......	66
Table 2.5: Constants $C_1$ and $C_2$ in expressions for $\rho_c$ [11]. ....	67
Table 2.6: Values of shape factor $\alpha$ [12]......	69
Table 2.7: Values of $\kappa$ factor for member with longitudinal welds [12]. ....	74
Table 2.8: Values of $\alpha$ and $\lambda_0$ for flexural buckling [12]......	75
Table 2.9: Values of $\alpha$ , $\lambda_0$ and $A_{eff}$ for torsional and torsional-flexural buckling [12]. .....	75
Table 2.10: Buckling length factor $k$ for struts [12]. ....	77
Table 2.11: Durability class for wrought aluminium alloys [13]. ....	84
Table 2.12: General corrosion protection of aluminium structures [13]. ....	85
Table 3.1: Characteristic values of 0,2% proof strength $f_0$ , ultimate strength $f_u$ and minimum elongation $A$ for 6063 T66 alloy. ....	95
Table 3.2: Comparison between Eurocode 9 and experimental data of the mechanical properties of 6082 T6 and 6060 T5 alloys.....	101
Table 4.1: Natural period, frequency and modal participation mass of the first three vibration modes for the existing building. ....	113
Table 4.2: PGA values and risk index for masonry piers evaluated in both directions with linear analysis for the existing building.....	116
Table 4.3: Percentage of reconstruction cost for each limit state. ....	117
Table 4.4: Assignment of the IS-V class based on the safety index. ....	118
Table 4.5: Assignment of the PAM class based on the annual average expected losses. .....	119
Table 4.6: Maximum inter-storey drift according to FEMA 356. ....	132
Table 4.7: Parameters of the SDOF system in both directions for the existing building. .....	135

Table 4.8: PGA values and risk index evaluated in both directions with nonlinear analysis for the existing building.....	137
Table 4.9: Comparison between the seismic risk index evaluated with linear and nonlinear analysis for the existing building.....	138
Table 5.1: Height/width ratio of shear walls. ....	144
Table 5.2: Span/depth ratio for beams.....	144
Table 5.3: Natural period, frequency and modal participation mass of the first three vibration modes for the retrofitted building. ....	145
Table 5.4: PGA values and risk index for masonry piers evaluated in both directions with linear analysis for the retrofitted building. ....	147
Table 5.5: Maximum inter-storey drift according to FEMA 356.....	151
Table 5.6: Parameters of the SDOF system in both directions for the retrofitted building.....	154
Table 5.7: PGA values and risk index evaluated in both directions with nonlinear analysis for the retrofitted building. ....	156
Table 5.8: Comparison between the seismic risk index evaluated with linear and nonlinear analysis for the existing building retrofitted with the first model of exoskeleton. ....	157
Table 5.9: Natural period, frequency and modal participation mass of the first three vibration modes for the retrofitted building with the second model of exoskeleton. ....	161
Table 5.10: PGA values and risk index for masonry piers evaluated in both directions with linear analysis for the retrofitted building with the second model of exoskeleton. ....	162
Table 5.11: Parameters of the SDOF system in x direction for the retrofitted building with the second model of the exoskeleton.....	166
Table 5.12: PGA values and risk index evaluated in both directions with nonlinear analysis for the retrofitted building with the second model of the exoskeleton.....	168
Table 5.13: Comparison between the seismic risk index evaluated with linear and nonlinear analysis for the existing building retrofitted with the second model of the exoskeleton. ....	169
Table 5.14: Comparison between the behaviour factor and the risk index evaluated in both directions for the nine solutions of the exoskeleton. ....	177
Table 5.15: Comparison between the nine solutions of the exoskeleton with reference to the total kilos of aluminium involved.....	180
Table 5.16: Maximum tensile actions at the base of the vertical mullions of the exoskeleton for the nine solutions. ....	182
Table 5.17: Cost of retrofit normalized to the gross internal area of the building. ..	182
Table A.1: Parameters of the SDOF system in both directions for EB-EX 3. ....	190

Table A.2: Risk index for the Life Safety limit state in both directions for EB-EX 3. .....	190
Table A.3: Parameters of the SDOF system in both directions for EB-EX 4.....	192
Table A.4: Risk index for the Life Safety limit state in both directions for EB-EX 4. .....	192
Table A.5: Parameters of the SDOF system in both directions for EB-EX 5.....	194
Table A.6: Risk index for the Life Safety limit state in both directions for EB-EX 5. .....	194
Table A.7: Parameters of the SDOF system in both directions for EB-EX 6.....	196
Table A.8: Risk index for the Life Safety limit state in both directions for EB-EX 6. .....	196
Table A.9: Parameters of the SDOF system in both directions for EB-EX 7.....	198
Table A.10: Risk index for the Life Safety limit state in both directions for EB-EX 7. .....	198
Table A.11: Parameters of the SDOF system in both directions for EB-EX 8.....	200
Table A.12: Risk index for the Life Safety limit state in both directions for EB-EX 8. .....	200
Table A.13: Parameters of the SDOF system in both directions for EB-EX 9.....	202
Table A.14: Risk index for the Life Safety limit state in both directions for EB-EX 9. .....	202



## *Chapter 1*

# INTRODUCTION

## 1.1 GENERAL OVERVIEW

Over the past decades, earthquakes have seriously hit countries causing catastrophic effects such as the loss of human life and considerable damage to buildings and infrastructures with subsequent significant economic losses. As a matter of fact, earthquakes caused approximately 2.5 million deaths and over 2.9 trillion US dollars of damage since 1900. It is clear that the seismic risk reduction is one of the most important concerns for engineers. From a structural point of view, this means the development of new strategies aimed at the mitigation of the seismic risk. The seismic risk is expressed through the well-known pseudo-equation:  $\text{seismic risk} = \text{hazard} \times \text{vulnerability} \times \text{exposure}$ . The programs of mitigation of the seismic risk are focused on the exposure and mainly on the vulnerability through the application of adequate seismic design methodologies for new construction and the retrofit of existing buildings. According to a performance-based approach, modern seismic codes define performance levels aimed at avoiding collapse under moderate earthquakes and ensuring control and limitation of damage under more frequent but less severe earthquakes, in order to minimize economic and functionality losses. In this framework, the seismic vulnerability assessment of buildings is essential and it is evaluated identifying the seismic demand and the seismic capacity for each considered performance level (referred to as the limit states in the European code). Throughout Europe the deep renovation of the existing building heritage is therefore

now acknowledged as a priority. Also, in Italy many of the existing buildings have unsatisfactory seismic vulnerability as they were designed only for gravity loads or in compliance with old and inadequate seismic design code. In fact, in the post-WWII, particularly between the 60s and the 80s, many constructions were erected and were often affected by deficiencies in the design process and in the execution. The designed was in compliance with handbooks commonly used in practice, with the safety verifications performed according to the Allowable Stress Method. In those years only a small portion of the territory was classified under seismic risk until the last seismic zonation was made in 2003 and the first performance-based design seismic code released. The researchers and the industry are constantly involved in the improvement of the performance of traditional seismic structural typologies and in the development of more innovative solutions. Common typologies for masonry are for example the reinforced grouted cavity masonry, where a steel rebars grid is placed in the cavity between two masonry walls and then filled with cast concrete, or the confined masonry, which is a masonry wall confined on all edges by reinforced concrete elements. For the concrete common typology is the hoop reinforcement of columns with metallic materials or the use of high-strength concrete. A modern strategy to improve the seismic performance is represented by energy dissipating devices that absorb the seismic input energy reducing the demand in other members and consequently the damages of the building. Another modern strategy is the base isolation where specific devices are inserted between the superstructure and the foundations in order to reduce the ground motion transmitted to the structure. [1] In the last years new technique for the retrofit of existing buildings has been proposed by researchers. It consists of an external bracing system, also called exoskeleton. The external arrangement of the bracing system allows to minimize the impact on the existing building, without disruption during the retrofitting works. This represents a remarkable advantage under both the economical and functional points of view. This avoids the occupant's relocation and can implement dry technologies to speed up the construction time. This solution also avoids

the increase of loads on the existing foundations. In fact, the seismic loads absorbed by the additional bracing systems are transferred directly towards suitable foundations appropriately built at their bases. In the past year, many research efforts have been dedicated to an in-depth study of seismic retrofit of existing buildings using external exoskeletons made of steel. Formisano et al. [2] proposed a steel concentric bracing systems, Labò et al. [3] proposed a diagrid system composed by triangular modules.

## **1.2 MOTIVATION AND RESEARCH OBJECTIVES**

This thesis is the result of the industrial PhD carried out in collaboration with *Aliva S.r.l.* company, which has its headquarter in San Mauro Pascoli (FC), Italy and it develops customized solutions for ventilated facades. The ventilated façade is a multi-layer protective system for the building envelope consisting, from the inside to the outside, of a continuous insulation, a light bearing structure, a ventilation chamber and a modular cladding. The ventilated façade allows several benefits such as the thermo-hygrometric improvement, energy saving, acoustic insulation and the architectural renovation of the building. The light bearing structure is usually made of aluminium alloy for its property of lightness, durability, corrosion resistance, workability thanks to the extrusion process and eco-sustainability. The scope of this thesis is to investigate the use of aluminium alloys in application fields different from that of the ventilated façade. The use of aluminium alloys in structural engineering is a quite recent activity, because this family of materials is relatively new. In the 20<sup>th</sup> century the use of aluminium alloys spread in many fields, in the aeronautical, transport, automotive and shipping industry. In civil engineering structures, the use of aluminium alloys has been less widespread because they have to compete with steel, the most widely used metallic material in this field. Nowadays, after the several research carried out in order to characterize the design of aluminium alloys structures and the publication of Eurocode 9 *Design of Aluminium Structures*, there are many applications of aluminium alloys in structural engineering. The

main fields of structural applications are the roofing systems, bridges and prefabricated systems. However, there is still a lack of information about the ductility of this material and its use in seismic zones. In fact, to date there is no seismic regulations for aluminium alloys applications, only recently in the project for the development of the next generation of structural Eurocodes, it was decided to introduce the aluminium alloys among the new emerging materials for anti-seismic structures. This thesis aims to make a contribution to the study of the possible use of aluminium alloys in seismic areas and intends to study if it can be a competitive solution in the seismic retrofit field. This study is part of the European research project Pro-GET-onE that means Proactive synergy of inteGrated Efficient Technologies on building's Envelope, in which the Aliva company is involved together with the university of Bologna and other members. The distinctive feature of the project is the integration between energy deep renovation techniques and seismic retrofitting actions. The project aims to combine in a same holistic and integrated system based on preassembled components the highest performance in terms of energy requirements, safety and social sustainability increasing the real estate value of the buildings. This incremented value will be obtained through the development and application of integrated efficient technologies (GETs) that introduce a metal structure with efficient stiffness applied externally to the existing building, with benefits in regarding the construction site, since it does not require operations inside the buildings. Different solutions of GET systems were proposed and analysed to provide the strengthening of the existing buildings and these are made of timber, aluminium alloys or steel. The research objectives are the study and the development of the design of an external structural frame, also called exoskeleton, made of aluminium alloys. The evaluation of the seismic improvement achieved for the existing building with the addition of the aluminium alloy exoskeleton is performed using the structural analysis software Midas Gen. Considering the Italian case study taken into account in the European project, a social housing located in Reggio Emilia, the seismic vulnerability of the building before and after the



intervention is assessed with linear and nonlinear analyses. Finally, a possible improvement of the exoskeleton is examined, nine solutions of the additional aluminium frames are proposed and analysed. The nine proposed solutions are compared in terms of pushover curve, behaviour factor, seismic risk index and costs.

### **1.3 ORGANIZATION AND OUTLINE**

The thesis is organized in 6 Chapters, whose contents can be briefly summarized as follow:

Chapter 1 outlines the motivation and research objectives of the thesis.

Chapter 2 deals with the characteristics and applications of the aluminium alloys. The extrusion process and the aluminium alloys suitable for extrusion are described. The design criteria of aluminium structures according to Eurocode 9 is examined.

Chapter 3 presents the design of the aluminium alloy exoskeleton. Firstly, the feasibility study with a full scale visual mock-up realized at Aliva warehouse is depicted. The purpose of the mock-up is to confirm the feasibility of the idea of the European research project Pro-GET-onE, that is the integrated system based on preassembled components for energy renovation and seismic retrofit. The visual mock-up shows the advantages of the plug and play solution where all components are preassembled in the factory and ready to be installed reducing the construction times. Being a visual mock-up and not a performance mock-up, the aspects to be improved and optimized in order to obtain the maximum performance are highlighted. In fact, preliminary sections of the components and bolted connections are used and both will be improved in the design of final sections. Then, the steps and motivations that led to the design of the final sections of the exoskeleton components are illustrated.

Chapter 4 presents the numerical analysis for the Italian case study considering in the European project. It is a social housing of four storeys composed by reinforced concrete and masonry. For the masonry the force-deformation relationship and the maximum inter-storey drift for each performance level are evaluated according to the FEMA 356 guidelines [4]. The numerical analysis is performed using the structural analysis software Midas Gen. The seismic vulnerability of the existing building is assessed with both linear and nonlinear analyses.

Chapter 5 deals with the seismic improvement assessment achieved for the existing building with the addition of the aluminium alloy exoskeleton. The seismic vulnerability of the strengthened building is assessed with both linear and nonlinear analyses. In the first design of the external exoskeleton, the bracings of the concentric frames are placed in the transverse direction due to the architectural requirements. In order to get better performance, a second model of the exoskeleton is developed by adding bracings in the longitudinal side of the building. To find the optimal solution of the exoskeleton, nine solutions are proposed and analysed and they are compared in terms of pushover curve, behaviour factor, seismic risk index and costs.

Chapter 6 presents the conclusions from the research and suggestion for future research.

## **1.4 PROGETONE**

The four-year European research project Pro-GET-onE (Proactive synergy of inteGrated Efficient Technologies on building's Envelope) is part of the Horizon 2020 program of research and innovation. This research and innovation project starts in 2016 and involves fifteen members coming from many parts of Europe. There are universities, municipalities, construction companies and energy consulting under the coordination of the University of Bologna. The research project Pro-GET-

onE is based on the integration of different technologies to achieve a multi-benefits approach by a closer integration between different aspects:

1. Energy requirements: by adding (or substituting the existing with) new prefab and plug and play high energy performing envelopes and HVAC (Heating, Ventilation, Air Conditioning) systems;
2. Safety: using appropriate external structures to increase the overall structural capacity of the building while supporting the new envelope consisting of timber based components for opaque parts/surface, and aluminium, glass, PV photovoltaic, solar panels;
3. Social and economic sustainability: increasing the real estate value of the buildings and the desirability of retrofit options by providing tailored and customized solutions for users, owners and house managers, increasing safeness and minimizing disturbance to inhabitants.

This incremented value will be obtained through the development and application of integrated efficient technologies (GETs) with the strategic aim of creating a new and attractive market in the deep renovation of existing buildings towards the target of nearly zero energy buildings nZEBs. Pro-GET-onE proposes a technique that until now has not been commonly used and can be configured as an exoskeleton connected to the reinforced concrete frame of the existing buildings. [5] The exoskeleton is applied externally to the existing building with benefits in regarding the construction site since it does not require the performance of operations inside the buildings. This avoids the occupant's relocation and implements dry technologies to speed up the construction time. Dry technologies consist of several factory-built components or units that are assembled on-site. Dry construction is best known in the context of prefabrication because of factory tolerances and workmanship is of a higher quality and consistency to that achieved on site. Prefabrication is the practice of assembling units or components of a structure in a factory or other manufacturing site and transporting complete assemblies or subassemblies to the construction site where the structure is to be located. A project that has adopted this strategy is the requalification of the office

and warehouse buildings of the Magneti Marelli factory in Crevalcore (Italy) made by Teleios Srl [6,7]. In the office building, the external structure is composed of steel frames connected to the existing reinforced concrete building where the vertical elements have been released from horizontal loads, being completely assigned to the new structure. (Figure 1.1). However, in the described case, the exoskeleton does not provide integrated solutions for energy improvement and possible volumetric expansion, as in the case of this research project.

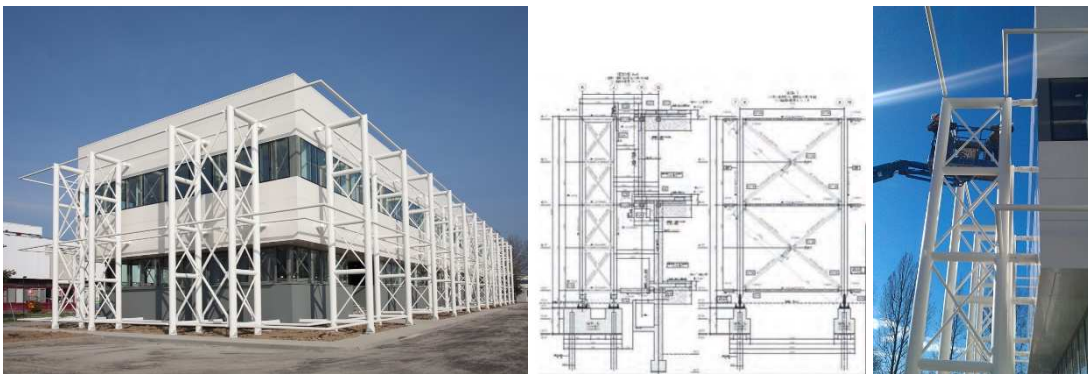


Figure 1.1: Magneti Marelli factory seismic retrofit after seismic event of 2012 [6,7].

This solution also avoids the increase of loads on the existing foundations. In fact, the seismic loads absorbed by the additional bracing systems are transferred directly towards suitable foundations appropriately built at their bases. The element of great importance for the system is the bond that can link the existing structure and the exoskeleton. In order not to burden the existing structure with vertical loads due to the new metal structure, but rather to create an effective collaboration to horizontal actions, this is configured as a vertically sliding joint that allows only vertical movement, leaving the structures autonomous for static loads (Figure 1.2). This connection consists of a steel profile connected to the exoskeleton by means of a flange and connected to the concrete joint with an UPN profiles fixed along the perimetral beams.

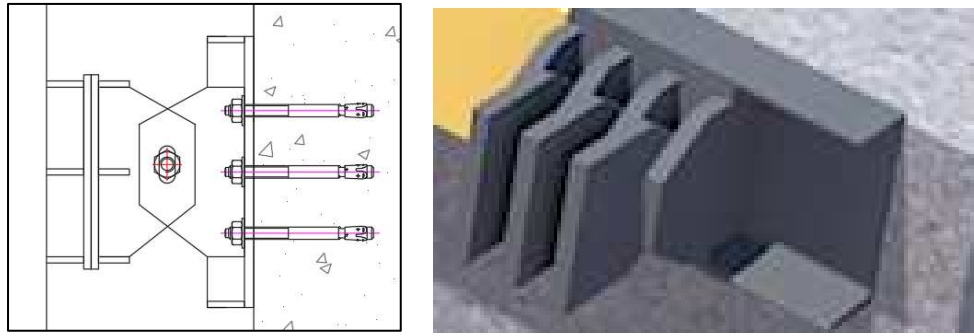


Figure 1.2: Connection linking the existing building and the exoskeleton.

The exoskeleton can be designed according to different geometrical solutions and materials. Both timber, aluminium alloy and steel are proposed and analyzed in Pro-GET-onE to find the optimal solution for strengthening existing buildings. Figure 1.3 outlines different solutions of additional structures and Figure 1.4 shows some of the different options for the new envelope: balcony, sunspace and extra-room. Information from SHARE project [8] indicates Italy, Greece, Romania and the Mediterranean countries of the European Union as the areas with the highest probability of an earthquake. In these areas, recent seismic events have shown how relevant is the issue of seismic vulnerability for existing buildings of reinforced concrete and in particular for those designed without any reference to anti-seismic criteria, which constitute a very substantial part of the existing building stock. Pro-GET-onE focus on existing residential buildings from the 50's-60's on, since they represent the large majority of the European Union building stocks and the biggest source of energy loss: yet today only 1% per year is renovated. Four case studies are selected in the research project and they are located in Groningen in Netherlands, Peristeri in Greece, Reggio Emilia in Italy and Brasov in Romania. These residential buildings are student house and social housing that embed a great potential for change, for energy, architectural and economic reasons.

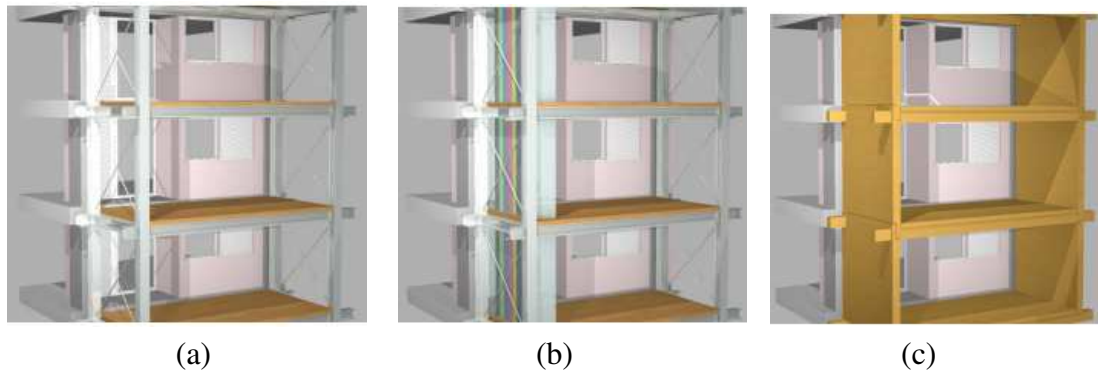


Figure 1.3: (a) Interaction between the existing façade and steel-aluminium structure; (b) the possible positioning of ducts/pipes/storage; (c) the same external structure in timber or X-Lam structure [5].

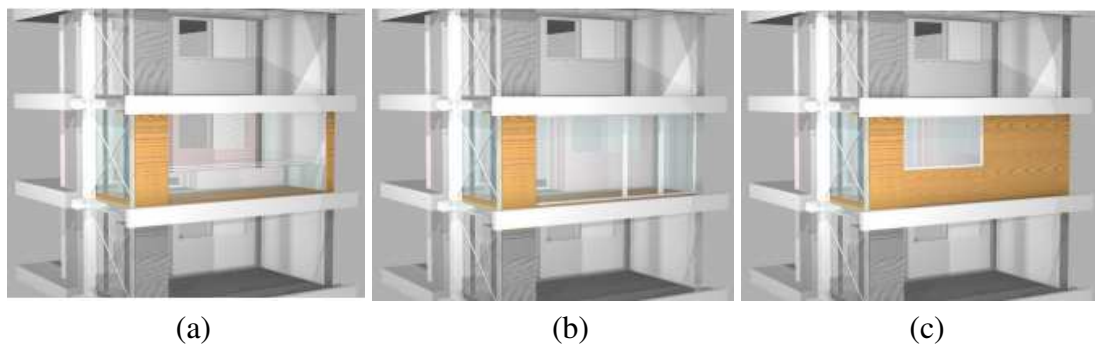


Figure 1.4: Different options for the new envelope.  
 (a) Balconies; (b) sun spaces; (c) extra room.

Some solutions of steel exoskeleton and results of the seismic strengthening of the case studies are presented by Fotopoulou et al. [9, 10].

## 1.5 STATE OF THE ART OF EXOSKELETON APPLICATIONS

As described in the previous paragraph, the “exoskeleton” is an innovative system adopted for the retrofitting of the existing building that is applied from the outside. This intervention is applied to a significant construction portion and it is able to protect the existing construction mainly by increasing its resistance and stiffness towards lateral actions. Referring to the global analysis of the system, the transfer of shear may occur through bi-dimensional (e.g. shear walls) or three-dimensional (e.g. cores) elements. In the first case, walls can be placed in perpendicular ( $2D\perp$ ) or parallel ( $2D//$ ) position to the façade (Figure 1.5.).

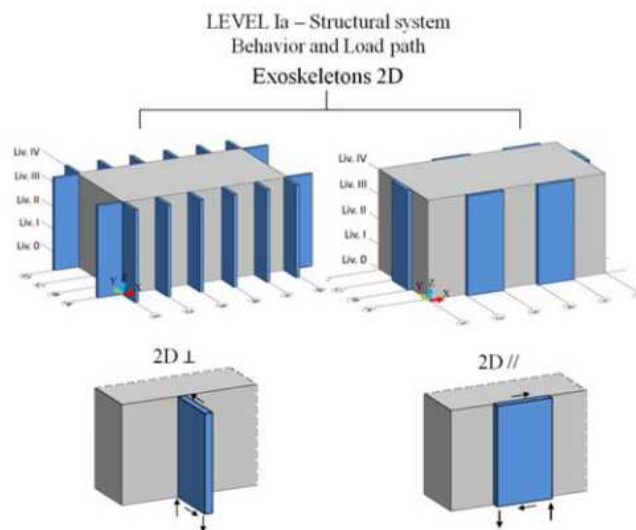


Figure 1.5: Exoskeleton 2D with shear walls arranged perpendicular ( $2D\perp$ ) or parallel ( $2D//$ ) to the façade [11].

$2D\perp$  systems detach from the structural grid to regulate the dynamic response of the existing building and they meet the demand in terms of stiffness and strength only by increasing the walls number and, therefore, they are suitable to be industrialized.  $2D//$  systems represent the most common solution and they are placed in parallel position to the façade. They require appropriate devices for transferring shear to each floor [11].

An alternative to bidimensional systems is represented by three-dimensional structures. These systems are more expensive and can absorb the base shear in all directions independently from their orientation. Figure 1.6 represents 3D systems with flat or curve shells with single or double curvature.

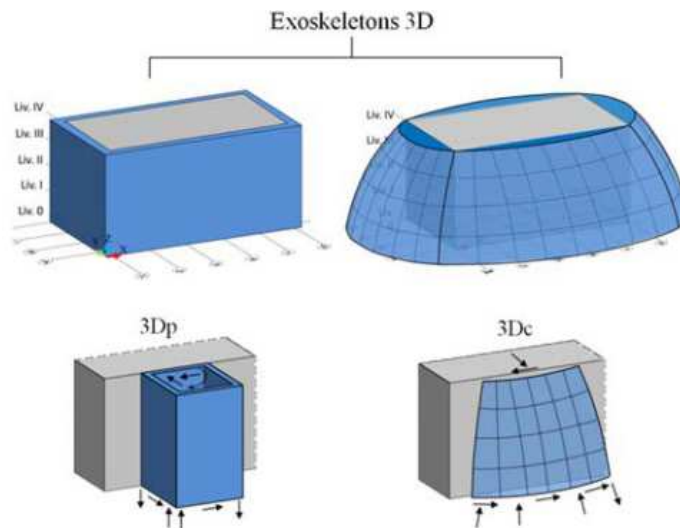


Figure 1.6: Exoskeleton 3D with plane (3Dp) and curved (3Dc) structures [11].

There are different structural configurations of steel exoskeletons, namely Concentric Bracing Frame (CBF), Eccentric Bracing Frame (EBF), Buckling-Restrained Bracing frame (BRB) and Moment Resisting Frame (MRF). The arrangement of braces in CBF systems can be usually done according to X, Inverted-V, portal and K schemes [11].

In the following, three cases of existing RC building retrofitted by steel exoskeletons are described and illustrated. The first case is the requalification of the office complex of Magneti Marelli in Crevalcore (Italy). The retrofit realization has been carried out in 2013-2014 and a bidimensional exoskeleton with shear walls arranged perpendicular to the façade (2D $\perp$ ) was used. Figure 1.1 shows the steel concentric bracing frames with diagonal arrangement according to the X scheme.

The second case is a 2D// system applied to the Hospital Ángeles Clínica Londres in Mexico City (Mexico). The Hospital was built in 1970 and is



a 12-storeys RC building. The 1979 Mexico City earthquake caused several damages to the structural elements and in 1980 the retrofit intervention was carried out to increase the global strength and stiffness of the building (Figure 1.7).



Figure 1.7: Retrofit intervention with 2D// steel exoskeleton of the Hospital Ángeles Clínica Londres in Mexico City [11].

The last example is a tridimensional plane system (3Dp) applied to the Hörsaalgebäude Physik building in Zurich (Switzerland). The building is an auditorium constructed in 1970-1971 without regard to seismic action. The structural weakness referring to seismic performance of the original building is the open entrance hall under the supporting floor of the auditoriums creating a typical weak storey (soft-storey). In addition, there is a very large eccentricity of over 40 metres between the centre of stiffness of the reinforced concrete walls on the rear side of the ground floor level and the centre of mass of the overlying storeys. As a consequence, the building experiences severe torsional stresses under seismic action. The weak ground floor level was retrofitted with a new, inclined, steel pipe truss. In this way, stiffness and resistance could be increased and the unfavourable eccentricity of the bracing system in the ground floor level could be eliminated. Figure 1.8 shows the retrofit intervention carried out in 1994.



Figure 1.8: Retrofit intervention with 3Dp steel exoskeleton of the Hörsaalgebäude Physik building in Zurich [11].

These applications have focused only on the achievement of the building structural security. The security index of the existing building is increased from initial values of 0,2-0,25 to values greater than 1 after the intervention. The state of the art highlighted that the exoskeletons design is still not carried out following a holistic vision to obtain a global structural, energetic and architectural retrofit.

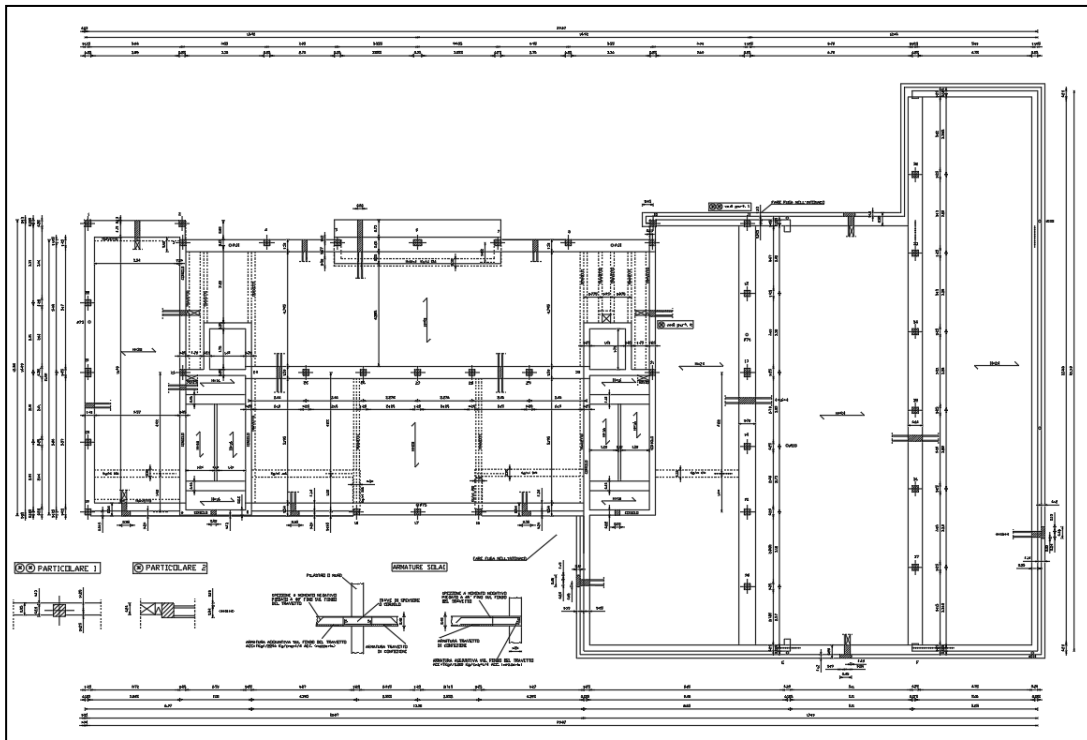
## 1.6 CASE STUDY

The Italian case study consists in a series of building located in different areas around the periphery of Reggio Emilia (Bagnolo in Piano, Castelnuovo di Sotto, Cavriago, Correggio and Poviglio). The buildings were built in the period from 1970 to 2001 and the building type has been identically reproduced. The buildings are for residential use and the apartments are a property of the Social Housing Association called ACER. In this thesis the building located in the town of Bagnolo in Piano (RE) is examined. It is a social housing consisting of 13 apartments built in 2001-2004.

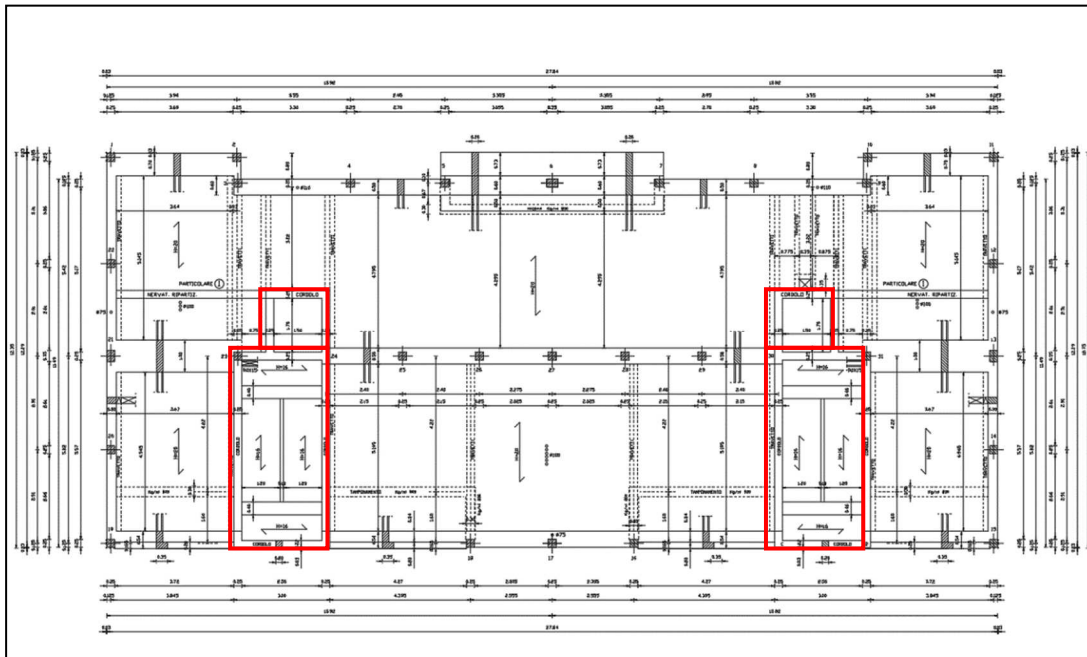


Figure 1.9: Case study of Bagnolo in Piano, Reggio Emilia.

The building has a rectangular plan with dimensions of 27,90 m by 12,35 m. On the ground floor there is an additional body intended for garages having dimensions 12 m by 23,38 m. The main building consists of four storeys of 2,70 m height each and an attic floor 2,2 m maximum height. The case study building has a mixed structure composed by reinforced concrete frame and masonry stairwells, highlighted in red in Figure 1.10. Figure 1.12 shows the plan of the inverted beam foundations.



(a)



(b)

Figure 1.10: Structural plan. (a) First storey plan; (b) Typical plan.

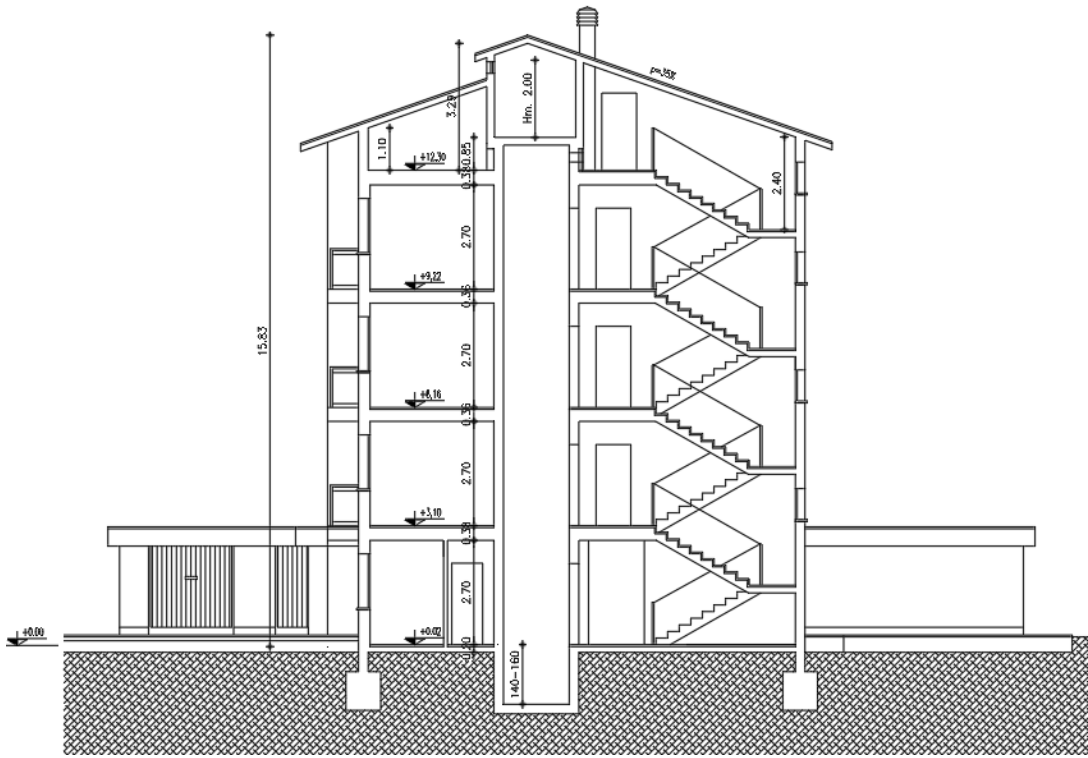


Figure 1.11: Vertical section.

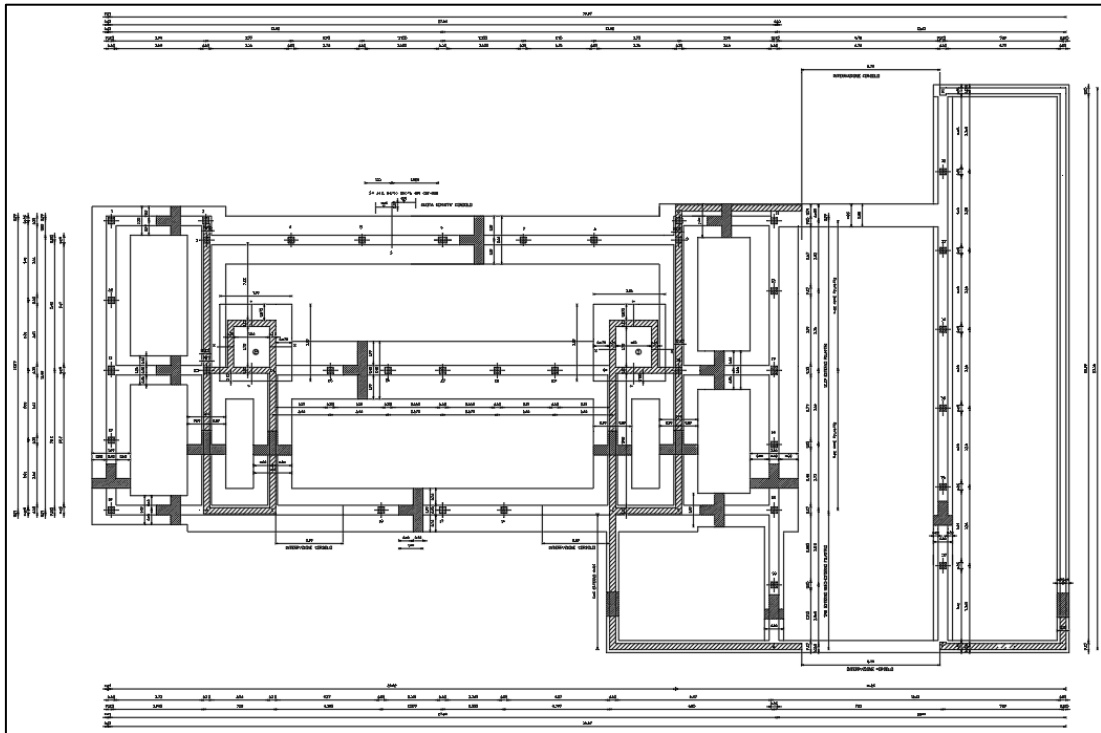


Figure 1.12: Plan of the foundations.

The materials used in the reinforced concrete frames are the C25/C30 concrete class (reference value  $f_{ck} = 25$  MPa) and the FeB44k (reference value  $f_{yk} \geq 430$  MPa) reinforcing steel. For the foundations, the C20/C25 concrete class (reference value  $f_{ck} = 20$  MPa) is used. The stairwells are made of masonry walls with a thickness of 25 cm. The masonry is made by semi-solid bricks and cement mortar. The absence of tests certifying the masonry performance leads to consider the knowledge level 1. The elastic and tangent modulus of masonry are respectively  $E = 4550$  MPa and  $G = 1137,5$  MPa, the compressive strength is  $f = 5$  MPa and the initial shear strength is  $f_{v0} = 0,20$  MPa. The reinforced concrete columns have sections 25 cm by 25 cm and 25 cm by 35 cm. Table 1.1 shows the geometry and the rebars for each column and storey. The ties have a diameter  $\varnothing 8$  and they are spaced 10 cm at the ends and 20 cm at the centre of the columns. Table 1.2 shows the geometry of the beams and Figure 1.13 illustrates the beam construction details with rebars and stirrups. The horizontal structures consist of reinforced brick concrete slabs ( $h=20+4$  cm), while a predalle precast slab is provided for the garage area ( $h=4+16+4$  cm). During the design phase of the building in 1999, the slabs were planned to be 20 cm high. In the structural test report dated 2005, it is indicated that the slabs were realized with a height of 20+4 cm. The structure is not designed for seismic actions because there are only one-directional beams. The imposed loads are listed below in Table 1.3. The seismic action is represented by the response spectrum defined in according with the Italian standard NTC 2018 [12]. For the limit states of Damage Limitation (DL) and Life Safety (LS) considered in this thesis, the value of the parameters that define the spectral shape are listed in Table 1.4.

Table 1.1: Table of reinforced concrete columns.

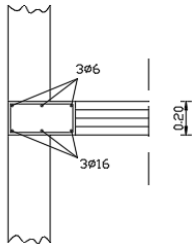
Column number	Section (cm)	Ground floor rebars	1 <sup>st</sup> floor rebars	2 <sup>nd</sup> - 3 <sup>rd</sup> floor rebars	Attic floor rebars
21-6-13	25x35	4 Ø18	4 Ø16	4 Ø14	4 Ø12
4-5-7-8-16-18-23-25-26-27-28-29-31	25x25	4 Ø18	4 Ø16	4 Ø14	4 Ø12
1-11-15-19 17	25x25 25x25	4 Ø16 4 Ø16	4 Ø16 4 Ø14	4 Ø16 4 Ø14	4 Ø16 4 Ø12
2-3-9-10 12-14	25x25 25x25	4 Ø14 4 Ø14	4 Ø14 4 Ø12	4 Ø14 4 Ø12	4 Ø12
20-22	25x25	4 Ø12	4 Ø12	4 Ø12	
32-33-34-35-36-37-38	25x25	4 Ø12			

Table 1.2: Table of reinforced concrete beams.

Beam nodes	Section (cm)	Slab
1-19	40x24	1 <sup>st</sup>
11-G	70x24	1 <sup>st</sup> at garage
E-F	60x24	1 <sup>st</sup> at garage
21-23 31-13	100x24	2 <sup>nd</sup> 3 <sup>rd</sup> 4 <sup>th</sup>
24-30	50x24	1 <sup>st</sup> 2 <sup>nd</sup> 3 <sup>rd</sup> 4 <sup>th</sup>
1-2 10-11	70x24	1 <sup>st</sup> 2 <sup>nd</sup> 3 <sup>rd</sup> 4 <sup>th</sup>
3-5 7-9	50x24	1 <sup>st</sup> 2 <sup>nd</sup> 3 <sup>rd</sup> 4 <sup>th</sup>
5-7	60x24	1 <sup>st</sup> 2 <sup>nd</sup> 3 <sup>rd</sup> 4 <sup>th</sup>
16-18	50x24	1 <sup>st</sup> 2 <sup>nd</sup> 3 <sup>rd</sup> 4 <sup>th</sup>
19-A B-18 16-C D-15	L shaped 54x39	1 <sup>st</sup> 2 <sup>nd</sup> 3 <sup>rd</sup> 4 <sup>th</sup>
1-19 11-15	30x24	2 <sup>nd</sup> 3 <sup>rd</sup> 4 <sup>th</sup>

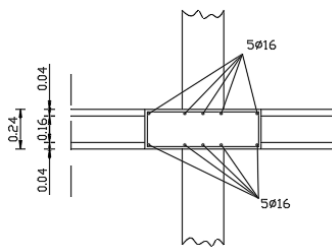
1-19

ST.Ø6/15°



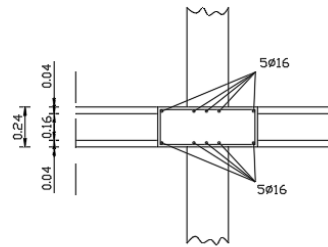
11-G

ST.Ø6/10°-15°



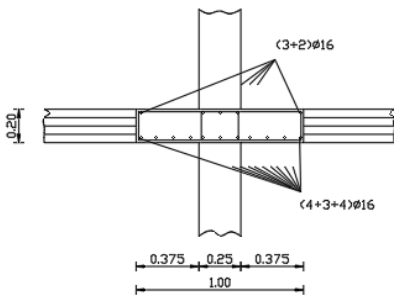
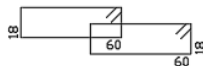
E-F

ST.Ø6/10°-15°



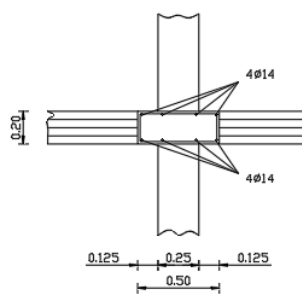
21-23 e 31-13

st. Ø6/15°



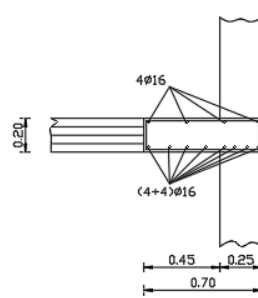
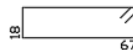
24-30

st. Ø6/15°



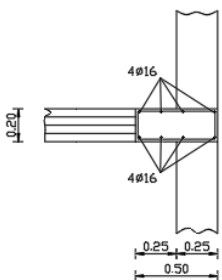
1-2 e 10-11

st. Ø8/10°-15°

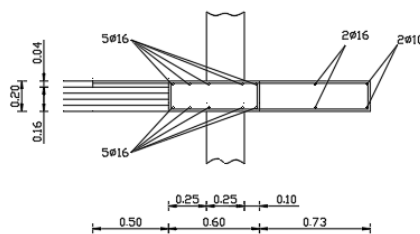
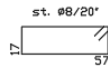
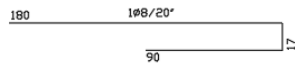


3-4-5 e 7-8-9

st. Ø6/10°-15°

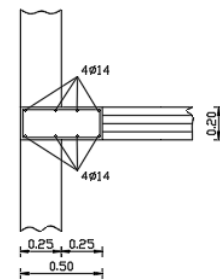


5-6-7



18-17-16

st. Ø6/15°





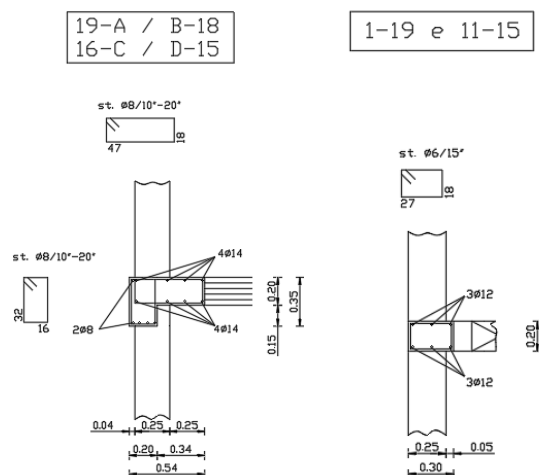


Figure 1.13: Beam construction details.

Table 1.3: Load patterns

Reinforced brick concrete slabs		
Self-weight $1,8 \frac{kN}{m^2}$	Dead load $2,5 \frac{kN}{m^2}$	Live load $2,0 \frac{kN}{m^2}$
Predall precast slabs		
Self-weight $3,3 \frac{kN}{m^2}$	Dead load $2,7 \frac{kN}{m^2}$	Live load $1,3 \frac{kN}{m^2}$
Roof slab		
Self-weight $1,8 \frac{kN}{m^2}$	Dead load $1,2 \frac{kN}{m^2}$	Live load $1,3 \frac{kN}{m^2}$

Table 1.4: Parameters defining the spectral shape.

Limit state	Probability of exceedance $P_{VR}$	Return period $T_R$	Maximum site acceleration $a_g/g$	Amplification factor $F_0$	Reference value $T_c^*$
DL	63%	50 years	0,054	2,511	0,263 s
LS	10%	475 years	0,148	2,424	0,284 s

## 1.7 REFERENCES

- [1] Fiorino L., Founti M., Herfurth D., Holl D., Iurio O., Kramer G., Landolfo R., Macillo V., Pali T. (2015) Lightweight steel drywall constructions for seismic areas. Design, research and applications. Knauf Gips KG , Germany.
- [2] Formisano A., Massimilla A., Di Lorenzo G., Landolfo R. (2020) Seismic retrofit of gravity load designed RC buildings using external steel concentric bracing systems. *Engineering Failure Analysis*, 111, 104485 <https://doi.org/10.1016/j.engfailanal.2020.104485>
- [3] Labò S., Passoni C., Marini A., Belleri A. (2020) Design of diagrid exoskeletons for the retrofit of existing buildings. *Engineering Structures*, 220, 110899. <https://doi.org/10.1016/j.engstruct.2020.110899>
- [4] FEMA 356 (2000) *Prestandard and Commentary for the Seismic Rehabilitation of Buildings*. Washington, D.C.
- [5] Ferrante A., Mochi G., Predari G., Badini L., Fotopoulou A., Gulli R., Semprini G. (2018) A European Project for Safer and Energy Efficient Buildings: Pro-GET-onE (Proactive Synergy of inteGrated Efficient Technologies on Buildings' Envelopes). *Sustainability* 10, 812, p. 1-26. <https://doi.org/10.3390/su10030812>
- [6] Inarcos. (2014) I segni della ricostruzione post terremoto maggio 2012: l'adeguamento sismico della palazzina uffici nello stabilimento Magneti Marelli di Crevalcore. Inarcos, Ingegneri Architetti Costruttori, p. 53-62. Available online: [https://www.teleios-ing.it/UserFiles/File/FRANCESCHINI/Articolo-Inarcos738\\_Ricostruzione%20terremoto%202012\\_Franceschini-Semproli-Secci.pdf](https://www.teleios-ing.it/UserFiles/File/FRANCESCHINI/Articolo-Inarcos738_Ricostruzione%20terremoto%202012_Franceschini-Semproli-Secci.pdf) (last access October 2020)

[7] Material provided by Teleios S.r.l. (società di ingegneria impegnata in un processo interdisciplinare di progettazione delle opere civili, impianti ed energia), via Salvatore Quasimodo, 44 40013 Castel Maggiore [BO]. Available online: [www.teleios-ing.it](http://www.teleios-ing.it) (accessed October 2020).

[8] SHARE Project, Seismic Hazard Harmonization in Europe. Available online: <http://www.share-eu.org/> (last access September 2020).

[9] Fotopoulou A., Badini L., Mochi G., Predari G., Roijackers R., Cojocaru R. (2018) Seismic strengthening through external exoskeleton. *Tema*, V.4, N.3 – Special Issue, p. 34-51. <https://doi.org/10.17410/tema.v4i3.203>

[10] Fotopoulou A., Ferrante A., Badini L., Predari G., Mochi G., Semprini G., Gulli R., Assimakopoulos M., Papadaki D. (2019) An integrated system for façade additions combining safe, energy efficient and user-orientated solutions. *Tema*, V.5, N.1, p. 72-81. <https://doi.org/10.17410/tema.v5i1.216>

[11] Di Lorenzo G., Colacurcio E., Di Filippo A., Formisano A., Massimilla A., Landolfo R. (2020) State-of-the-art on steel exoskeletons for seismic retrofit of existing RC buildings. *Ingegneria Sismica*, V.37, N.1, p. 33-50. 2-s2.0-85083758977, WOS:000522487600004

[12] Norme tecniche per le costruzioni (NTC 2018). D.M. 17 gennaio 2018.



## *Chapter 2*

# **ALUMINIUM ALLOYS: CHARACTERISTICS AND APPLICATIONS**

## **2.1 INTRODUCTION**

Aluminium is a very new material. The use of aluminium alloys in structural engineering is a quite recent activity, because this family of materials is very young and its history is very short. Aluminium comprises eight per cent of the earth's crust. Since aluminium occurs in extremely stable oxygen compounds, it took quite some time for scientists to figure out how to reduce it into pure metal. In fact, aluminium and its alloys are available since the end of the 19<sup>th</sup> century only. The possibility of isolating the aluminium element was foreseen by Sir Humphry Davy at the beginning of the 19<sup>th</sup> century (1807), but the first concrete result was obtained by Wohler after 20 years of research (1827). Some small-scale commercial production was achieved, but even five decades later aluminium remained more costly and coveted than gold. In 1886 started the industrial production of aluminium. Independently of each other, the American scientist Charles Martin Hall and the French scientist Paul Louis Touissant Héroult invented the electrolytic reduction process. The method is based on alumina derived from bauxite. Although improvements have been made in the process over the past century, the industrial production of aluminium is essentially based on the same process today. The production of primary aluminium is highly energy-intensive. Roughly 12-14 kWh are required to produce one kg of pure aluminium using the electrolytic reduction process. However, since the metal's melting point is

low (approximately 660 °C), the re-melting requires only about five per cent of the original energy input. This means that efficient aluminium recycling is profitable. The secondary production of aluminium, that is the process of recycling aluminium scrap into aluminium, currently accounts for about one-third of world aluminium consumption. [1] The aluminium recycling industry has almost quadrupled its output from 5 million tonnes in 1980 to close to 18 million tonnes in 2007 from old and traded new scrap. During the same time, primary metal use has grown from 15 to 38 million tonnes (Figure 2.1).

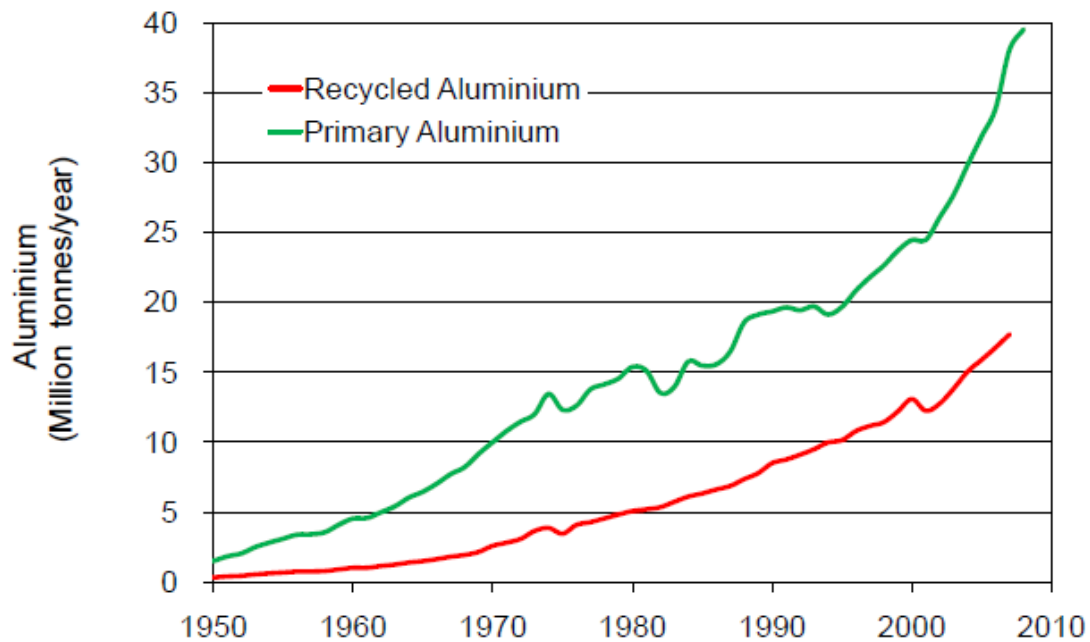


Figure 2.1: Worldwide evolution of recycled and primary aluminium [2].

At the end of their useful life, if pre-treated and/or sorted, aluminium products can be recycled for use in almost applications without loss of properties since the metal's atomic structure is not altered during melting. The recycled product may be the same as the original product but is more often a completely different product. Transportation is the most important field of application for aluminium worldwide. In 2007, up to 30% of wrought and casting alloys put on the market were used in cars, commercial vehicles, aircraft, trains, ships, etc. (Figure 2.2). The high

strength to weight ratio offers the possibility to reduce vehicle weight reducing consumption and greenhouse gas emission. In aerospace aluminium usage has long dominated all other constructional materials. The metal constitutes about 80% of a civil airliner's structural weight. Aluminium trains and rolling stock are in widespread use as railroads seek for operational economics. On the water aluminium masts and spars are now more common than wood for small craft and larger vessels have been built with aluminium superstructures [1].

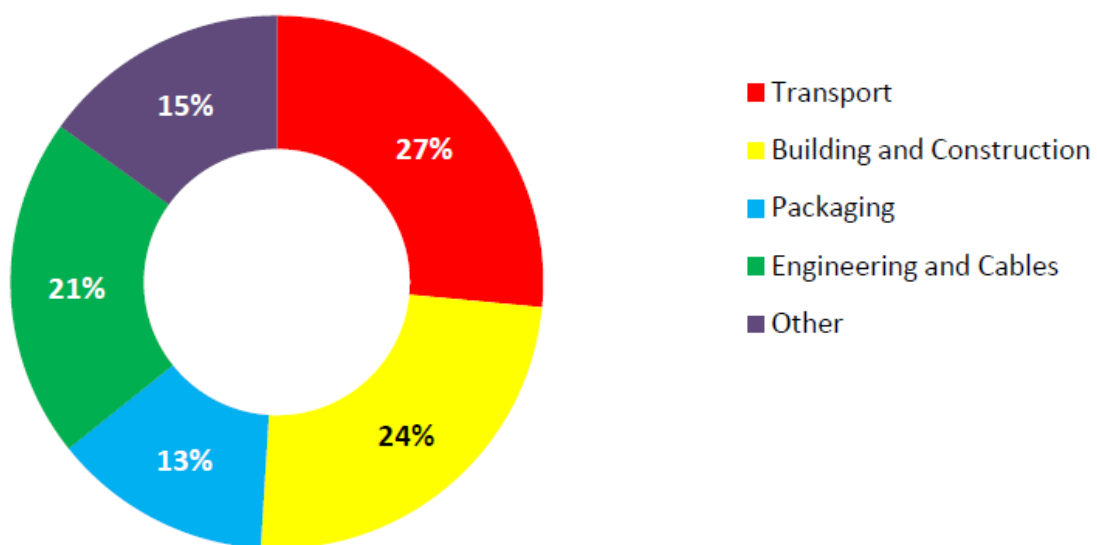


Figure 2.2: Global end-use markets for finished aluminium products, 2007 [2].

In building and construction, the aluminium's formability, high strength to weight ratio, corrosion resistance and easy of recycling make it the ideal material for a wide range of applications. The main uses of aluminium are in the construction of windows, doors and facades. Aluminium can also be found in the support structures for solar panels, solar collectors and light shelves. The lightness of aluminium is a characteristic that contributes to its wide structural application and provides many advantages in transportation and erection, especially for prefabricated system. In addition, in structures like swimming pool roofs, harbor elements and river bridges, which are characterized by humid

environments, the choice of aluminium is preferable due to its corrosion resistance and durability. [3] In the electric field, aluminium is widely used for long distance high voltage transmission lines. Virtually all high voltage transmission lines use aluminium conductor. The aluminium has a good electrical conductivity equal to 65% that of copper. Because of its low specific gravity, the mass electrical conductivity of pure aluminium is more than twice that of annealed copper and greater than that of any other metal. Therefore, allows larger pylon spacing and easier stringing. Furthermore, aluminium possesses unique barrier and physical properties and is therefore used extensively for the packaging of food, beverages and pharmaceuticals. Even in its thinnest form, aluminium effectively protects contents against the quality-reducing effects of oxygen, light, moisture, micro-organisms and unwanted aromas.

## **2.2 CHARACTERISTICS AND CIVIL-ENGINEERING APPLICATIONS**

The success of aluminium alloys as construction material is based on some prerequisites, which are connected to the physical properties, the production process and the technological features. In particular, it is commonly recognised that aluminium alloys can be economical, and therefore competitive in those applications where full advantage is taken on the following prerequisites:

1. Lightness: the density is  $\gamma = 2700 \text{ kg/m}^3$ , one third of that of steel. The low specific weight makes it possible to simplify the erection phases, transport fully prefabricated components, reduce the loads transmitted to foundations, economize energy either during erection and/or in service, reduce the physical labour.
2. Corrosion resistance: the exposed surface of aluminium combines with oxygen to form a thin and inert aluminium oxide film which blocks further oxidation. The formation of the protective oxide film on the surface makes it possible to reduce the maintenance expenses and to provide good performance in corrosive environments.



3. Functionality of structural shape: the extrusion process makes it possible to improve the geometrical properties of the cross-section by designing a shape which simultaneously gives the minimum weight and the highest structural efficiency. It allows to obtain stiffened shapes without using built-up sections, thus avoiding welding or bolting, and to simplify connecting systems among different component improving joint details. Finally, the extrusion process makes it possible to combine different functions of the structural component achieving a more economical and rational profile. [4]

Aluminium is also a ductile material. The metal can be hot rolled or cold rolled down to thicknesses of 6-7  $\mu\text{m}$  (foil), it can be extruded down to wall thicknesses of 0,5 mm and it can also be pressed, drawn, forged, stamped or cast by traditional methods. Furthermore, the aluminium can be described as the “green metal”: it is non-toxic and recyclable. From the point of view of mechanical resistance, pure aluminium has a strength varying from 30  $\text{N/mm}^2$  to 150  $\text{N/mm}^2$ , therefore it is reluctantly used for structural purposes in construction. However, when it is added to other metals, such as Mg, or with metalloids like Si, aluminium alloys are formed whose strength is high and, in some cases, can reach up to 500  $\text{N/mm}^2$ . A comparison with steel is important in order to identify the conditions and fields of applications where aluminium alloys can be competitive. From the comparison of the two typical stress-strain curves (Figure 2.3), it can be observed that both materials behave linear elastically with a different slope of the  $\sigma$ - $\varepsilon$  curve up to the elastic limit at a residual strain of 0,2% for aluminium  $f_{0,2}$  and the yield stress for steel  $f_y$ . After the elastic range, aluminium alloys have a continuous strain-hardening behaviour which is not preceded by a perfectly plastic branch corresponding to the yielding plateau as for steel. The ultimate deformation for aluminium alloys is lower (around 8-12%) than that of steel (greater than 20%). The ratio between the ultimate strength  $f_t$  and the elastic limit  $f_{0,2}$  for aluminium alloys is normally lower than that of steel, depending on the degree of hardening.

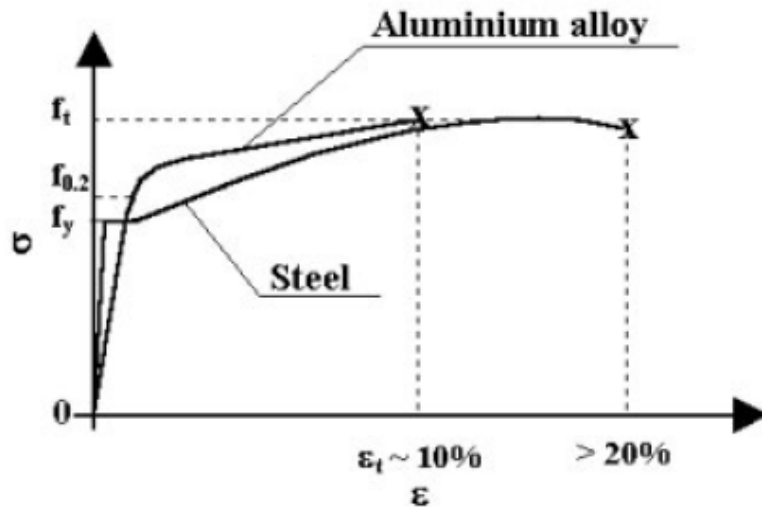


Figure 2.3: Comparison between typical stress-strain curves for aluminium alloy and steel [5].

Table 2.1 shows a summary comparison among some aluminium alloy extrusions (one work-hardened 5083 F, two heat-treated 6063 T6 and 7020 T6) and the most commonly used mild steels for hot-rolled sections (Fe 360, Fe 430 and Fe 510). The main mechanical properties are compared: elastic limit at a residual strain of 0,2% for aluminium  $f_{0,2}$  or yield stress for steel  $f_y$ , ultimate strength  $f_t$ , Young's modulus  $E$ , ultimate elongation  $\epsilon_t$ , density  $\gamma$  and thermal expansion coefficient  $\alpha$ .

Table 2.1: Comparison of properties among three aluminium alloys and the common mild steel [6].

Properties	Aluminium alloys			Steels		
	5083 F	6063 T6	7020 T6	Fe 360	Fe 430	Fe 510
$f_{0,2}/f_y$ (N/mm <sup>2</sup> )	110	190	290	235	275	355
$f_t$ (N/mm <sup>2</sup> )	270	220	350	360	430	510
$\epsilon_t$ (%)	12	10	10	28	24	22
$E$ (N/mm <sup>2</sup> )	70 000			206 000		
$\gamma$ (N/mm <sup>3</sup> )	27 000			78 500		
$\alpha$ (°C <sup>-1</sup> )	0,00002			0,00001		

The elastic modulus of the aluminium is 70 GPa, one-third of that of steel, and gives a high susceptibility to instability. To reduce the deformability of the aluminium, stiffened sections must be used in the structural design. The thermal expansion coefficient of the aluminium is twice the one of steel. This fact makes the aluminium alloys sensitive to thermal variations and it has to be taken into account particularly when designing support apparatus.

The mechanical characteristics of the aluminium alloys can be described through a generalized  $\varepsilon = \varepsilon(\sigma)$  relationship known as Ramberg-Osgood law [6]:

$$\varepsilon = \frac{\sigma}{E} + 0,002 \left( \frac{\sigma}{f_{0,2}} \right)^n \quad (2.1)$$

where:

$E$  is the Young's modulus;

$f_{0,2}$  is the elastic limit at a residual strain of 0,2%;

$n$  is the exponent of the Ramberg-Osgood law and it is given by:

$$n = \frac{\ln 2}{\ln \left( \frac{f_{0,2}}{f_{0,1}} \right)} \quad (2.2)$$

where  $f_{0,1}$  is the stress at a residual strain of 0,1%.

Depending on the ratio  $f_{0,2}/f_{0,1}$ , which characterizes the “knee” of the  $\sigma$ - $\varepsilon$  curve, the value of  $n$  are useful in classifying aluminium alloys from the point of view of the strain-hardening rate of stress-strain behaviour. In fact, when the ratio tends to 1, the exponent  $n$  tends to infinity and the Ramberg-Osgood law represents the behaviour of mild steel. On the contrary,  $n = 1$  provides a linear elastic behaviour. Intermediate values of  $n$  express the different behaviour of aluminium alloys, by means of decreasing values of  $n$  as far as the rate of strain-hardening increases. An effective interpretation of structural materials by means of the exponent  $n$  of the Ramberg-Osgood law is given in Figure 2.4 as a function of the  $f_{0,2}/f_{0,1}$  ratio, where aluminium alloys are identified by means of the four classical Sutter classes, which are limited by given increasing values of the  $f_{0,2}/f_{0,1}$  ratio as far as the degree of hardening decreases.

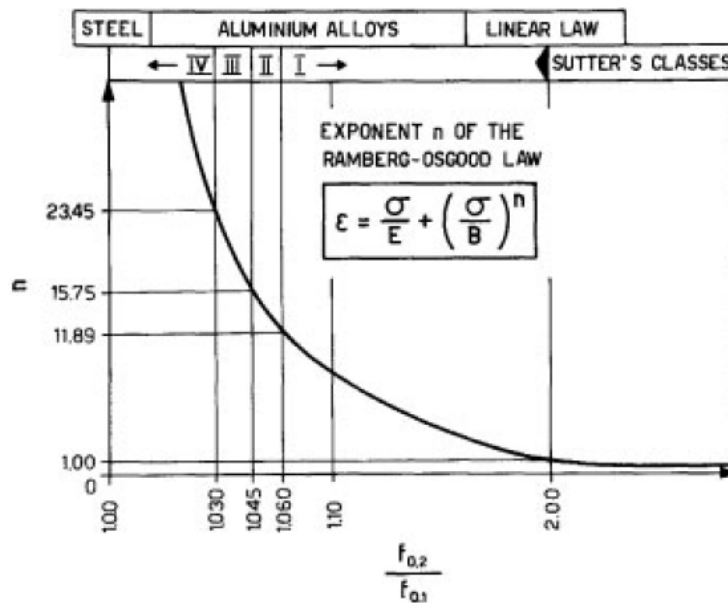
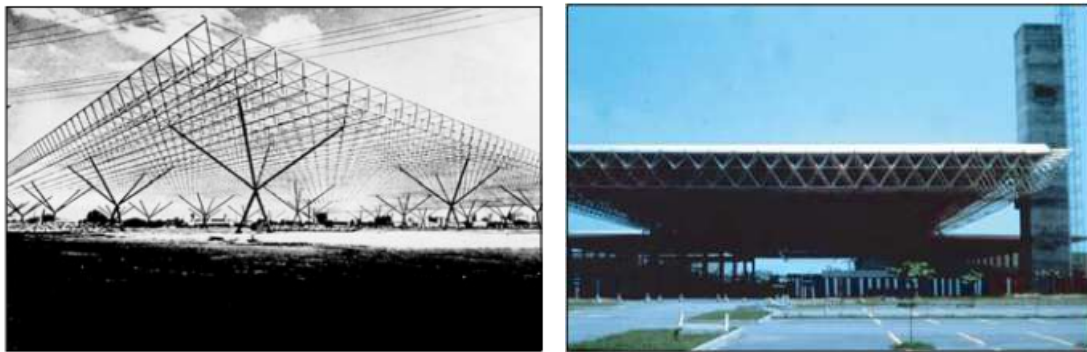


Figure 2.4: Comparison between the exponent  $n$  of the Ramberg-Osgood law and the values of ratio  $f_{0,2}/f_{0,1}$ , which are related to the Sutter classes [5].

With the advantages depicted above, the aluminium alloys are increasingly used in civil-engineering applications all over the world. The use of aluminium has been adopted in roofing systems, in which the live loads are small compared with dead loads and lightness is fundamental to cover a large surface. Several applications of reticular space structures can be found in South American (Brazil, Colombia, Ecuador). A very spectacular structure has been erected for the Interamerican Exhibition Center at Sao Paulo in Brazil, 1969. This structure covers an area of about 67 600 m<sup>2</sup>, with a mesh of 60 x 60 m and a depth of the reticular layer of 2,36 m (Figure 2.5a). The materials were: aluminium alloys of 6063 and 6351 series T6 for cylindrical bars; pure aluminium Al 99.5% for trapezoidal sheeting and galvanized steel bolts for connections. A very similar structure has been used for the International Congress Center in Rio de Janeiro, with the same mesh 60 x 60 m, covering in total 33 000 m<sup>2</sup> (Figure 2.5b). Figure 2.6 shows some roofing structures erected in UK (the Conference Center in Glasgow and the roof of the Millennium Stadium in Welles) [7]. The first important aluminium dome, called

“Dome of Discovery” was built in UK in 1951 for the Festival of Britain. It was the largest in the World at that time, with a diameter of 100 m, made of three-directional reticulated arches and having a total weight of 24 kg/m<sup>2</sup> (Figure 2.7).



(a)

(b)

Figure 2.5: (a) The reticular space structure of the Interamerican Exhibition Center of Sao Paulo (Brazil); (b) the International Congress Center of Rio de Janeiro (Brazil) [4].



(a)

(b)

Figure 2.6: (a) The Conference Center in Glasgow; (b) roof of the Millennium Stadium in Welles [7].

Several structural applications of aluminium domes followed in both industrial and architectural fields. Many structural systems have been proposed for reticular space structures, among which the Italian system Geo-system and the American system Tem-Cor. Geo-system is based on cylindrical bars with conical ends and hollow spherical nodes. Recently,

Geo-system structures have been used in the restoration of the “Mercati Traianei” Museum in Rome in the form of cylindrical vaults and geodetic domes (Figure 2.8). Two significant examples from USA are given in Figure 2.9: the Epoct Center in Florida (a) and of the University of Connecticut (b).

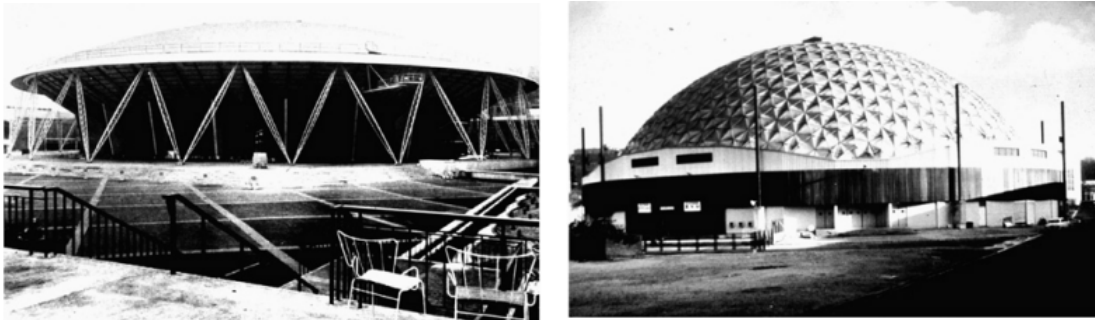


Figure 2.7: The “Dome of Discovery” in UK [7].

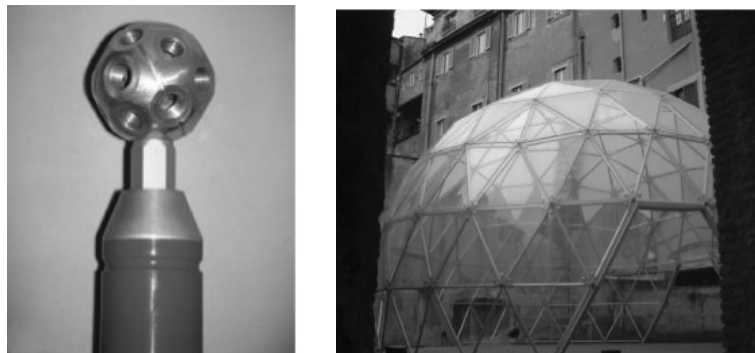


Figure 2.8: The Geo-system and its application in the geodetic dome of the “Mercati Traianei” Museum, Rome, Italy [6].



Figure 2.9: (a) Epoct Center in Florida; (b) the University of Connecticut in USA [7].

The properties of lightness and corrosion resistance of aluminium alloys have allowed their extended use in the field of bridges, covering all the main structural types, for which steel normally is used. The Arvida Bridge (Figure 2.10a) in Quebec, Canada (1950), was one of first motorway bridge made of aluminium alloy. A new important field of application is the one of military bridges. They are made of modular systems, consisting of one or more bridge segments dimensioned with the goal of minimum structural weight (Figure 2.10b). Aluminium alloys are successfully used in footbridges, owing to the low live load. Examples of aluminium footbridges can be found in France, Germany, The Netherlands, Italy, Canada. The features of aluminium alloys have been suitably exploited in the restoration and rehabilitation of old suspension bridges, where a new deck was necessary in order to fulfil new structural requirements. In the late 1970s, three 19th century suspension bridges were retrofitted by means of aluminium alloys deck in France. More recently (1998), the oldest Italian suspension bridge, the ‘Real Ferdinando’ bridge on the Garigliano river (erected in 1832) was restored by using an aluminium alloy deck and so became the first aluminium bridge in Italy (Figure 2.11).

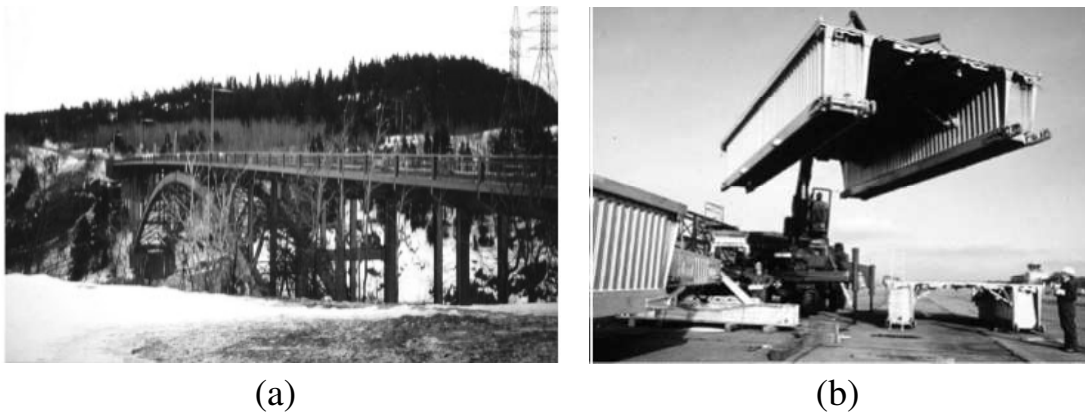


Figure 2.10: (a) Arvida bridge, Quebec, Canada; (b) German military bridge: erection phases [6].



Figure 2.11: The Real Ferdinando Bridge on the Garigliano River, Italy [8].

There are special structures having the function to support fixed elements, which are located at a given distance from the ground. The prevalent dimension can be horizontal, as in case of gantries for traffic signs, or vertical, as in case of antennas, electrical transmission tower and lighting towers. For these structures, the elimination of maintenance represents a fundamental prerequisite. In addition, the lightness of aluminium allows prefabricated systems, very easy for transportation and erection, giving rise to competitive solutions in comparison with other materials. Many towers for electrical transmission lines have been erected in Europe. Two important aluminium towers have been erected in Naples. The first is the tower for the parabolic antennas of the Electrical Department erected in 1986, which received the international award “Hundred Years of Aluminium” (Figure 2.12a). The second is the Information Tower near the football stadium in Naples (1990), which has been equipped with antennas and screens in order to display games outside the stadium (Figure 2.12b). A field where the properties of aluminium play a determinant role is the hydraulic applications, such as pipelines, reservoirs and sewage plants. In particular, the corrosion resistance allows to eliminate protection in the presence of corrosive environments, while the lightness corresponds to energy saving during the operating phases of the plant. Nowadays the offshore applications can be considered the main future trend for aluminium alloys. Helidecks are made of aluminium alloys and they are



erected not only on offshore platforms, but also on the top of multi-storey buildings.

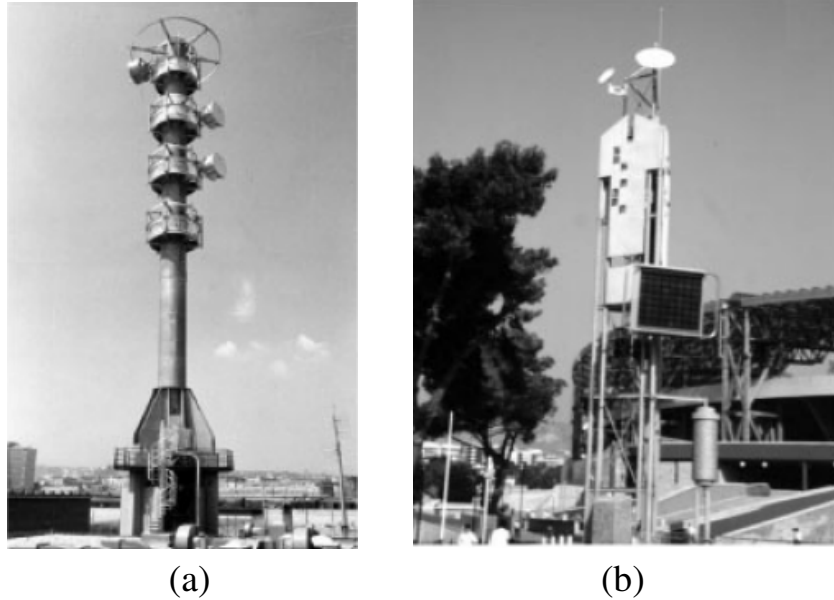


Figure 2.12: (a) The Enel Tower, Naples, Italy; (b) the Information Tower, Naples, Italy [6].

### 2.3 ALUMINIUM ALLOYS

Aluminium is not just one material but it is a family of different alloys. The properties of a particular aluminium product depend on the alloy chosen. The knowledge of these alloys is the key to the effective use of aluminium. The first official alloy designation that denotes commercially pure aluminium dates back to 1888. Since then, the introduction of new wrought and casting alloys, each developed for specific qualities, has continued steadily until the present day. The range of alloy choice is important. The number of widely used commercial alloys is of course much smaller. The aluminium alloys are divided into wrought alloys and casting alloys. Wrought alloys are classified according to the International Alloy Designation of the Aluminium Association [9]. Each alloy is described by a four digit number plus further letter and number indicating

the temper or condition of the alloy. The first of the four digits in the designation indicates the alloy group in terms of the major alloying elements as follows:

- 1xxx aluminium of 99% minimum purity and higher
- 2xxx aluminium and copper alloys
- 3xxx aluminium and manganese alloys
- 4xxx aluminium and silicon alloys
- 5xxx aluminium and magnesium alloys
- 6xxx aluminium, magnesium and silicon alloys
- 7xxx aluminium, zinc and magnesium alloys
- 8xxx other alloys (e.g. aluminium lithium)

1xxx Group. In this group for minimum purities of 99,00% and greater, the last two of the four digits indicate the minimum percentage of aluminium. For example, 1070 indicates aluminium purity of 99,70%. The second digit indicates modifications in impurity limits or alloying elements. If the second digit is zero it indicates unalloyed aluminium having natural impurity limits; integers 1-9 indicated special control of one or more individual impurities or alloying elements.

2xxx to

8xxx Group. In these groups the last two of the four digits have no special significance but serve only to identify the different alloys in the group. The second digit indicates alloy modifications; if it is zero it indicates the original alloy.

These alloys fall into two main groups (Figure 2.13). The work hardening alloys, where strength is related to the amount of cold work applied by rolling or forming, and the heat treatable alloys or precipitation hardening alloys. With the latter strength and other properties are enhanced by heat treatment of various kinds [1].

WORK HARDENING		HEAT TREATABLE	
1XXX	(Al)	2XXX	(Al/Cu)
3XXX	(Al/Mn)	6XXX	(Al/Mg/Si)
5XXX	(Al/Mg)	7XXX	(Al/Zn/Mg)
8XXX	(Al/Other)	8XXX	(Al/Other)

The 4xxx series in wrought form is almost exclusively used for welding rod and wire as well as for braze cladding.

Figure 2.13: Wrought aluminium alloys by group [1].

The European reference for the alloys will be identified with the preface EN and AW which indicated European Normative Aluminium Wrought alloys. In all other respects the alloy numbers and composition limits are identical to those registered by the Aluminium Association (Figure 2.14).

		Major alloying element	Atoms in solution	Work hardening	Precipitation hardening	
WROUGHT ALLOYS*) EN AW-	1XXX	None (min. 99.00% Al)		X		Non-heat treatable alloys
	3XXX	Mn	X	X		
	4XXX	Si	X	X		
	5XXX	Mg	X	X		
	2XXX	Cu	X	(X)	X	
	6XXX	Mg + Si	X	(X)	X	
	7XXX	Zn	X	(X)	X	
	8XXX	Other	X	(X)	X	

CASTING ALLOYS*) EN AB- EN AC- EN AM-	1XXX0	None (min. 99.00% Al)				*) letters preceding the alloy numbers have the following meaning EN = European Standard A = Aluminium B = Ingot C = Cast Alloy M = Master Alloy W = Wrought Alloy
	2XXX0	Cu				
	4XXX0	Si				
	5XXX0	Mg				
	7XXX0	Zn				
	8XXX0	Sn				
	9XXX0	Master Alloys				

Figure 2.14: European aluminium alloy designation [1].

The temper designation follows the alloy designation; these are separated by a hyphen. Basic temper designation consists of letters, according to EN 515 [10]:

F – as fabricated

O – Annealed

H – Strain-hardened

W – Solution heat-treated

T – Thermally treated (for heat treatable alloys only)

For the non-heat treatable alloys, in which the mechanical properties are enhanced by the amount of cold work introduced after the last annealing operation, the first digit after H indicates the specific combination of basic operations as follows:

H1: strain-hardened only

H2: strain-hardened and partially annealed

H3: strain-hardened and stabilized by low temperature treatment

H4: strain-hardened and lacquered or painted

For the heat treatable alloys, the first digit following the letter T is used to identify the specific sequences of basic treatments as follows:

T1: cooled from an elevated temperature and naturally aged

T2: cooled from an elevated temperature, cold worked and naturally aged

T3: solution heat-treated, cold worked and naturally aged

T4: solution heat-treated and naturally aged

T5: cooled from an elevated temperature shaping process and artificially aged

T6: solution heat-treated and artificially aged

T7: solution heat-treated and over-aged/stabilized

T8: solution heat-treated, cold worked and artificially aged

T9: solution heat-treated, artificially aged and cold worked

T10: cooled from an elevated temperature shaping process, cold worked and artificially aged

### **1000 series: pure aluminium**

Commercially pure aluminium (99,0% pure) is soft, ductile and of little structural value, but as extracted it normally contains up to 1,5% impurities; mainly iron and silicon. These have a marked effect on the properties of the metal, so that, with the further hardness acquired during rolling, commercial purity aluminium has a useful degree of strength and is widely produced in sheet form. Its elastic limit is very low in the annealed condition  $f_{0,2} \approx 30$  MPa and in it greater in strain-hardened condition  $f_{0,2} \approx 100$  MPa. It is very ductile in the annealed condition with ultimate elongation equal to  $\varepsilon_t \approx 30-40\%$ , whereas the ductility drastically reduced if the material is cold worked. This series has excellent corrosion resistance and it is ideal for use in the food and chemical industries. It is rolled to foil thickness for use in food, confectionery and cigarette packaging and has even been used for making shaped panels for vehicles where its high elongation was of prime importance for the forming processes involved.

### **2000 series: aluminium-copper alloys**

With copper as the principle element, these alloys require solution heat treatment to achieve optimum mechanical properties, which can exceed that of mild steel. The elastic limit  $f_{0,2}$  can increase up to 300 MPa when heat-treated, with a sufficient ductility of  $\varepsilon_t \approx 10\%$ . Generally, these alloys have limited cold formability, except in the annealed condition, and less corrosion resistance than other alloys; they are therefore generally anodised for protection from aggressive environments. They are also more difficult to weld. Alloys in this family are particularly useful for aircraft and military applications.

### **3000 series: aluminium-manganese alloys**

The addition of approximately 1% manganese increases the strength by approximately 10-15% compared with 1200 alloy, without any major loss in ductility. This series cannot be heat treated and uses hard cold-forming

processes to increase the material strength. It is corrosion resistant and its major end uses are roofing sheet and vehicle panelling.

#### **4000 series: aluminium-silicon alloys**

Silicon can be added to aluminium alloys in quantities sufficient to cause a substantial lowering of the melting point. For this reason, this alloy system is used entirely for welding wire and brazing filler alloys, where melting points lower than the parent metal are required.

#### **5000 series: aluminium-magnesium alloys**

This series of alloys is non heat-treatable and exhibits the best combination of high strength with resistance to corrosion; in fact, they are frequently used in marine/sea water applications. The elastic limit  $f_{0,2}$  reaches about 200 MPa when they are cold worked, and the ductility is quite high ( $\epsilon_t$  up to 10%). This series also exhibits good weldability but when the Mg level exceed 3% there is a tendency for stress corrosion resistance to be reduced, dependent on the temper used and temperature of operation. Major end uses of these alloys are pressure vessels, bulk road and rail vehicles, ships structures, chemical plant.

#### **6000 series: aluminium-silicon-magnesium alloys**

This group of heat-treatable alloys uses a combination of magnesium and silicon to render it heat-treatable. These alloys find their greatest strength, combined with good corrosion resistance, ease of formability and excellent ability to be anodised. The elastic limit is high  $f_{0,2} \approx 250$  MPa with a quite ductility  $\epsilon_t$  up to 12%. They are particularly suitable for extrusion, but also rolled sections as well as tubes can be produced. Typical alloys in this group include 6061, 6063 and 6082 used for building structure applications, and land and sea transport applications.

### **7000 series: aluminium-zinc-magnesium alloys**

This group of alloys exhibits the highest strength as far as aluminium is concerned and in many cases they are superior to that of high tensile steels. These alloys are produced in the form of extruded and rolled heat-treated profiles. They can be subdivided into two sub-families, depending upon the percentage of copper as the third alloying element:

- AlZnMg alloys have an elastic limit  $f_{0,2}$  greater than 250 MPa and quite good ductility ( $\epsilon_t \approx 10\%$ ). They are corrosion resistant and they are generally used in structural applications being suitable in welded structures.
- AlZnMgCu alloys are the highest resistance alloys after heat treatment, reaching  $f_{0,2} \approx 500$  MPa. They have low weldability and are not corrosion resistant, because of the presence of copper, and therefore require protection by plating or painting.

### **8000 series: aluminium-plus other elements which do not fall into any of the patterns outlined above**

The compositions of the alloys of this series are very different from each other, and their application can be very different. There are alloys for electrical conductors, for thin packaging foils and some complex alloys containing lithium for aeronautic.

Figure 2.15 shows typical stress-strain curves for four different aluminium alloys and compares them with a range of engineering metals. The alloys are: 99,5% pure aluminium (1050A) in the fully annealed state, a 4,5% magnesium-aluminium alloy (5083) after strain-hardening, a magnesium-silicon alloy 6082 in the fully heat-treated condition T6 and a zinc-magnesium-copper-aluminium alloy 7075-T6.

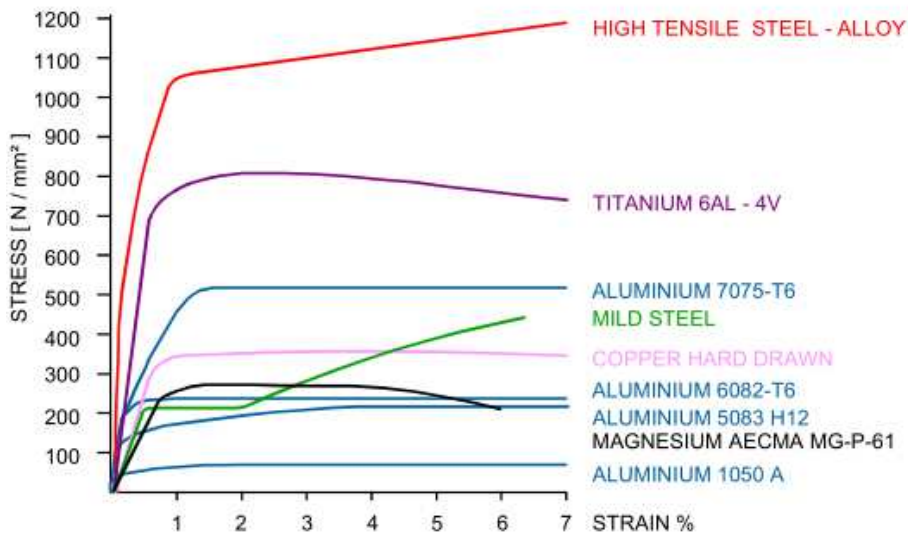


Figure 2.15: Stress-strain curves of aluminium in comparison with various metals and alloys [1].

## 2.4 THE EXTRUSION PROCESS

The extrusion is a transformation technique adopted for many metals, but particularly important for aluminium alloys, because it allows the production with high productivity of semi-finished products of complex shape with good properties and performance. The principle of extrusion is very simple: a cylindrical billet is inserted at a high temperature in a container and it is pushed by a ram against a shaped die, provided with a special slit, through which the metal exits assuming the section, see Figure 2.16.

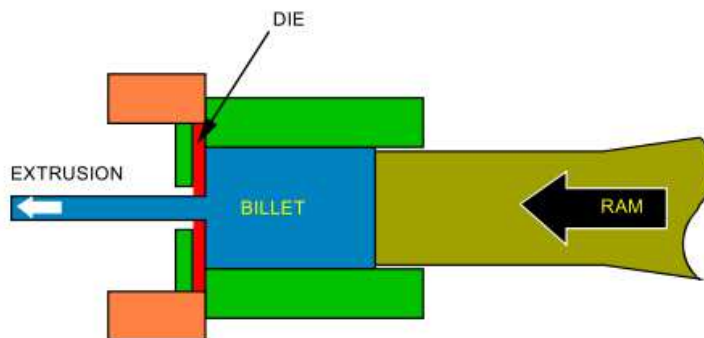


Figure 2.16: Direct extrusion [1].



When the heated billet is located in the heated container, the actual temperatures of both are around 450 °C – 500 °C. At these temperatures the flow stress of the aluminium alloys is very low and by applying pressure by means of a ram to the end of the billet, the metal flows through the steel die, located at the other end of the container to produce a section, the cross sectional shape of which is defined by the shape of the die. The maximum length of the section depends on the volume of the billet (cross-section x length) and on the extrusion ratio, i.e. the ratio of cross-section of the billet to the cross-section of the extrusion. When it is necessary to obtain very long length of section, as for instance in electrical conductors, it is possible to introduce successive billets into the container and produce a continuous product. The interaction between alloy composition, conditions of billet and container, extrusion ratio and extrusion speed affects metal flow and the resulting properties and structure of the section and its surface finish. The temperature at which the section leaves the die must not be so high as to cause cracking of the product surface. Since for economic reasons it is desirable to extrude as fast as possible, thus obtaining maximum output from the press, much attention has been paid to design of the bearings and to various die cooling techniques. The metal flow through the die must be controlled by die bearing design and section orientation with respect to the die axis so that uniform speed by all parts of the section is achieved; otherwise the section will deflect on emerging and suffer shape distortion. When the sections of heat treated alloys leave the die they can, depending on the alloy and section thickness, be quenched either in water or by air cooling, thus rendering a "solution heat treatment", or be taken from the press for formal solution heat treatment in a furnace. After either of these operations the sections receive a stretch of between 1 and 2% to remove residual stress followed by artificial ageing to stabilize their properties. The temper designations for extrusion products are shown in the previous paragraph; the most common are T4, T5 and T6. A typical extrusion plant layout is shown in Figure 2.17 [1].

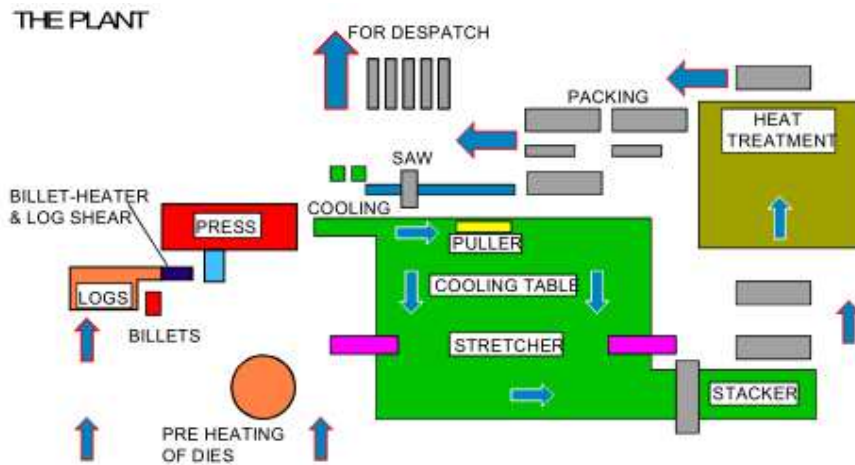


Figure 2.17: Typical extrusion plant layout [1].

The machine intended to operate the extrusion is the press, see Figure 2.18. Press load capacities range from a few hundred tonnes to as high as 20000 tonnes although the majority range between 1000 and 3000 tonnes. Billet sizes cover the range from 50 mm diameter to 500 mm with length usually about 2-4 times the diameter and while most presses have cylindrical containers a few have rectangular ones for the production of wide shallow sections.



Figure 2.18: 6050 tonnes extrusion press (picture Metra).

The overall dimensions of a section are related to the billet diameter (Figure 2.19), and the minimum section thickness relates to the location of the section within this "circumscribing circle", the complexity of the section and the alloy. The minimum thickness possible is about 0.5 mm. All aluminium alloys can be extruded but some are less suitable than others, requiring higher pressures, allowing only low extrusion speeds and having less than acceptable surface finish and section complexity. The term "extrudability" is used to embrace all of these issues. Pure aluminium has the greatest extrudability, while alloys with higher mechanical properties, as the aluminium-zinc-magnesium-copper alloys, have lower extrudability as shown in Figure 2.20 and 2.21.

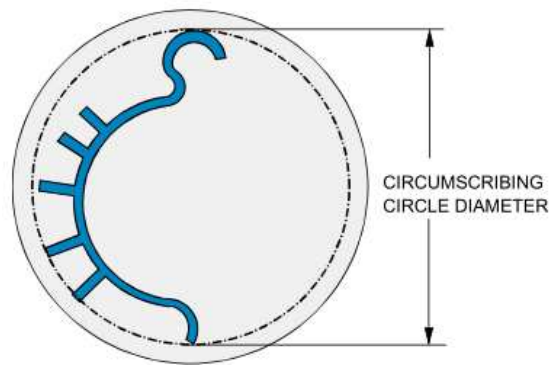


Figure 2.19: Cylindrical billet [1].

ALLOY	RATING	ALLOY	RATING
EC	150	6063	100
1060	150	6066	40
1100	150	6101	100
1150	150	6151	70
2011	15	6253	80
2014	20	6351	60
2024	15	6463	100
3003	100	6663	100
5052	80	7001	7
5083	20	7075	10
5086	25	7079	10
5154	50	7178	7
5254	50		
5454	50		
5456	20		
6061	60		

Figure 2.20: Relative extrudability of aluminium alloys [1].

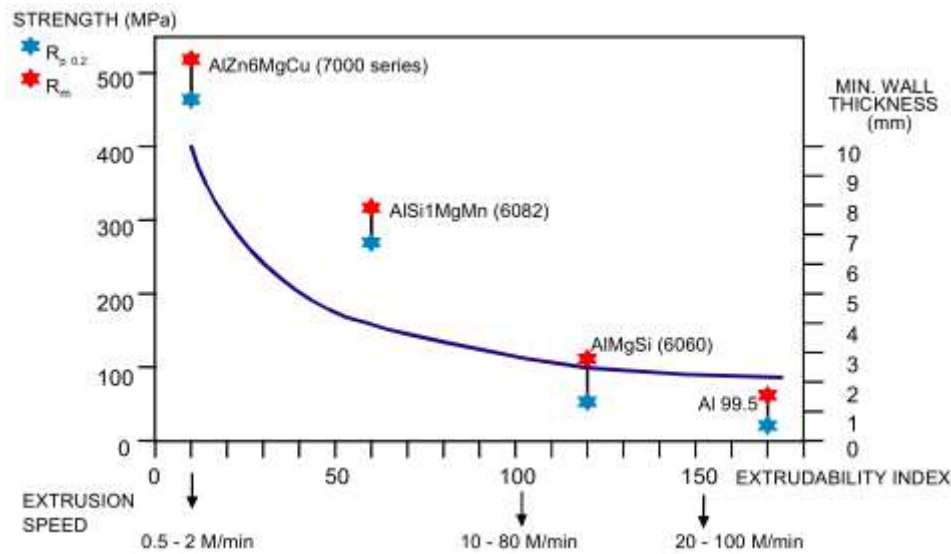


Figure 2.21: Relationship between mechanical strength and extrudability of some extrusion alloys [1].

Although large quantities of pure aluminium are extruded for production of electrical conductors, strong alloys in the 2000, 7000 and 8000 series used for spars and stringers in airframe construction and large sections in the 5000 series employed in marine structures, the biggest share of extrusion market is taken by the 6000, AlMgSi series. This group of alloys can be extruded with ease and their overall extrudability is good but those containing the lower limits of magnesium and silicon e.g. 6060 and 6063 extrude at very high speeds up to 100 m/min with good surface finish, anodising capability and maximum complexity of section shape combined with minimum section thickness.

In designing a section, a user is well advised to consult at an earlier stage with the suppliers for the manufacture of the dies and because some structural features of the product may require modification for better extrudability. The extrusion dies can be divided into the following categories:

- flat dies used for the extrusion of open profiles. Figure 2.22 shows the typical assembly of this type of die consisting of a die ring, which expands the equipment dimensions to allow it to be inserted

into the slide, a backer and a series of bolsters completing the support by filling the space available in the slide;

- porthole dies for hollow profiles. Figure 2.23a shows how it is possible to solve the problem of obtaining the hole in the simple case of circular section: a die reproduces the external contour of the profile, a mandrel the internal one. The metal split by extrusion die's bridges is joined together in welding chamber by means of solid state bonding, and then the joined metal flow through lower die's bearing to form a hollow cross-section profile (Figure 2.23b). In Figure 2.24, the typical assembly of a porthole die is represented [11].

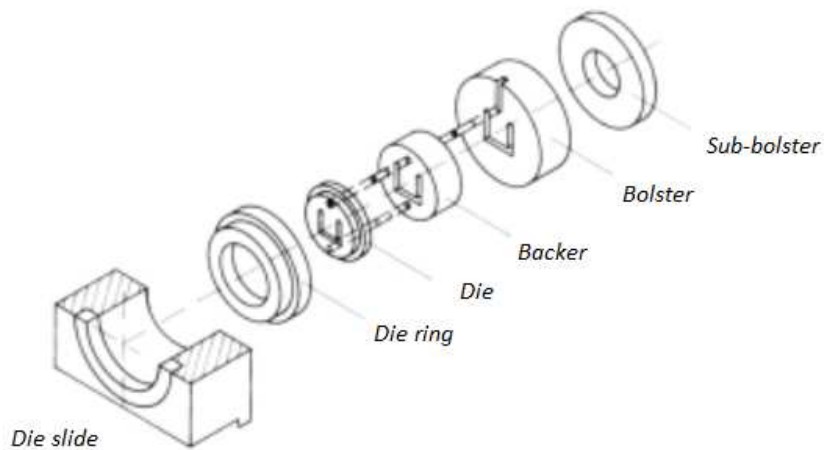


Figure 2.22: Typical assembly of flat die [11].

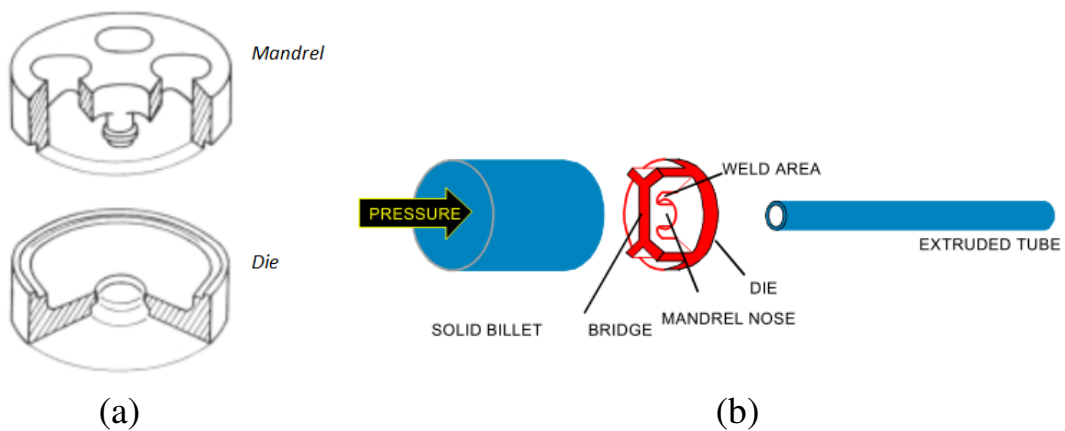


Figure 2.23: (a) Porthole die to realize a circular section tube [11]; (b) extrusion of hollow section [1].

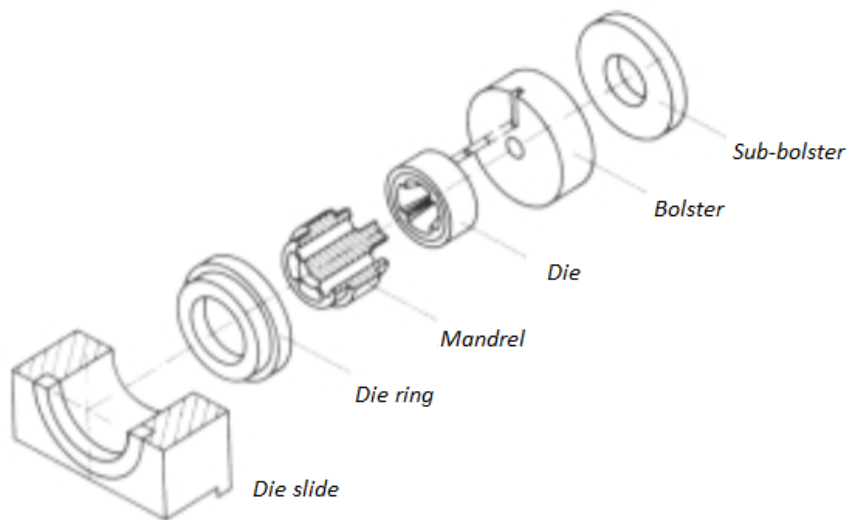


Figure 2.24: Typical assembly of porthole die [11].

In figure 2.25 examples of open flat section extrusions and hollow section extrusions are represented.

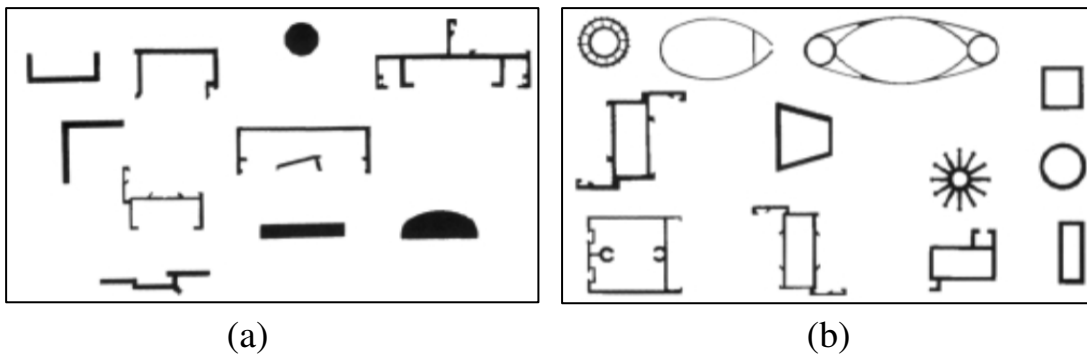
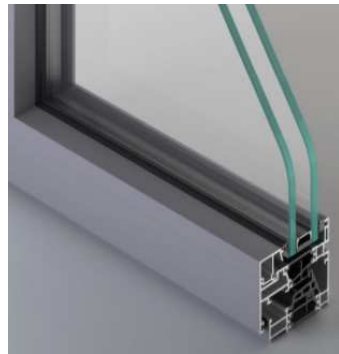
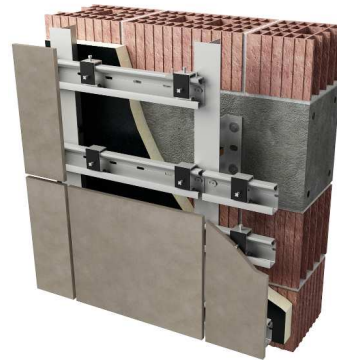


Figure 2.25: (a) Examples of open flat section extrusions; (b) examples of hollow section extrusions.

Below are shown some examples of aluminium extrusions (Figure 2.26).



(a)



(b)



(a)



(d)

Figure 2.26: Examples of aluminium extrusions. (a) Doors and windows (Metra); (b) ventilated facades (Aliva); (c) automotive (Metra); (d) naval transport (Metra).

## 2.5 DESIGN CRITERIA

Until 1950s there was a lack of codification and recommendations for the design of aluminium alloys structures. In 1971 Professor Mazzolani F.M. was appointed Chairman of the ECCS Committee on Aluminium structures and carried out extensive research in order to characterize the design of aluminium alloy structures in accordance with the current trend of safety principles already established for steel. This led to the publication of the European Recommendations for Aluminium Alloys Structures in 1978. Immediately after, during the 1980s, the main European codes, such as UK (BS8118), Italian (UNI 8634), Swedish (SVR), French (DTU), German (DIN 4113) and Austrian (ON) specifications, have been published or revised accordingly. In the USA,

the Aluminium Association Recommendations have been recently updated and the ultimate limit state design has been introduced beside the traditional allowable stress design. The 1990s saw the development of Eurocode 9 “Design of Aluminium Structures”, under the chairmanship of Mazzolani. [6] The EN version was published in 1999 and now it has been superseded by the 2007 publication.

As shown in previous paragraphs, most of the structural aluminium alloys have relatively high strength compared to the modulus of elasticity. The low elastic modulus gives rise to deformability and instability issues and for this reason, when designing an aluminium alloy structure, it will often be the deflection criteria which is governing. The objective of this paragraph is to give a background to the design methods and recommendations in Eurocode 9: Design of aluminium structures - Part 1-1: general structural rules [12].

### 2.5.1 Design resistance and material properties

The material constants to be adopted in calculations for aluminium alloys are listed in Table 2.2.

Table 2.2: Design value of material constants [12].

Modulus of elasticity	$E = 70\,000\text{ MPa}$
Shear modulus	$G = 27\,000\text{ MPa}$
Poisson’s ratio	$\nu = 0,3$
Coefficient of linear thermal expansion	$\alpha = 23 \times 10^6\text{ per }^\circ\text{C}$
Density	$\rho = 2\,700\text{ kg/m}^3$

The design value of strength at the ultimate limit state may be defined as follows:

$$R_d = \frac{1}{\gamma_M} R_k \quad (2.3)$$

where:



$R_k$  is the characteristic value of resistance of a cross section or member determined with characteristic or nominal values for the material properties and cross-sectional dimensions.

$\gamma_M$  is the global partial factors for the particular resistance, see Table 2.3.

Table 2.3: Partial safety factors for ultimate limit states

Resistance of cross-sections whatever the class is	$\gamma_{M1} = 1,10$
Resistance of members to instability assessed by member check	
Resistance of cross-sections in tension to fracture	$\gamma_{M2} = 1,25$

Characteristic values of 0,2% proof strength  $f_0$  and ultimate tensile strength  $f_u$  for wrought aluminium alloys are reported in Table 3.2a of Eurocode 9 for sheet, strip and plate (see Figure 2.27) and Table 3.2b for extruded profiles, extruded tube, extruded rod/bar and drawn tube (see Figure 2.28). Table 3.2a and table 3.2b also show the minimum elongation  $A$ , the reduction factors  $\rho_{o,haz}$  and  $\rho_{u,haz}$  in heat affected zones HAZ, the buckling class and the exponent  $n_p$  of the Ramberg-Osgood law. In the design of welded structures using strain hardened or heat treatable alloys the reduction in strength properties that occurs in the vicinity of welds shall be allowed for. For design purposes it is assumed that throughout the heat affected zone (HAZ) the strength properties are reduced on a constant level. The reduction factors  $\rho_{o,haz}$  and  $\rho_{u,haz}$  are determined by the following relationships:

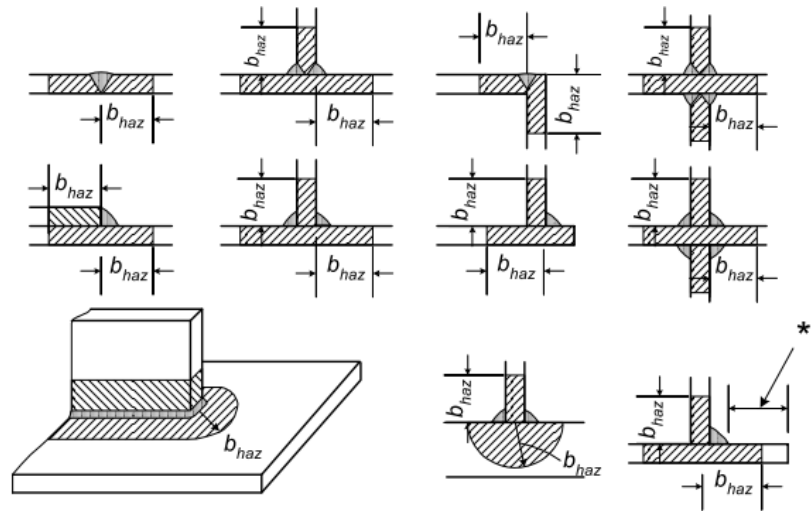
$$\rho_{o,haz} = \frac{f_{o,haz}}{f_0} \quad (2.4)$$

$$\rho_{u,haz} = \frac{f_{u,haz}}{f_0} \quad (2.5)$$

The HAZ is assumed to extend a distance  $b_{haz}$  in any direction from a weld, measured as follows (see Figure 2.29):

- a) transversely from the centre line of an in-line butt weld;
- b) transversely from the point of intersection of the welded surfaces at fillet welds;

- c) transversely from the point of intersection of the welded surfaces at butt welds used in corner, tee or cruciform joints;
- d) in any radial direction from the end of a weld.



\*) If this distance is less than  $3b_{haz}$  assume that the HAZ extends to the full width of outstand, see 6.1.6.3(7)

Figure 2.27: The extend of heat affected zones (HAZ) [12].

For a MIG weld laid on unheated material, and with interpass cooling to  $60^{\circ}\text{C}$  or less when multi-pass welds are laid, values of  $b_{haz}$  are as follows:

- $0 < t \leq 6 \text{ mm}$ :  $b_{haz} = 20 \text{ mm}$
- $6 < t \leq 12 \text{ mm}$ :  $b_{haz} = 30 \text{ mm}$
- $12 < t \leq 25 \text{ mm}$ :  $b_{haz} = 35 \text{ mm}$
- $t > 25 \text{ mm}$ :  $b_{haz} = 40 \text{ mm}$

For a TIG weld the extent of the HAZ is greater because the heat input is greater than for a MIG weld. TIG welds for in-line butt or fillet welds in 6000, 7000 or work-hardened 5000 series alloys, have a value of  $b_{haz}$  given by:

- $0 < t \leq 6 \text{ mm}$ :  $b_{haz} = 30 \text{ mm}$

Alloy EN- AW	Temper <sup>1)</sup>	Thick- ness mm <sup>1)</sup>	$f_0$ <sup>1)</sup>	$f_u$	$A_{50}$ <sup>1) 6)</sup>	$f_{0,haz}$ <sup>2)</sup>	$f_{u,haz}$ <sup>2)</sup>	HAZ-factor <sup>2)</sup>		BC 4)	$n_p$ 1), 5)														
			N/mm <sup>2</sup>		%	N/mm <sup>2</sup>		$\rho_{0,haz}$ <sup>1)</sup>	$\rho_{u,haz}$																
3004	H14   H24/H34	≤ 6   3	180   170	220	1   3	75	155	0,42   0,44	0,70	B	23   18														
	H16   H26/H36	≤ 4   3	200   190	240	1   3			0,38   0,39	0,65	B	25   20														
3005	H14   H24	≤ 6   3	150   130	170	1   4	56	115	0,37   0,43	0,68	B	38   18														
	H16   H26	≤ 4   3	175   160	195	1   3			0,32   0,35	0,59	B	43   24														
3103	H14   H24	≤ 25   12,5	120   110	140	2   4	44	90	0,37   0,40	0,64	B	31   20														
	H16   H26	≤ 4	145   135	160	1   2			0,30   0,33	0,56	B	48   28														
5005/ 5005A	O/H111	≤ 50	35	100	15	35	100	1	1	B	5														
	H12   H22/H32	≤ 12,5	95   80	125	2   4	44	100	0,46   0,55	0,80	B	18   11														
	H14   H24/H34	≤ 12,5	120   110	145	2   3			0,37   0,40	0,69	B	25   17														
5052	H12   H22/H32	≤ 40	160   130	210	4   5	80	170	0,50   0,62	0,81	B	17   10														
	H14   H24/H34	≤ 25	180   150	230	3   4			0,44   0,53	0,74	B	19   11														
5049	O / H111	≤ 100	80	190	12	80	190	1	1	B	6														
	H14   H24/H34	≤ 25	190   160	240	3   6	100	190	0,53   0,63	0,79	B	20   12														
5454	O/H111	≤ 80	85	215	12	85	215	1	1	B	5														
	H14   H24/H34	≤ 25	220   200	270	2   4	105	215	0,48   0,53	0,80	B	22   15														
5754	O/H111	≤ 100	80	190	12	80	190	1	1	B	6														
	H14   H24/H34	≤ 25	190   160	240	3   6	100	190	0,53   0,63	0,79	B	20   12														
5083	O/H111	≤ 50	125	275	11	125	275	1	1	B	6														
		50 < t ≤ 80	115	270	14 <sup>3)</sup>	115	270			B															
	H12   H22/H32	≤ 40	250   215	305	3   5	155	275	0,62   0,72	0,90	B	22   14														
H14   H24/H34	≤ 25	280   250	340	2   4	0,55   0,62			0,81	A	22   14															
6061	T4 / T451	≤ 12,5	110	205	12	95	150	0,86	0,73	B	8														
	T6 / T651	≤ 12,5	240	290	6	115	175	0,48	0,60	A	23														
	T651	12,5 < t ≤ 80	240	290	6 <sup>3)</sup>																				
6082	T4 / T451	≤ 12,5	110	205	12	100	160	0,91	0,78	B	8														
	T61/T6151	≤ 12,5	205	280	10							125	185	0,61	0,66	A	15								
	T6151	12,5 < t ≤ 100	200	275	12 <sup>3)</sup>													0,63	0,67	A	14				
	T6/T651	≤ 6	260	310	6																	0,48	0,60	A	25
		6 < t ≤ 12,5	255	300	9																				
T651	12,5 < t ≤ 100	240	295	7 <sup>3)</sup>	0,52	0,63	A	21																	
7020	T6	≤ 12,5	280	350	7	205	280	0,73	0,80	A	19														
	T651	≤ 40			9 <sup>3)</sup>																				
8011A	H14   H24	≤ 12,5	110   100	125	2   3	37	85	0,34   0,37	0,68	B	37   22														
	H16   H26	≤ 4	130   120	145	1   2			0,28   0,31	0,59		33   33														

1) If two (three) tempers are specified in one line, tempers separated by “|” have different technological values but separated by “/” have same values. (The tempers show differences for  $f_0$ ,  $A$  and  $n_p$ ).

2) The HAZ-values are valid for MIG welding and thickness up to 15mm. For TIG welding strain hardening alloys (3xxx, 5xxx and 8011A) up to 6 mm the same values apply, but for TIG welding precipitation hardening alloys (6xxx and 7xxx) and thickness up to 6 mm the HAZ values have to be multiplied by a factor 0,8 and so the  $\rho$ -factors. For higher thickness – unless other data are available – the HAZ values and  $\rho$ -factors have to be further reduced by a factor 0,8 for the precipitation hardening alloys (6xxx and 7xxx) and by a factor 0,9 for the strain hardening alloys (3xxx, 5xxx and 8011A). These reductions do not apply in temper O.

3) Based on  $A$  ( $= A_{5,65} \sqrt{A_0}$ ), not  $A_{50}$ .

4) BC = buckling class, see 6.1.4.4, 6.1.5 and 6.3.1.

5)  $n$ -value in Ramberg-Osgood expression for plastic analysis. It applies only in connection with the listed  $f_0$ -value.

6) The minimum elongation values indicated do not apply across the whole range of thickness given, but mostly to the thinner materials. In detail see EN 485-2.

Figure 2.28: Characteristic values of 0,2% proof strength  $f_0$ , ultimate tensile strength  $f_u$ , min. elongation  $A$ , reduction factors  $\rho_{0,haz}$  and  $\rho_{u,haz}$  in HAZ, buckling class and exponent  $n_p$  for wrought aluminium alloys – Sheet, strip and plate.

Alloy EN-AW	Product form	Temper	Thick-ness $t$ mm 1) 3)	$f_o$ 1)	$f_u$ 1)	$A$ 5) 2)	$f_{o,haz}$ 4)	$f_{u,haz}$ 4)	HAZ-factor 4)		BC 6)	$n_p$ 7)
				N/mm <sup>2</sup>	%	N/mm <sup>2</sup>		$\rho_{o,haz}$	$\rho_{u,haz}$			
5083	ET, EP, ER/B	O / H111, F, H112	$t \leq 200$	110	270	12	110	270	1	1	B	5
	DT	H12/22/32	$t \leq 10$	200	280	6	135	270	0,68	0,96	B	14
		H14/24/34	$t \leq 5$	235	300	4			0,57	0,90	A	18
6060	EP, ET, ER/B	T5	$t \leq 5$	120	160	8	50	80	0,42	0,50	B	17
	EP		$5 < t \leq 25$	100	140	8			0,50	0,57	B	14
	ET, EP, ER/B	T6	$t \leq 15$	140	170	8	60	100	0,43	0,59	A	24
	DT		$t \leq 20$	160	215	12			0,38	0,47	A	16
	EP, ET, ER/B	T64	$t \leq 15$	120	180	12	60	100	0,50	0,56	A	12
	EP, ET, ER/B	T66	$t \leq 3$	160	215	8	65	110	0,41	0,51	A	16
	EP		$3 < t \leq 25$	150	195	8			0,43	0,56	A	18
6061	EP, ET, ER/B, DT	T4	$t < 25$	110	180	50	95	150	0,86	0,83	B	8
	EP, ET, ER/B, DT	T6	$t \leq 20$	240	260	8	115	175	0,48	0,67	A	55
6063	EP, ET, ER/B	T5	$t \leq 3$	130	175	8	60	100	0,46	0,57	B	16
	EP		$3 < t \leq 25$	110	160	7			0,55	0,63	B	13
	EP, ET, ER/B	T6	$t \leq 25$	160	195	8	65	110	0,41	0,56	A	24
	DT		$t \leq 20$	190	220	10			0,34	0,50	A	31
	EP, ET, ER/B	T66	$t \leq 10$	200	245	8	75	130	0,38	0,53	A	22
	EP		$10 < t \leq 25$	180	225	8			0,42	0,58	A	21
	DT		$t \leq 20$	195	230	10			0,38	0,57	A	28
6005A	EP/O, ER/B	T6	$t \leq 5$	225	270	8	115	165	0,51	0,61	A	25
			$5 < t \leq 10$	215	260	8			0,53	0,63	A	24
			$10 < t \leq 25$	200	250	8			0,58	0,66	A	20
	EP/H, ET	T6	$t \leq 5$	215	255	8	115	165	0,53	0,65	A	26
	$5 < t \leq 10$		200	250	8	0,58			0,66	A	20	
6106	EP	T6	$t \leq 10$	200	250	8	95	160	0,48	0,64	A	20
6082	EP, ET, ER/B	T4	$t \leq 25$	110	205	14	100	160	0,91	0,78	B	8
	EP/O, EP/H	T5	$t \leq 5$	230	270	8	125	185	0,54	0,69	B	28
	EP/O, EP/H	T6	$t \leq 5$	250	290	8	125	185	0,50	0,64	A	32
			$5 < t \leq 15$	260	310	10			0,48	0,60	A	25
	ER/B	T6	$t \leq 20$	250	295	8			0,50	0,63	A	27
			$20 < t \leq 150$	260	310	8			0,48	0,60	A	25
	DT	T6	$t \leq 5$	255	310	8			0,49	0,60	A	22
$5 < t \leq 20$			240	310	10	0,52			0,60	A	17	
7020	EP, ET, ER/B	T6	$t \leq 15$	290	350	10			205	280	0,71	0,80
	EP, ET, ER/B	T6	$15 < t < 40$	275	350	10	0,75	0,80			A	19
	DT	T6	$t \leq 20$	280	350	10	0,73	0,80			A	18

Key: EP - Extruded profiles                      EP/O - Extruded open profiles  
EP/H - Extruded hollow profiles              ET - Extruded tube  
ER/B - Extruded rod and bar                    DT - Drawn tube

Figure 2.29: Characteristic values of 0,2% proof strength  $f_o$ , ultimate tensile strength  $f_u$ , min. elongation A, reduction factors  $\rho_{o,haz}$  and  $\rho_{u,haz}$  in HAZ, buckling class and exponent  $n_p$  for wrought aluminium alloys – Extruded profiles, extruded tube, extruded rod/bar and drawn tube [12].

## 2.5.2 Stress-strain relationship

Stress-strain relationships are given in Annex E of Eurocode 9. The analytical characterization of the  $\sigma - \varepsilon$  relationship of an aluminium alloy can be done by means of piecewise models or continuous models. Piecewise linear models are based on the assumption that material  $\sigma - \varepsilon$  law is described by means of a multi linear curve, each branch of it representing the elastic, inelastic and plastic region. Both bi-linear model and three-linear model can be used. Continuous models are based on the assumption that the  $\sigma - \varepsilon$  law is described by means of a continuous relationship representing the elastic, inelastic and plastic region.

### ***Bi-linear model***

If a bi-linear model with hardening is used (Figure 2.30 a), the following relationships may be assumed:

$$\sigma = E\varepsilon \quad \text{for } 0 < \varepsilon \leq \varepsilon_p \quad (2.6)$$

$$\sigma = f_p + E_1(\varepsilon - \varepsilon_p) \quad \text{for } \varepsilon_p < \varepsilon \leq \varepsilon_{max} \quad (2.7)$$

where:

$f_p$  is the conventional elastic limit of proportionality

$\varepsilon_p$  is the strain corresponding to the stress  $f_p$

$\varepsilon_{max}$  is the strain corresponding to the stress  $f_{max}$

$E$  is the elastic modulus

$E_1$  is the hardening modulus.

In case the “Elastic-Perfectly plastic” model is assumed (Figure 2.30 b), the material remains perfectly elastic until the elastic limit stress  $f_p$ . plastic deformation without hardening ( $E_1 = 0$ ) should be considered up to  $\varepsilon_{max}$ .

In the absence of more accurate evaluation of the above parameters, the following values may be assumed for both bi-linear and three-linear models:

$f_p =$  nominal value of  $f_o$

$f_{max} =$  nominal value of  $f_u$

$$\varepsilon_{max} = 0,5\varepsilon_u$$

$\varepsilon_u$  = nominal value of ultimate strain

$$\varepsilon_p = f_o/E$$

$$E_1 = (f_u - f_o)/(0,5 \varepsilon_u - \varepsilon_p)$$

According to experimental data, the values of  $\varepsilon_u$  for several alloys could be calculated using an analytical expression obtained by means of interpolation of available results. This expression, which provides an upper bound limit for the elongation at rupture, can be synthesized by the following expressions:

$$\varepsilon_u = 0,30 - 0,22 \frac{f_o(N/mm^2)}{400} \quad \text{if } f_o < 400 \text{ N/mm}^2 \quad (2.8)$$

$$\varepsilon_u = 0,08 \quad \text{if } f_o \geq 400 \text{ N/mm}^2 \quad (2.9)$$

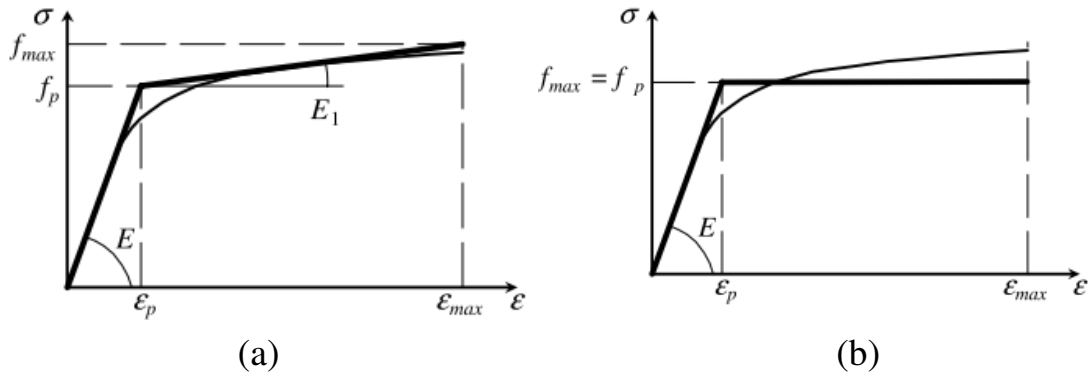


Figure 2.30: (a) Bi-linear model with hardening; (b) Elastic-perfectly plastic model [12].

### **Three-linear model**

If three-linear model with hardening is used (Figure 2.31a), the following relationships may be assumed:

$$\sigma = E\varepsilon \quad \text{for } 0 < \varepsilon \leq \varepsilon_p \quad (2.10)$$

$$\sigma = f_p + E_1(\varepsilon - \varepsilon_p) \quad \text{for } \varepsilon_p < \varepsilon \leq \varepsilon_e \quad (2.11)$$

$$\sigma = f_e + E_2(\varepsilon - \varepsilon_e) \quad \text{for } \varepsilon_e < \varepsilon \leq \varepsilon_{max} \quad (2.12)$$

where:

$f_p$  is the limit of proportionality ( $= R_{p0,001}$ )

$f_e$  is the limit of elasticity ( $= R_{p0,02}$ )

$\varepsilon_p$  is the strain corresponding to the stress  $f_p$

$\varepsilon_e$  is the strain corresponding to the stress  $f_e$

$\varepsilon_{max}$  is the strain corresponding to the stress  $f_{max}$

$E$  is the elastic modulus

$E_1$  is the first hardening modulus

$E_2$  is the second hardening modulus.

In case of “Perfectly plastic” model is assumed (Figure 2.31b), plastic deformations without hardening ( $E_2 = 0$ ) should be considered for strain ranges from  $\varepsilon_e$  to  $\varepsilon_{max}$ .

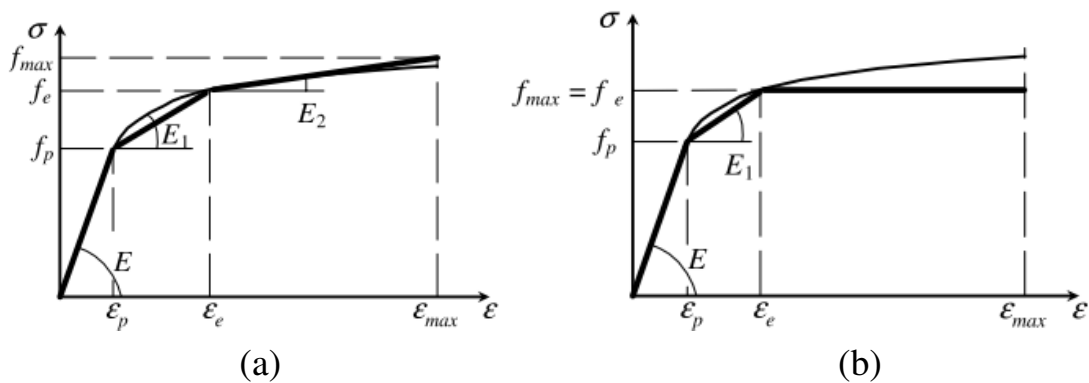


Figure 2.31: (a) Three-linear model with hardening; (b) Perfectly plastic model [12].

### Continuous model in the form $\varepsilon = \varepsilon(\sigma)$

The Ramberg-Osgood model may be applied to describe the stress versus strain relationship in the form  $\varepsilon = \varepsilon(\sigma)$  described by Equation 2.1. The exponent  $n$  of the law depends on the choice of the second reference point, based on the strain range corresponding to the phenomenon under investigation. The following limit cases may be considered:

- if the analysis concerns the range of elastic deformations, the proof stress evaluated by means of 0,1% offset method may be assumed as the second reference point (see Figure 2.32a), giving the Equation 2.2;

b) if the analysis concerns the range of plastic deformations, the tensile stress at the top point of the  $\sigma - \varepsilon$  curve may be assumed as the second reference point (see Figure 2.32b), giving:

$$n = \frac{\ln(0,002/\varepsilon_{0,max})}{\ln(f_0/f_{max})} \quad (2.13)$$

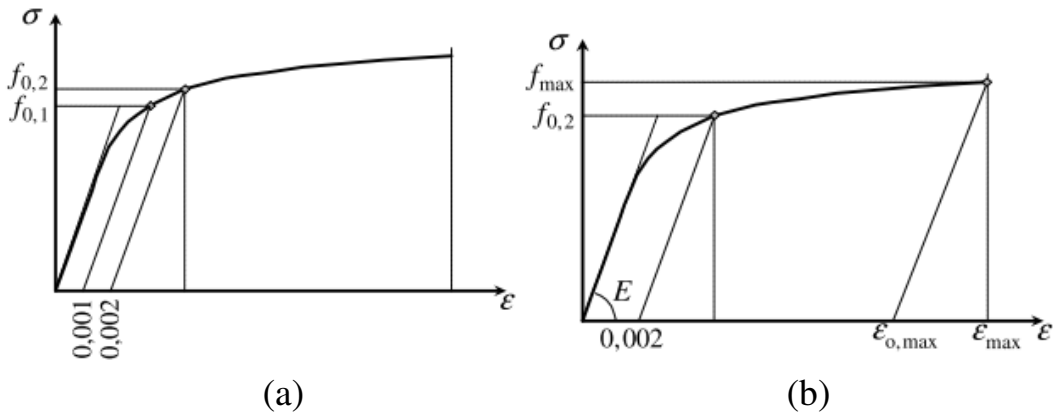


Figure 2.32: Continuous models in the form  $\varepsilon = \varepsilon(\sigma)$  [12].

Based on extensive tests, the following values may be assumed:

a) elastic range:

$$n = \frac{\ln(0,000001/0,002)}{\ln(f_p/f_0)} \quad (2.14)$$

where the proportional limit  $f_p$  only depends on the value of the  $f_0$  yield stress:

$$f_p = f_{0,2} - 2\sqrt{10f_{0,2}(N/mm^2)} \quad \text{if } f_{0,2} > 160 \text{ N/mm}^2 \quad (2.15)$$

$$f_p = f_{0,2}/2 \quad \text{if } f_{0,2} \leq 160 \text{ N/mm}^2 \quad (2.16)$$

b) plastic range:

$$n = n_p = \frac{\ln(0,002/\varepsilon_u)}{\ln(f_0/f_u)} \quad (2.17)$$



### 2.5.3 Classification of cross-sections

A four-class classification criteria has been proposed in Eurocode 9. In particular, referring to a generalized force  $F$  versus displacement  $D$  relationship, cross-sections can be divided as follows (see Figure 2.33):

- Class 1: ductile sections that develop the collapse resistance without having local instability in the section. The full exploitation of the hardening properties of material is allowed until the ultimate value of deformation, depending on the type of alloy, is reached.
- Class 2: compact sections that are capable of developing the plastic limit resistance. The full exploitation of the hardening properties of material is prevented by the onset of plastic instability phenomena.
- Class 3: semi-compact sections able to develop the elastic limit resistance only without getting into inelastic range owing to instability phenomena. Only small plastic deformations occur within the section, whose behaviour remains substantially brittle.
- Class 4: slender sections characterized by the occurring of local buckling phenomena in the elastic range. No plastic deformations are allowed within the section, whose behaviour is remarkably brittle.

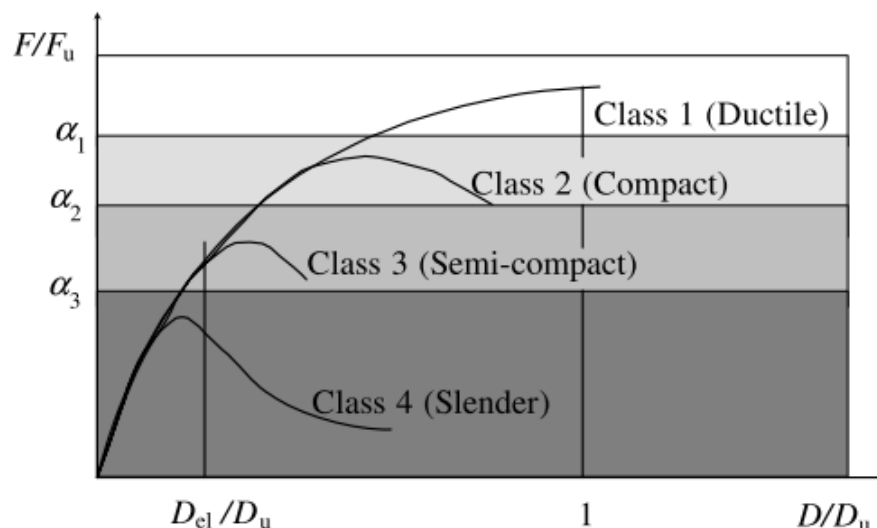


Figure 2.33: Classification of cross-sections [12].

The classification of a cross-section depends on the width to thickness ratio of the parts subject to compression. The various compression parts in a cross-section (such as web or flange) can be in different classes. A cross-section is classified according to the highest class of its compression parts. The following basic types of thin-walled part are identified in the classification process:

- a) flat outstand parts;
- b) flat internal parts;
- c) curved internal parts.

These parts can be un-reinforced or reinforced by longitudinal stiffening ribs or edge lips or bulbs (see Figure 2.34).

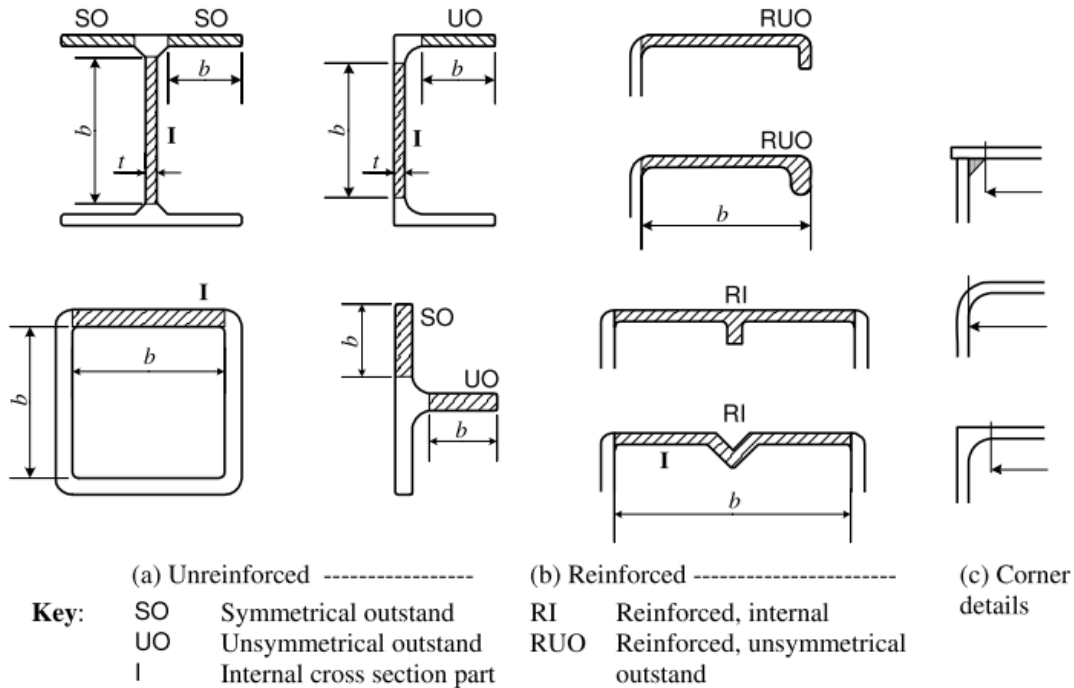


Figure 2.34: Types of cross-section parts [12].

The susceptibility of an un-reinforced flat part to local buckling is defined by the parameter  $\beta$ , which has the following values:

- a) flat internal parts with no stress gradient or flat outstands with no stress gradient or peak compression at toe:  $\beta = b/t$  (2.18)

b) internal parts with a stress gradient that results in a neutral axis at the center:  

$$\beta = 0,40 b/t \quad (2.19)$$

c) internal parts with stress gradient and outstands with peak compression at root:  

$$\beta = \eta b/t \quad (2.20)$$

where:

$b$  is the width of a cross-section part;

$t$  is the thickness of a cross-section;

$\eta$  is the stress gradient factor given by the expressions:

$$\eta = 0,70 + 0,30\psi \quad (1 \geq \psi \geq -1)$$

$$\eta = 0,80 / (1 - \psi) \quad (\psi < -1), \text{ see Figure 2.35}$$

where

$\psi$  is the ratio of the stresses at the edges of the plate under consideration related to the maximum compressive stress. In general the neutral axis should be the elastic neutral axis, but in checking whether a section is class 1 or 2 it is permissible to use the plastic neutral axis.

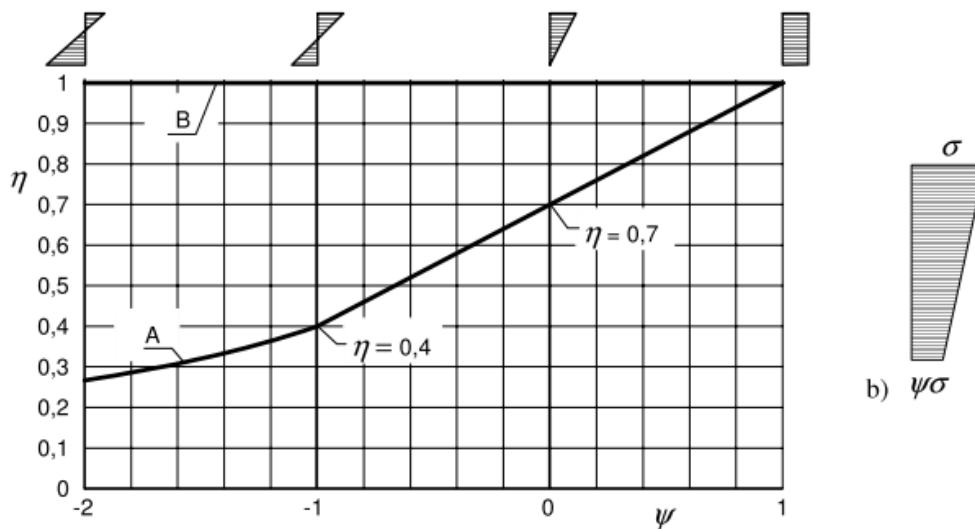


Figure 2.35: Flat internal parts under stress gradient, values of  $\eta$ . For internal parts or outstands (peak compression at root) use curve A. For outstands (peak compression at toe) use line B [12].

When considering the susceptibility of a reinforced flat part to local buckling, three possible buckling modes should be considered, as shown in Figure 2.36:

- a) Mode 1: the reinforced part buckles as a unit, so that the reinforcement buckles with the same curvature as the part. This mode is often referred to as distortional buckling.
- b) Mode 2: the sub-parts and the reinforcement buckle as individual parts with the junction between them remaining straight.
- c) Mode 3: this is a combination of modes 1 and 2 in which sub-part buckles are superimposed on the buckles of the whole part.

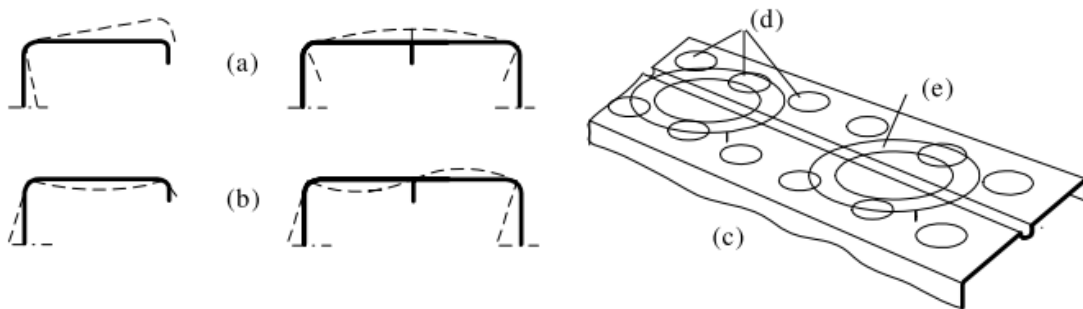


Figure 2.36: Buckling modes for flat reinforced parts. (a) Mode 1; (b) mode 2; (c) mode 3; (d) sub-part buckles; (e) whole reinforced part buckles [12].

For the mode 1, uniform compression and standard reinforcement the parameter  $\beta$  is given by:

$$\beta = \eta b/t \quad (2.21)$$

where  $\eta$  is read from Figure 2.37. In this figure the depth  $c$  of the rib or lip is measured to the inner surface of the plate.

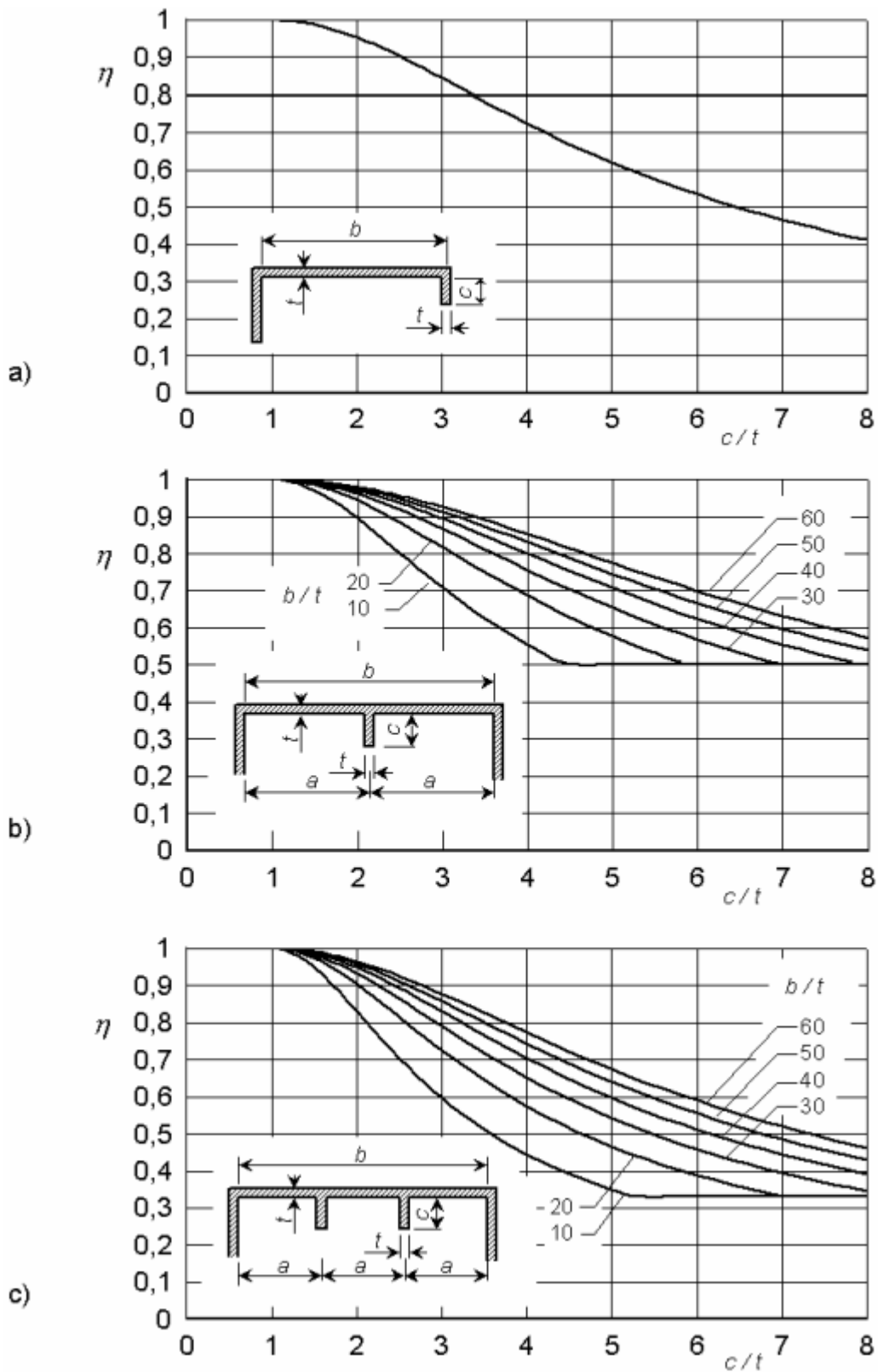


Figure 2.37: Values of  $\eta$  for reinforced cross section parts [12].

The classification of parts of cross-sections is linked to the values of the slenderness parameter  $\beta$  as follows:

Parts in beams	Parts in struts
$\beta \leq \beta_1$ : class 1	$\beta \leq \beta_2$ : class 1 or 2
$\beta_1 < \beta \leq \beta_2$ : class 2	$\beta_2 < \beta \leq \beta_3$ : class 3
$\beta_2 < \beta \leq \beta_3$ : class 3	$\beta_3 < \beta$ : class 4
$\beta_3 < \beta$ : class 4	

Values of  $\beta_1$ ,  $\beta_2$  and  $\beta_3$  are given in Table 2.4.

Table 2.4: Slenderness parameters  $\beta_1 / \varepsilon$ ,  $\beta_2 / \varepsilon$  and  $\beta_3 / \varepsilon$  [12].

Material classification	Internal part			Outstand part		
	$\beta_1 / \varepsilon$	$\beta_2 / \varepsilon$	$\beta_3 / \varepsilon$	$\beta_1 / \varepsilon$	$\beta_2 / \varepsilon$	$\beta_3 / \varepsilon$
Class A, without welds	11	16	22	3	4,5	6
Class A, with welds	9	13	18	2,5	4	5
Class B, without welds	13	16,5	18	3,5	4,5	5
Class B, with welds	10	13,5	15	3	3,5	4
$\varepsilon = \sqrt{250/f_0}$ , $f_0$ in N/mm <sup>2</sup>						

Local buckling in class 4 members is generally allowed for by replacing the true section by an effective section. The effective section is obtained by employing a local buckling factor  $\rho_c$  to factor down the thickness.  $\rho_c$  is applied to any uniform thickness class 4 part that is wholly or partly in compression. The factor  $\rho_c$  is given by expressions (2.22) and (2.23), separately for different parts of the section, in terms of the ratio  $\beta / \varepsilon$ .

$$\rho_c = 1,0 \quad \text{if } \beta \leq \beta_3 \quad (2.22)$$

$$\rho_c = \frac{C_1}{(\beta/\varepsilon)} - \frac{C_2}{(\beta/\varepsilon)^2} \quad \text{if } \beta > \beta_3 \quad (2.23)$$

The constant  $C_1$  and  $C_2$  are defined in Table 2.5.

Table 2.5: Constants  $C_1$  and  $C_2$  in expressions for  $\rho_c$  [11].

Material classification	Internal part		Outstand part	
	$C_1$	$C_2$	$C_1$	$C_2$
Class A, without welds	32	220	10	24
Class A, with welds	29	198	9	20
Class B, without welds	29	198	9	20
Class B, with welds	25	150	8	16

## 2.5.4 Resistance of cross-sections

### Tension

The design value of the tensile force  $N_{Ed}$  shall satisfy:

$$\frac{N_{Ed}}{N_{t,Rd}} \leq 1,0 \quad (2.24)$$

The design tension resistance of the cross-section  $N_{t,Rd}$  should be taken as the lesser of  $N_{o,Rd}$  and  $N_{u,Rd}$  where:

a) general yielding along the member:  $N_{o,Rd} = A_g f_o / \gamma_{M1} \quad (2.25)$

b) local failure at a section with holes:  $N_{u,Rd} = 0,9 A_{net} f_u / \gamma_{M2} \quad (2.26)$

c) local failure at a section with HAZ:  $N_{u,Rd} = A_{eff} f_u / \gamma_{M2} \quad (2.27)$

where:

$A_g$  is either the gross section or a reduced cross-section to allow for HAZ softening due to longitudinal welds. In the latter case  $A_g$  is found by taking a reduced area equal to  $\rho_{o,haz}$  times the area of HAZ;

$A_{net}$  is the net section area, with deduction for holes and a deduction if required to allow for the effect of HAZ softening in the net section through the hole. The latter deduction is based on the reduced thickness of  $\rho_{u,haz} t$ ;

$A_{eff}$  is the effective area based on the reduced thickness of  $\rho_{u,haz} t$ .

## Compression

The design value of the axial compression force  $N_{Ed}$  shall satisfy:

$$\frac{N_{Ed}}{N_{c,Rd}} \leq 1,0 \quad (2.28)$$

The design resistance for uniform compression  $N_{c,Rd}$  should be taken as the lesser of  $N_{u,Rd}$  and  $N_{c,Rd}$  where:

a) in sections with unfilled holes:  $N_{u,Rd} = A_{net} f_u / \gamma_{M2}$  (2.29)

b) other sections:  $N_{c,Rd} = A_{eff} f_0 / \gamma_{M1}$  (2.30)

in which:

$A_{net}$  is the net section area, with deductions for unfilled holes and HAZ softening if necessary. For holes located in reduced thickness regions the deduction may be based on the reduced thickness, instead of the full thickness;

$A_{eff}$  is the effective section area based on reduced thickness allowing for local buckling and HAZ softening but ignoring unfilled holes.

## Bending moment

The design value of the bending moment  $M_{Ed}$  shall satisfy:

$$\frac{M_{Ed}}{M_{Rd}} \leq 1,0 \quad (2.31)$$

The design resistance for bending about one principal axis of a cross section  $M_{Rd}$  is determined as the lesser of  $M_{u,Rd}$  and  $M_{c,Rd}$  where:

$$M_{u,Rd} = W_{net} f_u / \gamma_{M2} \quad \text{in a net section} \quad (2.32)$$

$$M_{c,Rd} = \alpha W_{el} f_0 / \gamma_{M1} \quad \text{at each cross-section} \quad (2.33)$$

where:



$\alpha$  is the shape factor, see Table 2.6;

$W_{el}$  is the elastic modulus of the gross section;

$W_{net}$  is the elastic modulus of the net section allowing for holes and HAZ softening, if welded. The latter deduction is based on the reduced thickness of  $\rho_{u,haz}t$ .

Table 2.6: Values of shape factor  $\alpha$  [12].

Cross-section class	Without welds	With longitudinal welds
1	$W_{pl} / W_{el}$	$W_{pl,haz} / W_{el}$
2	$W_{pl} / W_{el}$	$W_{pl,haz} / W_{el}$
3	$\alpha_{3,u}$	$\alpha_{3,w}$
4	$W_{eff} / W_{el}$	$W_{eff,haz} / W_{el}$

In table 2.6 the various section moduli  $W$  and  $\alpha_{3,u}$ ,  $\alpha_{3,w}$  are defined as:

$W_{pl}$  plastic modulus of the gross section;

$W_{eff}$  effective elastic section modulus, obtained using a reduced thickness  $t_{eff}$  for the class 4 parts;

$W_{el,haz}$  effective elastic modulus of the gross section, obtained using a reduced thickness  $\rho_{o,haz}t$  for the HAZ material;

$W_{pl,haz}$  effective plastic modulus of the gross section, obtained using a reduced thickness  $\rho_{o,haz}t$  for the HAZ material;

$W_{eff,haz}$  effective elastic section modulus, obtained using a reduced thickness  $\rho_c t$  for the class 4 parts or a reduced thickness  $\rho_{o,haz}t$  for the HAZ material, whichever is the smaller;

$\alpha_{3,u} = 1$  or may alternatively be taken as:

$$\alpha_{3,u} = \left[ 1 + \left( \frac{\beta_3 - \beta}{\beta_3 - \beta_2} \right) \left( \frac{W_{pl}}{W_{el}} - 1 \right) \right] \quad (2.34)$$

$\alpha_{3,w} = W_{el,haz} / W_{el}$  or may alternatively be taken as:

$$\alpha_{3,w} = \left[ \frac{W_{el,haz}}{W_{el}} + \left( \frac{\beta_3 - \beta}{\beta_3 - \beta_2} \right) \left( \frac{W_{pl,haz} - W_{el,haz}}{W_{el}} \right) \right] \quad (2.35)$$

## Shear

The design value of the shear force  $V_{Ed}$  shall satisfy:

$$\frac{V_{Ed}}{V_{Rd}} \leq 1,0 \quad (2.36)$$

where:

$V_{Rd}$  is the design shear resistance of the cross-section.

For non-slender sections,  $h_w / t_w < 39\varepsilon$ :

$$V_{Rd} = A_v \frac{f_0}{\sqrt{3} \gamma_{M1}} \quad (2.37)$$

where  $A_v$  is the shear area, taken as:

a) for sections containing shear webs

$$A_v = \sum_{i=1}^n [(h_w - \sum d)(t_w)_i - (1 - \rho_{o,haz})b_{haz}(t_w)_i] \quad (2.38)$$

where:

$h_w$  is the depth of the web between flanges;

$b_{haz}$  is the total depth of HAZ material occurring between the clear depth of the web between flanges. For sections with no welds,  $\rho_{o,haz} = 1$ .

If the HAZ extends the entire depth of the web panel  $b_{haz} = h_w - \sum d$ ;

$t_w$  is the web thickness;

$d$  is the diameter of holes along the shear plane;

$n$  is the number of webs.

b) for a solid bar and a round tube

$$A_v = \eta_v A_e \quad (2.39)$$

where:

$\eta_v = 0,8$  for a solid bar;

$\eta_v = 0,6$  for a round tube;

$A_e$  is the full section area of an unwelded section, and the effective section area obtained by taking a reduced thickness  $\rho_{o,haz}t$  for the HAZ material of a welded section.

## Torsion

For members subjected to torsion for which distortional deformations and warping torsion may be disregarded the design value of the torsional moment  $T_{Ed}$  at each cross-section shall satisfy:

$$\frac{T_{Ed}}{T_{Rd}} \leq 1,0 \quad (2.40)$$

where:

$T_{Rd} = W_{T,pl} f_0 / (\sqrt{3} \gamma_{M1})$  is the design St. Venants torsion moment resistance of the cross-section in which  $W_{T,pl}$  is the plastic torsion modulus.

For members subjected to torsion for which distortional deformations may be disregarded but not warping torsion, the total torsional moment at any cross-section should be considered as the sum of two internal effects:

$$T_{Ed} = T_{t,Ed} + T_{w,Ed} \quad (2.41)$$

where:

$T_{t,Ed}$  is the internal St. Venants torsion moment;  
 $T_{w,Ed}$  is the internal warping torsion moment.

## Combined shear force and torsional moment

For combined shear force and torsional moment the shear force resistance accounting for torsional effects shall be reduced from

$V_{Rd}$  to  $V_{T,Rd}$  and the design shear force shall satisfy:

$$\frac{V_{Ed}}{V_{T,Rd}} \leq 1,0 \quad (2.42)$$

in which  $V_{T,Rd}$  may be derived as follows:

- for an I or H section

$$V_{T,Rd} = \sqrt{1 - \frac{\tau_{t,Ed} \sqrt{3}}{1,25 \frac{f_0}{\gamma_{M1}}}} V_{Rd} \quad (2.43)$$

- for a channel section

$$V_{T,Rd} = \left[ \sqrt{1 - \frac{\tau_{t,Ed} \sqrt{3}}{1,25 \frac{f_0}{\gamma_{M1}}} - \frac{\tau_{w,Ed} \sqrt{3}}{\frac{f_0}{\gamma_{M1}}}} \right] V_{Rd} \quad (2.44)$$

- for a hollow section

$$V_{T,Rd} = \left[ 1 - \frac{\tau_{t,Ed} \sqrt{3}}{\frac{f_0}{\gamma_{M1}}} \right] V_{Rd} \quad (2.45)$$

## Bending and shear

If the shear force  $V_{Ed}$  is less than half the shear resistance  $V_{Rd}$  its effect on the moment resistance may be neglected except where shear buckling reduces the section resistance. Otherwise, the reduced moment resistance should be taken as the design resistance of the cross-section, calculated using a reduced strength:

$$f_{0,V} = f_0 \left[ 1 - \left( \frac{2 V_{ed}}{V_{Rd} - 1} \right)^2 \right] \quad (2.46)$$

## Bending and axial force

For doubly symmetric cross-sections the following two criteria should be satisfied:

$$\left( \frac{N_{Ed}}{\omega_0 N_{Rd}} \right)^{\xi_0} + \frac{M_{y,Ed}}{\omega_0 M_{y,Rd}} \leq 1,0 \quad (2.47)$$

$$\left( \frac{N_{Ed}}{\omega_0 N_{Rd}} \right)^{\eta_0} + \left( \frac{M_{y,Ed}}{\omega_0 M_{y,Rd}} \right)^{\gamma_0} + \left( \frac{M_{z,Ed}}{\omega_0 M_{z,Rd}} \right)^{\xi_0} \leq 1,0 \quad (2.48)$$

where:

$\eta_0 = 1,0$  or may alternatively be taken as  $\alpha_z^2 \alpha_y^2$  but  $1 \leq \eta_0 \leq 2$ ;

$\gamma_0 = 1,0$  or may alternatively be taken as  $\alpha_z^2$  but  $1 \leq \gamma_0 \leq 1,56$ ;

$\xi_0 = 1,0$  or may alternatively be taken as  $\alpha_y^2$  but  $1 \leq \xi_0 \leq 1,56$ ;

$N_{Ed}$  is the design value of the axial compression or tension force;

$M_{y,Ed}$  and  $M_{z,Ed}$  are the bending moments about the y-y and z-z axis;

$N_{Rd} = A_{eff} f_0 / \gamma_{M1}$

$M_{y,Rd} = \alpha_y W_{y,el} f_0 / \gamma_{M1}$

$M_{z,Rd} = \alpha_z W_{z,el} f_0 / \gamma_{M1}$

$\alpha_y$ ,  $\alpha_z$  are the shape factors for bending about the y and z axis, with allowance for local buckling and HAZ softening from longitudinal welds;  
 $\omega_0 = 1$  for sections without localized welds or holes.

### 2.5.5 Buckling resistance of members

#### Members in compression

A compression member shall be verified against both flexural and torsional or torsional-flexural buckling as follows:

$$\frac{N_{Ed}}{N_{b,Rd}} \leq 1,0 \quad (2.49)$$

where:

$N_{Ed}$  is the design value of the compression force;

$N_{b,Rd}$  is the design buckling resistance of the compression member given by the expression:

$$N_{b,Rd} = \kappa \chi A_{eff} f_o / \gamma_{M1} \quad (2.50)$$

where:

$\chi$  is the reduction factor for the relevant buckling mode;

$\kappa$  is a factor to allow for the weakening effects of welding. For longitudinally welded member  $\kappa$  is given in Table 2.7 for flexural buckling and  $\kappa = 1$  for torsional and torsional-flexural buckling. In case of transversally welded member  $\kappa = \omega_x$ ;

$A_{eff}$  is the effective area allowing for local buckling for class 4 cross-section. For torsional and torsional-flexural buckling see Table 2.9.

$A_{eff} = A$  for class 1, 2 or 3 cross-section.

Table 2.7: Values of  $\kappa$  factor for member with longitudinal welds [12].

Class A material	Class B material
$\kappa = 1 - \left(1 - \frac{A_1}{A}\right) 10^{-\bar{\lambda}} - \left(0,05 + 0,1 \frac{A_1}{A}\right) \bar{\lambda}^{1,3(1-\bar{\lambda})}$ with $A_1 = A - A_{haz} (1 - \rho_{0,haz})$ in which $A_{haz}$ = area of HAZ	$\kappa = 1$ if $\bar{\lambda} \leq 0,2$ $\kappa = 1 + 0,04(4\bar{\lambda})^{(0,5-\bar{\lambda})} - 0,22\bar{\lambda}^{1,4(1-\bar{\lambda})}$ if $\bar{\lambda} > 0,2$

For axial compression in members the value of  $\chi$  for the appropriate value of  $\bar{\lambda}$  should be determined from the relevant buckling curve according to:

$$\chi = \frac{1}{\phi + \sqrt{\phi^2 - \bar{\lambda}^2}} \quad \text{but } \chi < 1,0 \quad (2.51)$$

where:

$$\phi = 0,5(1 + \alpha(\bar{\lambda} - \bar{\lambda}_0)) + \bar{\lambda}^2 \quad (2.52)$$

$\alpha$  is an imperfection factor;

$\bar{\lambda}_0$  is the limit of the horizontal plateau;

$\bar{\lambda}$  is the relative slenderness.

The imperfection factor  $\alpha$  and limit of horizontal plateau  $\bar{\lambda}_0$  corresponding to appropriate buckling curve should be obtained from Table 2.8 for flexural buckling and Table 2.9 for torsional or torsional-flexural buckling.

Table 2.8: Values of  $\alpha$  and  $\bar{\lambda}_0$  for flexural buckling [12].

Material buckling class	$\alpha$	$\bar{\lambda}_0$
Class A	0,20	0,10
Class B	0,32	0,00

Table 2.9: Values of  $\alpha$ ,  $\bar{\lambda}_0$  and  $A_{eff}$  for torsional and torsional-flexural buckling [12].

Cross-section	$\alpha$	$\bar{\lambda}_0$	$A_{eff}$
General	0,35	0,4	$A_{eff}$
Composed entirely of radiating outstands	0,20	0,6	A

Values of the reduction factor  $\chi$  for the appropriate relative slenderness  $\bar{\lambda}$  may be obtained from Figure 2.38 for flexural buckling and Figure 2.39 for torsional or torsional-flexural buckling.

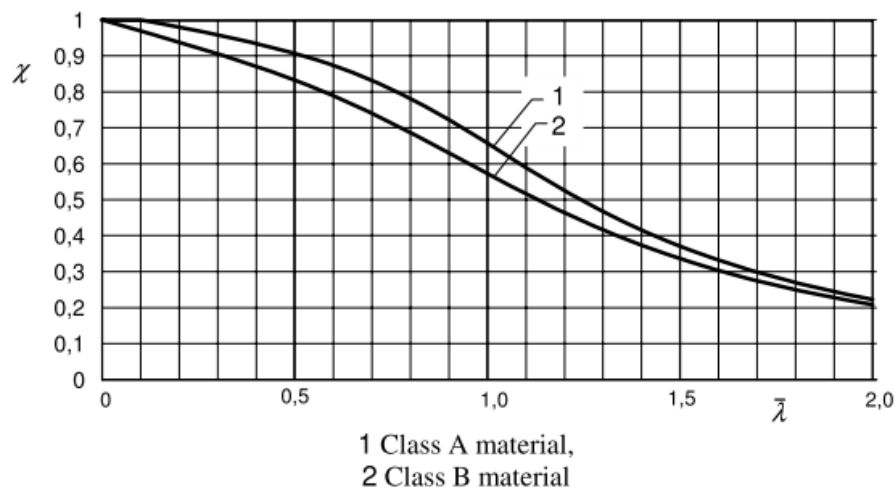


Figure 2.38: Reduction factor  $\chi$  for flexural buckling [12].

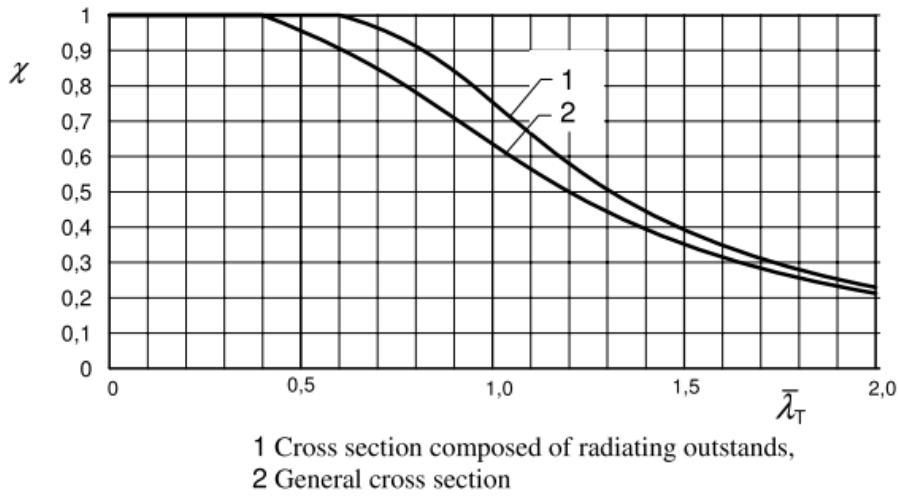


Figure 2.39: Reduction factor  $\chi$  for torsional and torsional-flexural buckling [12].

The relative slenderness  $\bar{\lambda}$  is given by:

$$\bar{\lambda} = \sqrt{\frac{A_{eff} f_o}{N_{cr}}} \quad (2.53)$$

$N_{cr}$  is the elastic critical force for the relevant buckling mode based on the gross cross-sectional properties.

As  $N_{cr} = \frac{\pi^2 EI}{L_{cr}^2}$ , then:

$$\bar{\lambda} = \frac{L_{cr}}{\pi i} \sqrt{\frac{A_{eff} f_o}{A E}} \quad (2.54)$$

where:

$L_{cr}$  is the buckling length in the buckling plane considered;

$i$  is the radius of gyration about the relevant axis, determined using the properties of gross cross-section.

The buckling length  $L_{cr}$  should be taken as  $kL$ , where  $L$  is the length between points of lateral support; for a cantilever strut,  $L$  is its length. The value of  $k$ , the buckling length factor for struts, should be assessed from a knowledge of the end conditions; Table 2.10 gives guidance.



Table 2.10: Buckling length factor  $k$  for struts [12].

End conditions	$k$
1. Held in position and restrained in direction at both ends	0,7
2. Held in position at both ends and restrained in direction at one end	0,85
3. Held in position at both ends, but not restrained in direction	1,0
4. Held in position at one end, and restrained in direction at both ends	1,25
5. Held in position and restrained in direction at one end, and partially restrained in direction but not held in position at the other end	1,5
6. Held in position and restrained in direction at one end, but not held in position or restrained at the other end	2,0

### Members in bending

A laterally unrestrained member subject to mayor axis bending shall be verified against lateral-torsional buckling as follows:

$$\frac{M_{Ed}}{M_{b,Rd}} \leq 1,0 \quad (2.55)$$

where:

$M_{Ed}$  is the design value of the bending moment;

$M_{b,Rd}$  is the design buckling resistance moment given by the expression:

$$M_{b,Rd} = \chi_{LT} \alpha W_{el,y} f_o / \gamma_{M1} \quad (2.56)$$

where:

$W_{el,y}$  is the elastic section modulus of the gross section, without reduction for HAZ softening, local buckling or holes;

$\alpha$  is taken from Table 2.6 subject to the limitation  $\alpha \leq W_{pl,y} / W_{el,y}$ ;

$\chi_{LT}$  is the reduction factor for lateral torsional buckling for the appropriate relative slenderness  $\bar{\lambda}_{LT}$ , determined from:

$$\chi_{LT} = \frac{1}{\phi_{LT} + \sqrt{\phi_{LT}^2 - \bar{\lambda}_{LT}^2}} \quad \text{but } \chi_{LT} < 1,0 \quad (2.57)$$

where:

$$\phi_{LT} = 0,5(1 + \alpha_{LT}(\bar{\lambda}_{LT} - \bar{\lambda}_{0,LT})) + \bar{\lambda}_{LT}^2 \quad (2.58)$$

$\alpha_{LT}$  is an imperfection factor;

$\bar{\lambda}_{LT}$  is the relative slenderness;

$\bar{\lambda}_{0,LT}$  is the limit of the horizontal plateau.

The value of  $\alpha_{LT}$  and  $\bar{\lambda}_{0,LT}$  should be taken as:

$\alpha_{LT} = 0,10$  and  $\bar{\lambda}_{0,LT} = 0,6$  for class 1 and 2 cross-sections;

$\alpha_{LT} = 0,20$  and  $\bar{\lambda}_{0,LT} = 0,4$  for class 3 and 4 cross-sections.

Values of the reduction factor  $\chi_{LT}$  for the appropriate relative slenderness  $\bar{\lambda}_{LT}$  may be obtained from Figure 2.40.

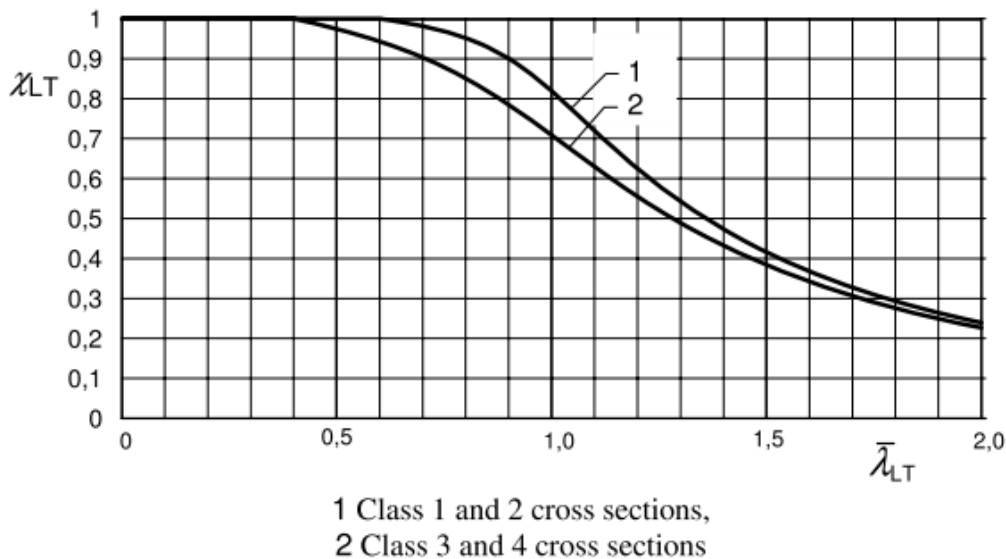


Figure 2.40: Reduction factor for lateral-torsional buckling [12].

The relative slenderness parameter  $\bar{\lambda}_{LT}$  should be determined from:

$$\bar{\lambda}_{LT} = \sqrt{\frac{\alpha W_{el,y} f_o}{M_{cr}}} \quad (2.59)$$

where:

$\alpha$  is taken from Table 2.6 subject to the limitation  $\alpha \leq W_{pl,y} / W_{el,y}$ ;

$M_{cr}$  is the elastic critical moment for lateral-torsional buckling.

Expressions for  $M_{cr}$  for certain sections and boundary conditions are given in Annex I.1 and approximate values of  $\bar{\lambda}_{LT}$  for certain I-sections and channels are given in Annex I.2.

### Members in bending and axial compression

The stability of uniform members should be checked as given in the following clause, where a distinction is made for:

- members that are not susceptible to torsional deformations, e.g. circular hollow sections or sections restrained from torsion (flexural buckling only);
- members that are susceptible to torsional deformations, e.g. members with open cross-sections not restrained from torsion (lateral-torsional buckling or flexural buckling).

#### Flexural buckling

For a member with open doubly symmetric cross-section, one of the following criteria should be satisfied:

- for major axis (y-axis) bending:

$$\left( \frac{N_{ed}}{\chi_y \omega_x N_{Rd}} \right)^{\xi_{yc}} + \frac{M_{y,Ed}}{\omega_0 M_{y,Rd}} \leq 1,0 \quad (2.60)$$

- for minor axis (z-axis) bending:

$$\left( \frac{N_{ed}}{\chi_z \omega_x N_{Rd}} \right)^{\eta_c} + \left( \frac{M_{z,Ed}}{\omega_0 M_{z,Rd}} \right)^{\xi_{zc}} \leq 1,0 \quad (2.61)$$

where:

$\eta_c = 0,8$  or may alternatively be taken as  $\eta_c = \eta_0 \chi_z$  but  $\eta_c \geq 0,8$ ;

$\xi_{yc} = 0,8$  or may alternatively be taken as  $\xi_{yc} = \xi_0 \chi_y$  but  $\xi_{yc} \geq 0,8$ ;

$\xi_{zc} = 0,8$  or may alternatively be taken as  $\xi_{zc} = \xi_0 \chi_z$  but  $\xi_{zc} \geq 0,8$ ;

$\omega_x = \omega_0 = 1$  for beam-columns without localized welds and with equal end moments. Otherwise see (2.63).

$N_{Ed}$  is the design value of the axial compressive force;

$M_{y,Ed}$  and  $M_{z,Ed}$  are the bending moments about the y-y and z-z axis. The moments are calculated according to first order theory;

$N_{Rd} = Af_0 / \gamma_{M1}$  or  $A_{eff} f_0 / \gamma_{M1}$  for class 4 cross-sections. For members with longitudinal welds but without localized welds  $N_{Rd} = \kappa Af_0 / \gamma_{M1}$  or  $\kappa A_{eff} f_0 / \gamma_{M1}$ ;

$M_{y,Rd} = \alpha_y W_y f_0 / \gamma_{M1}$  bending capacity about the y-axis;

$M_{z,Rd} = \alpha_z W_z f_0 / \gamma_{M1}$  bending capacity about the z-axis;

$\alpha_y, \alpha_z$  are the shape factors, but  $\alpha_y$  and  $\alpha_z$  should not be taken larger than 1,25.

### Lateral-torsional buckling

Members with open cross-section symmetrical about major axis, centrally symmetric or doubly symmetric cross-section, the following criterion should satisfy:

$$\left( \frac{N_{Ed}}{\chi_z \omega_x N_{Rd}} \right)^{\eta_c} + \left( \frac{M_{y,Ed}}{\chi_{LT} \omega_{xLT} M_{y,Rd}} \right)^{\gamma_c} + \left( \frac{M_{z,Ed}}{\omega_0 M_{z,Rd}} \right)^{\xi_{zc}} \leq 1,0 \quad (2.62)$$

where:

$N_{Ed}$  is the design value of the axial compressive force;

$M_{y,Ed}$  is bending moments about the y-axis. In the case of beam-columns with hinged ends and in the case of members in non-sway frames,  $M_{y,Ed}$  is moment of the first order. For members in frames free to sway,  $M_{y,Ed}$  is bending moment according to second order theory;

$M_{z,Ed}$  is bending moments about the z-axis.  $M_{z,Ed}$  is bending moment according to first order theory;

$N_{Rd} = Af_0 / \gamma_{M1}$  or  $A_{eff} f_0 / \gamma_{M1}$  for class 4 cross-sections. For members with longitudinal welds but without localized welds  $N_{Rd} = \kappa Af_0 / \gamma_{M1}$  or  $\kappa A_{eff} f_0 / \gamma_{M1}$ ;

$\chi_z$  is the reduction factor for buckling when one or both flanges deflects laterally (buckling in the x-y plane or lateral-torsional buckling);

$M_{y,Rd} = \alpha_y W_y f_0 / \gamma_{M1}$  bending capacity about the y-axis;

$M_{z,Rd} = \alpha_z W_z f_0 / \gamma_{M1}$  bending capacity about the z-axis;

$\alpha_y$ ,  $\alpha_z$  are the shape factors, but  $\alpha_y$  and  $\alpha_z$  should not be taken larger than 1,25;

$\chi_{LT}$  is the reduction factor for lateral torsional buckling;

$\eta_c = 0,8$  or alternatively  $\eta_0 \chi_z$  but  $\eta_c \geq 0,8$ ;

$\gamma_c = \gamma_0$ ;

$\xi_{zc} = 0,8$  alternatively  $\xi_0 \chi_z$  but  $\xi_{zc} \geq 0,8$ ;

$\omega_x$ ,  $\omega_0$  and  $\omega_{LT}$  = HAZ-softening factors.

The value of  $\omega_x$ ,  $\omega_0$  and  $\omega_{LT}$  for a member subject to HAZ softening, should generally be based on the ultimate strength of the HAZ softened material. It could be referred to the most unfavourable section in the bay considered. If such softening occurs only locally along the length, then  $\omega_x$ ,  $\omega_0$  and  $\omega_{LT}$  are:

$$\omega_0 = \omega_x = \omega_{xLT} = \frac{\rho_{u,haz} f_u / \gamma_{M2}}{f_0 / \gamma_{M1}} \text{ but } \leq 1,0 \quad (2.63)$$

where  $\rho_{u,haz}$  is the reduction factor for the heat affected material.

However, if HAZ softening occurs close to the ends of the bay, or close to points of contra flexure only,  $\omega_x$  and  $\omega_{LT}$  may be increased in considering flexural and lateral-torsional buckling, provided that such softening does not extend a distance along the member greater than the least width (e.g. flange width) of the section.

$$\omega_x = \frac{\omega_0}{\chi + (1-\chi) \sin \frac{\pi x_s}{l_c}} \quad (2.64)$$

$$\omega_{xLT} = \frac{\omega_0}{\chi_{LT} + (1-\chi_{LT}) \sin \frac{\pi x_s}{l_c}} \quad (2.65)$$

$$\omega_0 = \frac{\rho_{u,haz} f_u / \gamma_{M2}}{f_0 / \gamma_{M1}} \text{ but } \leq 1,0 \quad (2.66)$$

where:

$\chi = \chi_y$  or  $\chi_z$  depending on buckling direction;

$\chi_{LT}$  is the reduction factor for lateral-torsional buckling of the beam-column in bending only;

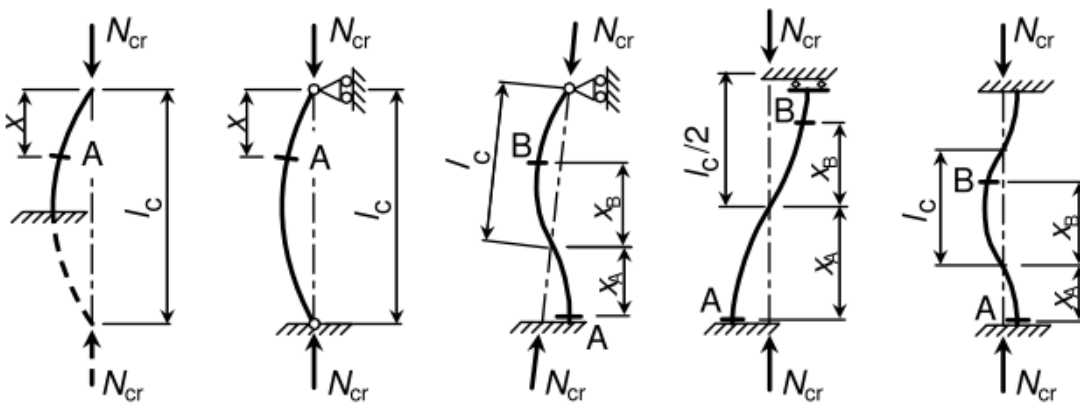
$x_s$  is the distance from the localized weld to a support or point of contra flexure for the deflection curve for elastic buckling of axial force only, compare Figure 2.41;

$l_c$  is the buckling length.

Calculation of  $\chi$  ( $\chi_y$  or  $\chi_z$ ) and  $\chi_{LT}$  in the section with the localized weld should be based on the ultimate strength of the heat affected material for the relative slenderness parameters:

$$\bar{\lambda}_{haz} = \bar{\lambda} \sqrt{\omega_0} \quad (2.67a)$$

$$\bar{\lambda}_{haz,LT} = \bar{\lambda}_{LT} \sqrt{\omega_0} \quad (2.67b)$$



A and B are examples of studied sections marked with transverse lines.

See Table 6.8 for value of buckling length  $l_c = KL$ .

Figure 2.41: Buckling length  $l_c$  and definition of  $x_s$  ( $=x_A$  or  $x_B$ ) [12].

## 2.6 DURABILITY AND PROTECTION SYSTEMS

The necessity of electrolytic processes for the production of aluminium, utilising molten melts, signals immediately the high reactivity of the metal. In fact, immediately after the exposure to the atmosphere, a protective oxide film called alumina forms on the aluminium surface. This film is usually invisible, relatively inert and forms naturally as a result of exposure to air or oxygen and in many other complex environments containing oxygen. The high affinity of aluminium for oxygen also ensures that similar films will develop in damaged or scratched regions of the substrate. Thus, at face value, an ideal situation arises where the metal is protected by a very thin, self-repairing aluminium film. However, in real-life, the ideal situation of perfection over the macroscopic aluminium surfaces is rarely, if ever, achieved. Thus, defects of various kinds, generally called flaws, are present in the air-formed film on the aluminium surface. In reality, whilst the total area occupied by such flaws is low, processes proceeding at them largely determine the effective behaviour of aluminium. In general, aluminium alloys have good corrosion resistance in normal atmospheric conditions. The term “good corrosion resistance” means that in many cases aluminium alloys can be used without surface protection and will give long service life. Depending on the aggressiveness of the environment for a given application as well as on the function of the product and the expected service requirements and life, measure may have to be taken to prevent or limit the extent of corrosion attack [1]. In siliceous or highly alkaline environments, the discoloration and roughening of the surface of the elements will be more evident, with the formation of visible white pulverized oxides and the possibility that the protective oxide film is itself soluble. The metal is then no longer fully protected and additional protection must be considered. In marine environments, the surface of the aluminium alloy structural elements acquires a grey colour and it is necessary to provide for the protection of the alloy. The aluminium alloys are grouped according to three levels of durability in the Italian instructions for the design, execution and control

of aluminium structures [13]. Table 2.11 illustrates the durability class for wrought alloys. There are three levels of durability: A (excellent), B and C in decreasing order of durability. These levels are used to determine the need and degree of protection required. In constructions where more than one alloy is used, including filler metals related to welded constructions, the degree of protection should be determined in relation to the lower of the relative durability levels. Table 2.12 provides recommendations for corrosion protection for the three durability classes [13].

Table 2.11: Durability class for wrought aluminium alloys [13].

Alloy designation		Shape of the semi-finished product	Durability class
Numeric	Alphanumeric		
EN AW-3004	EN AW-AlMn1Mg1	SH, ST, PL	A
EN AW-3005	EN AW-AlMn1Mg0,5	SH, ST, PL	A
EN AW-3103	EN AW-Al Mn1	SH, ST, PL, ET, EP, ER/B	A
EN AW-5005/5005A	EN AW-AlMg1(B)/(C)	SH, ST, PL	A
EN AW-5049	EN AW-AlMg2Mn0,8	SH, ST, PL	A
EN AW-5052	EN AW-Al Mg2,5	SH, ST, PL, ET <sup>1)</sup> , EP <sup>1)</sup> , ER/B, DT	A
EN AW-5083	EN AW-Al Mg4,5Mn0,7	SH, ST, PL, ET <sup>1)</sup> , EP <sup>1)</sup> , ER/B, DT, FO	A
EN AW-5454	EN AW-Al Mg3Mn	SH, ST, PL, ET <sup>1)</sup> , EP <sup>1)</sup> , ER/B	A
EN AW-5754	EN AW-Al Mg3	SH, ST, PL, ET <sup>1)</sup> , EP <sup>1)</sup> , ER/B, DT, FO	A
EN AW-6060	EN AW-Al MgSi	ET, EP, ER/B, DT	B
EN AW-6061	EN AW-Al Mg1SiCu	SH, ST, PL, ET, EP, ER/B, DT	B
EN AW-6063	EN AW-Al Mg0,7Si	ET, EP, ER/B, DT	B
EN AW-6005A	EN AW-Al SiMg(A)	ET, EP, ER/B	B
EN AW-6082	EN AW-Al Si1MgMn	SH, ST, PL, ET, EP, ER/B, DT, FO	B
EN AW-6106	EN AW-AlMgSiMn	EP	B
EN AW-7020	EN AW-Al Zn4,5Mg1	SH, ST, PL, ET, EP, ER/B, DT	C
EN AW-8011A	EN AW-AlFeSi	SH, ST, PL	B
Legend:		ER/B – Extruded rod or bar (EN 755)	
SH – Sheet (EN 485)		DT – Drawn tube (EN 754)	
ST – Strip (EN 485)		FO – Forged (EN 586)	
ET – Extruded tube (EN 755)		<sup>1)</sup> Only solid extruded sections (open)	
EP – Extruded profile (EN 755)		or seamless tubes	



Table 2.12: General corrosion protection of aluminium structures [13].

Protection degree in relation to environmental conditions									
Dura- bility level of the alloy	Material thickness [mm]	Kind of atmosphere						Kind of immersion	
		Rural	Industrial/urban		Marine			Fresh water	Salt water
			moderate	severe	not industrial	Mo- derate	severe		
A	Any	0	0	P	0	0	P	0	(P)
B	< 3	0	(P)	P	(P)	(P)	P	P	P
	≥ 3	0	0	P	0	(P)	P	(P)	P
C	Any	0	(P)	P	(P)	(P)	P	(P)	NR

Legend:  
 0: normally no protection is needed.  
 P: Protection normally required, except for special cases decided by the designer.  
 (P): The need for protection depends on the special conditions of the structure, as determined by the designer.  
 NR: The immersion in salt water is not recommended.

The type of corrosion protection must be adapted to the corrosive mechanism, such as pitting corrosion, galvanic corrosion, crevice corrosion and corrosion due to contact with other materials. Pitting corrosion is a localized corrosion that occurs in aerated aqueous solutions and in the presence of Cl<sup>-</sup> ions and it is characterized by the formation of pits in the protected oxide film. Very high purity aluminium (1099) has excellent resistance to pitting. Among commercial alloys, the aluminium-magnesium alloys (5xxx) have the lowest pitting probability and penetration rates. With low (<0.04%) copper content aluminium-manganese (3xxx) alloys show comparable pitting behaviour. In aluminium-magnesium-silicon (6xxx) alloys pitting is combined with intergranular corrosion. Aluminium-copper (2xxx) and aluminium-zinc-magnesium-copper (7xxx) alloys are normally clad to protect against pitting [1]. Crevice corrosion can occur in any type of crevice, even between metal and plastic. To prevent crevice corrosion, the crevice should be sealed with a non-hardening elastomer to prevent the entry of moisture. This elastomer requirement is essential because some sealants become hard and crack on aging, allowing moisture to enter. If a protection of the contact surface is specified for structures in a severe industrial or marine environment or for structures immersed in water, both contact surfaces shall be assembled so that no crevices exist where water

can penetrate. Both contact surfaces, including bolt and rivet holes shall, before assembly, be cleaned, pre-treated and receive one priming coat or sealing compound, extending beyond the contact area. Due to the fact that different metals must be used very often electrically coupled in an integrated structure a galvanic corrosion can occur resulting in acceleration of the corrosion process in less resistant metals. To minimize galvanic corrosion, it is recommended to provide complete electrical insulation of the two metals and all fixing elements. This may be done by using insulating gaskets, sleeves and washers to prevent metallic and electrical contact between the materials. The use of additional coating or sealants may be necessary. For contact with wood a coating is not required, unless the wood has been treated with an aluminium harming product (e.g. cooper sulphate). In such cases a coating protection is necessary. If protection measures are specified on the aluminium surface in cases of direct or indirect contact between aluminium components with concrete, brickwork or plaster, before assembly the aluminium surface shall be covered with a bitumen layer or another suitable coating with a thickness of at least 100  $\mu\text{m}$ , if not otherwise specified. In contact with soils the coating of the aluminium surface shall be done in two layers of bitumen or another suitable coating with a thickness of at least 100  $\mu\text{m}$  [14]. The surface treatments for aluminium can be coating, anodizing and passivation. The surfaces to be protected should be cleaned using suitable equipment such as fibre brushes, cleaning wool, careful abrasive-blast cleaning using suitable blasting material and thereafter carefully degreased. If sheets, profiles or parts of the structure already have been pre-treated or primed before assembly, all parts that were in contact with grease should be cleaned once more with a suitable method before subsequent coats are deposited. Coating of the whole structure should be carried out before or directly after the assembly. The execution of coatings should only be done when the surface temperature of the parts to be coated is higher than 5 °C, relative humidity is less than 85 % and the surface temperature is 3 °C above the dew point, unless other limits are permitted by the manufacturer of the coating. Directly after drying a suitable priming

coat should be deposited onto the cleaned and degreased surfaces if these are not already pre-treated in another way. Pre-treated surfaces should be covered with a base coat with an appropriate inhibiting pigment compatible with the aluminium substrate and any subsequent coats. Lead, copper, mercury or tin, graphite, cadmium or carbonaceous materials as pigments are not allowed in basic coatings. After sufficient drying of the base coat, a suitable final coat should be applied depending on the exposure conditions. For the anodizing, a minimum thickness of the oxide layer of 20  $\mu\text{m}$  is required if it is to be used as corrosive protection. A method for specifying decorative and protective anodic oxidation coatings on aluminium is given in EN 12373-1. Any required passivation or special surface treatment should be specified. The requirements for the application published by the manufacturer of the passivation agent should be followed. If the required type of passivation is not specified, the minimum should be a chromic acidic solution (chromating) or if possible, phosphoric acidic solution (phosphating). Passivation of aluminium without additional coating is only a short-term protection or for mild conditions. [14].

## 2.7 REFERENCES

- [1] TALAT Training in Aluminium Application Technologies. (1999) EAA – European Aluminium Association, Brussels, Belgium.
- [2] International Aluminium Institute. (2009) Global aluminium recycling: A cornerstone of sustainable development. Available online: [https://www.world-aluminium.org/media/filer\\_public/2013/01/15/fl0000181.pdf](https://www.world-aluminium.org/media/filer_public/2013/01/15/fl0000181.pdf) (last access November 2020)
- [3] Efthymiou E., Cöcen O. N., Ermolli S. R. (2010) Sustainable aluminium systems. *Sustainability* 2010, 2, p. 3100-3109. <https://doi.org/10.3390/su2093100>
- [4] Mazzolani F. M. (2006) Structural applications of aluminium in civil engineering. *Structural Engineering International*, 4.
- [5] Mazzolani F. M. (1994) *Aluminium Alloy Structures* (second edition). E&FN Spon, an imprint of Chapman & Hall, London.
- [6] Mazzolani F. M. (2004) Competing issues for aluminium alloys in structural engineering. *Prog. Struct. Engng. Mater.*, 6, p. 185-196. <https://doi.org/10.1002/pse.178>
- [7] Mazzolani F. M. (2012) 3D aluminium structures. *Thin-Walled Structures*, 61, p. 258-266. <http://dx.doi.org/10.1016/j.tws.2012.07.017>
- [8] Mazzolani F. M. (2006) Aluminium Structures in Refurbishment: the case of the “Real Ferdinando” bridge on the Garigliano river. *Structural Engineering International*, 16, 4, p. 352-355. <https://doi.org/10.2749/101686606778995182>

[9] International Alloy Designations and Chemical Composition Limits for Wrought Aluminium and Wrought Aluminium Alloys. (2015) The Aluminium Association, Arlington, VA.

[10] EN 515 (2017) Aluminium and aluminium alloys – Wrought products - Temper designations.

[11] Conserva M., Bonollo F., Donzelli G. (2004) Alluminio manuale degli impieghi. Edimet.

[12] CEN-TC250 (2007) Eurocode 9: Design of aluminium structures. Part 1-1: general structural rules.

[13] CNR DT 208/2011 Istruzioni per la Progettazione, l'Esecuzione ed il Controllo di Strutture di Alluminio.

[14] EN 1090-3 (2019) Execution of steel structures and aluminium structures - Part 3: Technical requirements for aluminium structures.



## *Chapter 3*

# **DESIGN OF THE ALUMINIUM ALLOY EXOSKELETON**

## **3.1 INTRODUCTION**

As introduced in Chapter 1, the main aim of this thesis is the development of the design of an external structural frame, also called exoskeleton, made of aluminium alloys for the seismic retrofit of existing buildings. Although several studies have been carried out in recent years on the seismic retrofit of existing buildings using steel exoskeletons, studies on this technology made of aluminium alloys are very rare. The Japanese Sumikei-Nikkei Engineering Company invented the SNE-Truss as a seismic retrofit technology to reinforce existing RC buildings. SNE-Truss reinforces existing RC buildings from the outside of the structure using aluminium alloy space grids latticed wall. The purpose of the reinforcement by SNE-Truss is to improve the seismic capacity of existing RC buildings by the in-plane strength and stiffness of the aluminium lattice wall. Figure 3.1 shows a computer graphic drawing of existing buildings reinforced by SNE-Truss. The main characteristics of this technology include:

- 1) the adaptability with existing RC buildings for retrofitting works;
- 2) the minimal self-weight and a high strength of aluminium used in SNE-Truss;
- 3) the high performance of corrosion resistance of aluminium [1].

Despite the three-dimensional geometry, the structural behaviour of these systems is similar to that of vertical bracing applied parallel and externally to the building façade, indicated with exoskeleton 2D// in chapter 1.5.



Figure 3.1: Computer graphic drawing of existing RC buildings reinforced by SNE-Truss [1, 2].

Figure 3.2 shows the shape and materials of the connection that is adopted in SNE-Truss and mainly composed of aluminium alloy. All the struts, hubs, collar and end plugs are extruded aluminium (6061 T6).

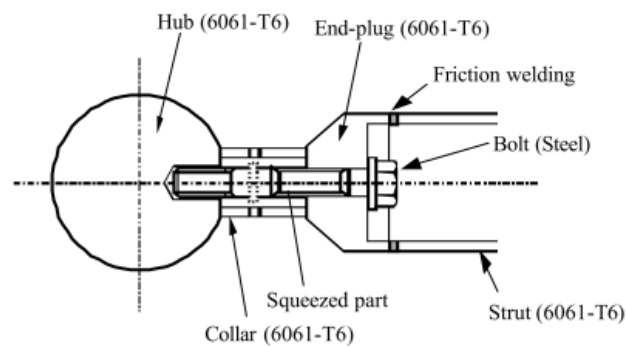


Figure 3.2: Shape and material of SNE-Truss connection [2].

The simple beam loading test and in-plane loading test were carried out (Figure 3.3).





Figure 3.3: Loading tests of SNE-Truss [2].

### **3.2 FEASIBILITY STUDY WITH A FULL SCALE MOCK-UP**

Within the scope of the European project Pro-GET-onE, described in chapter 1.4, a full-scale functional mock-up was created in San Mauro Pascoli on the ALIVA premises. Although the materials, sections and aesthetics are not the final ones, the purpose of the mock-up is to confirm the feasibility of the solution proposed by Pro-GET-onE for the seismic retrofit and energy renovation. The mock-up is made up of an aluminium exoskeleton, which is seismic-resistant; therefore, it is quite realistic in terms of weights, dimensions and installation times. The system can be classified as an exoskeleton 2D $\perp$  with shear walls arranged perpendicular to the façade as indicated in chapter 1.5. The structure is composed by two main concentric bracing frames with diagonal arrangement according to the X scheme, connected by longitudinal beams. The system under investigation has a structural behaviour completely different from the SNE-Truss solution, cited in the previous chapter because it is entirely made of aluminium. The mock-up is made in aluminium, except for cross-laminated timber slabs and wooden-framed walls. The frame is raised from the foundation floor by 0,5 m and it has two inter-storeys of 2,5 m and 1 m cantilever at the top. The total height is 6,5 m and the plan dimensions are 1,2 m by 4 m (see Figure 3.4 and 3.5).

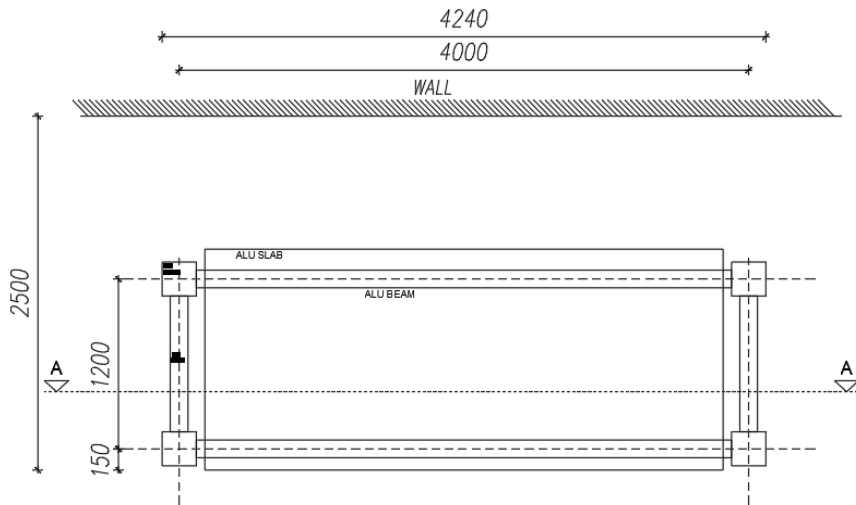


Figure 3.4: Plan view of the full scale mock-up.

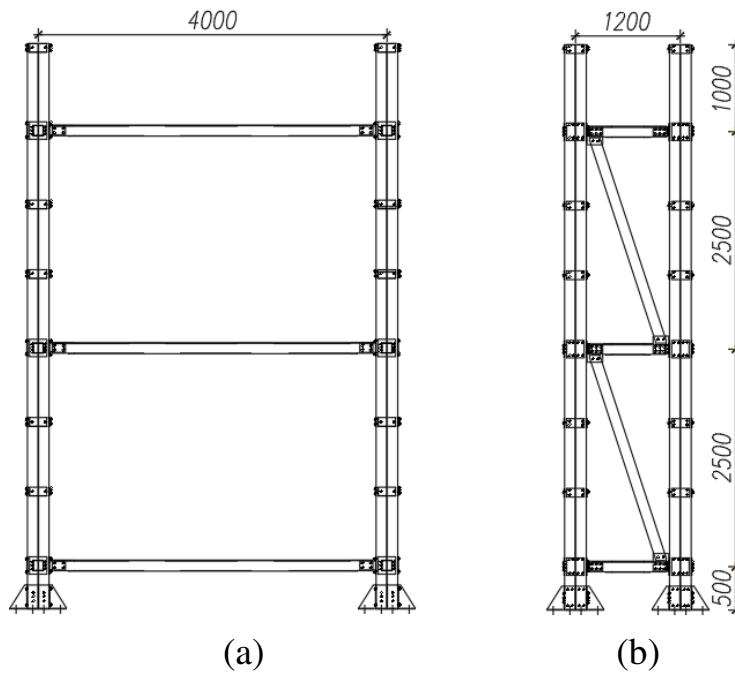


Figure 3.5: (a) Longitudinal section of the full scale mock-up; (b) transverse section.

Since the purpose of this structure is to act as a full scale visual mock-up, the class of use I (temporary construction) is considered.

Commercial extruded profiles in aluminium alloy 6063 T66 CE marked are used. The 6063 T66 is an AlMgSi heat treated alloy whose characteristic values of 0,2% proof strength  $f_0$ , ultimate strength  $f_u$  and minimum elongation  $A$ , are shown in Table 3.1 according to Eurocode 9.

Table 3.1: Characteristic values of 0,2% proof strength  $f_0$ , ultimate strength  $f_u$  and minimum elongation  $A$  for 6063 T66 alloy.

Alloy EN-AW	Thickness (mm)	$f_0$ (N/mm <sup>2</sup> )	$f_u$ (N/mm <sup>2</sup> )	$A$ (%)
6063 T66	$t \leq 10$	200	245	8

The section of the vertical mullions is obtained by assembling together four commercial extruded tubular profiles with side 120 mm and thickness 5 mm through bolted crosses (see Figure 3.6). The crosses are obtained from welded plates and the bolted connection between the tubular profiles and crosses is made every 80 cm along the length of the profile.

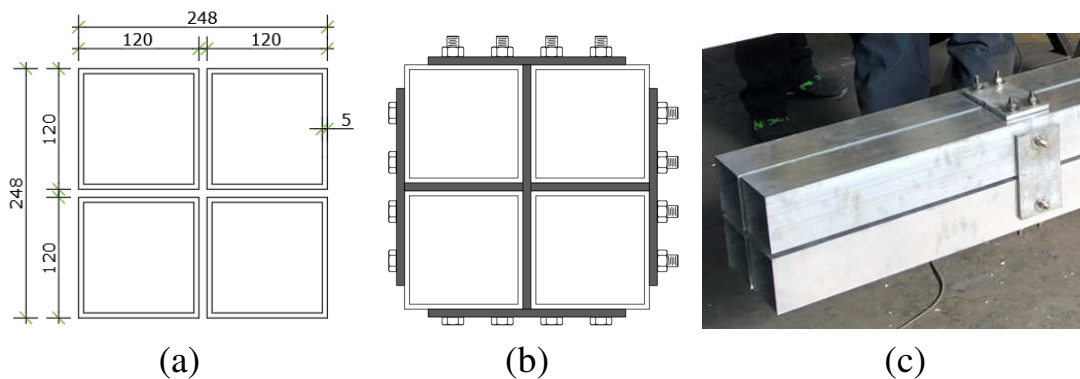


Figure 3.6: Section of the vertical mullions of the mock-up.

- (a) Commercial extruded tubular profiles; (b) four tubular profiles connected with bolted crosses; (c) picture of the section.

The beams are obtained by welding an extruded tubular profile with side 120 mm and thickness 5 mm and a plate with dimensions 200 mm by 8 mm (see Figure 3.7).



Figure 3.7: Section of the beams of the mock-up.

For the bracing the same extruded tubular profile with side 120 mm and thickness 5 mm is used. With reference to the classification of cross-section (see chapter 2.5.3), all sections are class 4 and the effective section, obtained by reducing the thickness of factor  $\rho_c$ , has been considered in the calculations. For the ultimate limit states, the resistance and buckling verification have been carried out according to chapter 2.5.4. At the serviceability limit states, the deformability verification in case of seismic actions has been carried out assuming a maximum inter-storey drift of 1%. The preliminary geometry of the mock up shows the presence of joints eccentricity. These eccentricities produce bending moments that have been considered in the design of the mock up chord members. The final geometry of the aluminium exoskeleton will consist of customized sections which will be illustrated in chapter 3.5. These allow to minimize the joints eccentricity and to consider the secondary bending moments as negligible. The visual mock-up shows the advantages of the plug and play solution where all components are preassembled in the factory and ready to be installed reducing the construction times. The assembly phases of the prefabricated components in the factory are depicted in Figure 3.8. The parallel beams are also pre-assembled in the factory with x-lam slabs (see Figure 3.9).



Figure 3.8: Assembly phases of the prefabricated components of the mock-up.



Figure 3.9: Parallel beams pre-assembled with x-lam slabs.

The erection phases and the installation of the mock-up are illustrated in Figure 3.10. Subsequently, the wooden-framed walls, the windows and parts of the technical building equipment were installed (see Figure 3.11). The aluminium exoskeleton provides integrated solutions for seismic retrofit and energy improvement and possible volumetric expansion, as described in chapter 1.4. The mock-up shows the various possibilities of the additional spaces. Downstairs is a sunspace, above it an extra room and at the top a balcony, as can be seen from Figure 3.12. The construction of the visual mock-up has highlighted the main aspects of this technology, as the assembly process and the critical connections. These will help to further improve the design of the aluminium exoskeleton. In fact, the preliminary sections of the components, constituted by the union of commercial profiles, will be replaced by customized sections to obtain the maximum performance and a more rational profile. The bolted connections will be improved by designing an innovative connection system. The extrusion process, illustrated in chapter 2.4, allows individually tailored products to be designed and to simplify connection systems avoiding welding or bolting.

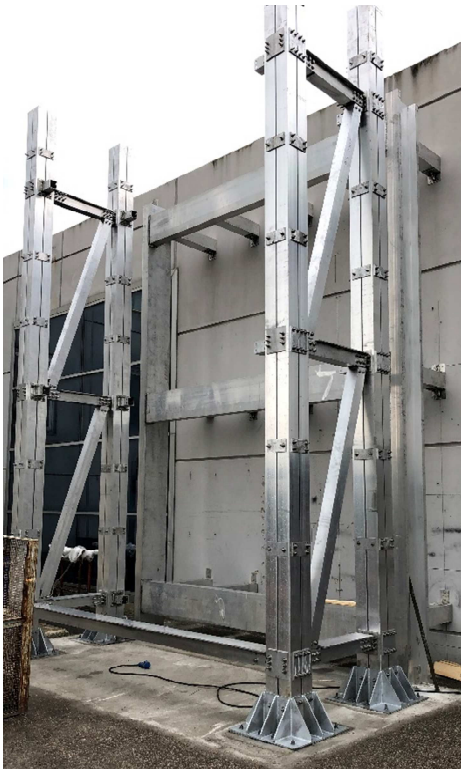
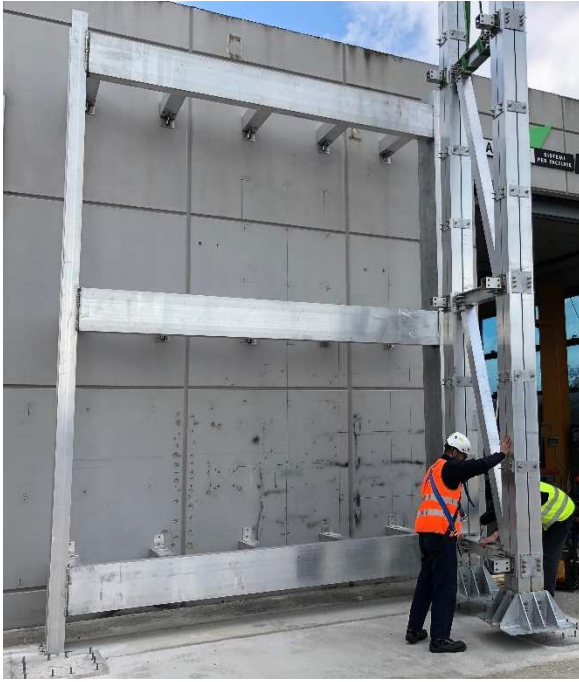


Figure 3.10: Erection phases and installation of the mock-up.



Figure 3.11: Installation of wooden-framed walls, windows and parts of the technical building equipment.



Figure 3.12: Various possibilities of the additional spaces: sunspace, extra room and balcony.



### 3.3 ALUMINIUM ALLOYS SELECTED

Within the group of the wrought aluminium alloys, the 6000 series has been chosen. It is a magnesium-silicon alloy and it is heat treatable. This group of alloys has high strength, good corrosion resistance and high extrudability index and it is the most used in the extrusion process. For the vertical mullions and beams of the exoskeletons, the alloy 6082 T6 has been selected. It is the alloy with the greatest strength among those of the 6000 series included in the Eurocode 9. The bracings of the exoskeleton have dissipative function absorbing the seismic input energy. For this reason, the alloy 6060 T5 that has the lowest elastic limit at a residual strain of 0,2%  $f_{0,2}$  has been selected. The mechanical properties of the two alloys are obtained from tests performed by the manufacturer. The main mechanical properties are the elastic limit at a residual strain of 0,2%  $f_{0,2}$ , the ultimate strength  $f_u$  and the ultimate elongation  $A$ . For extruded profiles, the ultimate elongation  $A$  is expressed as percentage of the original gauge length of  $5,65 \sqrt{S_0}$ , where  $S_0$  is the original cross-sectional area of the parallel length. Table 3.2 show the comparison between experimental data and European Standard of the mechanical properties of 6082 T6 and 6060 T5 alloys.

Table 3.2: Comparison between Eurocode 9 and experimental data of the mechanical properties of 6082 T6 and 6060 T5 alloys.

Alloy EN-AW	Eurocode 9				Experimental data			
	$f_{0,2}$ [MPa]	$f_u$ [MPa]	$A$ [%]	$n_p$ [-]	$f_{0,2}$ [MPa]	$f_u$ [MPa]	$A$ [%]	$n_p$ [-]
6082 T6	260	310	10	25	350	390	12	38
6060 T5	100	140	8	14	189	215	12,5	32

The experimental values of elastic limit, ultimate strength and elongation are greater than those provided by the standard code. Also, the exponent  $n_p$  of the Ramberg-Osgood law experimentally assumes greater values

than the standard ones. The comparison between the experimental and theoretical  $\sigma - \varepsilon$  curve of the 6082 T6 and 6060 T5 alloys is shown in Figure 3.13 and 3.14 respectively.

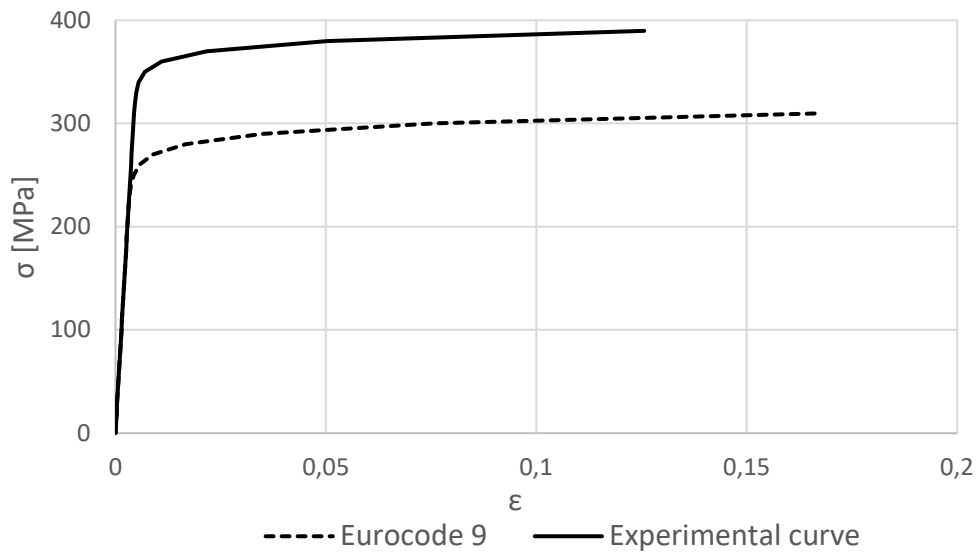


Figure 3.13: Comparison between the experimental and theoretical  $\sigma - \varepsilon$  curve of the 6082 T6 alloy.

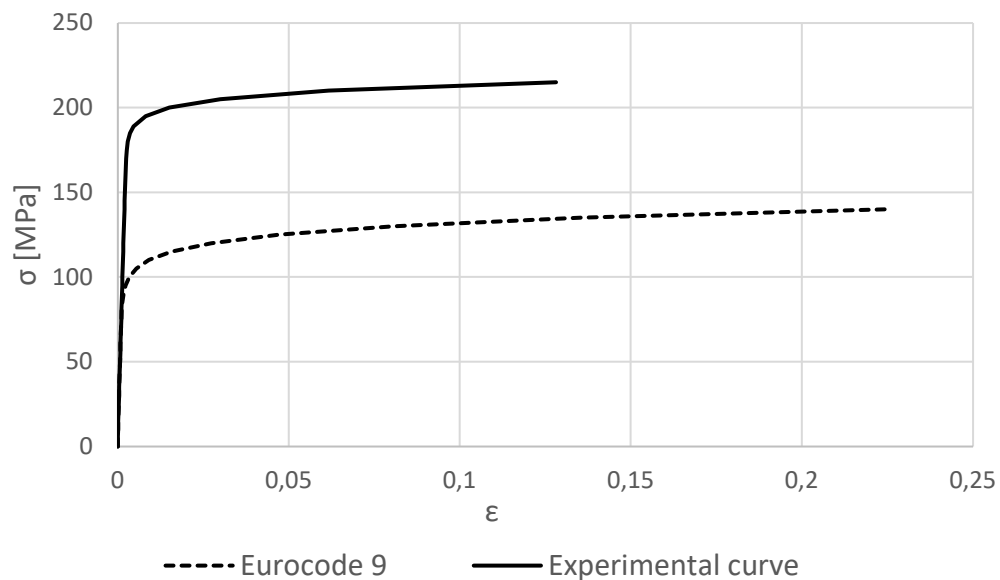


Figure 3.14: Comparison between the experimental and theoretical  $\sigma - \varepsilon$  curve of the 6060 T5 alloy.

The experimental data, used to calibrate the parameters of the constitutive model in accordance with Annex E of Eurocode 9 (see chapter 2.5.2), will be assumed in the nonlinear analysis for the seismic improvement assessment. In the last phase of the aluminium exoskeleton design, nine solutions will be proposed and analysed in order to find the best solution. Among these, the hypothesis of using the lowest performance alloy 6060 T5 for all the components (vertical mullions, beams and diagonals) will be evaluated.

### **3.4 DESIGN OF THE CUSTOMIZED SECTIONS OF THE EXTRUDED PROFILES**

The feasibility study with a full scale mock-up, described in chapter 3.2, has highlighted the main aspects of the technology that need to be improved in the design of the aluminium exoskeleton. In particular, the connections and the design of the optimal sections of the profiles. The use of commercial profiles does not allow to obtain high performance and simplified connections, therefore it is necessary to design customized sections for the extruded profiles. In designing a section, a preliminary consultation with the suppliers for the manufacture of the dies is advised to well know the maximum extrusion sizes, the minimum thickness and some structural features of the product that may require modification for better extrudability. As described in chapter 2.4, the overall dimensions of a section are related to the billet diameter, and the minimum section thickness relates to the complexity of the section and the alloy. The minimum thickness is about 0.5 mm. The maximum extrusion sizes in the Italian market for a square section is 320 mm by 320 mm. The sections have to be designed in order to avoid a brittle behaviour and local buckling phenomena in the elastic range. Therefore, sections in class 1, 2 or 3 according with the classification of cross-section described in chapter 2.5.3 are recommended. Finally, the design of the customized sections has to allow a plug and play solution with the main frame assembled in the factory and the simplicity of connections. An innovative connection

system has been studied consisting of special connectors fixed by blind rivets nuts that create threads for the installation of bolts and they can be fitted from one side only. The customized section of vertical mullions includes open chambers for the accommodation of the connectors, to which the beams and diagonals are subsequently fixed with bolted connection. Figure 3.15 shows a computer graphic drawing of the connection system.

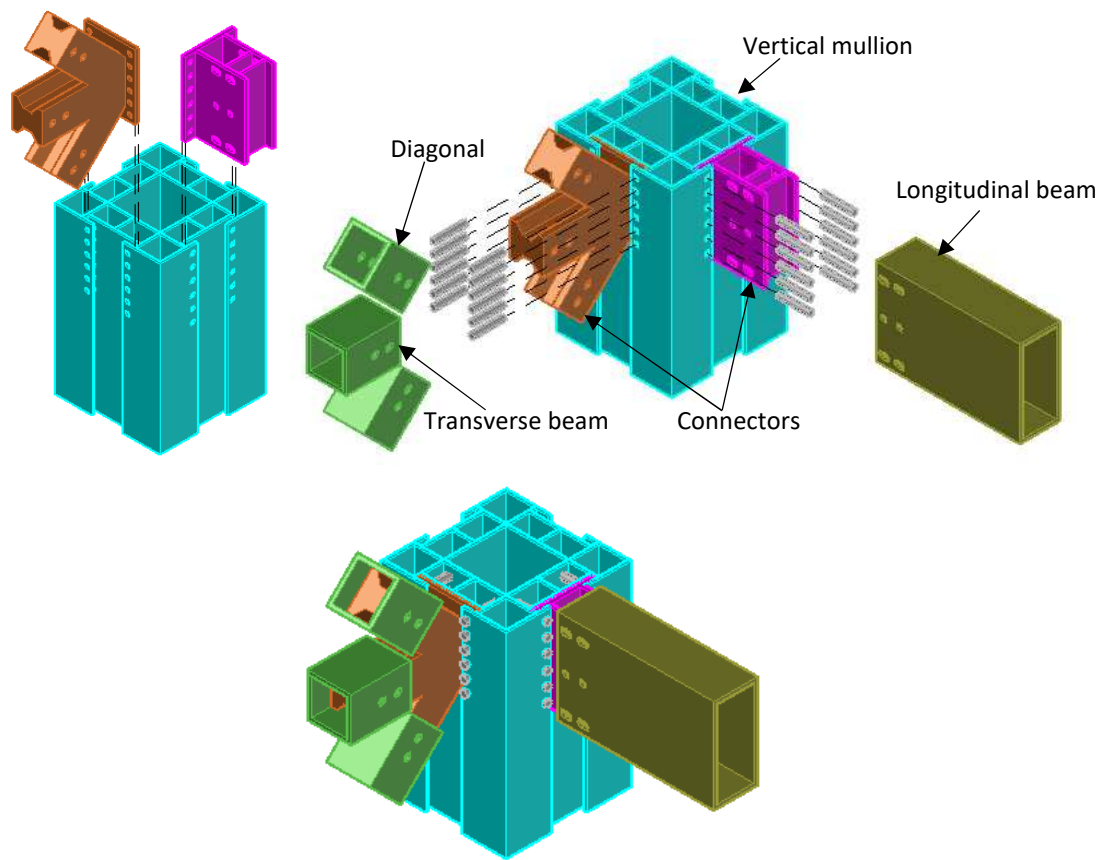


Figure 3.15: Computer graphic drawing of the innovative connection system.

Figure 3.16 shows the study of the customized section of the extruded profile from the preliminary section used in the full scale visual mock up to the final design. In the visual mock up four commercial hollow profiles joined with cross bolted connection were used. The study moved towards the design of a single section with multiple internal chambers to increase

the stiffness and then, a further modification of the chambers for the accommodation of the connectors led to the final section design.

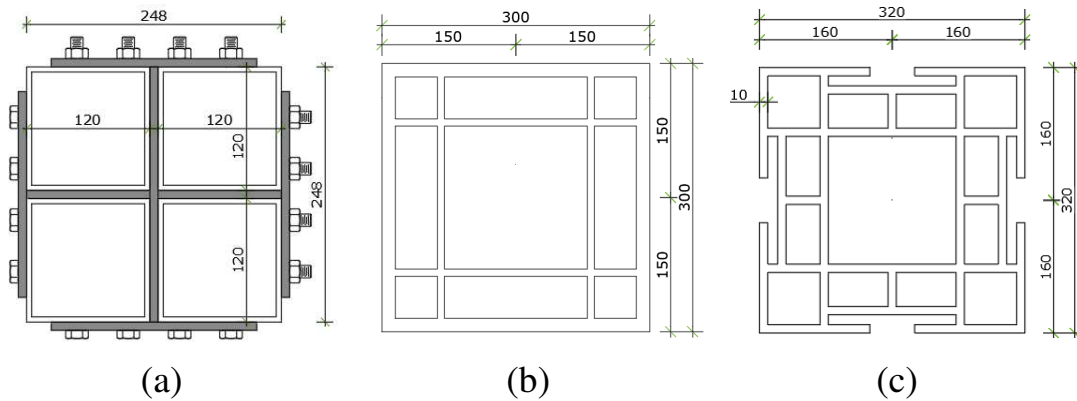


Figure 3.16: The study of the customized extruded section.  
 (a) Preliminary section used in the full scale mock up; (b) single section with multiple internal chambers; (c) final section design.

For the vertical mullions of the exoskeleton, the customized section with dimensions 320 mm by 320 mm and thickness 10 mm is considered at the first and second floor (indicated in the following as type A for simplicity). Vertical mullions with a reduced thickness of 6 mm, indicated as type B, are considered at the third and fourth floor. During the study of the improvement to the external aluminium alloy exoskeleton (see chapter 5.3), the mullion type A is result not efficient and only the geometry of mullion type B with reduced thickness was used at all floors. The geometrical properties of mullions type A and B are described in Figure 3.17, where:  $A$  is the cross-section area,  $I_y$  is the second moment of area of major axis,  $W_{e,y}$  is the elastic modulus of the gross section of major axis and  $P$  is the unit weight. The final section design of these profile was not carried out in order to optimize the weight, in fact the profiles have high cross-section area and unit weight. Their geometry has been studied to meet the requirements of instability, ease of assembly and prefabrication. The longitudinal beams have a tubular section of dimension 126 mm by 256 mm and thickness 16 mm. The transverse beams and the diagonals have a square hollow section with side 110 mm and thickness 12 mm.

Figure 3.18 shows the geometrical properties of beams and diagonals.

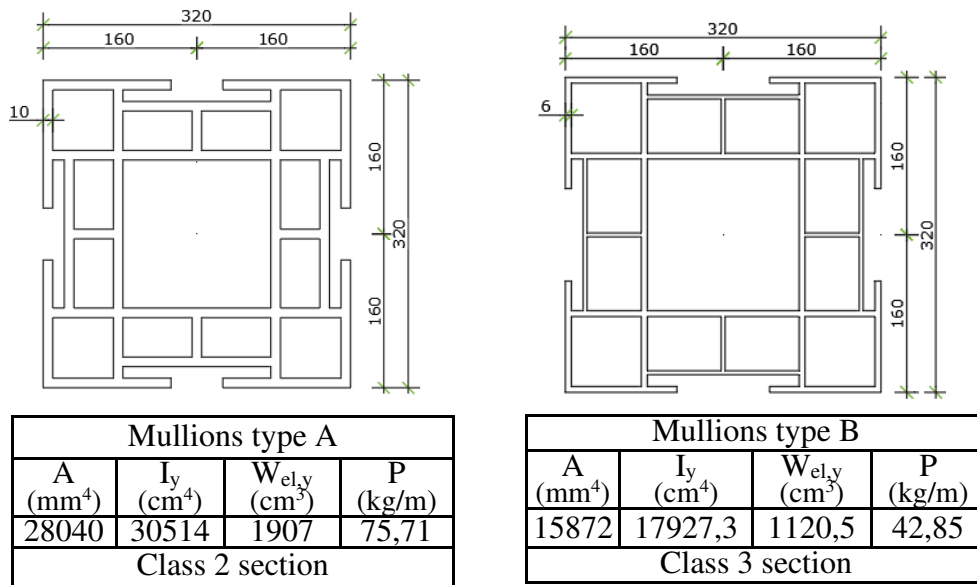


Figure 3.17: Geometrical properties of mullions type A and type B.

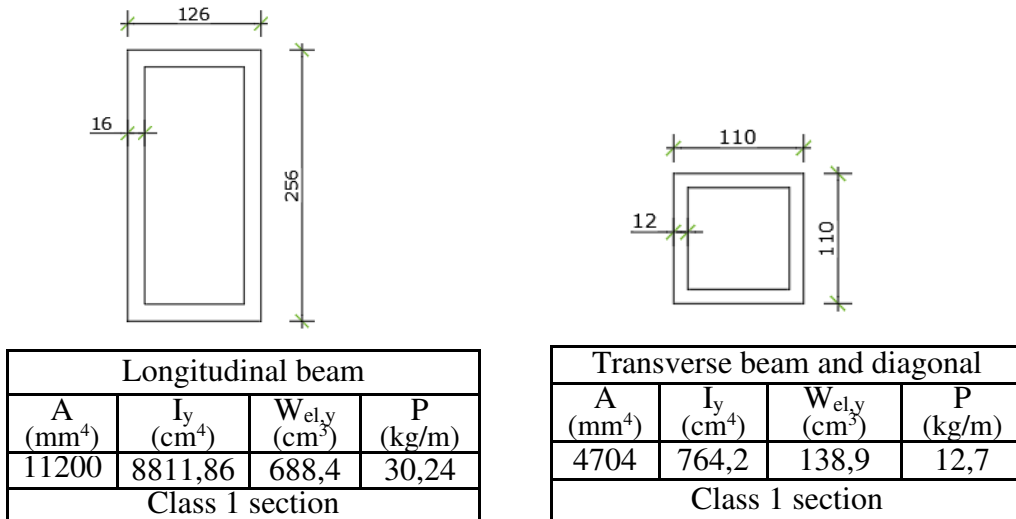


Figure 3.18: Geometrical properties of longitudinal beams and transverse beams and diagonals.

### **3.5 REFERENCES**

[1] Bayat B., Ghazali M. Z. M., Tahir M. (2013) Space shear wall as an innovative seismic resistant system for structures. *International Journal of Civil and Structural Engineering*, 3, 2, p. 203-214.  
doi: 10.6088/ijcser.201304010021

[2] Japan Building Disaster Prevention Association. (2005) *Recent Development of Seismic Retrofit Methods in Japan*.





## *Chapter 4*

# NUMERICAL ANALYSIS FOR CASE STUDY

### 4.1 NUMERICAL MODEL

The numerical analysis of the case study described at chapter 1.6 is performed using Midas Gen software [1]. The finite element model shows the composite structure of the building: the reinforced concrete frames and the masonry stairwells, see Figure 4.1.

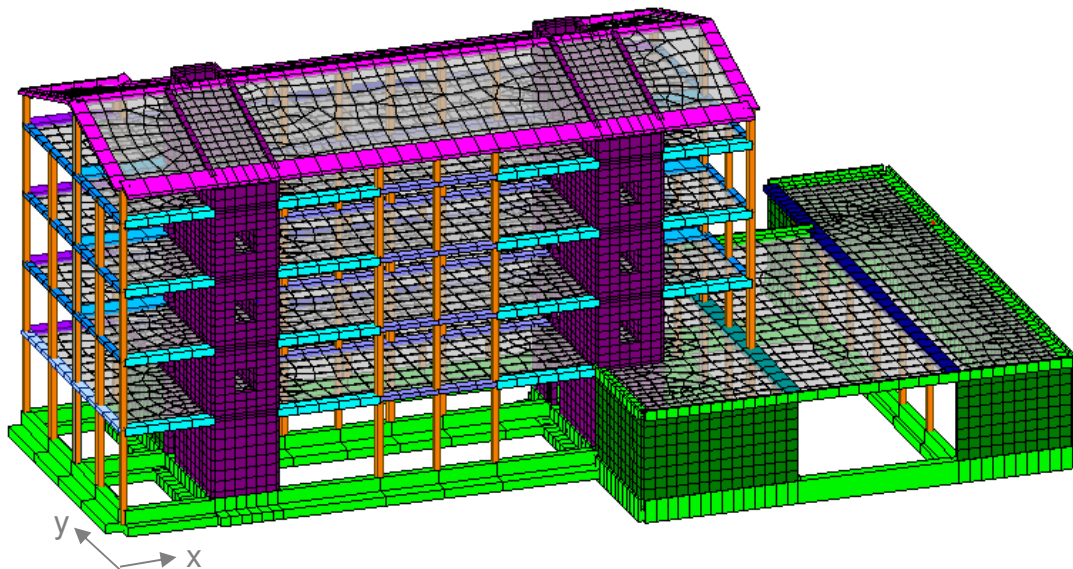


Figure 4.1: The finite element model of the case study developed with Midas Gen software.

Figure 4.2 shows the typical plan of the finite element model of the case study. Figure 4.3 shows the vertical section of the finite element model.

See also Table 1.1 and 1.2 at chapter 1.6 for the geometry and rebars of columns and beams.

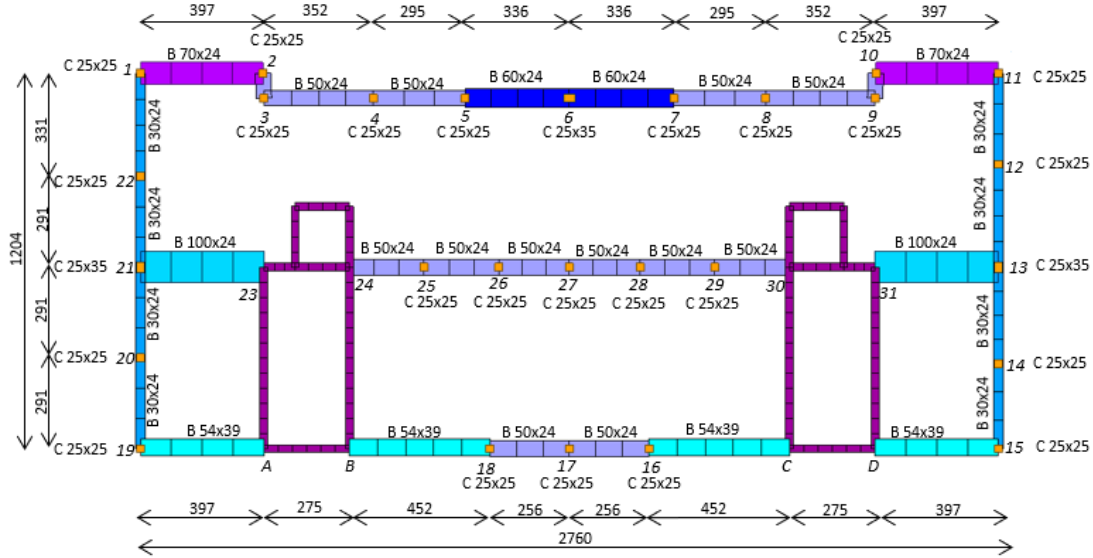


Figure 4.2: Structural plan of the finite element model of the case study – Type plan.

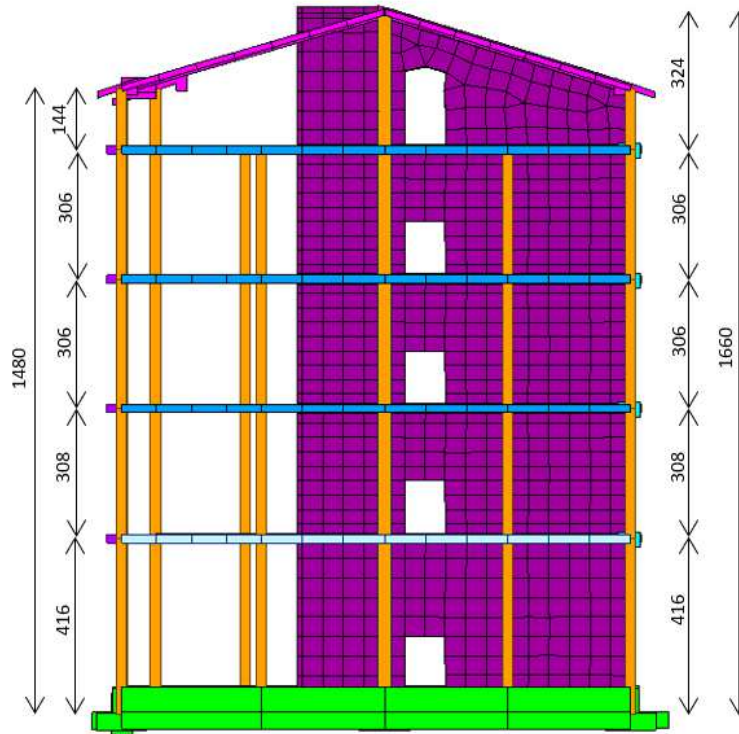


Figure 4.3: Vertical section of the finite element model of the case study.

The frame components are modelled as beam elements, while the masonry stairwells, the slabs and the walls of the additional body intended for garages are modelled as plate elements. The slabs are considered as rigid floor diaphragms being made of reinforced brick concrete with 4 cm slab. The capacities of the building are explored and the verifications are carried out according to the European [2] and the national [3] building codes. The elastic response spectrum of the horizontal components of the seismic action  $S_e(T)$  is defined by the following expressions according to the national standard [3]:

$$0 \leq T < T_B \quad S_e(T) = a_g S \eta F_o \left[ \frac{T}{T_B} + \frac{1}{\eta F_o} \left( 1 - \frac{T}{T_B} \right) \right] \quad (4.1)$$

$$T_B \leq T < T_C \quad S_e(T) = a_g S \eta F_o \quad (4.2)$$

$$T_C \leq T < T_D \quad S_e(T) = a_g S \eta F_o \left( \frac{T_C}{T} \right) \quad (4.3)$$

$$T_D \leq T \quad S_e(T) = a_g S \eta F_o \left( \frac{T_C T_D}{T^2} \right) \quad (4.4)$$

where:

$a_g, F_o$  are the parameters that define the spectral shape and are listed in Table 1.4;

$S$  is the coefficient that considers the soil category and the topographic conditions;

$\eta$  is the damping correction factor  $\eta = \sqrt{10/(5 + \xi)}$ , being  $\xi$  the viscous damping expressed as a percentage;

$T_B$  is the period corresponding to the beginning of the constant acceleration branch of the spectrum;

$T_C$  is the period corresponding to the beginning of the constant velocity branch of the spectrum;

$T_D$  is the period corresponding to the beginning of the constant displacement branch of the spectrum.

For the case study the soil category is  $C$ , the topographic category is  $T_I$  and the viscous damping is 5%.

The design response spectrum is obtained by replacing in the equations (4.1), (4.2), (4.3) and (4.4)  $\eta$  with  $1/q$ , where  $q$  is the behaviour factor. The value of the behaviour factor  $q$  considered in the linear analysis is 1,5 according with chapter C8 for existing building of the circular of the Italian technical standard [4]. The design response spectrum at the Life Safety (LS) and Damage Limitation limit state (DL) are shown in Figure 4.4 and Figure 4.5 respectively.

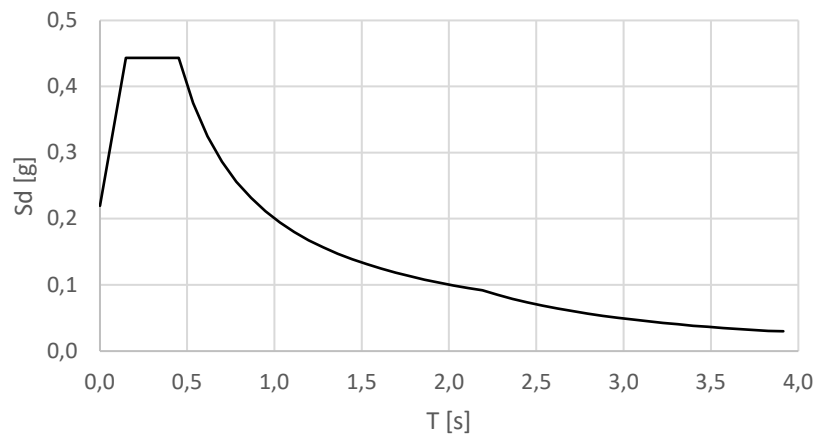


Figure 4.4: Design response spectrum at the Life Safety limit state.

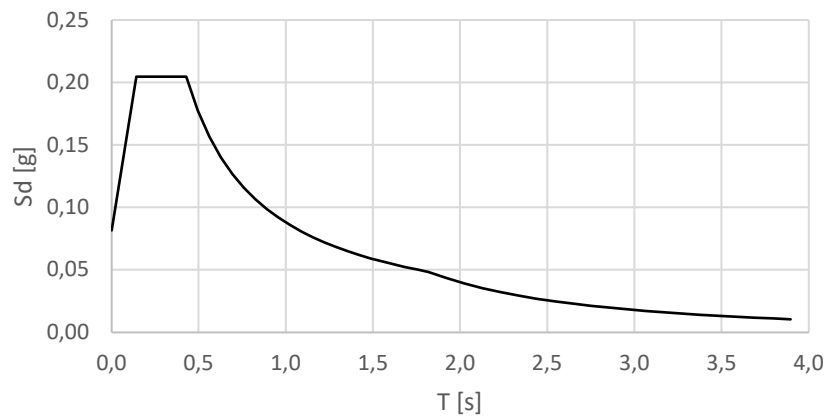


Figure 4.5: Design response spectrum at the Damage Limitation limit state.

The natural period  $T$ , the frequency  $f$  and the modal participation mass  $M$  for the first three vibration modes are listed in Table 4.1. The modal shapes are illustrated in Figure 4.6. The first vibration mode is a translational mode in the longitudinal direction of the building (x direction), the second mode is characterised by a deformation along the shorter side of the building (y direction) and by a rotation along the vertical direction (z direction). The third vibration mode is mainly characterized by a rotation along the vertical direction.

Table 4.1: Natural period, frequency and modal participation mass of the first three vibration modes for the existing building.

Mode	Frequency $f$ [cycle/s]	Period $T$ [s]	$M_x$ [%]	$M_y$ [%]	$M_{\theta_z}$ [%]
1	2,49	0,40	54	0	0
2	4,17	0,24	0	46	17
3	4,55	0,22	0	7	18

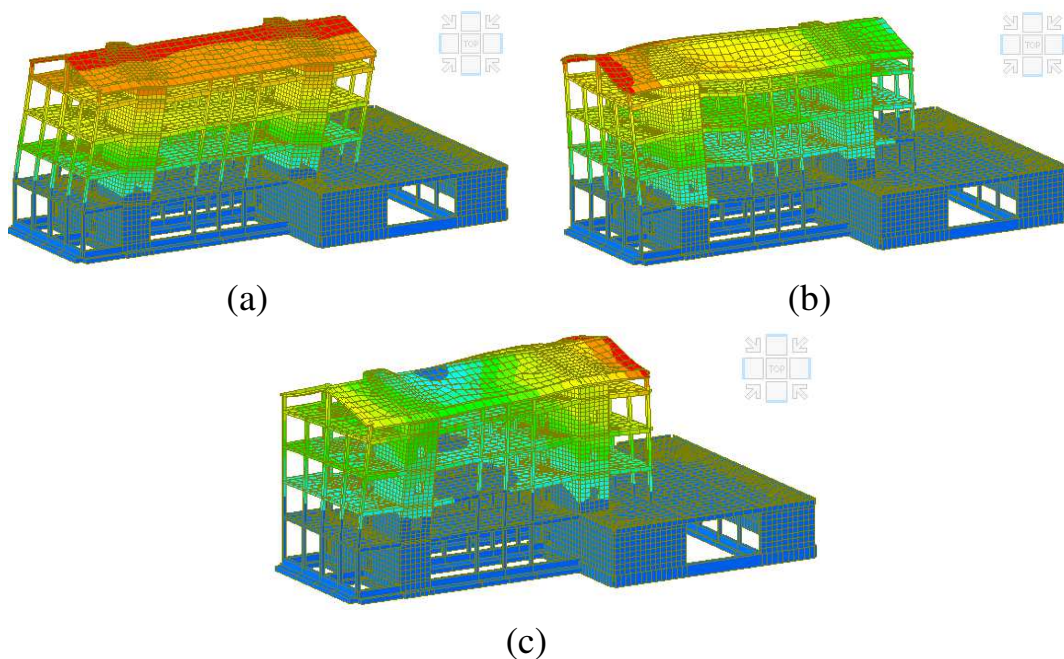


Figure 4.6: Modal shapes of the existing building.

## 4.2 SEISMIC VULNERABILITY WITH LINEAR STATIC ANALYSIS

The seismic vulnerability is based on the definition of the risk index. The risk index of the building is defined, for the linear static analysis, as the ratio between the capacity and the seismic demand in terms of Peak Ground Acceleration (PGA). The seismic demand is the representation of earthquake ground motion and the capacity is the representation of the structure's ability to resist the seismic demand. Referring to the Life Safety (LS) and Damage Limitation limit state (DL), the risk index are defined by the following ratios:

$$\alpha_u = \frac{PGA_{c,LS}}{PGA_{D,LS}} ; \quad \alpha_e = \frac{PGA_{c,DL}}{PGA_{D,DL}}$$

where:

$PGA_{C,LS}$  is the peak ground acceleration determined at the achievement of the Life Safety limit state;

$PGA_{C,DL}$  is the peak ground acceleration determined at the achievement of the Damage Limitation limit state;

$PGA_{D,LS}$  is the peak ground acceleration with probability of exceedance 10% in the reference period  $V_R$ ;

$PGA_{D,DL}$  is the peak ground acceleration with probability of exceedance 63% in the reference period  $V_R$ .

Values close to or greater than one characterize buildings in which the level of risk is close to that require by standards, while low values close to zero characterize high risk buildings. The peak ground acceleration  $PGA_{C,LS}$  and  $PGA_{C,DL}$  are evaluated both for reinforced concrete and masonry. The masonry is the weak element of the structure and the bending and shear verification are evaluated according with the national standard [3, 4]. The bending verification is assessed comparing the design moment with the ultimate resistant moment calculated assuming that the

masonry has no tensile strength. For a rectangular section and a compression diagram with the resistance value equal to  $0,85f_d$ , the ultimate resistant moment can be calculated by the following equation:

$$M_u = \left( l^2 t \frac{\sigma_0}{2} \right) \left( 1 - \frac{\sigma_0}{0.85 f_d} \right) \quad (4.5)$$

where:

$l$  is the overall length of the wall (including the tensile area);

$t$  is the thickness of the compressive zone of the wall;

$\sigma_0$  is the average normal strength, referred to the total area of the section,  $\sigma_0 = N/(l t)$ , with  $N$  the compression axial force;

$f_d$  is the design compressive strength of masonry,  $f_d = \frac{f_m}{\gamma_{MFC}}$ .

For existing buildings, the shear verification for actions in the plane of the masonry wall can be evaluated by the equation:

$$V_t = l t \frac{f_{td}}{b} \sqrt{1 + \frac{\sigma_0}{f_{td}}} \quad (4.6)$$

where:

$l$  is the wall length;

$t$  is the wall thickness;

$\sigma_0$  is the average normal strength, referred to the total area of the section,  $\sigma_0 = N/(l t)$ , with  $N$  the compression axial force;

$f_{td}$  is the design value of tensile strength for diagonal cracking,  $f_{td} = 1,5 \tau_{0d}$ , with  $\tau_{0d}$  the design shear strength of the masonry;

$b$  is a corrective coefficient correlated to the distribution of stresses on the section, depending on the wall slenderness. It can be assumed equal to  $h/l$ , in any case lower than 1,5 and higher than 1, with  $h$  the height of the wall.

The first RC columns that reach the bending capacity at the Life Safety limit state are those at the fourth floor. The risk index  $\alpha_u$  at LS limit state is 0,50. The presence of very slender masonry piers subjected to low compression axial forces, leads to the achievement of the considered limit

states for low values of peak ground acceleration. The results are presented in Table 4.2.

Table 4.2: PGA values and risk index for masonry piers evaluated in both directions with linear analysis for the existing building.

Limit state	Element	PGA <sub>C-X</sub> [g]	PGA <sub>C-Y</sub> [g]	PGA <sub>D</sub> [g]	α <sub>X</sub> [-]	α <sub>Y</sub> [-]
LS	Masonry piers - shear	0,066	0,198	0,22	0,30	0,90
	Masonry piers - bending	0,048	0,11	0,22	0,22	0,50
DL	Masonry piers - shear	0,0492	0,082	0,082	0,60	1,00
	Masonry piers - bending	0,0328	0,082	0,082	0,40	1,00

The risk index of the building is determined by the achievement of the bending capacity of masonry piers evaluated with equation (4.5). The risk index of the building at the LS limit is  $\alpha_{u,X} = 0,22$  in the longitudinal direction (x direction) and  $\alpha_{u,Y} = 0,50$  in the transverse direction (y direction). The seismic risk class of the existing building can be evaluated according to the Annex A of the national standard [5]. The seismic risk assessment refers to two parameters: the risk index at the LS limit state, also called safety index IS-V, and the annual average expected loss PAM. The PAM is an economic parameter which considers the economic losses associated with damage to the structural and non-structural elements referring to the reconstruction costs of the building (CR). Eight seismic risk classes are defined from the class A<sup>+</sup> of lower risk to the class G of highest risk. Once the capacity peak ground acceleration at LS and DL are known, the corresponding return periods  $T_{rC}$  can be determined by the following equation:

$$T_{rC} = T_{rD} (PGA_C / PGA_D)^\eta \quad (4.7)$$

where  $\eta = 1/0,41$ .

For each of the identified return periods, the value of the exceeding annual average frequency is determined by  $\lambda = 1/T_{rC}$ .



For the Operational and Near Collapse limit states, the following values of  $\lambda$  can be attributed:

$$\lambda_O = 1,67 \lambda_{DL} ; \lambda_{NC} = 0,49 \lambda_{LS} \quad (4.8)$$

Other two limit states are defined: the Starting Damage limit state, to which are associated no economic losses and the Reconstruction limit state to which is associated an economic loss equal to 100%. Table 4.3 defines the value of the percentage of the reconstruction cost for each of the considered limit states.

Table 4.3: Percentage of reconstruction cost for each limit state.

Limit state	Reconstruction cost $CR$
Reconstruction	100%
Near Collapse	80%
Life Safety	50%
Damage Limitation	15%
Operational	7%
Starting Damage	0%

The PAM parameter is evaluated by the area subtended by the piecewise curve identified by points  $(\lambda, CR)$  for each of the limit states by the following expression:

$$PAM = \sum_{i=2}^5 [\lambda(SL_i) - \lambda(SL_{i-1})] \cdot \frac{[CR(SL_i) + CR(SL_{i-1})]}{2} + \lambda(SLC) \cdot CR(SLR) \quad (4.9)$$

The evaluation of the PAM parameter for the existing building is represented in Figure 4.7.

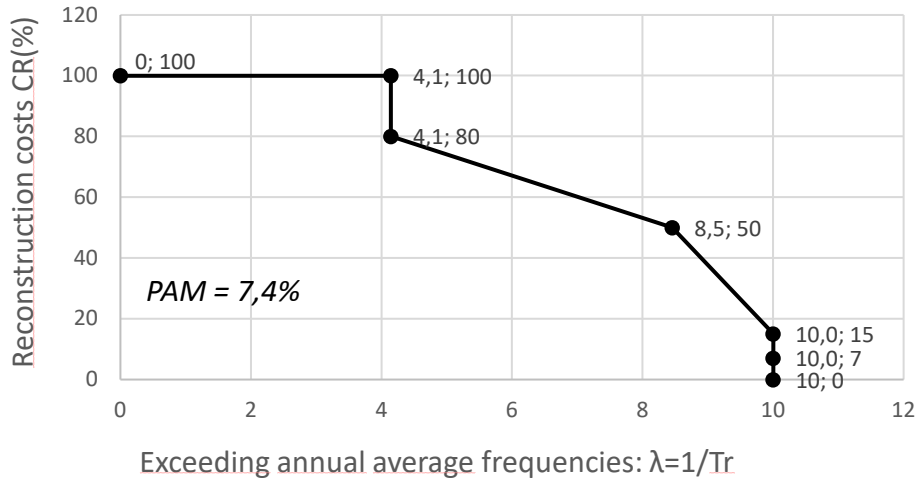


Figure 4.7: Evaluation of the annual average expected loss parameter (PAM) for the existing building.

The IS-V class based on the safety index, calculated as the ratio between  $PGA_{C,LS}$  and  $PGA_{D,LS}$ , is determined by Table 4.4. The PAM class is determined by Table 4.5. The seismic risk class of the building is the lower between the two classes.

Table 4.4: Assignment of the IS-V class based on the safety index.

Security index	IS-V class
$100\% < IS-V$	$A^+_{IS-v}$
$80\% \leq IS-V < 100\%$	$A_{IS-v}$
$60\% \leq IS-V < 80\%$	$B_{IS-v}$
$45\% \leq IS-V < 60\%$	$C_{IS-v}$
$30\% \leq IS-V < 45\%$	$D_{IS-v}$
$15\% \leq IS-V < 30\%$	$E_{IS-v}$
$IS-V \leq 15\%$	$F_{IS-v}$

Table 4.5: Assignment of the PAM class based on the annual average expected losses.

Annual average expected loss	PAM class
$PAM \leq 0,50\%$	$A^+_{PAM}$
$0,50\% < PAM \leq 1,0\%$	$A_{PAM}$
$1,0\% < PAM \leq 1,5\%$	$B_{PAM}$
$1,5\% < PAM \leq 2,5\%$	$C_{PAM}$
$2,5\% < PAM \leq 3,5\%$	$D_{PAM}$
$3,5\% < PAM \leq 4,5\%$	$E_{PAM}$
$4,5\% < PAM \leq 7,5\%$	$F_{PAM}$
$7,5\% \leq PAM$	$G_{PAM}$

The seismic risk class of the existing building appears to be class F.

### 4.3 SEISMIC VULNERABILITY WITH NONLINEAR STATIC ANALYSIS

Building loaded beyond elastic range can be analysed with nonlinear static analysis (pushover analysis). The pushover analysis procedure is considered as one of the powerful tools for performance evaluation of buildings with respect to objectives set in performance-based earthquake engineering. The modelling is one of the important steps to be considered while conducting pushover analysis. Appropriate model requires the determination of the nonlinear properties of each component in the structure that are quantified by strength and deformation capacities. In the pushover analysis the equivalent frame modelling for the masonry is assumed. Midas Gen software is not a specific program for masonry, so it is necessary to manually create the equivalent frame. The method proposed by Dolce (1989) is used to define the equivalent frame. The masonry pier is supposed to be constituted by a deformable central part having a finite resistance and by two infinitely rigid parts at the ends. The height of the deformable part, or effective height  $H_{eff}$ , takes into account the deformability of the masonry at the ends and in the central wall between two openings. The effective height  $H_{eff}$  can be defined as:

$$H_{eff} = h' + \frac{l(H' - h')}{3h'} \leq H' \quad (4.10)$$

where:

$H'$  is the inter-storey height;

$l$  is the masonry pier length;

$h'$  is a conventional parameter of height.

The masonry piers and spandrels are modelled as beam elements. The infinitely rigid parts at the ends of the masonry piers are modelled as rigid links. Figure 4.8 shows the finite element model of the case study in order to perform the nonlinear analysis.

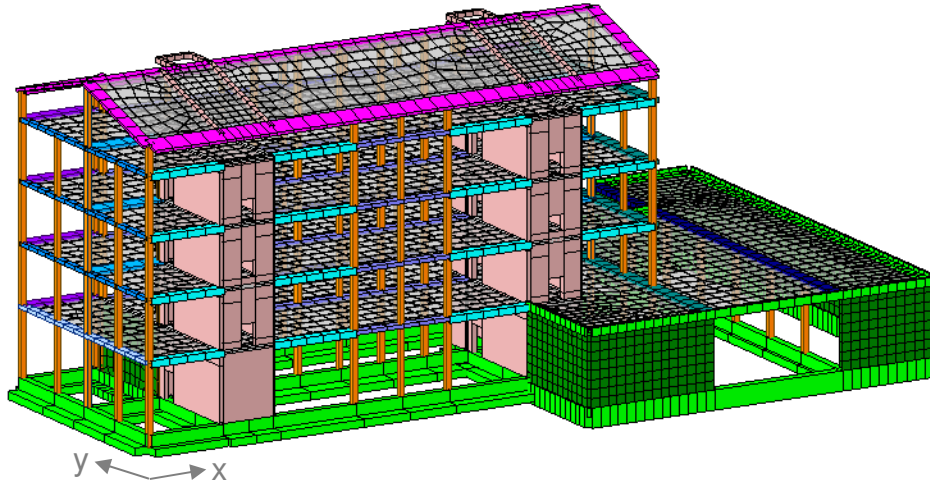


Figure 4.8: The finite element model for nonlinear analysis.

The linear analysis showed that the masonry represents the weak element of the building and that RC column and beams do not exhibit brittle failure for shear. For the nonlinear static analysis, the shear verification of the columns was carried out on the most stressed section. The value of the shear force acting on the section is equal to 50 KN and the design shear resistance is equal to 83 KN. Modelling the inelastic behaviour of the structural elements for different levels of performance is an important step towards performance evaluation of building. The inelastic behaviour of reinforced concrete and masonry is accounted for by means of lumped plastic hinges.

#### 4.3.1 Inelastic deformation capacity of reinforced concrete

For reinforced concrete beams and columns, the capacity is defined in terms of ultimate chord rotation  $\theta_u$ . The national standard and Eurocode 8 define the ultimate rotational capacity at Near Collapse limit state by the following equation:

$$\theta_{um} = \frac{1}{\gamma_{el}} 0,016(0,3^v) \left[ \frac{\max(0,01;\omega')}{\max(0,01;\omega)} f_c \right]^{0,225} \left( \min \left( 9; \frac{L_v}{h} \right) \right)^{0,35} 25^{\left( \alpha \rho_{sx} \frac{f_{yw}}{f_c} \right)} (1,25^{100\rho_d}) \quad (4.11)$$

where:

$\gamma_{el}$  is equal to 1,5 for primary seismic elements and to 1,0 for secondary seismic elements;

$h$  is the depth of cross-section;

$L_v = M/V$  is the ratio moment/shear at the end section;

$v = N/bhf_c$  ( $b$  width of compression zone,  $N$  axial force positive for compression);

$\omega, \omega'$  is the mechanical reinforcement ratio of the tension and compression, respectively, longitudinal reinforcement;

$f_c$  and  $f_{yw}$  are the concrete compressive strength and the stirrup yield strength, respectively;

$\rho_{sx} = A_{sx}/b_w s_h$  is the ratio of transverse steel parallel to the direction  $x$  of loading ( $s_h$  is the stirrup spacing);

$\rho_d$  is the steel ratio of diagonal reinforcement in each diagonal direction;

$\alpha$  is the confinement effectiveness factor, that may be taken equal to:

$$\alpha = \left(1 - \frac{s_h}{2b_o}\right) \left(1 - \frac{s_h}{2h_o}\right) \left(1 - \frac{\sum b_i^2}{6h_o b_o}\right)$$

( $b_o$  and  $h_o$  is the dimension of confined core to the centreline of the hoop,  $b_i$  is the spacing of longitudinal bars laterally restrained by a stirrup corner or a cross-tie along the perimeter of the cross-section).

The chord rotation capacity corresponding to Life Safety limit state may be assumed to be  $\frac{3}{4}$  of the ultimate chord rotation  $\theta_u$ .

In the American guidelines FEMA 356 [6] the capacity is expressed in terms of chord rotation. The chord rotation  $\theta$  is the summation of yield rotation  $\theta_y$  plus plastic rotation  $\theta_p$ . The generalized load-deformation relation is shown in Figure 4.9. The load-deformation relation shall be described by linear response from A to an effective yield B, then a linear response at reduced stiffness from point B to C, then sudden reduction in lateral load resistance to point D, then response at reduced resistance to E, and final loss of resistance thereafter. Typically, the responses shown in Figure 4.9 are associated with flexural response and the resistance  $Q/Q_y = 1,0$  is the yield value followed by strain hardening. When the response is associated with shear, the resistance  $Q/Q_y = 1,0$  is the value at which the

design shear strength is reached, and no strain hardening follows. The deformations used for the load-deformation relation shall be defined in one of two ways, as follows:

- (a) Deformation, or Type I. In this curve, deformations are expressed directly using terms such as strain, curvature, rotation, or elongation. The parameters  $a$  and  $b$  shall refer to the plastic deformation. The parameter  $c$  is the reduced resistance after the sudden reduction from C to D. Parameters  $a$ ,  $b$  and  $c$  are defined numerically in various tables.
- (b) Deformation ratio, or Type II. In this curve, deformations are expressed in terms such as shear angle and tangential drift ratio. The parameters  $d$  and  $e$  refer to total deformations measured from the origin. Parameters  $c$ ,  $d$  and  $e$  are defined numerically in various tables.

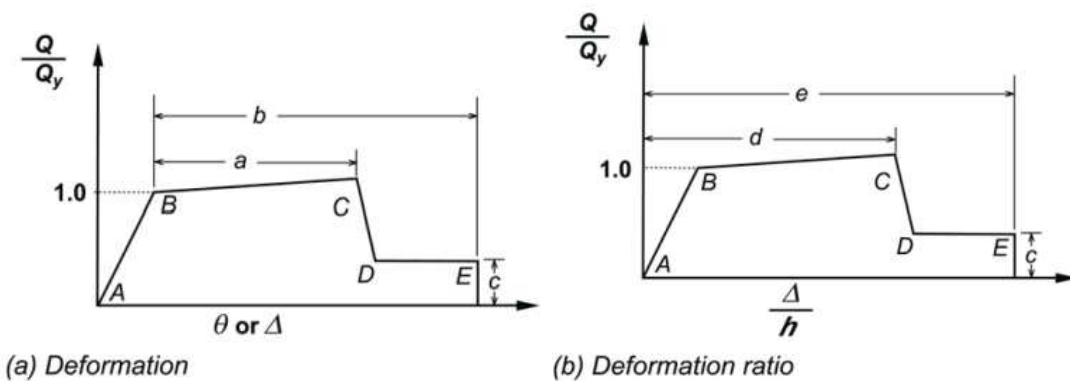


Figure 4.9: Generalized Force-Deformation relations for concrete elements [6].

For reinforced concrete beams and columns the generalized deformation in Figure 4.9 is the chord rotation. The parameter  $a$ ,  $b$  and  $c$  are defined in Table 6-7 and Table 6-8 of FEMA 356 for beams and columns (see Figure 4.10 and 4.11). Tables includes also the acceptance criteria for the three limit states:

- Immediate Occupancy (IO), corresponding to Damage Limitation (DL) level of Eurocode;
- Life Safety (LS), corresponding to Significant Damage (SD) level of Eurocode;

- Collapse prevention (CP), corresponding to the Near Collapse (NC) level of Eurocode.

Acceptable limiting values have been specified for primary or secondary components of the structural system as a function of the type of reinforcement, axial and shear force levels and detailing of RC members.

**Table 6-7 Modeling Parameters and Numerical Acceptance Criteria for Nonlinear Procedures—Reinforced Concrete Beams**

Conditions	Modeling Parameters <sup>3</sup>					Acceptance Criteria <sup>3</sup>				
	Plastic Rotation Angle, radians			Residual Strength Ratio		Plastic Rotation Angle, radians				
						Performance Level				
	a			b		c		Component Type		
								Primary		Secondary
IO			LS		CP		LS		CP	
<b>i. Beams controlled by flexure<sup>1</sup></b>										
$\frac{\rho - \rho'}{\rho_{bal}}$	Trans. Reinf. <sup>2</sup>	$\frac{V}{b_w d_n \sqrt{f'_c}}$								
≤ 0.0	C	≤ 3	0.025	0.05	0.2	0.010	0.02	0.025	0.02	0.05
≤ 0.0	C	≥ 6	0.02	0.04	0.2	0.005	0.01	0.02	0.02	0.04
≥ 0.5	C	≤ 3	0.02	0.03	0.2	0.005	0.01	0.02	0.02	0.03
≥ 0.5	C	≥ 6	0.015	0.02	0.2	0.005	0.005	0.015	0.015	0.02
≤ 0.0	NC	≤ 3	0.02	0.03	0.2	0.005	0.01	0.02	0.02	0.03
≤ 0.0	NC	≥ 6	0.01	0.015	0.2	0.0015	0.005	0.01	0.01	0.015
≥ 0.5	NC	≤ 3	0.01	0.015	0.2	0.005	0.01	0.01	0.01	0.015
≥ 0.5	NC	≥ 6	0.005	0.01	0.2	0.0015	0.005	0.005	0.005	0.01
<b>ii. Beams controlled by shear<sup>1</sup></b>										
Stirrup spacing ≤ d/2			0.0030	0.02	0.2	0.0015	0.0020	0.0030	0.01	0.02
Stirrup spacing > d/2			0.0030	0.01	0.2	0.0015	0.0020	0.0030	0.005	0.01
<b>iii. Beams controlled by inadequate development or splicing along the span<sup>1</sup></b>										
Stirrup spacing ≤ d/2			0.0030	0.02	0.0	0.0015	0.0020	0.0030	0.01	0.02
Stirrup spacing > d/2			0.0030	0.01	0.0	0.0015	0.0020	0.0030	0.005	0.01
<b>iv. Beams controlled by inadequate embedment into beam-column joint<sup>1</sup></b>										
			0.015	0.03	0.2	0.01	0.01	0.015	0.02	0.03

1. When more than one of the conditions i, ii, iii, and iv occurs for a given component, use the minimum appropriate numerical value from the table.
2. "C" and "NC" are abbreviations for conforming and nonconforming transverse reinforcement. A component is conforming if, within the flexural plastic hinge region, hoops are spaced at ≤ d/3, and if, for components of moderate and high ductility demand, the strength provided by the hoops ( $V_h$ ) is at least three-fourths of the design shear. Otherwise, the component is considered nonconforming.
3. Linear interpolation between values listed in the table shall be permitted.

Figure 4.10: Modelling parameters and numerical acceptance criteria for nonlinear analysis for reinforced concrete beams [6].



**Table 6-8 Modeling Parameters and Numerical Acceptance Criteria for Nonlinear Procedures—Reinforced Concrete Columns**

Conditions	Modeling Parameters <sup>4</sup>					Acceptance Criteria <sup>4</sup>				
	Plastic Rotation Angle, radians		Residual Strength Ratio			Plastic Rotation Angle, radians				
						Performance Level				
	a		b			c			Component Type	
									Primary	
IO		LS		CP		LS		CP		
<b>i. Columns controlled by flexure<sup>1</sup></b>										
$\frac{P}{A_g f'_c}$	Trans. Reinf. <sup>2</sup>	$\frac{V}{b_w d_s \sqrt{f'_c}}$								
≤ 0.1	C	≤ 3	0.02	0.03	0.2	0.005	0.015	0.02	0.02	0.03
≤ 0.1	C	≥ 6	0.016	0.024	0.2	0.005	0.012	0.016	0.016	0.024
≥ 0.4	C	≤ 3	0.015	0.025	0.2	0.003	0.012	0.015	0.018	0.025
≥ 0.4	C	≥ 6	0.012	0.02	0.2	0.003	0.01	0.012	0.013	0.02
≤ 0.1	NC	≤ 3	0.006	0.015	0.2	0.005	0.005	0.006	0.01	0.015
≤ 0.1	NC	≥ 6	0.005	0.012	0.2	0.005	0.004	0.005	0.008	0.012
≥ 0.4	NC	≤ 3	0.003	0.01	0.2	0.002	0.002	0.003	0.006	0.01
≥ 0.4	NC	≥ 6	0.002	0.008	0.2	0.002	0.002	0.002	0.005	0.008
<b>ii. Columns controlled by shear<sup>1, 3</sup></b>										
All cases <sup>5</sup>			—	—	—	—	—	—	.0030	.0040
<b>iii. Columns controlled by inadequate development or splicing along the clear height<sup>1, 3</sup></b>										
Hoop spacing ≤ d/2			0.01	0.02	0.4	0.005	0.005	0.01	0.01	0.02
Hoop spacing > d/2			0.0	0.01	0.2	0.0	0.0	0.0	0.005	0.01
<b>iv. Columns with axial loads exceeding 0.70P<sub>o</sub><sup>1, 3</sup></b>										
Conforming hoops over the entire length			0.015	0.025	0.02	0.0	0.005	0.01	0.01	0.02
All other cases			0.0	0.0	0.0	0.0	0.0	0.0	0.0	0.0

1. When more than one of the conditions i, ii, iii, and iv occurs for a given component, use the minimum appropriate numerical value from the table.
2. "C" and "NC" are abbreviations for conforming and nonconforming transverse reinforcement. A component is conforming if, within the flexural plastic hinge region, hoops are spaced at ≤ d/3, and if, for components of moderate and high ductility demand, the strength provided by the hoops ( $V_s$ ) is at least three-fourths of the design shear. Otherwise, the component is considered nonconforming.
3. To qualify, columns must have transverse reinforcement consisting of hoops. Otherwise, actions shall be treated as force-controlled.
4. Linear interpolation between values listed in the table shall be permitted.
5. For columns controlled by shear, see Section 6.5.2.4.2 for acceptance criteria.

**Figure 4.11: Modelling parameters and numerical acceptance criteria for nonlinear analysis for reinforced concrete columns [6].**

The default moment-rotation hinge properties for RC beams and columns implemented in Midas Gen and used for the nonlinear analysis are shown in Figure 4.12. The acceptance criteria for the three limit states IO, LS and CP are shown in Figure 4.13. For IO limit state, the acceptable chord rotation is taken as 2 times the yield rotation  $\theta_y$ , for LS the acceptable chord rotation is  $4\theta_y$  and for CP is  $6\theta_y$ .

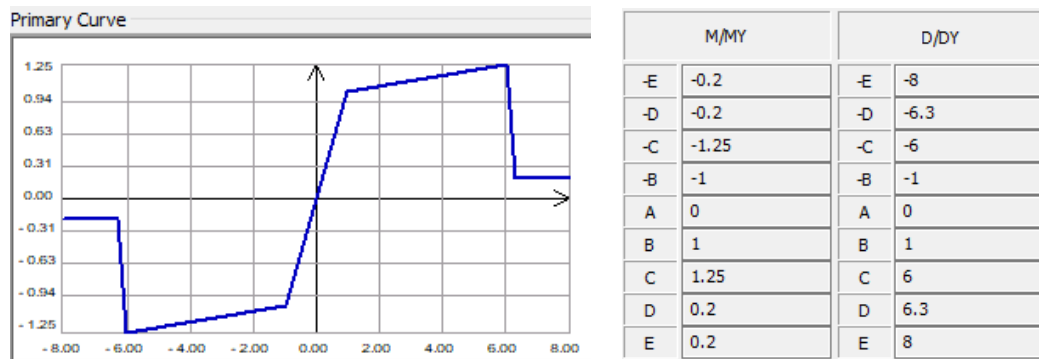


Figure 4.12: Default moment-rotation hinge properties for RC beams and columns implemented in Midas Gen.

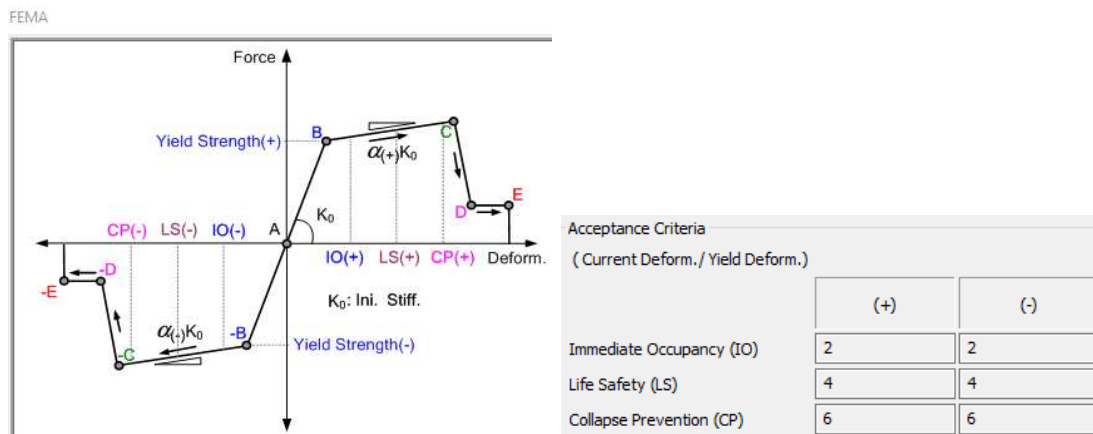


Figure 4.13: Acceptance criteria for RC beams and columns in Midas Gen.

### 4.3.2 Inelastic deformation capacity of masonry

For masonry, the capacity is defined in terms of drift  $\delta$  that is the ratio between the horizontal displacement and the height of the wall. Current codes propose different empirical models for the drift capacity of unreinforced masonry walls, which includes a number of factors including the failure mode, the slenderness, the aspect ratio, the axial load ratio and the normalized shear span. The Italian standard [3, 4] connects the drift capacity to the failure mode of the wall. At the Near Collapse limit state, the drift capacity is 0,5% for shear failure and 1,0% for flexural failure. The drift capacity at the Life Safety limit state is taken equal to 3/4 the

values at NC. EC8 [2] states that unreinforced masonry walls failing in shear have a drift capacity of 0,4% for primary seismic walls and 0,6% for secondary ones at Significant Damage limit state. For walls failing in flexure, EC8 propose drift values that increase linearly with the slenderness ratio  $H_0/D$ , where  $H_0$  is the distance between the section where the flexural capacity is attained and the contraflexure point and  $D$  is the depth of the wall. At the SD limit state, the drift capacity is equal to  $0,8\% H_0/D$  for primary seismic walls and  $1,2\% H_0/D$  for secondary ones. At the NC limit state, the drift capacity is equal to  $4/3$  of the values at SD. FEMA 356 assumes the generalized force-deformation relation shown in Figure 4.14. The parameters  $c$ ,  $d$  and  $e$  are defined in Table 7.4 of FEMA 356 for unreinforced masonry walls (see Figure 4.15).

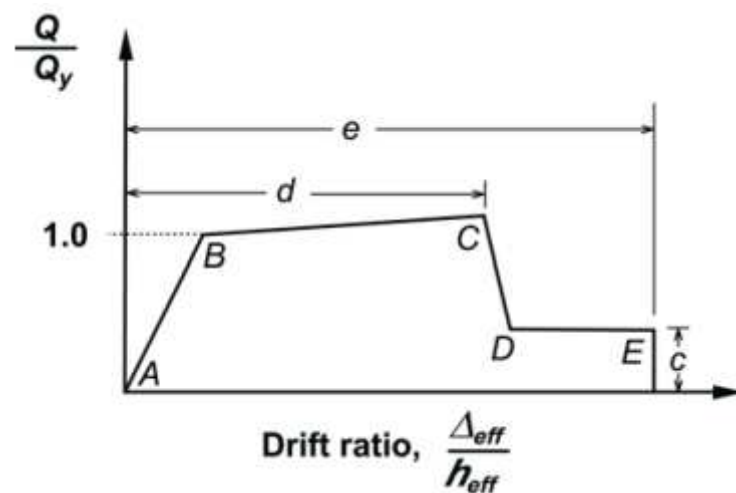


Figure 4.14: Generalized force-deformation relation for masonry [6].

A rotational plastic hinge at both ends and a shear plastic hinge in the middle is assigned at each masonry pier. The default hinge properties for masonry elements implemented in Midas Gen according with FEMA 356 are used in the nonlinear analysis. For the case study building, with the values of masonry characteristics reported in Figure 4.16, the capacity drift is 0,4% for shear failure and 0,6% for flexure failure (see Figure 4.17 and 4.18).

**Table 7-4 Nonlinear Static Procedure—Simplified Force-Deflection Relations for URM In-Plane Walls and Piers**

Limiting Behavioral Mode	Acceptance Criteria							
	Performance Level							
	c %	d %	e %	IO %	Primary		Secondary	
LS %					CP %	LS %	CP %	
Bed-Joint Sliding	0.6	0.4	0.8	0.1	0.3	0.4	0.6	0.8
Rocking	0.6	$0.4h_{eff}/L$	$0.8h_{eff}/L$	0.1	$0.3h_{eff}/L$	$0.4h_{eff}/L$	$0.6h_{eff}/L$	$0.8h_{eff}/L$

Interpolation shall be used between table values.

Figure 4.15: Modelling parameters and numerical acceptance criteria for nonlinear analysis for unreinforced masonry walls [6].

**Masonry Properties**

Building Type  
 New Buildings       Existing Buildings

Compressive Strength (fm)       N/mm<sup>2</sup>

Shear Strength (t0)       N/mm<sup>2</sup>

Vertical Stress Distribution Coefficient (k)

Figure 4.16: Masonry properties of the existing building for the nonlinear analysis.

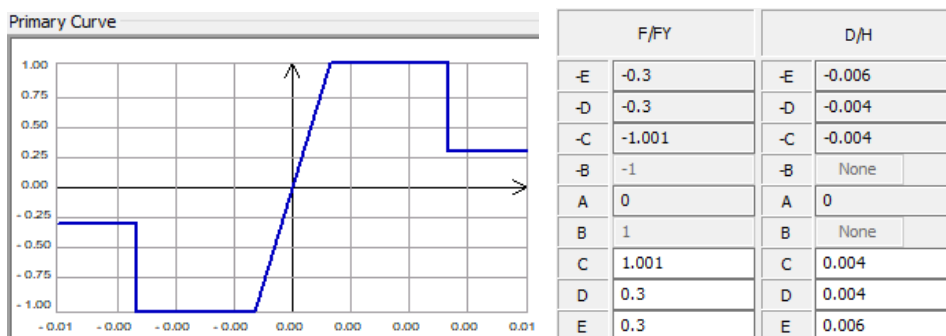


Figure 4.17: Default hinge properties for masonry failing in shear in Midas Gen.

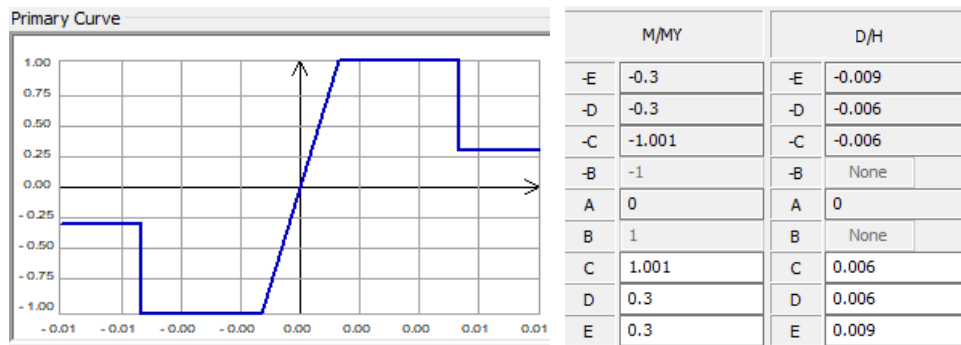


Figure 4.18: Default hinge properties for masonry failing in bending in Midas Gen.

### 4.3.3 Sensitivity of the pushover curve

Considering the plastic hinge properties for RC and masonry defined previously, the base shear-top displacement curves for the two directions are shown in Figure 4.19 and 4.20. In the weak direction of the masonry (x direction) both the base shear capacity and the ultimate displacement are lower.

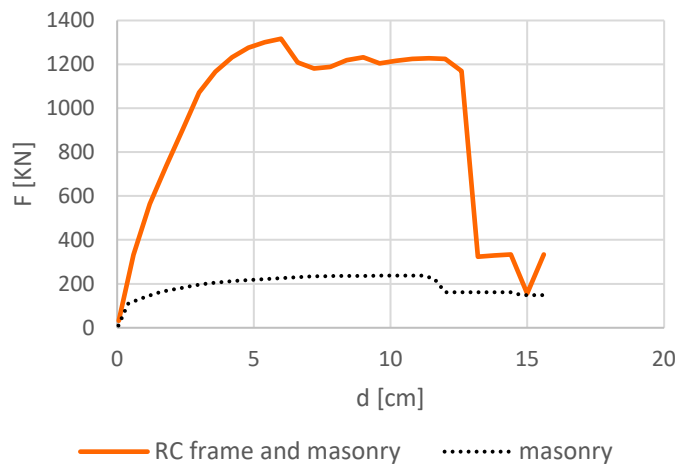


Figure 4.19: Capacity curve in x direction for the existing building.

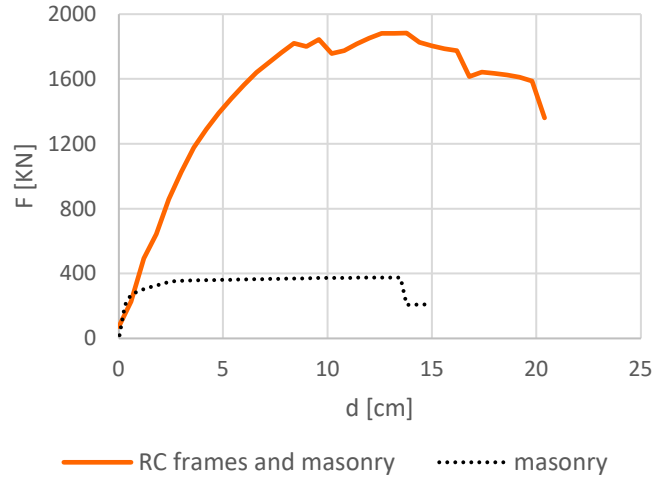


Figure 4.20: Capacity curve in y direction for the existing building.

The nonlinear analysis of the existing building is conducted according to the N2 method formulated by P. Fajfar to which the Italian standard [4] allows to reference. The base shear and the displacement of the equivalent SDOF system are obtained by the equations:

$$F^* = F/\Gamma \quad (4.12)$$

$$d^* = d/\Gamma \quad (4.13)$$

where:

$F$  is the base shear of the MDOF system;

$d$  is the displacement of the MDOF system;

$\Gamma$  is the participation factor defined by:

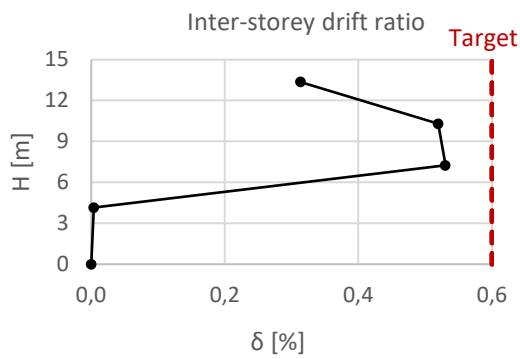
$$\Gamma = \frac{\varphi^T M \tau}{\varphi^T M \varphi} \quad (4.14)$$

with  $\tau$  the vector corresponding to the considered earthquake direction,  $\varphi$  the vector of the fundamental vibration mode of MDOF system normalized considering  $d=1$  and  $M$  the matrix of masses of MDOF system. The capacity curve of the equivalent SDOF system is replaced by a bilinear curve having an elasto-plastic force-displacement relationship. The elastic part is defined by imposing the correspondence between the actual curve and the approximate one at the 60% of the actual curve maximum force. The yield force is defined by imposing the area

equivalence between the two curves in the range defined by the displacement corresponding to the reduction of 15% of the maximum force of the actual curve. In the sensitivity study of the pushover curves, the ultimate displacement obtained from the curves equal to 12 cm in x direction and 20 cm in y direction was first considered. With this assumption, a behaviour factor  $q$  of the existing building equal to 4,06 in x direction and 3,77 in y direction is obtained. These values of ultimate displacement don't seem to be realistic and reliable. In fact, observing the development of plastic hinges it is possible to notice that all masonry piers achieved the drift capacity for bending and some RC columns at the first floor reached the ultimate rotation. It is therefore necessary to define specific design targets. Table 4.6 shows the limitations of inter-storey drift recommended by [6] for concrete frames and unreinforced masonry walls for each limit states. A maximum inter-storey drift equal to 0,6% for the Life Safety limit state is assumed. The drift target corresponds to a storey displacement at the top floor of 4,2 cm (see Figure 4.21). Figure 4.22a shows the pushover curve in x direction and the displacement target. The reliability of the design target can be confirmed by observing the development of the plastic hinges. At a displacement of 4,2 cm only few masonry piers of the left stairwells reach the ultimate drift for bending and they are no longer resistant to horizontal forces but only to vertical loads. After this displacement target value, all masonry piers fail for bending step by step until the formation of plastic hinges on concrete columns leading to the formation of the weak floor at the first storey (see Figure 4.22b, c and d). In Figure 4.23 the pushover curve in y direction with the displacement target and the development of the plastic hinges are represented. The curve  $F^*-d^*$  of SDOF system and the bilinear equivalent curve are shown in Figure 4.24 for both the main direction. The behaviour factor  $q$  of 1,5 in x direction and 1,2 in y direction is obtained.

Table 4.6: Maximum inter-storey drift according to FEMA 356.

Elements	Structural performance levels		
	Collapse prevention	Life safety	Immediate Occupancy
Concrete frames	drift 4%	drift 2%	drift 1%
Unreinforced masonry walls	drift 1%	drift 0,6%	drift 0,3%

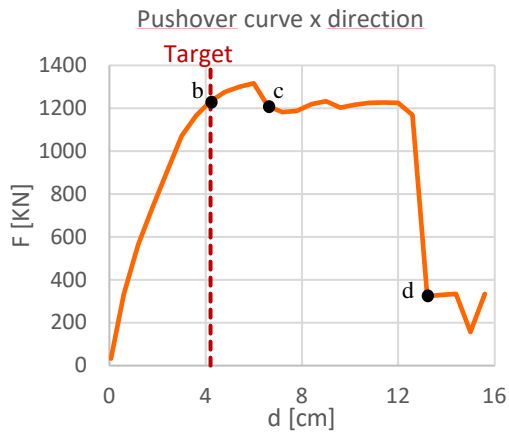


(a)

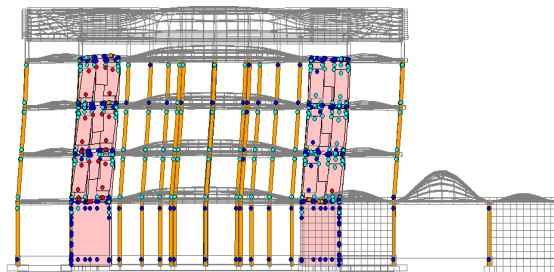


(b)

Figure 4.21: (a) Inter-storey drift; (b) storey displacement for the existing building.



(a)



(b)



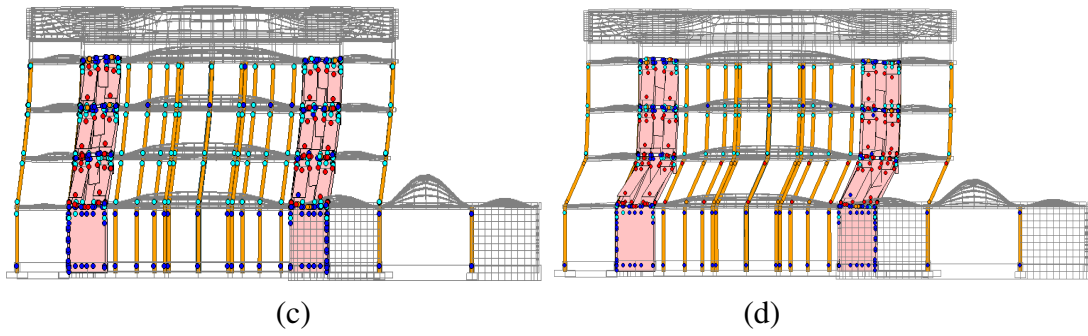


Figure 4.22: (a) Pushover curve in x direction and displacement target for the existing building; (b,c,d) development of plastic hinges in the corresponding points of the curve.

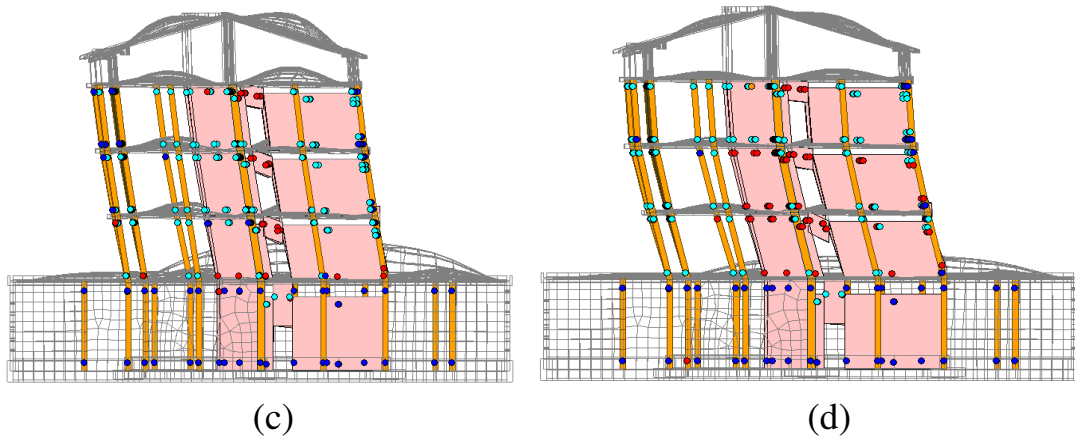
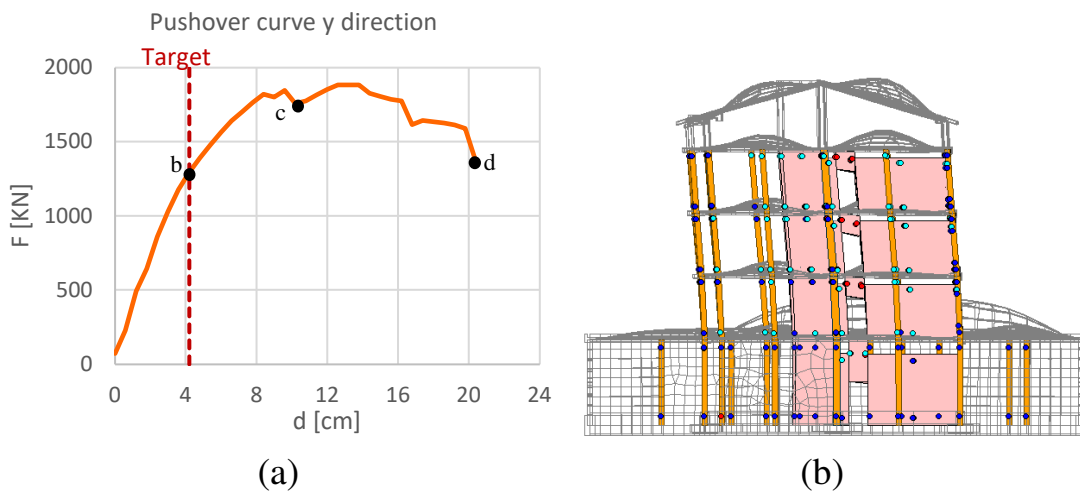


Figure 4.23: (a) Pushover curve in y direction and displacement target for the existing building; (b,c,d) development of plastic hinges in the corresponding points of the curve.

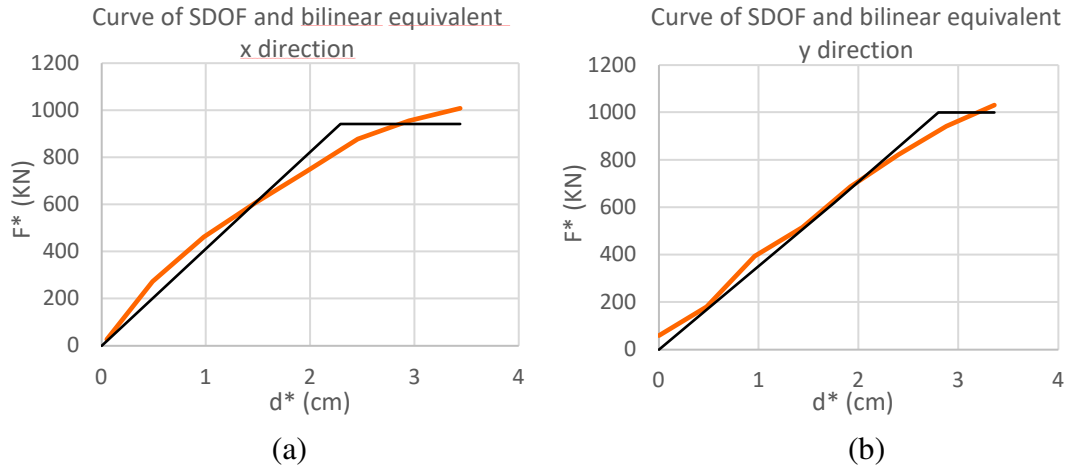


Figure 4.24: Curve of the SDOF system and bilinear equivalent curve for the existing building. (a) x direction; (b) y direction.

The fundamental period of the equivalent SDOF system is given by:

$$T^* = 2\pi \sqrt{\frac{m^*}{k^*}} \quad (4.15)$$

where:

$m^* = \varphi M \tau$  and  $k^*$  is the stiffness of the elastic part of the bilinear curve.

According to the N2 method, if  $T^* \geq T_C$  the displacement demand for the inelastic system is equal to that of the elastic system with the same period:

$$d_{max}^* = d_{e,max}^* = S_{De}(T^*) \quad (4.16)$$

If  $T^* \leq T_C$  the displacement demand for the inelastic system is greater than that of the elastic system with the same period and can be obtained from the following expression:

$$d_{max}^* = \frac{d_{e,max}^*}{q} \left[ 1 + (q^* - 1) \frac{T_C}{T^*} \right] \geq d_{e,max}^* \quad (4.17)$$

where:

$q^* = S_e(T^*) m^* / F_y$  is the ratio between the elastic force and the yielding force of the equivalent system. If results  $q^* \leq 1$ , then  $d_{max}^* = d_{e,max}^*$ .

The main parameters of the N2 method, which define the properties of the equivalent SDOF system, are reported in Table 4.7.

Table 4.7: Parameters of the SDOF system in both directions for the existing building.

Parameter	Symbol	Value	
		x direction	y direction
Mass	$m^*$	576626 kg	564091 kg
Partecipation factor	$\Gamma$	1,22	1,251
Yelding force	$F_y^*$	942 KN	999,6 KN
Yelding displacement	$\delta_y$	2,3 cm	2,8 cm
Ultimate displacement	$\delta_u$	3,4 cm	3,4 cm
Fundamental period	$T^*$	0,74	0,79
Displacement demand for LS limit state	$S_d(T^*)$	4,46 cm	4,7 cm

The displacement demand of the MDOF system is then obtained by:

$$d_{max} = \Gamma d_{max}^* \quad (4.18)$$

The vulnerability analysis of the existing building carried out with the nonlinear analysis is defined by the ratio capacity/demand in terms of displacement. The results for the Life Safety limit state are shown in Figure 4.25 for x direction and in Figure 4.26 for y direction.

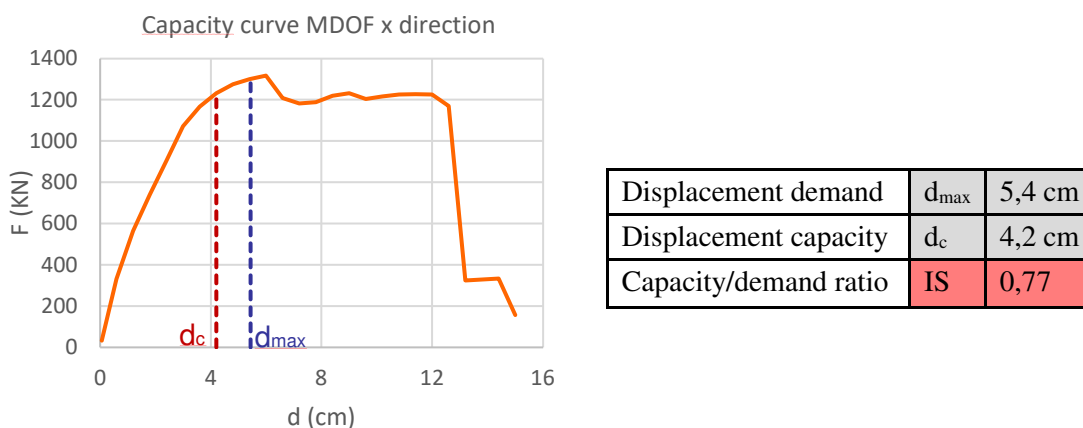


Figure 4.25: Capacity/demand ratio for the Life Safety limit state in x direction for the existing building.

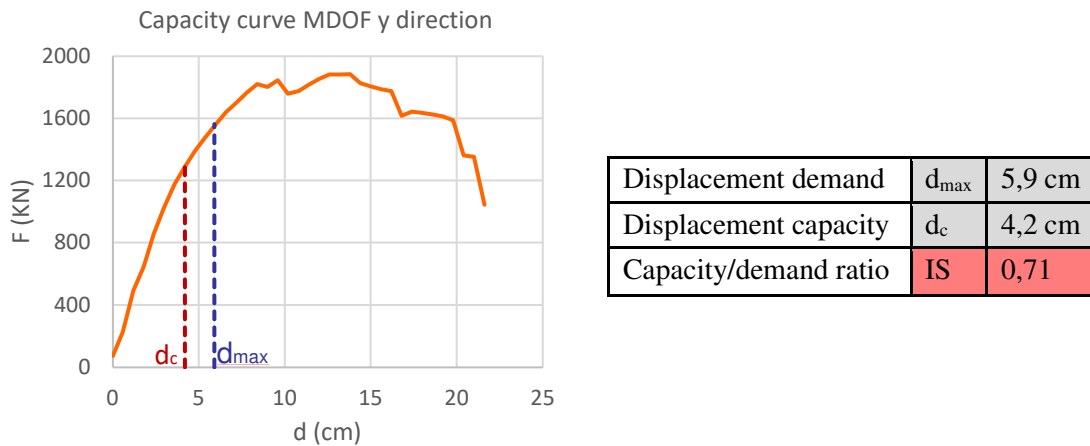


Figure 4.26: Capacity/demand ratio for the Life Safety limit state in y direction for the existing building.

For the Damage Limitation limit state, corresponding to Immediate Occupancy level in the American guidelines [6], the maximum inter-storey drift of 0,3% is considered. The verification of capacity/demand in terms of displacement for x direction and y direction is shown in Figure 4.27 and 4.28 respectively.

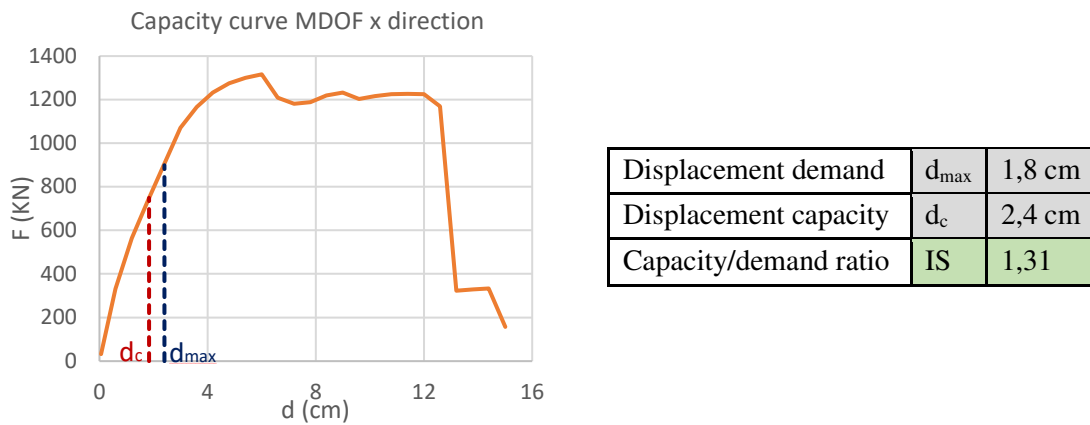


Figure 4.27: Capacity/demand ratio for the Damage Limitation limit state in x direction for the existing building.

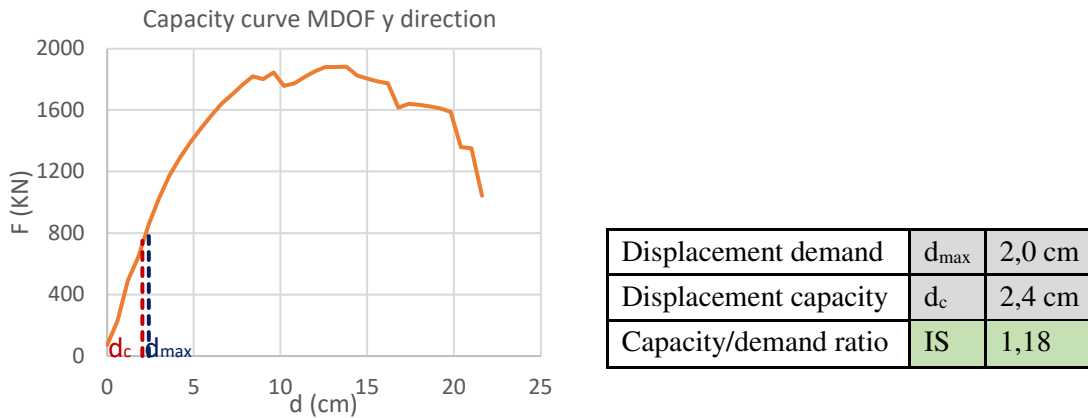


Figure 4.28: Capacity/demand ratio for the Damage Limitation limit state in y direction for the existing building.

The capacity/demand ratio in terms of Peak Ground Acceleration is represented in Table 4.8. Evaluating the return periods  $T_{rC}$  with equation (4.7) and the exceeding annual average frequencies  $\lambda$  with equation (4.8), the economic parameter PAM can be evaluated (see Figure 4.29). The seismic risk class is determined as the lower between the IS-V class (determined by Table 4.4) and the PAM class (determined by Table 4.5). The seismic risk class of the existing building evaluated with the nonlinear analysis is the B class.

Table 4.8: PGA values and risk index evaluated in both directions with nonlinear analysis for the existing building.

Limit state	$PGA_{C-X}$ [g]	$PGA_{C-Y}$ [g]	$PGA_D$ [g]	$\alpha_X$ [-]	$\alpha_Y$ [-]
LS	0,17	0,156	0,22	0,77	0,71
DL	0,107	0,097	0,082	1,31	1,18

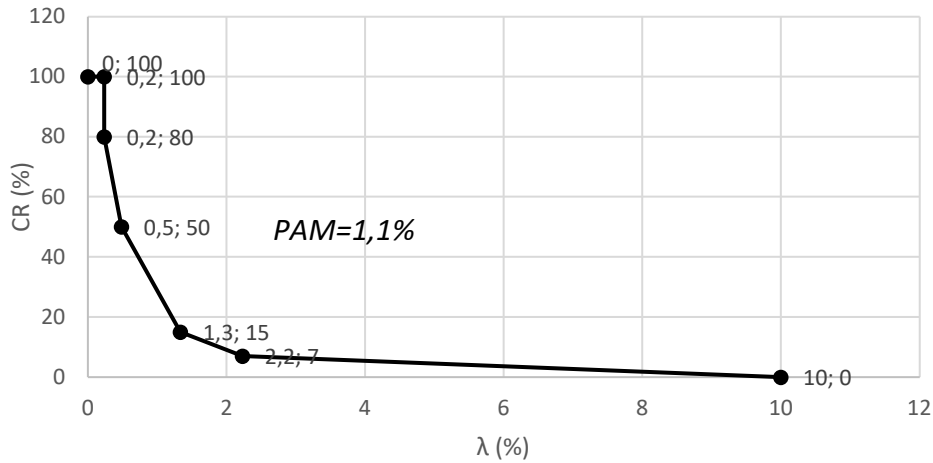


Figure 4.29: Evaluation of the annual average expected loss parameter (PAM) with nonlinear analysis for the existing building.

## 4.4 RESULTS

The risk index of the existing building has been evaluated with the linear analysis and nonlinear analysis. The results are shown in Table 4.9.

Table 4.9: Comparison between the seismic risk index evaluated with linear and nonlinear analysis for the existing building.

Limit state	Linear analysis		Nonlinear analysis	
	$\alpha_X$	$\alpha_Y$	$\alpha_X$	$\alpha_Y$
LS	0,22	0,50	0,77	0,71
DL	0,40	1,00	1,31	1,18

With the nonlinear analysis the seismic safety ratios in both the main directions of the building are greater. This is due to the fact that a maximum inter-storey drift of 0,6% is considered in the nonlinear analysis, while in the linear analysis the attainment of the LS limit state occurs for a value of inter-storey drift of 0,05%. Furthermore, with the linear analysis the risk class F is obtained, while nonlinear analysis leads to a risk class B (see Figure 4.30).

Linear analysis		Nonlinear analysis	
Security index	IS-V class	Security index	IS-V class
$100\% < \text{IS-V}$	$A^+_{\text{IS-V}}$	$100\% < \text{IS-V}$	$A^+_{\text{IS-V}}$
$80\% \leq \text{IS-V} < 100\%$	$A_{\text{IS-V}}$	$80\% \leq \text{IS-V} < 100\%$	$A_{\text{IS-V}}$
$60\% \leq \text{IS-V} < 80\%$	$B_{\text{IS-V}}$	$60\% \leq \text{IS-V} < 80\%$	$B_{\text{IS-V}}$
$45\% \leq \text{IS-V} < 60\%$	$C_{\text{IS-V}}$	$45\% \leq \text{IS-V} < 60\%$	$C_{\text{IS-V}}$
$30\% \leq \text{IS-V} < 45\%$	$D_{\text{IS-V}}$	$30\% \leq \text{IS-V} < 45\%$	$D_{\text{IS-V}}$
$15\% \leq \text{IS-V} < 30\%$	$E_{\text{IS-V}}$	$15\% \leq \text{IS-V} < 30\%$	$E_{\text{IS-V}}$
$\text{IS-V} \leq 15\%$	$F_{\text{IS-V}}$	$\text{IS-V} \leq 15\%$	$F_{\text{IS-V}}$
Annual average expected loss	PAM class	Annual average expected loss	PAM class
$\text{PAM} \leq 0,50\%$	$A^+_{\text{PAM}}$	$\text{PAM} \leq 0,50\%$	$A^+_{\text{PAM}}$
$0,50\% < \text{PAM} \leq 1,0\%$	$A_{\text{PAM}}$	$0,50\% < \text{PAM} \leq 1,0\%$	$A_{\text{PAM}}$
$1,0\% < \text{PAM} \leq 1,5\%$	$B_{\text{PAM}}$	$1,0\% < \text{PAM} \leq 1,5\%$	$B_{\text{PAM}}$
$1,5\% < \text{PAM} \leq 2,5\%$	$C_{\text{PAM}}$	$1,5\% < \text{PAM} \leq 2,5\%$	$C_{\text{PAM}}$
$2,5\% < \text{PAM} \leq 3,5\%$	$D_{\text{PAM}}$	$2,5\% < \text{PAM} \leq 3,5\%$	$D_{\text{PAM}}$
$3,5\% < \text{PAM} \leq 4,5\%$	$E_{\text{PAM}}$	$3,5\% < \text{PAM} \leq 4,5\%$	$E_{\text{PAM}}$
$4,5\% < \text{PAM} \leq 7,5\%$	$F_{\text{PAM}}$	$4,5\% < \text{PAM} \leq 7,5\%$	$F_{\text{PAM}}$
$7,5\% \leq \text{PAM}$	$G_{\text{PAM}}$	$7,5\% \leq \text{PAM}$	$G_{\text{PAM}}$
Risk class F		Risk class B	

Figure 4.30: Comparison between the risk class evaluated with linear and nonlinear analysis for the existing building.

## 4.5 REFERENCES

- [1] Midas Gen. Analysis Manual for Midas Gen.
- [2] CEN-TC250 (2005) Eurocode 8: Design of structures for earthquake resistance.
- [3] Norme tecniche per le costruzioni (NTC 2018). D.M. 17 gennaio 2018.
- [4] Consiglio Superiore dei Lavori Pubblici, Circolare 21 gennaio 2019, n.7. Istruzioni per l'applicazione dell'aggiornamento delle "Norme tecniche per le costruzioni" di cui al decreto ministeriale 17 gennaio 2018.
- [5] Consiglio Superiore dei Lavori Pubblici. D.M. 65 del 7 marzo 2017 Allegato A. Linee guida per la classificazione del rischio sismico delle costruzioni.
- [6] FEMA 356 (2000) Prestandard and commentary for the seismic rehabilitation of buildings. ASCE for the Federal Emergency Management Agency, Washington, D.C.



## *Chapter 5*

# **SEISMIC IMPROVEMET ASSESSMENT**

## **5.1 FIRST NUMERICAL MODEL OF EXTERNAL EXOSKELETON**

This chapter deals with the seismic improvement assessment achieved for the existing building with the addition of the aluminium alloy exoskeleton. Figure 5.1 shows the existing building and a computer graphic drawing of the new envelope with the different options of the additional spaces (balcony, sunspace and extra-room) described in chapter 1.4.

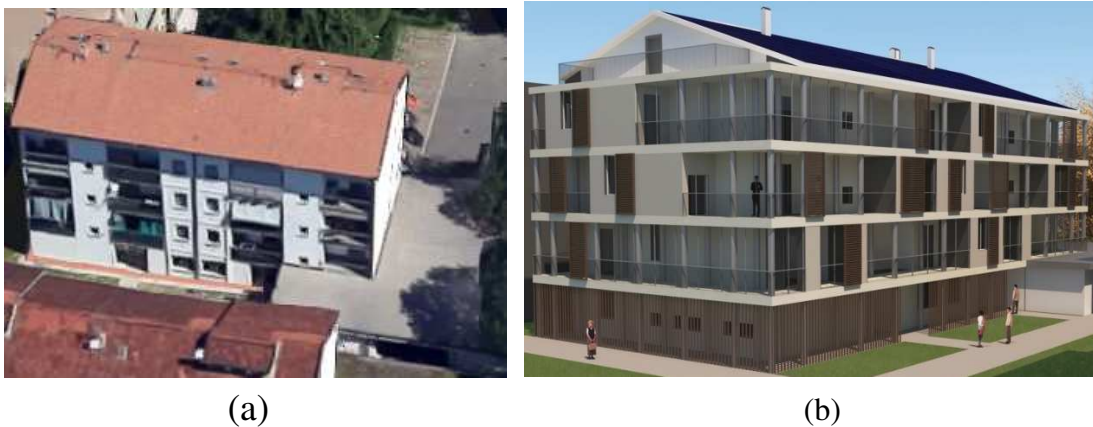


Figure 5.1: (a) Existing building. (b) Computer graphic drawing of the new envelope.

In the first numerical model of the external exoskeleton, the bracings of the concentric frames are placed in order to have the minimum architectural impact. Figure 5.2 shows the numerical model performed with Midas Gen software [1]. The system can be classified as an

exoskeleton 2D $\perp$  with shear walls arranged perpendicular to the façade as indicated in chapter 1.5. The exoskeleton consists of an aluminium alloy frame for each floor, with bracing in the transverse direction, connected to the existing building at the beam-column joints. These frames have a width of 2 m and they are connected by longitudinal beams to create the space suitable for housing the volumetric additions. Only diagonals under traction are considered in the numerical model. An analysis including also the compressed diagonals was performed which showed that these buckle out of their plane. The geometrical properties of all the components of the exoskeleton have been presented in chapter 3.4. The vertical mullions and beams are made of aluminium alloy 6082 T6 while the bracings are made of alloy 6060 T5 as described in chapter 3.3. The distance between the existing building and the internal mullion of the exoskeleton is 0,5 m. The aluminium mullion span is equal to that of the existing structure. Figure 5.3 illustrates the structural scheme of the external exoskeleton. The width of the shear walls in relation to their height and the span to depth ratio for beams are indicated in Table 5.1.

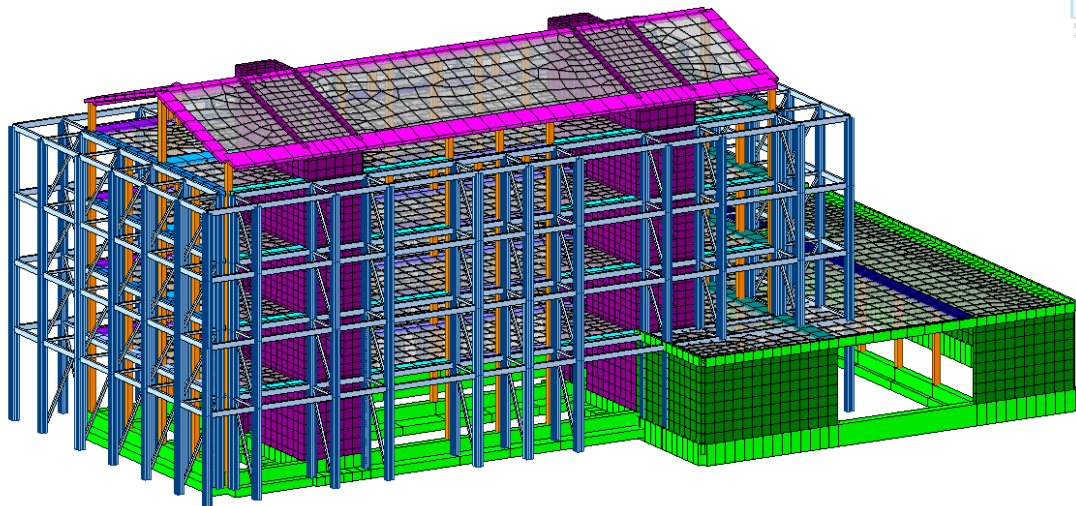
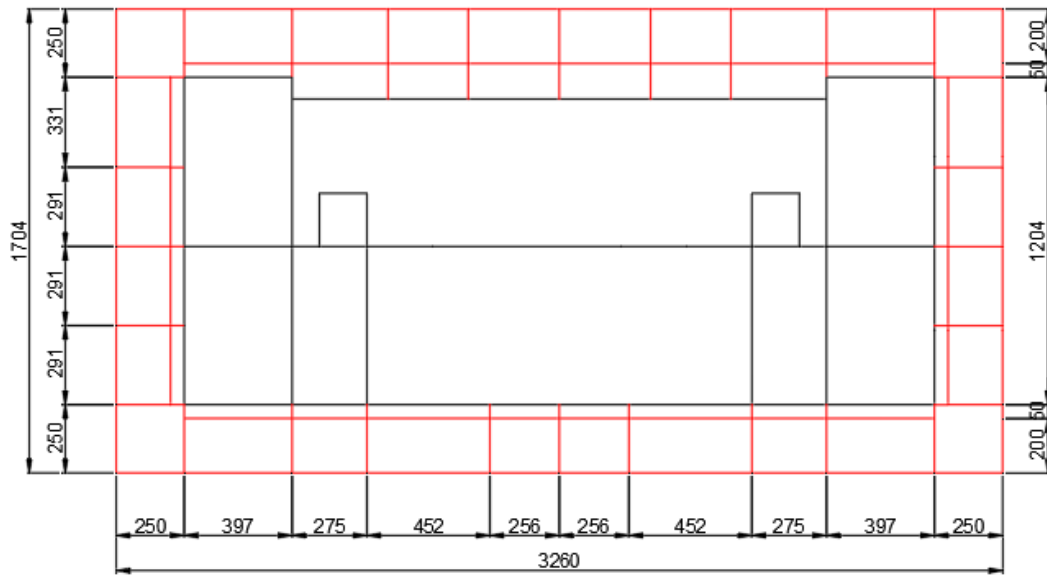
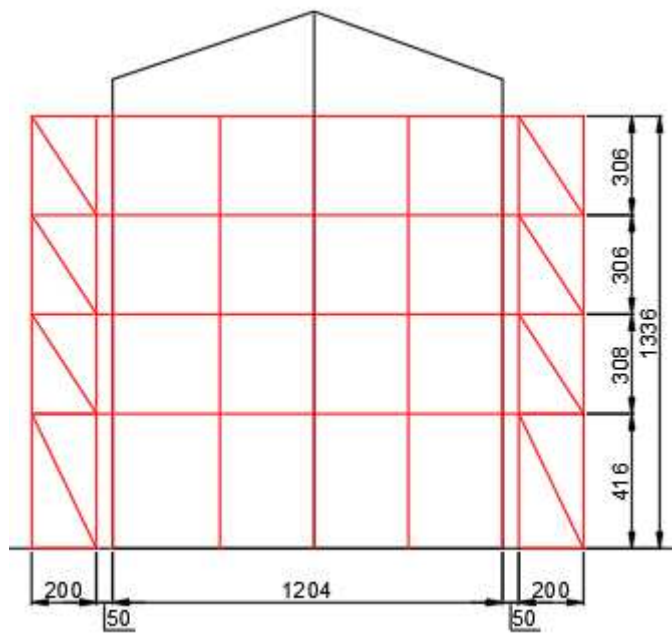


Figure 5.2: First numerical model of the external aluminium alloy exoskeleton.



(a)



(b)

Figure 5.3: Structural scheme of the external exoskeleton. (a) Plan view; (b) Front view.

Table 5.1: Height/width ratio of shear walls.

Floors	Height/width ratio
Ground floor	2,1
1 <sup>st</sup> floor	1,5
2 <sup>nd</sup> floor	1,5
3 <sup>rd</sup> floor	1,5

Table 5.2: Span/depth ratio for beams.

Beam span (cm)	Span/depth ratio
250	9,8
256	10
275	10,7
291	11,4
331	12,9
397	15,5
452	17,7

All the components of the exoskeleton are modelled as beam elements. The beam-mullion connection was illustrated in chapter 3.4 and it is modelled as a rigid connection. The joints eccentricity is very small and allows to consider the secondary bending moments as negligible. The application of the aluminium alloy external structure connected to the existing building increases the rigidity of the structure with a minimum mass increase, resulting in a decrease in the structure's period. The natural period  $T$ , the frequency  $f$  and the modal participation mass  $M$  for the first three vibration modes are listed in Table 5.3. The fundamental period is still on the plateau of the response spectrum, so the seismic demand remains unchanged. The modal shapes are illustrated in Figure 5.4.

Table 5.3: Natural period, frequency and modal participation mass of the first three vibration modes for the retrofitted building.

Mode	Frequency $f$ [cycle/s]	Period $T$ [s]	$M_x$ [%]	$M_y$ [%]	$M_{\theta_z}$ [%]
1	2,65	0,38	61,5	0	0
2	4,22	0,24	0	45	21
3	4,69	0,21	0	11	18

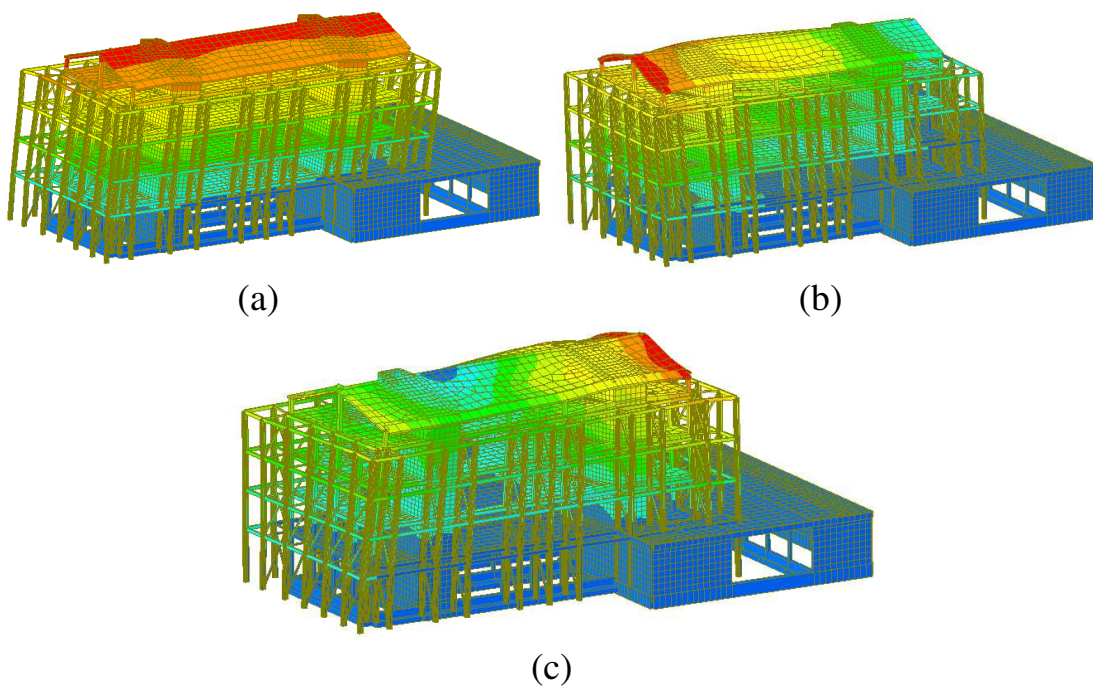


Figure 5.4: Modal shapes of the retrofitted building.

The connection between the existing building and the exoskeleton, illustrated in chapter 1.4, is a rigid link in the x-y plane to create an effective collaboration to horizontal actions. The vertical displacements are allowed leaving the structures autonomous for static loads. The connection includes a vertical slotted hole to allow the thermal expansion of the aluminium. As indicated in chapter 2.2, the aluminium has a high thermal expansion coefficient that has to be taken into account in the design. In fact, it is equal to  $2,3 \times 10^{-5} \text{ } ^\circ\text{C}^{-1}$  and it is twice the one of steel and concrete. For a four-storey building the difference of thermal expansion between aluminium and concrete is approximately 7/8 mm. The connection consists of a steel profile connected to the exoskeleton by means of a flange and connected to the concrete joint with an UPN profiles fixed along the perimetral beams. Figure 5.5 shows the connection realized by means of six steel S235 plates with dimensions 100x8 mm connected with a M20 grade 8.8 bolt.

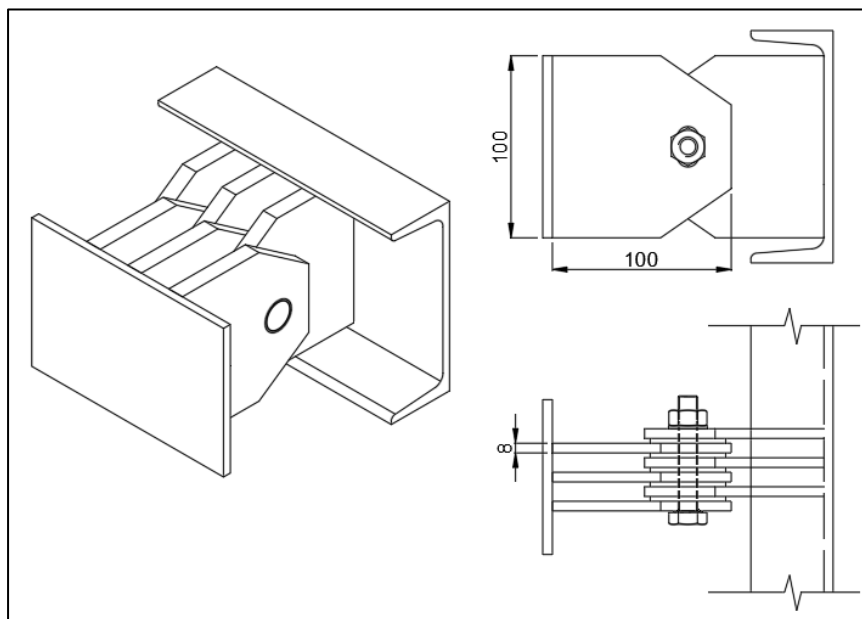


Figure 5.5: Connection detail between the existing building and the exoskeleton.

### 5.1.1 Seismic vulnerability with linear static analysis

The risk index of the building is determined by the achievement of the bending capacity of masonry piers evaluated with equation (4.5). Table 5.4 shows the results regarding the existing building retrofitted with the exoskeleton. It can be noted that the retrofitted building still shows a high vulnerability, especially in the longitudinal direction. The risk index at the LS limit state is  $\alpha_{u,X} = 0,24$  in x direction and  $\alpha_{u,Y} = 0,80$  in y direction. Considering the lower value of the two, the IS-V class, determined by Table 4.4, is the class E.

Table 5.4: PGA values and risk index for masonry piers evaluated in both directions with linear analysis for the retrofitted building.

Limit state	Element	PGA <sub>C-X</sub> [g]	PGA <sub>C-Y</sub> [g]	PGA <sub>D</sub> [g]	$\alpha_X$ [-]	$\alpha_Y$ [-]
LS	Masonry piers - shear	0,0814	0,22	0,22	0,37	1,00
	Masonry piers - bending	0,0528	0,176	0,22	0,24	0,80
DL	Masonry piers - shear	0,0656	0,082	0,082	0,80	1,00
	Masonry piers - bending	0,0476	0,082	0,082	0,58	1,00

The PAM parameter, evaluated by equation 4.9, is represented in Figure 5.6.

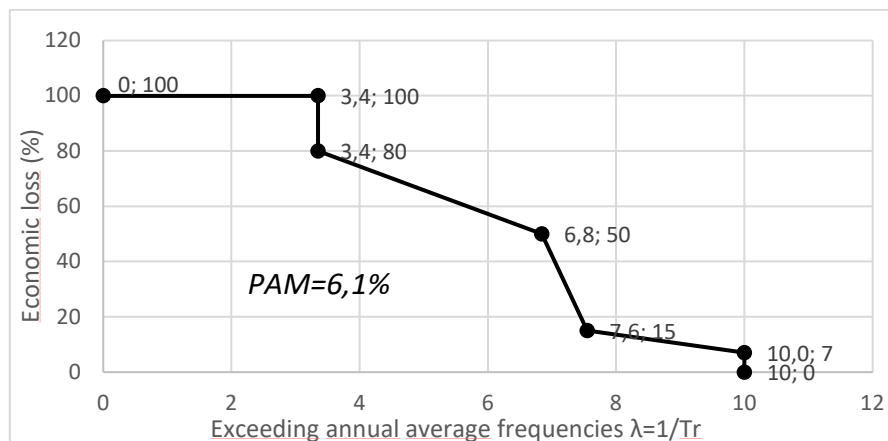


Figure 5.6: Evaluation of the annual average expected loss parameter (PAM) for the retrofitted building.

The PAM class, determined by Table 4.5, is the class F. Therefore, the risk class post-intervention remains the class F and consequently there is not a seismic improvement with the linear analysis.

### 5.1.2 Seismic vulnerability with nonlinear static analysis

User-defined hinges are assigned at the ends of aluminium members and they are based on the experimental  $\sigma - \varepsilon$  curves for the 6082 T6 and 6060 T5 alloys (Figure 3.13 and 3.14). The user-defined hinge properties are shown in Figure 5.7 for mullions and beams made of aluminium alloy 6082 T6 and in Figure 5.8 for diagonals made of 6060 T5 alloy.

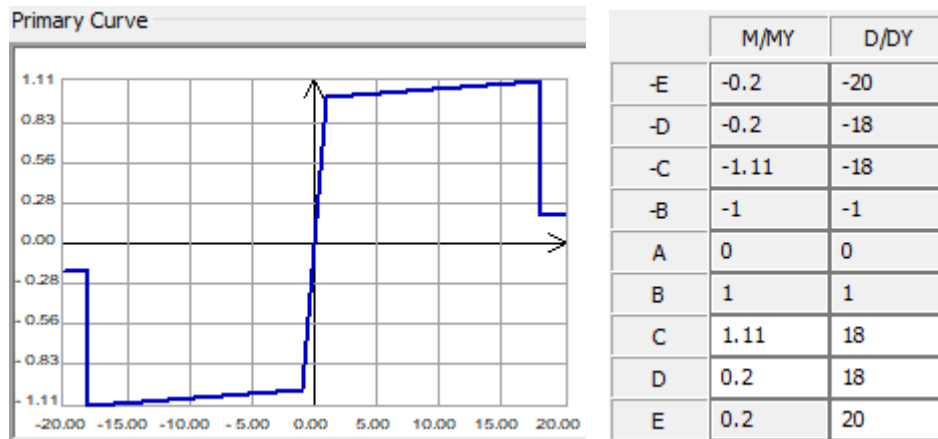


Figure 5.7: User-defined hinge properties for aluminium alloy 6082 T6.

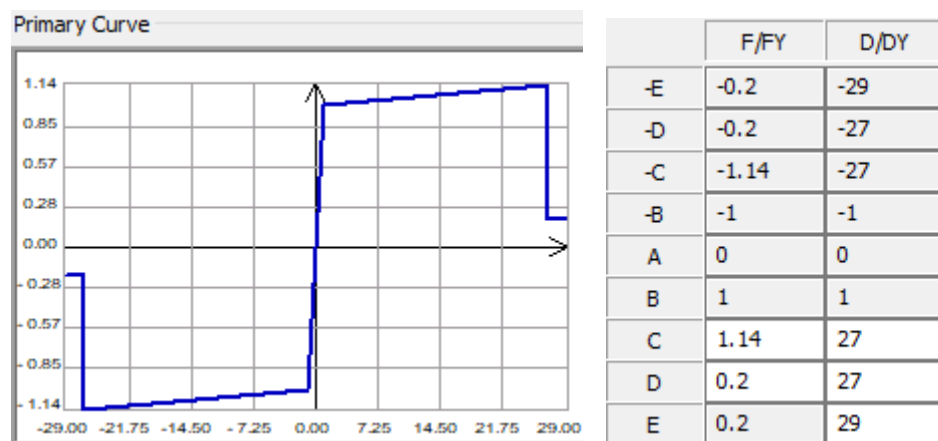


Figure 5.8: User-defined hinge properties for aluminium alloy 6060 T5.



The capacity curves of the existing building EB, the exoskeleton EX and the existing building retrofitted with exoskeleton EB-EX in x direction are shown in Figure 5.9.

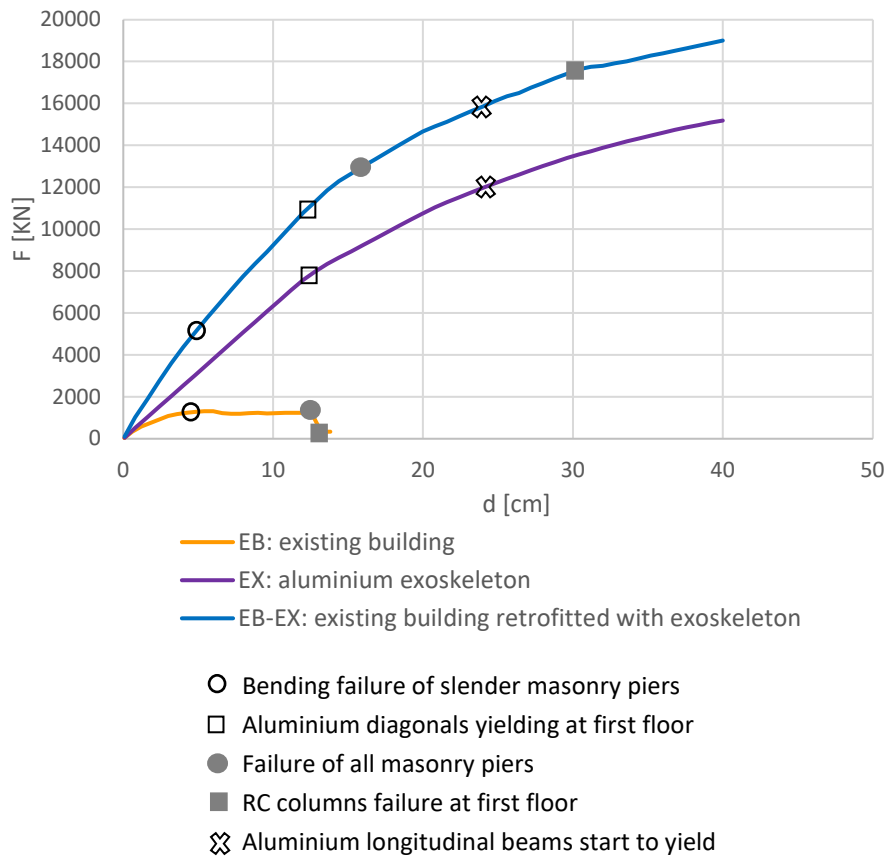


Figure 5.9: Capacity curves of the existing building, the exoskeleton and the retrofitted building in x direction.

At a displacement of about 12 cm there is the aluminium diagonals yielding at the first floor (see Figure 5.10a). The aluminium longitudinal beams start to yield at a displacement of 24 cm (see Figure 5.10b). The RC columns failure occurs at a displacement of 13 cm for the existing building and at 30 cm for the retrofitted building (see Figure 5.10c). In y direction the capacity curves of the three systems are overlapped in Figure 5.11.

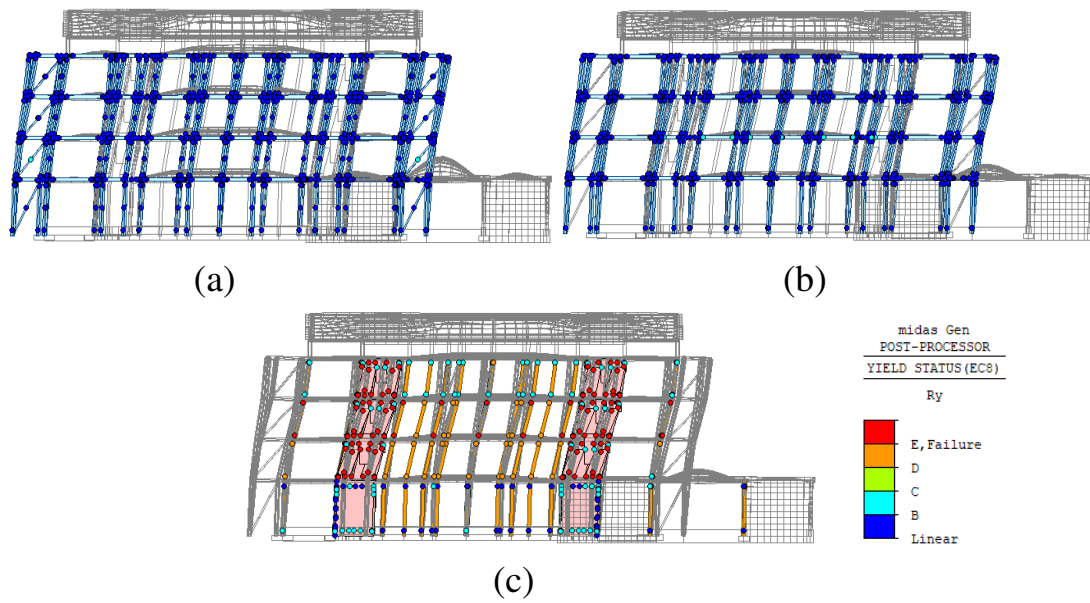


Figure 5.10: (a) Aluminium diagonals yielding at first floor at 12 cm. (b) Aluminium longitudinal beams start to yield at 24 cm. (c) RC columns failure at 30 cm.

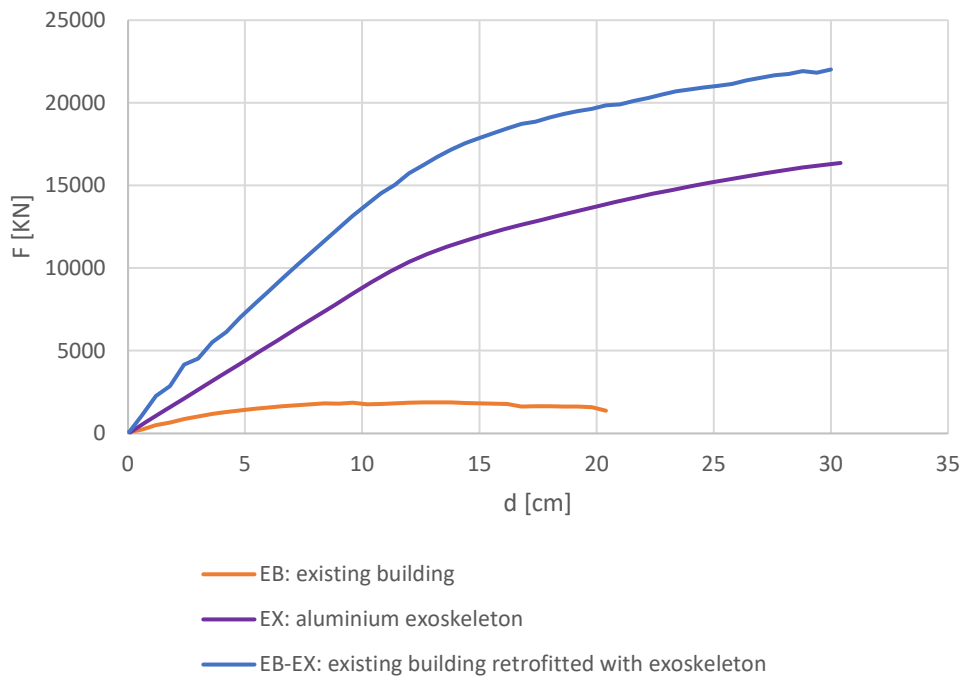


Figure 5.11: Capacity curves of the existing building, the exoskeleton and the retrofitted building in y direction.

The limitations of inter-storey drift recommended by [2] for concrete frames, unreinforced masonry walls and braced steel frame are reported in Table 5.5 for each limit states. Aluminium frames are not included in [2] so the limitation for steel frames is considered. A maximum inter-storey drift equal to 0,6% for the Life Safety limit state is assumed. The drift target corresponds to a storey displacement at the top floor of 4,8 cm in x direction and 4,2 cm in y direction (see Figure 5.12). At the displacement target only few slender masonry piers reach the ultimate bending drift and the RC columns come into the plastic field, while the aluminium exoskeleton remains in the elastic field (see Figure 5.13). The fast collapse of the masonry bearing structure does not allow the exploitation of the exoskeleton's ductile behaviour. Figure 5.14 shows how the exoskeleton increase the stiffness and the base shear in each analysis direction. In x direction there is an increase of base shear of 3,7 and an increase of stiffness of 2,3. In y direction the increased strength is 4,7 and the increased stiffness is 4,8. Although the exoskeleton has a greater resistance than the existing building, it is not possible to consider only the exoskeleton as seismic-resistant. In fact, the masonry is the weak element of the building that reach the ultimate drift for bending and it is no longer resistant to horizontal forces but only to vertical loads.

Table 5.5: Maximum inter-storey drift according to FEMA 356.

Elements	Structural performance levels		
	Collapse prevention	Life safety	Immediate Occupancy
Concrete frames	drift 4%	drift 2%	drift 1%
Unreinforced masonry walls	drift 1%	drift 0,6%	drift 0,3%
Braced steel frames	drift 2%	drift 1,5%	drift 0,5%

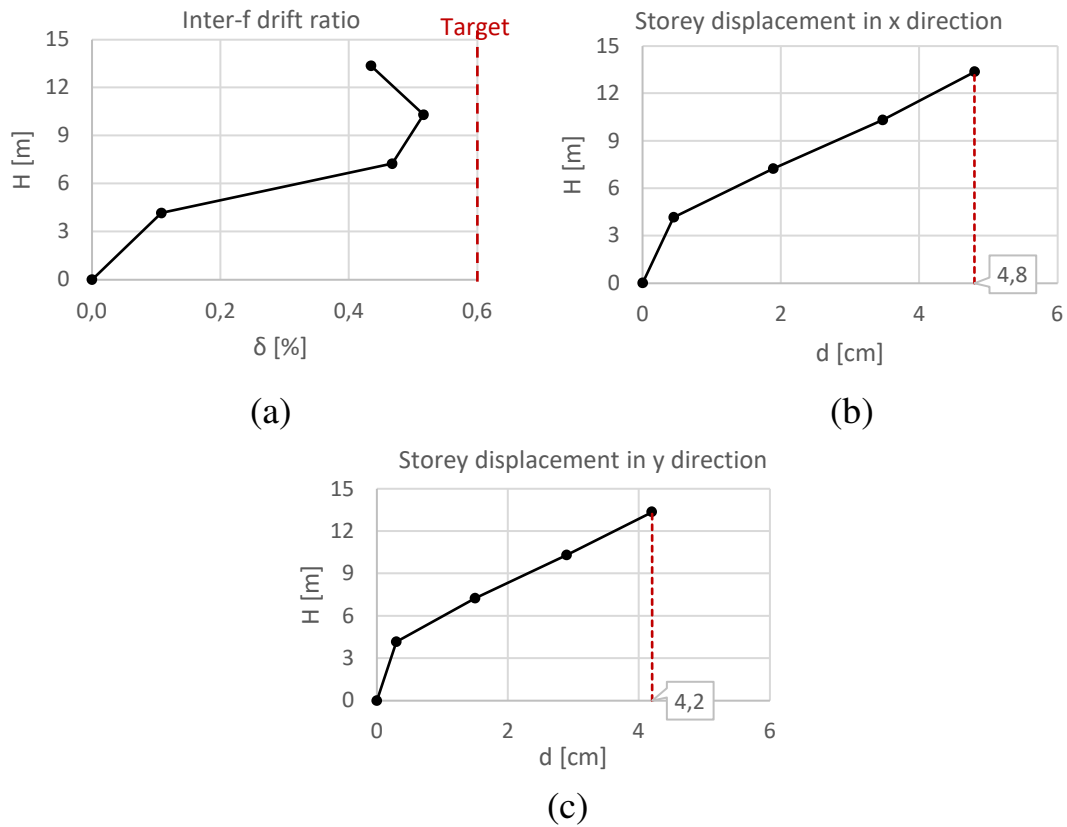
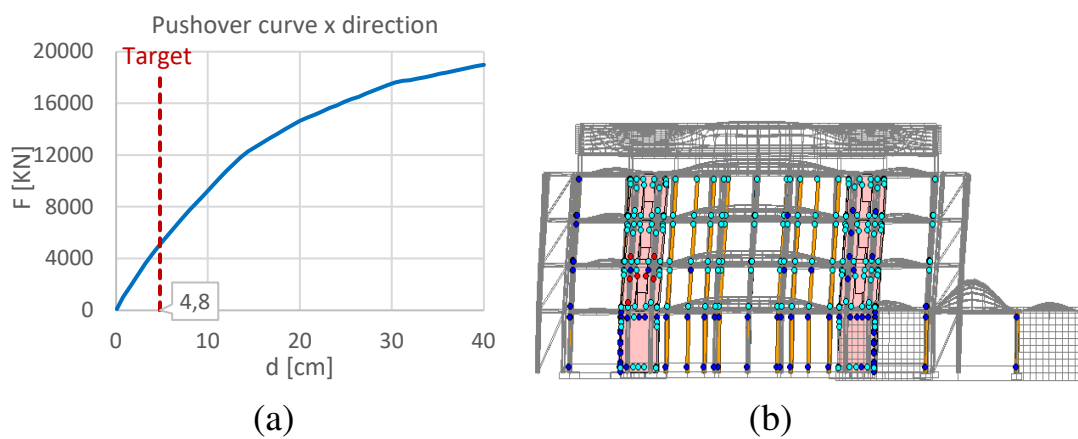
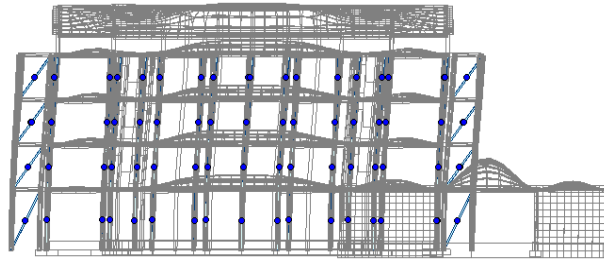


Figure 5.12: (a) Inter-storey drift; (b) storey displacement in x direction; (c) storey displacement in y direction.





(c)

Figure 5.13: (a) Pushover curve in x direction and displacement target; (b) plastic hinges on masonry and RC columns at displacement target; (c) plastic hinges on aluminium exoskeleton at displacement target.

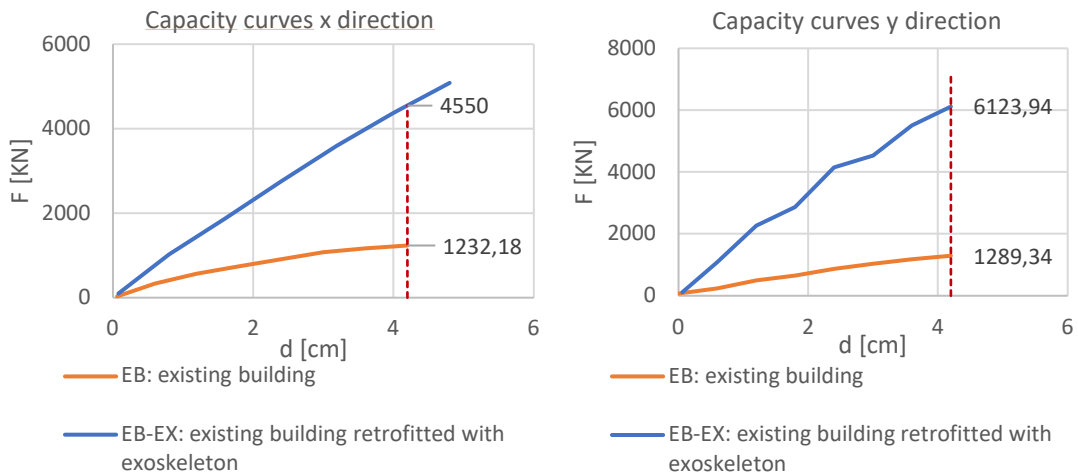


Figure 5.14: Evaluation of the increased strength and stiffness in both directions.

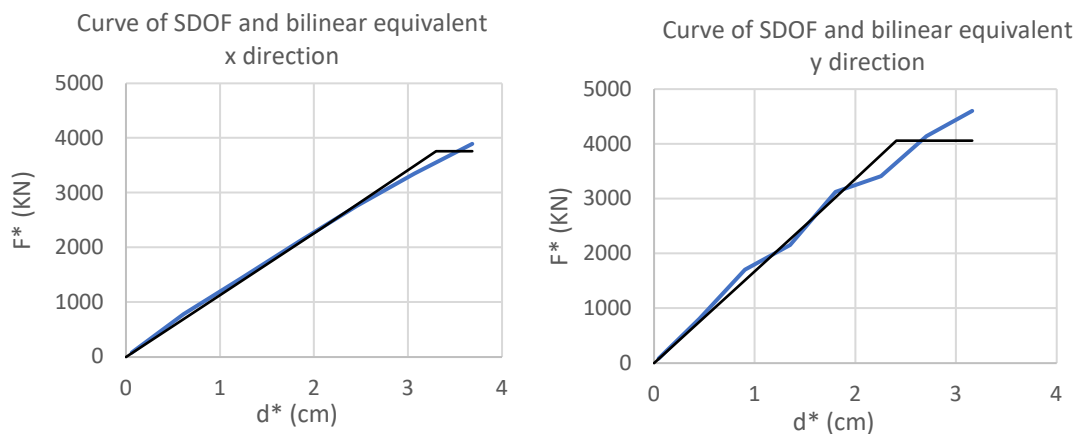


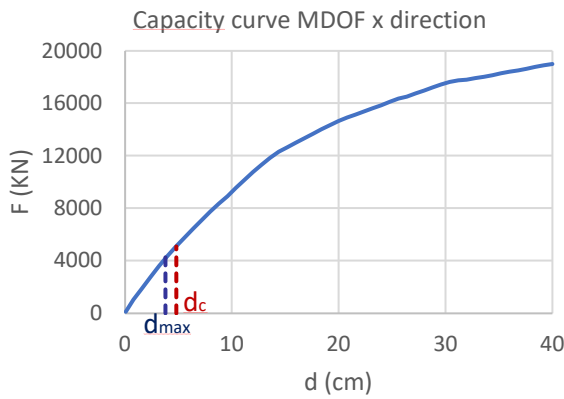
Figure 5.15: Curve of the SDOF system and bilinear equivalent curve in both directions for the retrofitted building.

The SDOF system curve and the bilinear equivalent curve evaluated with the N2 method are shown in Figure 5.15 for both the main direction. The main parameters of the SDOF system in both directions are reported in Table 5.6. The behaviour factor  $q$  of 1,12 in x direction and 1,31 in y direction is obtained.

Table 5.6: Parameters of the SDOF system in both directions for the retrofitted building.

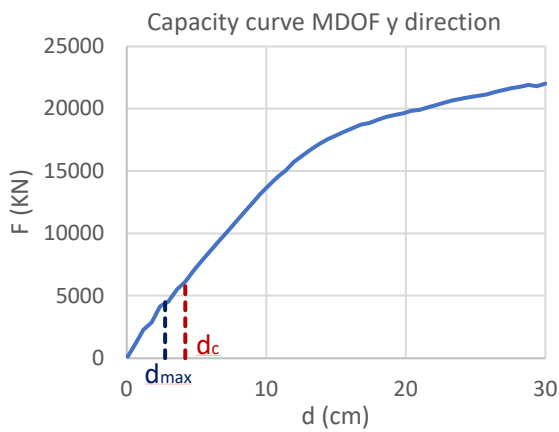
Parameter	Symbol	Value	
		x direction	y direction
Mass	$m^*$	682861 kg	664324 kg
Partecipation factor	$\Gamma$	1,30	1,33
Yelding force	$F_y^*$	3758 KN	4062 KN
Yelding displacement	$\delta_y$	3,3 cm	2,4 cm
Ultimate displacement	$\delta_u$	3,7 cm	3,2 cm
Fundamental period	$T^*$	0,49	0,40
Displacement demand for LS limit state	$S_d(T^*)$	2,91 cm	2,1 cm

The vulnerability analysis of the reinforced building carried out with the nonlinear analysis shows a significant seismic improvement. In fact, the risk index for the LS limit state is 1,27 in x direction (Figure 5.16) and 1,52 in y direction (Figure 5.17). For the DL limit state, the vulnerability analysis is performed by considering a maximum inter-storey drift of 0,3%. The risk index of 1,78 in x direction (Figure 5.18) and 2,36 in y direction (Figure 5.19) is obtained.



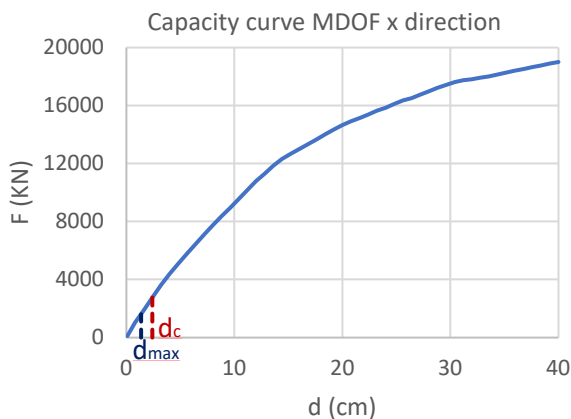
Displacement demand	$d_{max}$	3,8 cm
Displacement capacity	$d_c$	4,8 cm
Capacity/demand ratio	IS	1,27

Figure 5.16: Capacity/demand ratio for the Life Safety limit state in x direction for the retrofitted building.



Displacement demand	$d_{max}$	2,8 cm
Displacement capacity	$d_c$	4,2 cm
Capacity/demand ratio	IS	1,52

Figure 5.17: Capacity/demand ratio for the Life Safety limit state in y direction for the retrofitted building.



Displacement demand	$d_{max}$	1,4 cm
Displacement capacity	$d_c$	2,4 cm
Capacity/demand ratio	IS	1,78

Figure 5.18: Capacity/demand ratio for the Damage Limitation limit state in x direction for the retrofitted building.

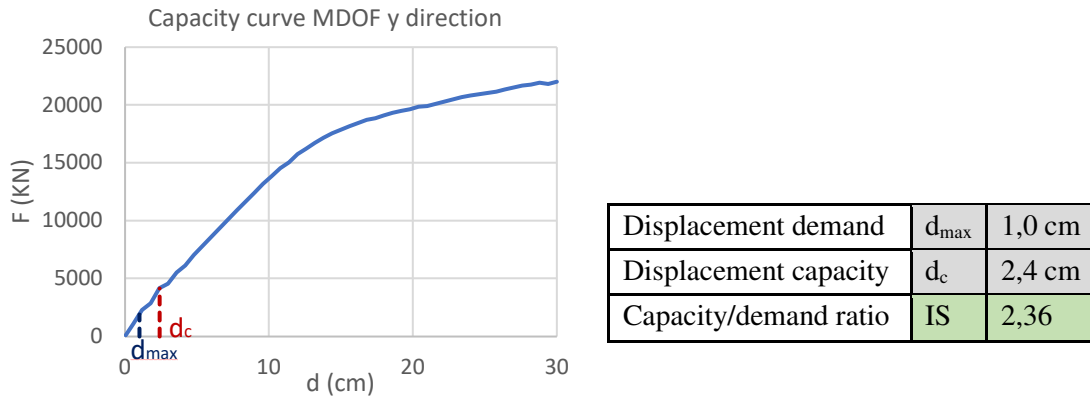


Figure 5.19: Capacity/demand ratio for the Damage Limitation limit state in y direction for the retrofitted building.

The capacity/demand ratio in terms of Peak Ground Acceleration is represented in Table 5.7. Evaluating the return periods  $T_{rC}$  with equation (4.7) and the exceeding annual average frequencies  $\lambda$  with equation (4.8), the economic parameter PAM can be evaluated. The latter is equal to 0,6% (Figure 5.20) and the PAM class obtained is class A. The seismic risk class of the retrofitted building evaluated with the nonlinear analysis and determined as the lower between the IS-V class and the PAM class is the class A.

Table 5.7: PGA values and risk index evaluated in both directions with nonlinear analysis for the retrofitted building.

Limit state	$PGA_{C-X}$ [g]	$PGA_{C-Y}$ [g]	$PGA_D$ [g]	$\alpha_X$ [-]	$\alpha_Y$ [-]
LS	0,279	0,334	0,22	1,27	1,52
DL	0,146	0,194	0,082	1,78	2,36



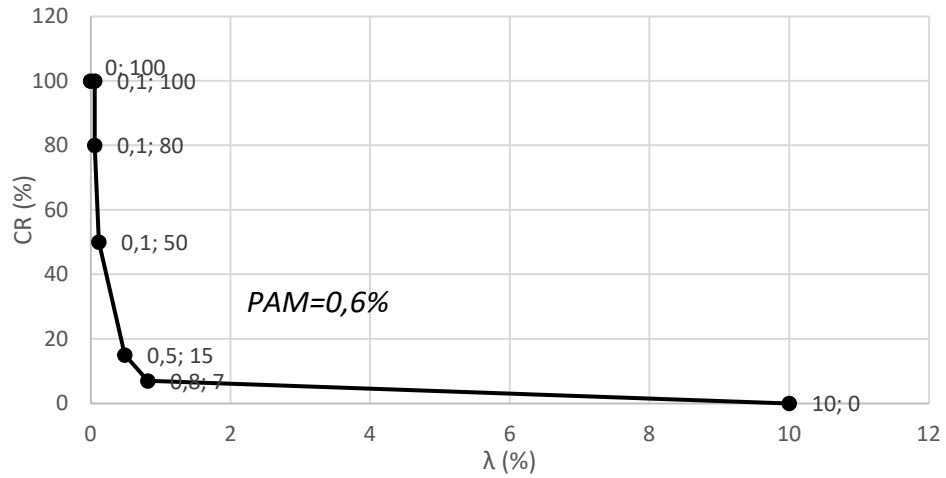


Figure 5.20: Evaluation of the annual average expected loss parameter (PAM) with nonlinear analysis for the retrofitted building.

### 5.1.3 Results

Table 5.8 shows the comparison between the seismic risk index of the existing building retrofitted with the first model of the exoskeleton evaluated with the linear analysis and nonlinear analysis.

Table 5.8: Comparison between the seismic risk index evaluated with linear and nonlinear analysis for the existing building retrofitted with the first model of exoskeleton.

Limit state	Linear analysis		Nonlinear analysis	
	$\alpha_X$	$\alpha_Y$	$\alpha_X$	$\alpha_Y$
LS	0,24	0,80	1,27	1,52
DL	0,58	1,00	1,78	2,36

The difference in the results is due to the fact that a maximum inter-storey drift of 0,6% is considered in the nonlinear analysis, while in the linear analysis the attainment of the LS limit state occurs for a value of inter-storey drift of 0,05%. In Figure 5.21 the comparison of the evaluation of the risk class with the linear and nonlinear analysis is shown. It can be

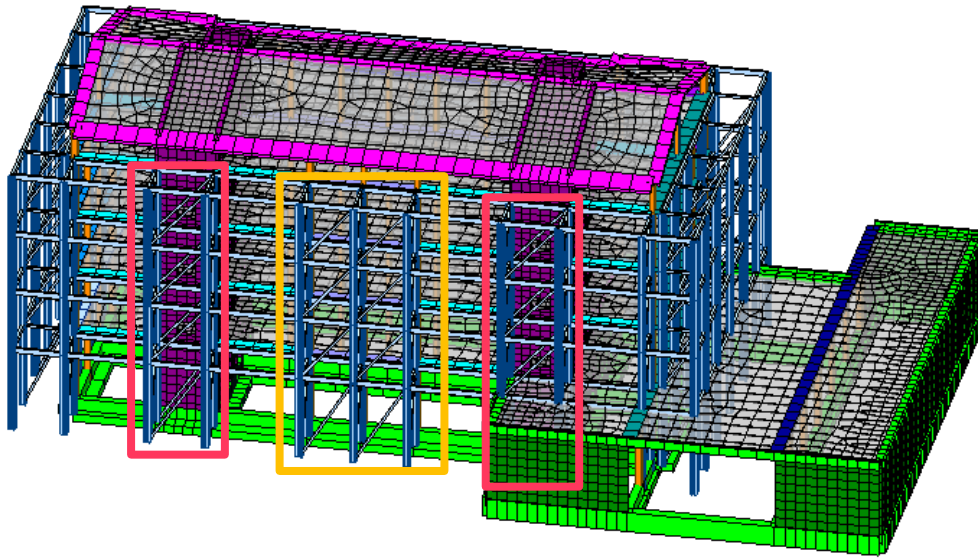
noted that the two analysis led to different results. With the linear analysis there is not a seismic improvement with the addition of the external exoskeleton. The risk class post-intervention remains the class F as for the existing building. On the contrary, the nonlinear analysis highlights a seismic improvement of the building leading to a low risk class A.

Linear analysis		Nonlinear analysis	
Security index	IS-V class	Security index	IS-V class
$100\% < \text{IS-V}$	$A^+_{\text{IS-V}}$	$100\% < \text{IS-V}$	$A^+_{\text{IS-V}}$
$80\% \leq \text{IS-V} < 100\%$	$A_{\text{IS-V}}$	$80\% \leq \text{IS-V} < 100\%$	$A_{\text{IS-V}}$
$60\% \leq \text{IS-V} < 80\%$	$B_{\text{IS-V}}$	$60\% \leq \text{IS-V} < 80\%$	$B_{\text{IS-V}}$
$45\% \leq \text{IS-V} < 60\%$	$C_{\text{IS-V}}$	$45\% \leq \text{IS-V} < 60\%$	$C_{\text{IS-V}}$
$30\% \leq \text{IS-V} < 45\%$	$D_{\text{IS-V}}$	$30\% \leq \text{IS-V} < 45\%$	$D_{\text{IS-V}}$
$15\% \leq \text{IS-V} < 30\%$	$E_{\text{IS-V}}$	$15\% \leq \text{IS-V} < 30\%$	$E_{\text{IS-V}}$
$\text{IS-V} \leq 15\%$	$F_{\text{IS-V}}$	$\text{IS-V} \leq 15\%$	$F_{\text{IS-V}}$
Annual average expected loss	PAM class	Annual average expected loss	PAM class
$\text{PAM} \leq 0,50\%$	$A^+_{\text{PAM}}$	$\text{PAM} \leq 0,50\%$	$A^+_{\text{PAM}}$
$0,50\% < \text{PAM} \leq 1,0\%$	$A_{\text{PAM}}$	$0,50\% < \text{PAM} \leq 1,0\%$	$A_{\text{PAM}}$
$1,0\% < \text{PAM} \leq 1,5\%$	$B_{\text{PAM}}$	$1,0\% < \text{PAM} \leq 1,5\%$	$B_{\text{PAM}}$
$1,5\% < \text{PAM} \leq 2,5\%$	$C_{\text{PAM}}$	$1,5\% < \text{PAM} \leq 2,5\%$	$C_{\text{PAM}}$
$2,5\% < \text{PAM} \leq 3,5\%$	$D_{\text{PAM}}$	$2,5\% < \text{PAM} \leq 3,5\%$	$D_{\text{PAM}}$
$3,5\% < \text{PAM} \leq 4,5\%$	$E_{\text{PAM}}$	$3,5\% < \text{PAM} \leq 4,5\%$	$E_{\text{PAM}}$
$4,5\% < \text{PAM} \leq 7,5\%$	$F_{\text{PAM}}$	$4,5\% < \text{PAM} \leq 7,5\%$	$F_{\text{PAM}}$
$7,5\% \leq \text{PAM}$	$G_{\text{PAM}}$	$7,5\% \leq \text{PAM}$	$G_{\text{PAM}}$
Risk class F		Risk class A	

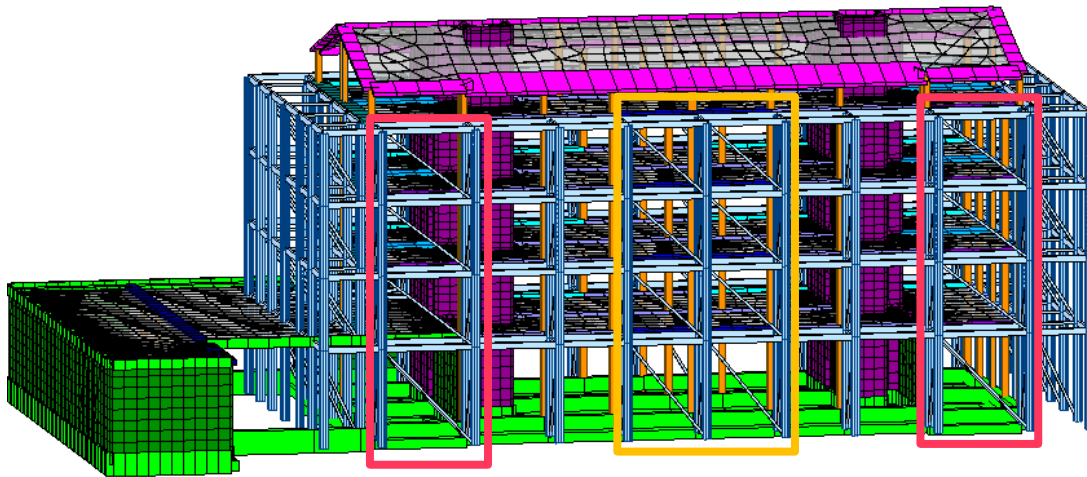
Figure 5.21: Comparison between the risk class evaluated with linear and nonlinear analysis for the existing building retrofitted with the first model of exoskeleton.

## **5.2 SECOND NUMERICAL MODEL OF EXTERNAL EXOSKELETON**

In order to obtain better performance of the building a second model of the external aluminium exoskeleton is developed. It consists of a strengthened exoskeleton obtained with the addition of bracings in the longitudinal and weak direction of the building. In this case, the system combines the  $2D\perp$  exoskeleton with a  $2D//$  exoskeleton with shear walls parallel to the building façade as indicated in chapter 1.5. Figure 5.22 shows the numerical model of this second design of the exoskeleton performed with Midas Gen software. This solution has a greater architectural impact, but the following assumptions are considered. Additional bracings on the internal and external side of the aluminium frame are considered at the stairwells in the South elevation. The addition of the bracings is highlighted by red boxes in Figure 5.22. It is assumed acceptable to have internal bracings at the stairwells because the windows are at a height of approximately 2 m from the landing and consequently, they are not accessible (Figure 5.23). In the North elevation additional bracings on both side of the exoskeleton are considered in positions where there are windows and balconies are not present. Additional bracings only on the external side of the exoskeleton are assumed in the position highlighted with orange box in Figure 5.22. This assumption allows the access at the extra room created by the exoskeleton but implies an opaque envelope.



(a)



(b)

Figure 5.22: Second numerical model of the external aluminium alloy exoskeleton. (a) South elevation; (b) North elevation.

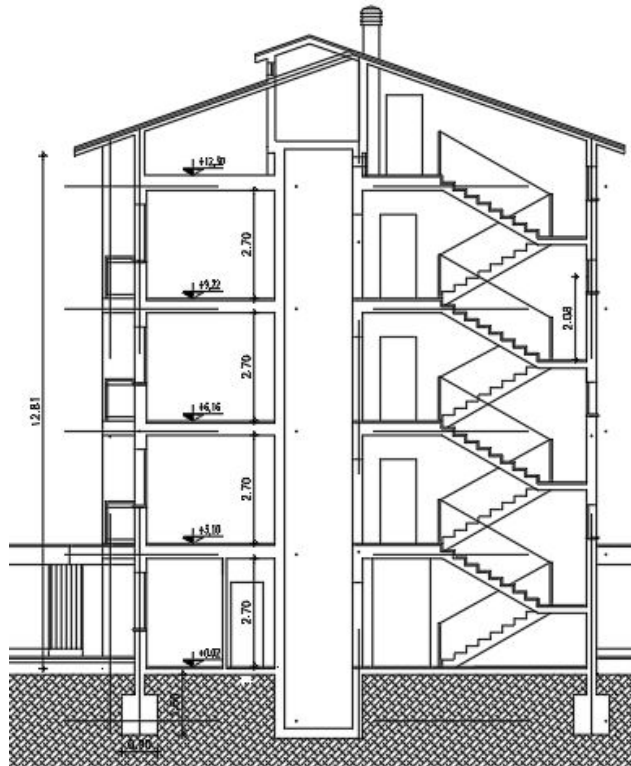


Figure 5.23: Vertical section and windows height from the landing.

The strengthened exoskeleton implies an increase in the rigidity of the structure and a decrease in the fundamental period. The latter is still located on the plateau of the response spectrum and does not involve a change in the seismic demand. The natural period  $T$ , the frequency  $f$  and the modal participation mass  $M$  for the first three vibration modes are listed in Table 5.9. The modal shapes are illustrated in Figure 5.24.

Table 5.9: Natural period, frequency and modal participation mass of the first three vibration modes for the retrofitted building with the second model of exoskeleton.

Mode	Frequency $f$ [cycle/s]	Period $T$ [s]	$M_x$ [%]	$M_y$ [%]	$M_{gz}$ [%]
1	2,92	0,34	62	0	0
2	4,24	0,24	0	48	18
3	4,77	0,21	0	8	20,5

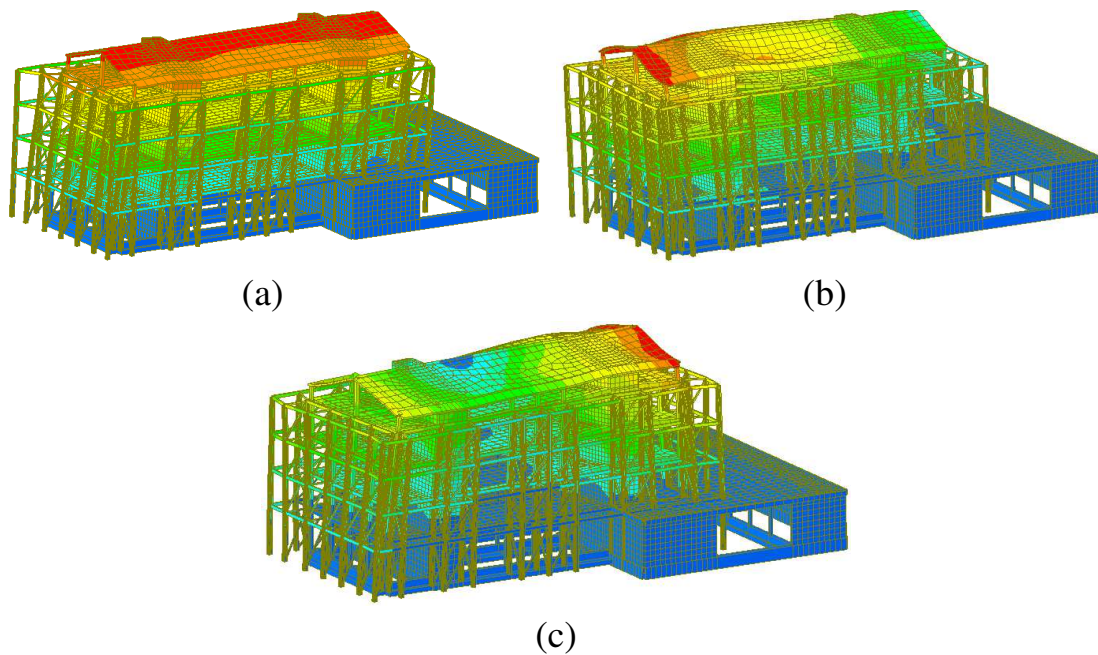


Figure 5.24: Modal shapes of the retrofitted building with the second model of the exoskeleton.

### 5.2.1 Seismic vulnerability with linear static analysis

Table 5.10 shows the PGA values and the risk index for masonry piers evaluated in both directions with the linear analysis for the retrofitted building with the second model of the exoskeleton. At the LS limit state the risk index is  $\alpha_{u,X} = 0,32$  in x direction and  $\alpha_{u,Y} = 1,00$  in y direction. The IS-V class, assessed considering the lower value between the two, is the class D.

Table 5.10: PGA values and risk index for masonry piers evaluated in both directions with linear analysis for the retrofitted building with the second model of exoskeleton.

Limit state	Element	PGA <sub>C-X</sub> [g]	PGA <sub>C-Y</sub> [g]	PGA <sub>D</sub> [g]	$\alpha_X$ [-]	$\alpha_Y$ [-]
LS	Masonry piers - shear	0,099	0,22	0,22	0,45	1,00
	Masonry piers - bending	0,0704	0,22	0,22	0,32	1,00
DL	Masonry piers - shear	0,082	0,082	0,082	1,00	1,00
	Masonry piers - bending	0,0533	0,082	0,082	0,65	1,00

The PAM parameter is equal to 4,0% (Figure 5.25) and the corresponding class is the E. For the existing building retrofitted with the second model of the exoskeleton, the risk class is the class E and there is an improvement of one class compared to the bare building.

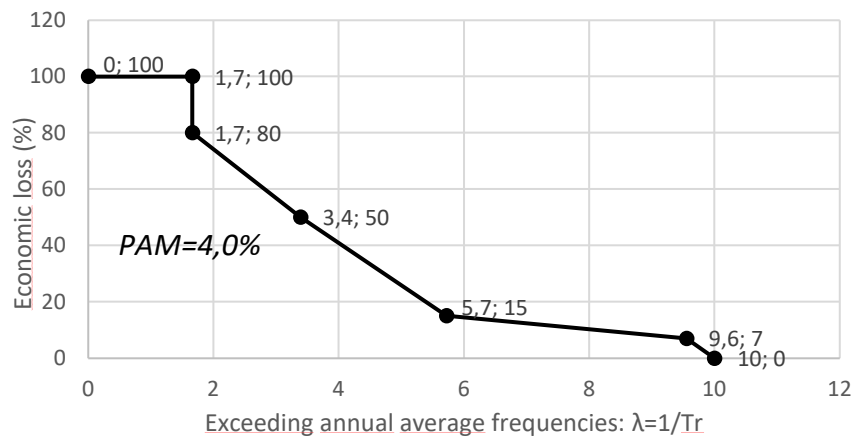


Figure 5.25: Evaluation of the annual average expected loss parameter (PAM) for the retrofitted building with the second model of exoskeleton.

### 5.2.2 Seismic vulnerability with nonlinear static analysis

The pushover analysis is performed considering the user-defined hinges properties for the 6082 T6 and 6060 T5 aluminium alloy described at Chapter 5.1.2. The pushover curve of the building retrofitted with the second model of the exoskeleton EB-EX 2 in x direction is shown in Figure 5.26. The capacity curve is compared with the curve of the existing building EB and that of the first model of the exoskeleton EB-EX 1. The EB-EX 2 curve in x direction shows higher stiffness and capacity. In the y direction there are no additional bracings and the capacity curve is the same as the previous case EB-EX 1 (Figure 5.27).

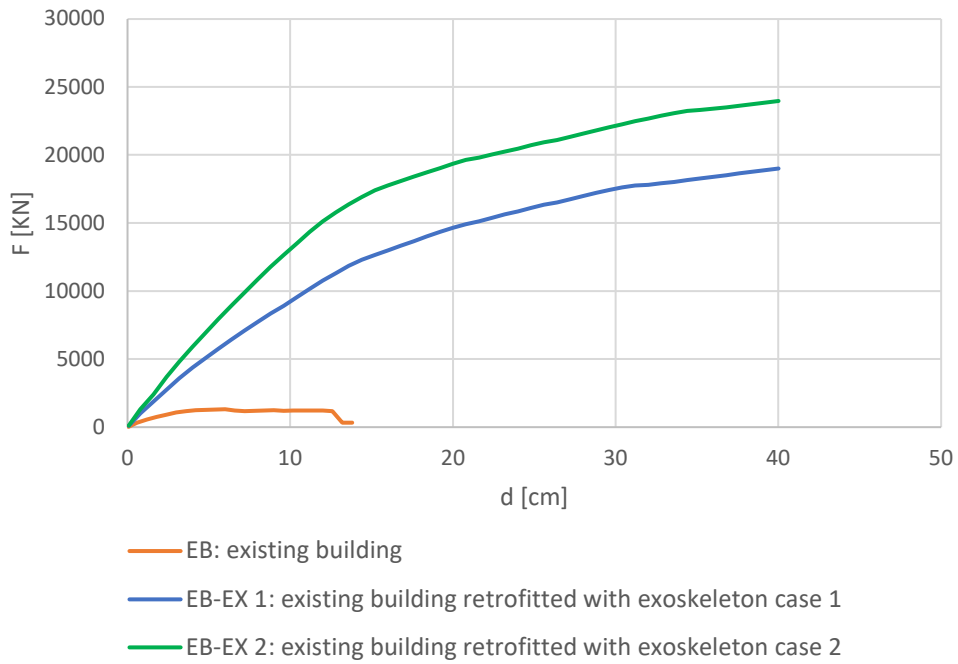


Figure 5.26: Capacity curves of the existing building EB, the retrofitted building with the first model of exoskeleton EB-EX 1 and the second model of the exoskeleton EB-EX 2 in x direction.

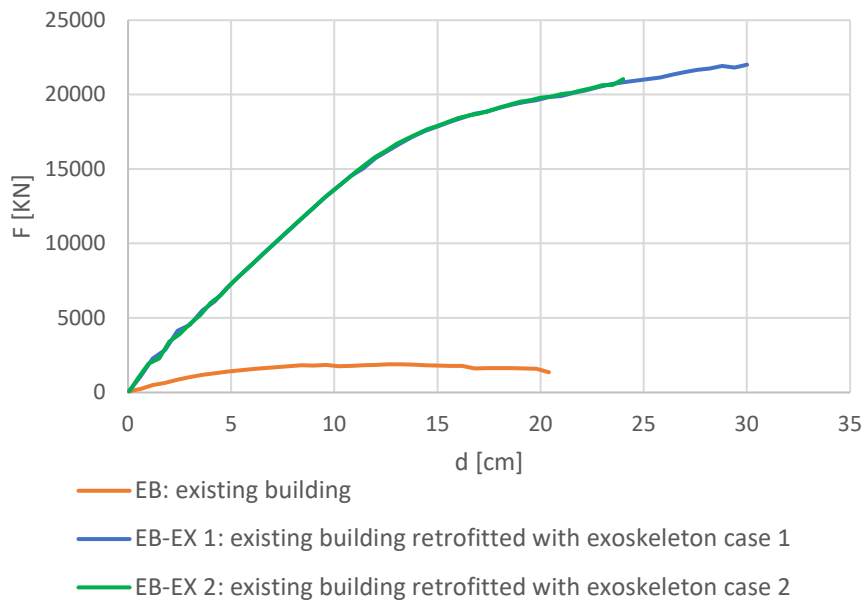


Figure 5.27: Capacity curves of the existing building EB, the retrofitted building with the first model of exoskeleton EB-EX 1 and the second model of the exoskeleton EB-EX 2 in y direction.



The maximum inter-storey drift of 0,6% for the Life Safety limit state and equal to 0,3% for the Damage Limitation limit state is assumed. The increase of stiffness achieved with the second model of the exoskeleton in x direction is 3,0 times the stiffness of the existing building:

$$\frac{K_{EB-EX2}}{K_{EB}} = 3,0$$

The capacity of the building retrofitted with the second model of the exoskeleton is 5 times the capacity of the existing building (Figure 5.28):

$$\frac{F_{EB-EX2}}{F_{EB}} = 5,0$$

The SDOF system curve and the bilinear equivalent curve evaluated with the N2 method are shown in Figure 5.29 for both the main direction. In the y direction the SDOF system curve and the behaviour factor are the same as the first model of the exoskeleton. In x direction the behaviour factor  $q$  equal to 1,12 is obtained. The main parameters of the SDOF system in x direction are reported in Table 5.11.

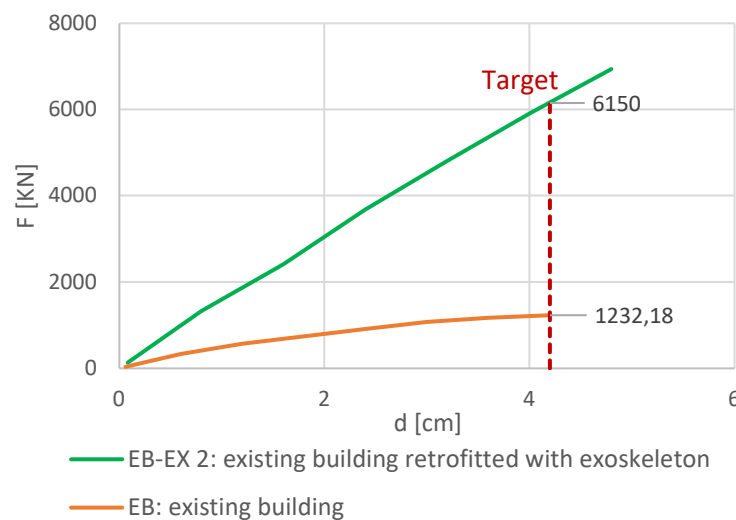


Figure 5.28: Evaluation of the increased strength and stiffness in x direction obtained with the second model of the exoskeleton.

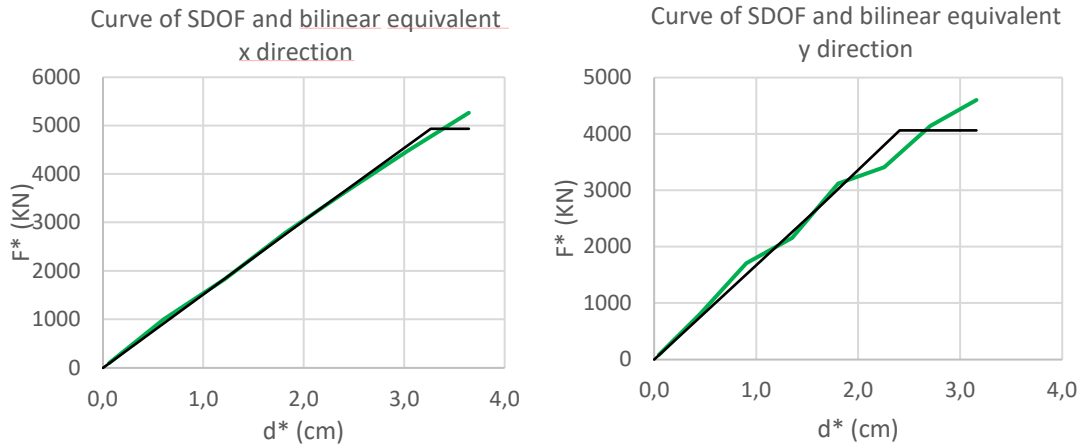
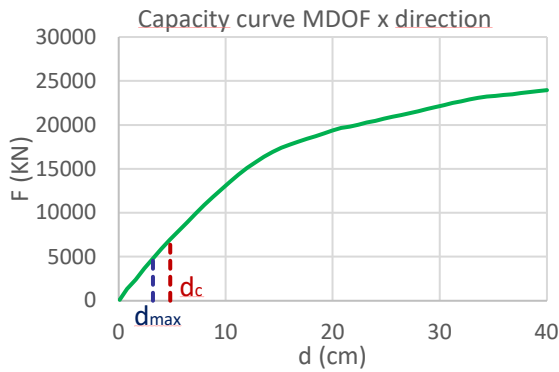


Figure 5.29: Curve of the SDOF system and bilinear equivalent curve in both directions for the retrofitted building with the second model of the exoskeleton.

Table 5.11: Parameters of the SDOF system in x direction for the retrofitted building with the second model of the exoskeleton.

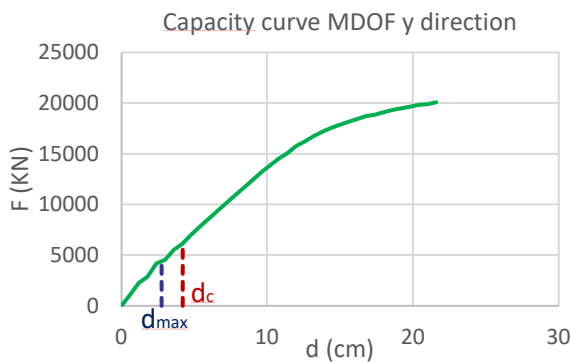
Parameter	Symbol	Value
		x direction
Mass	$m^*$	701290 kg
Partecipation factor	$\Gamma$	1,32
Yelding force	$F_y^*$	4933 KN
Yelding displacement	$\delta_y$	3,3 cm
Ultimate displacement	$\delta_u$	3,6 cm
Fundamental period	$T^*$	0,43
Displacement demand for LS limit state	$S_d(T^*)$	2,42 cm

The risk index for the LS limit state, evaluated by the ratio capacity/demand in terms of displacement, is 1,50 in x direction (Figure 5.30). In y direction the risk index is 1,52 as for the first model of the exoskeleton (Figure 5.31). For the DL limit state, the risk index of 1,94 in x direction (Figure 5.32) and 2,36 in y direction (Figure 5.33) is obtained.



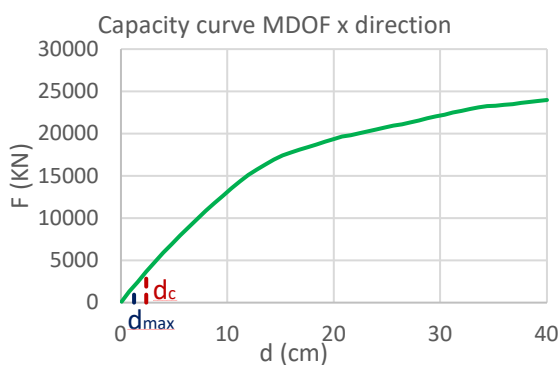
Displacement demand	$d_{max}$	3,2 cm
Displacement capacity	$d_c$	4,8 cm
Capacity/demand ratio	IS	1,50

Figure 5.30: Capacity/demand ratio for the Life Safety limit state in x direction for the retrofitted building with the second model of the exoskeleton.



Displacement demand	$d_{max}$	2,8 cm
Displacement capacity	$d_c$	4,2 cm
Capacity/demand ratio	IS	1,52

Figure 5.31: Capacity/demand ratio for the Life Safety limit state in y direction for the retrofitted building with the second model of the exoskeleton.



Displacement demand	$d_{max}$	1,2 cm
Displacement capacity	$d_c$	2,4 cm
Capacity/demand ratio	IS	1,94

Figure 5.32: Capacity/demand ratio for the Damage Limitation limit state in x direction for the retrofitted building with the second model of the exoskeleton.

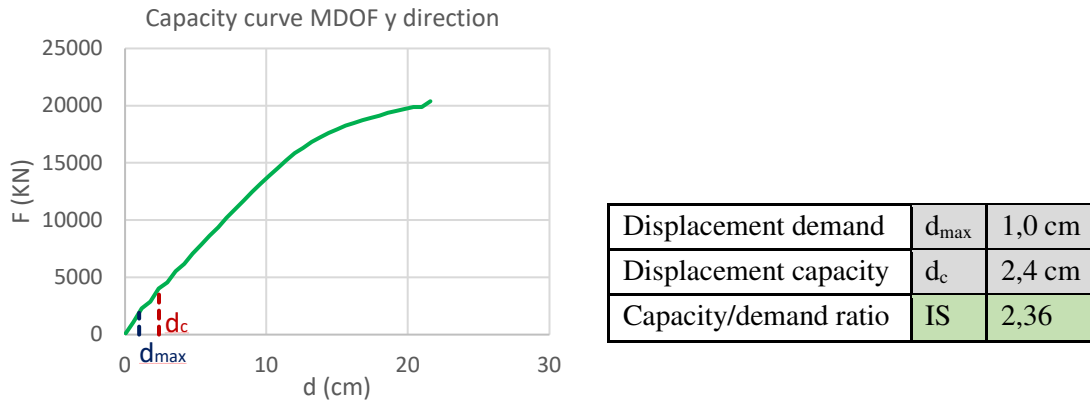


Figure 5.33: Capacity/demand ratio for the Damage Limitation limit state in y direction for the retrofitted building with the second model of the exoskeleton.

The capacity/demand ratio in terms of Peak Ground Acceleration is represented in Table 5.12. The economic parameter PAM, evaluated by the area subtended by the curve identified by points ( $\lambda$ , CR), is shown in Figure 5.34. The PAM class which determines the seismic risk class of the retrofitted building with the second model of the exoskeleton evaluated with the nonlinear analysis is the class A.

Table 5.12: PGA values and risk index evaluated in both directions with nonlinear analysis for the retrofitted building with the second model of the exoskeleton.

Limit state	PGA <sub>C-X</sub> [g]	PGA <sub>C-Y</sub> [g]	PGA <sub>D</sub> [g]	$\alpha_X$ [-]	$\alpha_Y$ [-]
LS	0,33	0,334	0,22	1,50	1,52
DL	0,159	0,194	0,082	1,94	2,36

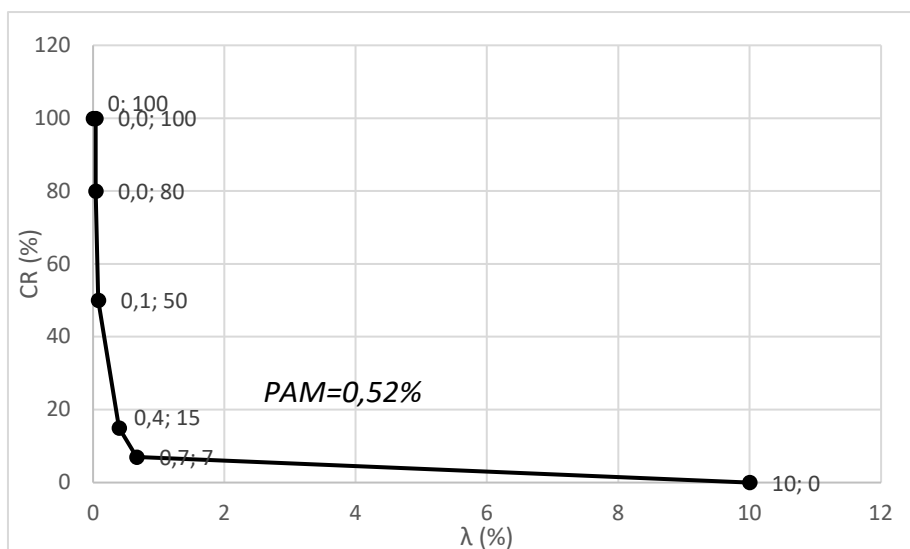


Figure 5.34: Evaluation of the annual average expected loss parameter (PAM) with nonlinear analysis for the retrofitted building with the second model of the exoskeleton.

### 5.2.3 Results

The comparison between the seismic risk index of the existing building retrofitted with the second model of the exoskeleton evaluated with the linear analysis and nonlinear analysis is shown in Table 5.13.

Table 5.13: Comparison between the seismic risk index evaluated with linear and nonlinear analysis for the existing building retrofitted with the second model of the exoskeleton.

Limit state	Linear analysis		Nonlinear analysis	
	$\alpha_X$	$\alpha_Y$	$\alpha_X$	$\alpha_Y$
LS	0,32	1,00	1,50	1,52
DL	0,65	1,00	1,94	2,36

With the linear analysis the risk class post-intervention is the class E and there is an improvement of one class compared to the existing building. The risk class assessed with nonlinear analysis is the class A. Figure 5.35 summarizes the results obtained with the two analysis.

Linear analysis		Nonlinear analysis	
Security index	IS-V class	Security index	IS-V class
$100\% < \text{IS-V}$	$A^+_{\text{IS-V}}$	$100\% < \text{IS-V}$	$A^+_{\text{IS-V}}$
$80\% \leq \text{IS-V} < 100\%$	$A_{\text{IS-V}}$	$80\% \leq \text{IS-V} < 100\%$	$A_{\text{IS-V}}$
$60\% \leq \text{IS-V} < 80\%$	$B_{\text{IS-V}}$	$60\% \leq \text{IS-V} < 80\%$	$B_{\text{IS-V}}$
$45\% \leq \text{IS-V} < 60\%$	$C_{\text{IS-V}}$	$45\% \leq \text{IS-V} < 60\%$	$C_{\text{IS-V}}$
$30\% \leq \text{IS-V} < 45\%$	$D_{\text{IS-V}}$	$30\% \leq \text{IS-V} < 45\%$	$D_{\text{IS-V}}$
$15\% \leq \text{IS-V} < 30\%$	$E_{\text{IS-V}}$	$15\% \leq \text{IS-V} < 30\%$	$E_{\text{IS-V}}$
$\text{IS-V} \leq 15\%$	$F_{\text{IS-V}}$	$\text{IS-V} \leq 15\%$	$F_{\text{IS-V}}$
Annual average expected loss	PAM class	Annual average expected loss	PAM class
$\text{PAM} \leq 0,50\%$	$A^+_{\text{PAM}}$	$\text{PAM} \leq 0,50\%$	$A^+_{\text{PAM}}$
$0,50\% < \text{PAM} \leq 1,0\%$	$A_{\text{PAM}}$	$0,50\% < \text{PAM} \leq 1,0\%$	$A_{\text{PAM}}$
$1,0\% < \text{PAM} \leq 1,5\%$	$B_{\text{PAM}}$	$1,0\% < \text{PAM} \leq 1,5\%$	$B_{\text{PAM}}$
$1,5\% < \text{PAM} \leq 2,5\%$	$C_{\text{PAM}}$	$1,5\% < \text{PAM} \leq 2,5\%$	$C_{\text{PAM}}$
$2,5\% < \text{PAM} \leq 3,5\%$	$D_{\text{PAM}}$	$2,5\% < \text{PAM} \leq 3,5\%$	$D_{\text{PAM}}$
$3,5\% < \text{PAM} \leq 4,5\%$	$E_{\text{PAM}}$	$3,5\% < \text{PAM} \leq 4,5\%$	$E_{\text{PAM}}$
$4,5\% < \text{PAM} \leq 7,5\%$	$F_{\text{PAM}}$	$4,5\% < \text{PAM} \leq 7,5\%$	$F_{\text{PAM}}$
$7,5\% \leq \text{PAM}$	$G_{\text{PAM}}$	$7,5\% \leq \text{PAM}$	$G_{\text{PAM}}$
Risk class E		Risk class A	

Figure 5.35: Comparison between the risk class evaluated with linear and nonlinear analysis for the existing building retrofitted with the second model of exoskeleton.

### **5.3 IMPROVEMENT TO THE EXOSKELETON**

This chapter presents the study of the improvement to the external aluminium alloy exoskeleton in order to find the optimal solution in terms of seismic improvement rate and costs. A total of nine solutions are proposed and analysed and the main results are shown in the present chapter. Appendix A contains the SDOF system curve and the bilinear equivalent curve for both the main directions for all the solutions. The main parameters of the SDOF system and the evaluation of the seismic risk index are also present.

The first design of the exoskeleton is presented at chapter 5.1. It consists of concentric frames for each floor, with bracing placed in the transverse direction to respect the architectural requirements. The vertical mullions and beams are made of aluminium alloy 6082 T6 while the bracings are made of alloy 6060 T5 as described in chapter 3.3. The frame geometry is characterized by mullions type A with thickness 10 mm at the first and second floor, and mullions type B with a reduced thickness of 6 mm at the third and fourth floor (Figure 3.17). The frames are connected by longitudinal beams having a tubular section of dimension 126 mm by 256 mm and thickness 16 mm. The transverse beams and the diagonals have a square hollow section with side 110 mm and thickness 12 mm (Figure 3.18).

The second case of the exoskeleton is described at chapter 5.2 and it consists of a strengthened exoskeleton obtained with the addition of bracings in the longitudinal direction of the building.

The previous chapter have highlighted how the fast collapse of the masonry bearing structure does not allow the exploitation of the exoskeleton's ductile behaviour. The maximum inter-story drift of 0,6% for the Life Safety limit state implies stopping the nonlinear analysis for very low levels of displacement of approximately 5 cm. For these levels

of displacement, it is not possible to exploit the ductile behaviour of the aluminium. The difference in stiffness between the existing and the retrofitted building is so high that the aluminium remains in the elastic field. For these reasons, solutions that provide for a lightening of the exoskeleton are considered. The following cases three, four and five take the first design of the exoskeleton as a starting point and each one examines only one variation.

The third case considers the first design of the exoskeleton with the variation of having the mullions type B with reduced thickness at all floors.

The fourth case examines the possibility of using the aluminium alloy 6060 T5 with lower performance for all the components of the exoskeleton.

In the fifth case the diagonals with a reduced thickness of 10 mm are considered (Figure 5.36). The reduced weight of the diagonals is 10,8 kg/m instead of 12,7 kg/m.

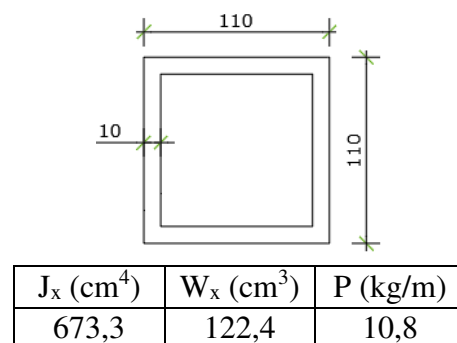


Figure 5.36: Geometrical properties of the diagonals considered in case 5 of the exoskeleton.

The cases six, seven and eight assume as initial data the second model of the exoskeleton characterized by high stiffness and capacity. These



solutions aim to have a lower yield threshold and a more ductile behaviour. Each case analyses some variations in order to lighten the structure and have lower production costs.

The sixth case combines the second model of the exoskeleton with the addition of bracings also at the four corners of the building (Figure 5.37). It considers the bracings with a reduced thickness of 10 mm and the longitudinal beams with a reduced thickness of 14 mm. Figure 5.38 shows the geometry of the lightened longitudinal beam having a weight of 26,2 kg/m instead of 30,2 kg/m.

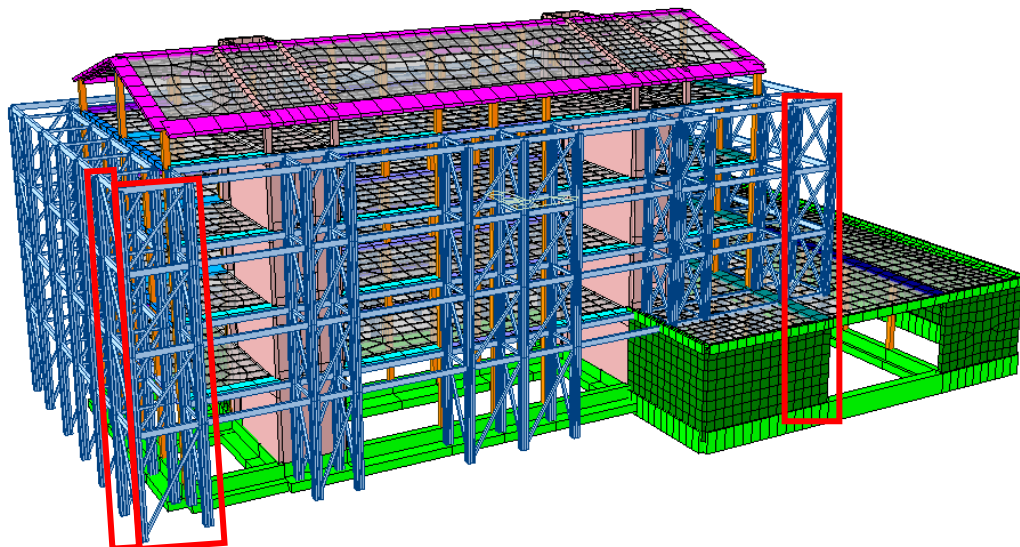
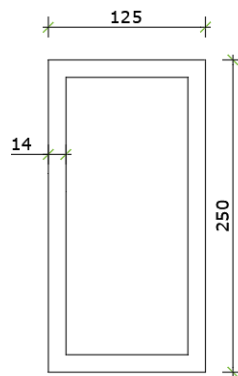


Figure 5.37: Sixth model of the exoskeleton with the addition of bracings at the four corners of the building.



$J_x$ (cm <sup>4</sup> )	$W_x$ (cm <sup>3</sup> )	P (kg/m)
7432	595	26,2

Figure 5.38: Geometrical properties of the longitudinal beam considered in case 6 of the exoskeleton.

The seventh case varies with respect to the sixth case for the use of aluminium alloy 6060 T5 with lower performance for all the components of the exoskeleton.

The eighth case adds to the previous case the use of mullions type B with reduced thickness at all floors.

The last ninth case of the exoskeleton is designed to have the cheapest solution. It is the same as the case eight without additional bracings on the longitudinal direction and on the corners of the building.

The nine solutions of the external exoskeleton are summarized in the Figure 5.39.

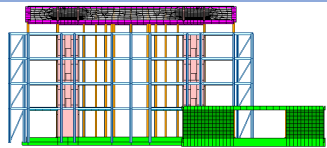
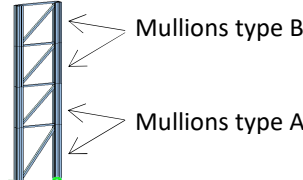
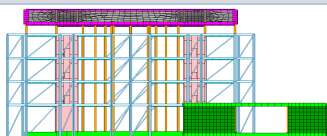
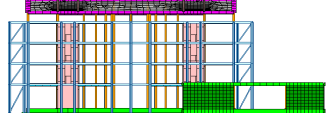

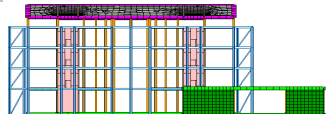
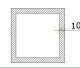
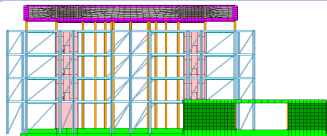
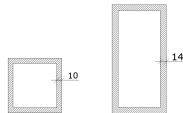

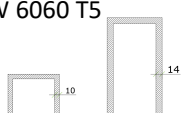
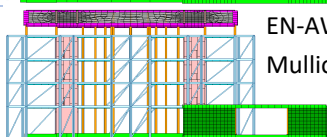
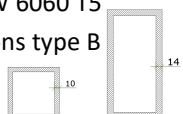
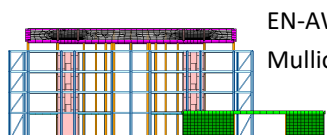
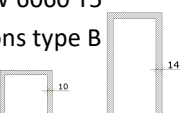
<b>EXOSKELETON FIRST DESIGN</b>		
<b>Case 1</b>	EN-AW 6082 T6 for mullions and beams	 
	EN-AW 6060 T5 for diagonals	
	Mullions type A at 1 <sup>st</sup> and 2 <sup>nd</sup> floors	
	Mullions type B at 3 <sup>rd</sup> and 4 <sup>th</sup> floors	
	Diagonals 12 mm th.	
<b>EXOSKELETON VARIATIONS</b>		
<b>Case 2</b>	Reinforced exoskeleton with additional diagonals on the longitudinal side (x direction)	
<b>Case 3</b>	Case 1 with mullions type B at all floors	 Mullions type B
<b>Case 4</b>	Case 1 with aluminium alloy EN-AW 6060 T5 for mullions, beams and diagonals	 EN-AW 6060 T5
<b>Case 5</b>	Case 1 with diagonals 10 mm thickness	 
<b>Case 6</b>	Case 2 with diagonals on the corners, diagonals 10 mm th. and longitudinal beams 14 mm th.	 
<b>Case 7</b>	Case 6 with aluminium alloy 6060 T5 for mullions, beams and diagonals	 EN-AW 6060 T5 
<b>Case 8</b>	Case 7 with mullions type B at all floors	 EN-AW 6060 T5 Mullions type B 
<b>Case 9</b>	Case 8 without additional diagonals	 EN-AW 6060 T5 Mullions type B 

Figure 5.39: Summary table of the nine cases studied for the improvement of the exoskeleton.

The nine solutions described above are compared in relation to their ductile behaviour and the seismic improvement rate. The risk index for the LS limit state is evaluated with a nonlinear analysis by the ratio capacity/demand in terms of displacement. Table 5.14 shows the results of behaviour factor  $q$  and risk index  $IS$  evaluated in both direction for the nine solutions. The values are obtained by performing a nonlinear analysis of the structure and considering the maximum inter-storey drift of 0,6% for masonry for the LS limit state. The drift target corresponds to a storey displacement at the top floor of approximately 5 cm. For this displacement, the pushover curves of all the solutions are almost straight lines and consequently the behaviour factors assume low values. All the solutions show a very similar behaviour factor in x direction  $q_x$  ranging from the value of 1,10 for case eight to the value of 1,16 for case nine. In y direction the behaviour factor  $q_y$  varies from the lowest value of 1,15 for cases six and seven to the higher value of 1,31 for the first three cases. Figures 5.40 and 5.41 represent the pushover curves for the nine solutions of the exoskeleton in x and y direction respectively. It can be noted that using the strengthened exoskeleton with additional bracings on the longitudinal direction of the building (EB-EX 2, EB-EX 6, EB-EX 7 and EB-EX 8), higher stiffness and capacity are obtained but with high costs. In the strong direction y of the building there are not additional bracings and the initial stiffness is the same. The use of an aluminium alloy with lower performance (EB-EX 4, EB-EX 7, EB-EX 8 and EB-EX 9) leads to a lower yield value and a more ductile behaviour with lower costs. However, when the diagonals yield at one floor, the lateral-torsional buckling of the mullions at the first floor, evaluated with equation (2.62), occurs. This happens for displacement values of approximately 10 cm, very far from the displacement target for which the curves are stopped. By using slender sections for diagonals and beams (EB-EX 6, EB-EX 7, EB-EX 8 and EB-EX 9) a lower curve with higher ductility and economic savings are obtained. The use of slender mullions (EB-EX 3, EB-EX 8 and EB-EX 9) allows for a more ductile behaviour and a reduction in costs.

Table 5.14: Comparison between the behaviour factor and the risk index evaluated in both directions for the nine solutions of the exoskeleton.

<i>Exoskeleton solutions</i>	<i>Description</i>	<i>Behaviour factor x direction</i> $q_x$	<i>Behaviour factor y direction</i> $q_y$	<i>Risk index x direction</i> $IS_x$	<i>Risk index y direction</i> $IS_y$
<i>Case 1</i>	First design	1,12	1,31	1,27	1,52
<i>Case 2</i>	Reinforced exoskeleton with additional diagonals on the longitudinal side	1,12	1,31	1,50	1,52
<i>Case 3</i>	Case 1 with mullions type B at all floors	1,13	1,31	1,20	1,30
<i>Case 4</i>	Case 1 with aluminium alloy 6060 T5 for mullions, beams and diagonals	1,14	1,29	1,26	1,51
<i>Case 5</i>	Case 1 with diagonals 10mm thickness	1,12	1,16	1,25	1,46
<i>Case 6</i>	Case 2 with diagonals on the corners, diagonals 10 mm th. and longitudinal beams 14 mm th.	1,13	1,15	1,49	1,62
<i>Case 7</i>	Case 6 with aluminium alloy 6060 T5 for mullions, beams and diagonals	1,13	1,15	1,49	1,62
<i>Case 8</i>	Case 7 with mullions type B at all floors	1,10	1,17	1,37	1,41
<i>Case 9</i>	Case 8 without additional diagonals	1,16	1,17	1,19	1,24

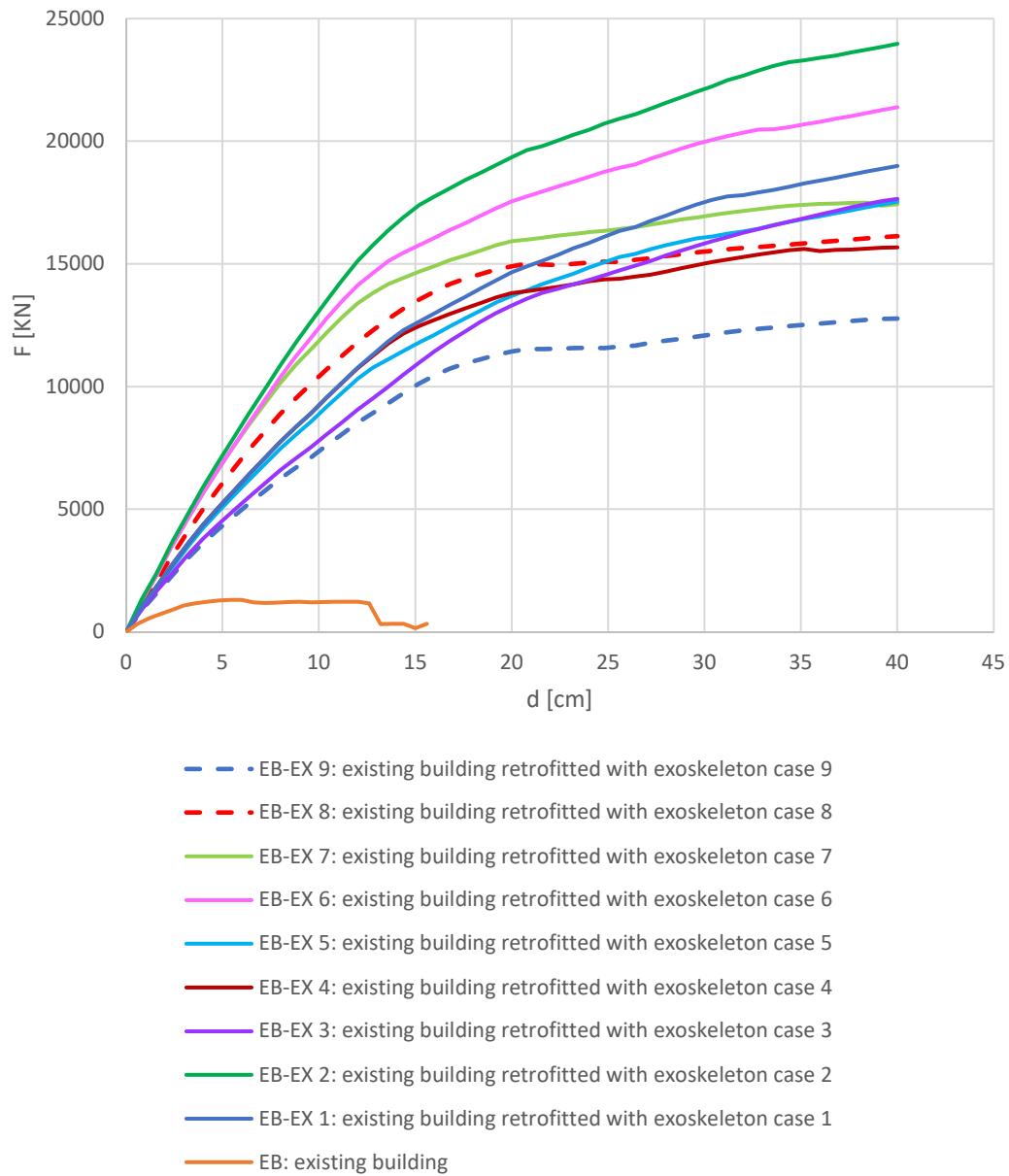


Figure 5.40: Capacity curves in x direction for the nine solutions of the exoskeleton.

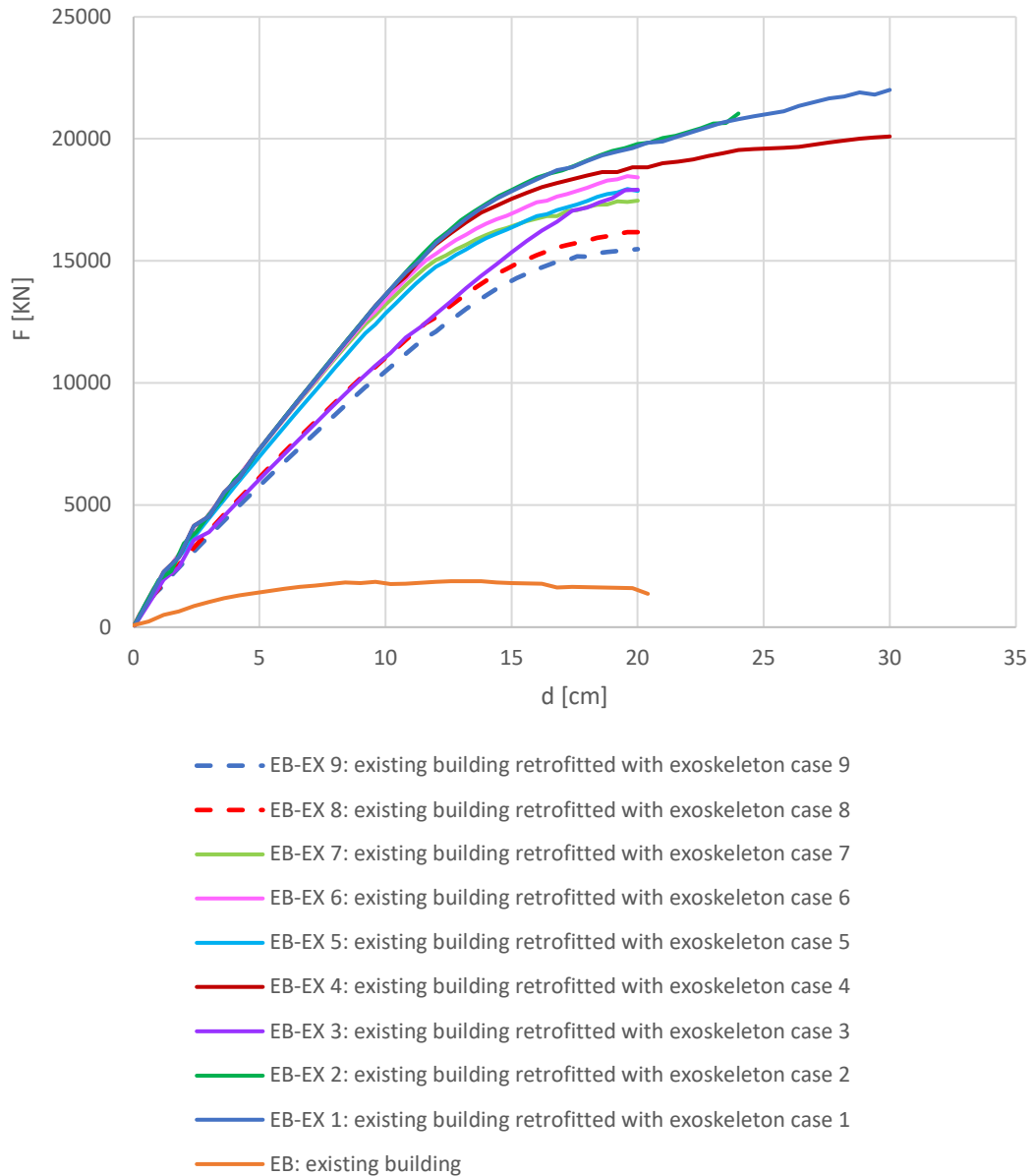


Figure 5.41: Capacity curves in y direction for the nine solutions of the exoskeleton.

The lateral-torsional buckling of the mullions at the first floor occurs for a displacement of approximately 20 cm, very far from the displacement target considered in the analysis.

## 5.4 ECONOMIC EVALUATION

The nine solutions of the exoskeleton are compared in Table 5.15 referring to the total kilos of aluminium involved. Considering the first model of the exoskeleton as the reference point, the cost difference respect to it expressed as a percentage is shown.

Table 5.15: Comparison between the nine solutions of the exoskeleton with reference to the total kilos of aluminium involved.

<i>Exoskeleton solutions</i>	<i>Description</i>	<i>Kilos of aluminium</i>	<i>Cost difference compared to the Reference</i>
<i>Case 1</i>	First design	<i>78617</i>	<i>Reference</i>
<i>Case 2</i>	Reinforced exoskeleton with additional diagonals on the longitudinal side	<i>80996</i>	<i>+2%</i>
<i>Case 3</i>	Case 1 with mullions type B at all floors	<i>64343</i>	<i>-19%</i>
<i>Case 4</i>	Case 1 with aluminium alloy 6060 T5 for mullions, beams and diagonals	<i>78617</i>	<i>-27%</i>
<i>Case 5</i>	Case 1 with diagonals 10mm thickness	<i>77361</i>	<i>-1%</i>
<i>Case 6</i>	Case 2 with diagonals on the corners, diagonals 10 mm th. and longitudinal beams 14 mm th.	<i>77847</i>	<i>-2%</i>
<i>Case 7</i>	Case 6 with aluminium alloy 6060 T5 for mullions, beams and diagonals	<i>77847</i>	<i>-28%</i>
<i>Case 8</i>	Case 7 with mullions type B at all floors	<i>63573</i>	<i>-41%</i>
<i>Case 9</i>	Case 8 without additional diagonals	<i>60201</i>	<i>-44%</i>



The addition of the bracings in the second model of the exoskeleton leads to an increase of costs of 2%. The use of slender mullions in the third case causes a very significant reduction in costs equal to 19%, while the use of slender diagonals causes a small cost reduction of 1%. The fourth and seventh case involve the use of extruded profiles with a less performing aluminium alloy and they are characterized by a considerable reduction in costs. The economic savings is 27% for case four and 28% for case seven. The sixth, seventh and eighth case, although using additional bracings, are characterized by economic savings thanks to the lightening of the exoskeleton. With case eight, in which all the components of the exoskeleton have a reduced weight and the aluminium alloy with lower performance is used, a cost reduction of 41% is achieved. The last case is the cheapest solution. It does not consider the additional bracings and it is characterized by profiles with reduced sections and the aluminium alloy 6060 T5. With this solution an economic saving of 44% is achieved compared to the first design of the exoskeleton. For the maximum displacement levels considered in the analysis, the latter represents the best solution as it is characterized by a risk index of approximately 1,2 and by a high cost reduction. Also comparing the tensile actions at the base of the vertical mullions of the exoskeleton, the last case represents the best solution. In fact, as shown in Table 5.16, the ninth case is characterized by the lowest value of the maximum tensile action that leads to a reduction cost in the foundations. With reference to this last case, a preliminary design of the foundations was carried out. From the geotechnical report, a soil capacity of 1,5 kg/cm<sup>2</sup> is deducted. It is considered necessary to realize a raft foundation three meters wide. Due to the high tensile forces at the base, the use of two micropiles for each mullion with a diameter of 20 cm and a length of 18 meters is provided. Table 5.17 shows the cost of the aluminium exoskeleton and the cost of foundations for each solution. Both costs are normalized to the gross internal area of the building equal to 1582,4 square meters.

Table 5.16: Maximum tensile actions at the base of the vertical mullions of the exoskeleton for the nine solutions.

Exoskeleton solutions	Maximum tensile action at the base (KN)
Case 1	723
Case 2	785
Case 3	526
Case 4	723
Case 5	673
Case 6	712
Case 7	712
Case 8	584
Case 9	498

Table 5.17: Cost of retrofit normalized to the gross internal area of the building.

Exoskeleton solutions	Cost of aluminium exoskeleton (€/m <sup>2</sup> )	Cost of foundations (€/m <sup>2</sup> )
Case 1	204,46	2164,16
Case 2	208,97	2349,75
Case 3	166,57	1574,48
Case 4	149,05	2164,16
Case 5	201,76	2014,50
Case 6	200,49	2131,24
Case 7	147,59	2131,24
Case 8	120,53	1748,09
Case 9	114,14	1490,67

## **5.5 REFERENCES**

[1] Midas Gen. Analysis Manual for Midas Gen.

[2] FEMA 356 (2000) Prestandard and commentary for the seismic rehabilitation of buildings. ASCE for the Federal Emergency Management Agency, Washington, D.C.



## *Chapter 6*

### **CONCLUSIONS**

This thesis is the result of the industrial PhD carried out in collaboration with *Aliva S.r.l.* company that develops customized solutions for ventilated facades. The scope of this thesis is to investigate the use of aluminium alloys in application fields different from that of the ventilated façade, especially in the seismic retrofit field. This study is part of the European research project Pro-GET-onE that means Proactive synergy of inteGrated Efficient Technologies on building's Envelope. The project proposes a technique that until now has not been commonly used and can be configured as an exoskeleton connected to the reinforced concrete frame of the existing buildings. The exoskeleton is applied externally to the existing building with benefits in regarding the construction site since it does not require the performance of operations inside the buildings. This avoids the occupant's relocation and implements dry technologies to speed up the construction time. Moreover, it avoids the increase of loads on the existing foundations. In fact, the seismic loads absorbed by the additional bracing systems are transferred directly towards suitable foundations appropriately built at their bases. The exoskeleton also provides integrated solutions for energy improvement and possible volumetric expansion increasing the real estate value of the buildings. The Italian case study considered in the European project, a social housing located in Reggio Emilia, has been subjected to a seismic vulnerability assessment with linear and nonlinear analyses. The reference building, composed by reinforced concrete and masonry, was built between the 60's and 70's and designed for gravity loads only. In fact, the building does not

have a good seismic performance, showing greater vulnerability in the longitudinal direction where slender masonry piers are present. The linear and nonlinear analysis have shown differences in the results of the seismic performance assessment. With the nonlinear analysis the seismic risk index in both the main directions of the building are greater. This is due to the fact that a maximum inter-storey drift of 0,6% has been considered in the nonlinear analysis, while in the linear analysis the attainment of the Life Safety limit state occurred for a value of inter-storey drift 10 times lower. In order to upgrade the seismic capacity of the original structure, the use of the external aluminium alloy exoskeleton has been adopted. The feasibility of the exoskeleton has been confirmed with the realization of a full scale visual mock-up. It has shown the advantages of the plug and play solution where all the components are preassembled in the factory and ready to be installed reducing the construction times. The mock-up also showed the various possibilities of the additional spaces, such as sunspace, extra room and balcony. The construction of the visual mock-up has highlighted the main aspects of the technology that needed to be improved. In particular, the connections and the design of the optimal sections of the profiles. The commercial profiles used in the mock-up does not allow to obtain high performance and simplified connections. The design phases of the exoskeleton have been shown. The in-depth study of the wide range of aluminium alloys led to the choice of 6000 AlMgSi series. The alloy 6082 T6 for vertical mullions and beams, and the alloy 6060 T5 for the bracings of the exoskeleton have been selected. The main aspects analysed in the design of the customized sections of the extruded profiles have been explained and the innovative connection system between the components has been shown. The seismic improvement assessment achieved for the existing building with the addition of the aluminium alloy exoskeleton has been performed with the linear and nonlinear analysis. Nine different solution of the external exoskeleton have been proposed and analysed. In the first design of the exoskeleton, the bracings have been placed in order to respect the architectural requirements and to not impact the appearance of the building. The results

have shown that with the linear analysis there is not a seismic improvement with the addition of the external exoskeleton. On the contrary, the nonlinear analysis has highlighted a seismic improvement of one risk class. The second case of the exoskeleton consists of a strengthened exoskeleton obtained with the addition of bracings in the longitudinal direction of the building. This solution has a greater architectural impact and the reasons that determined the choice of the arrangement of the bracings have been explained. With both linear and nonlinear analysis, the improvement of one risk class compared to the existing building has been obtained. It has been noticed that the fast collapse of the masonry bearing structure does not allow the exploitation of the exoskeleton's ductile behaviour. Finally, the possible improvement of the exoskeleton has been examined. Solutions that provide for a lightening of the exoskeleton have been considered. The use of slender sections and the use of the aluminium alloy with lowest performance for all the components of the exoskeleton have been studied. The nine proposed solutions have been compared in terms of pushover curve, behaviour factor, seismic risk index and costs. All the solutions have shown a very similar behaviour factor in x direction ranging from the value of 1,10 for the eighth case to the value of 1,16 for the ninth case. In y direction the behaviour factor varies from the lowest value of 1,15 for cases six and seven to the higher value of 1,31 for the first three cases. The pushover curves have pointed out that using the strengthened exoskeleton with additional bracings, higher stiffness and capacity are obtained but with high costs. The use of the aluminium alloy with lower performance has shown a more ductile behaviour and a considerable reduction in costs. By using slender sections, a lower curve with higher ductility and economic savings have been obtained. The results have shown that the proposed retrofit technique is effective in improving the seismic behaviour of the existing buildings.





# APPENDIX A

## Case 3 of the exoskeleton EB-EX 3

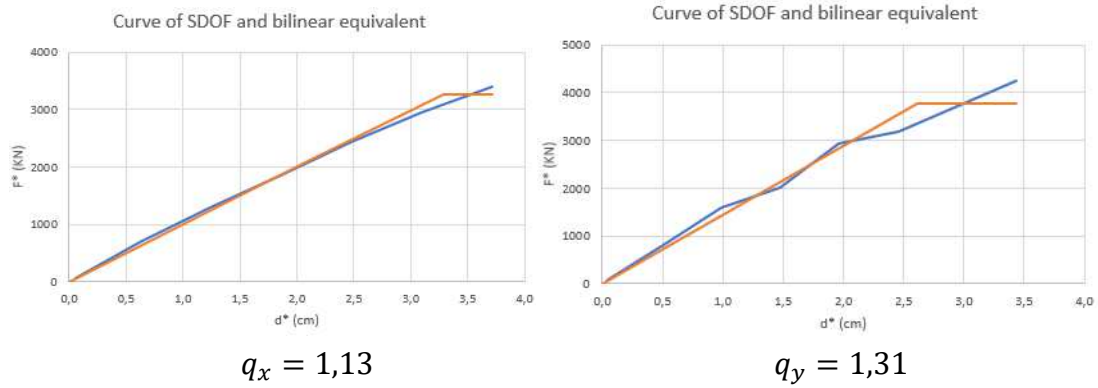


Figure A.1: Curve of the SDOF system and bilinear equivalent curve in both directions for EB-EX 3.

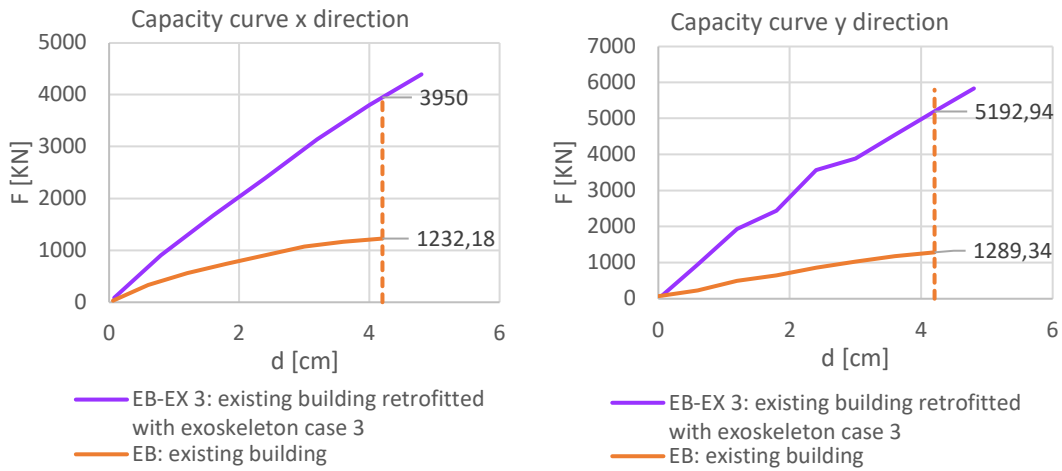


Figure A.2: Evaluation of the increased strength in both directions for EB-EX 3.

Table A.1: Parameters of the SDOF system in both directions for EB-EX 3.

Parameter	Symbol	Value	
		x direction	y direction
Mass	$m^*$	668988 kg	726599 kg
Partecipation factor	$\Gamma$	1,29	1,22
Yelding force	$F_y^*$	3256 KN	3765 KN
Yelding displacement	$\delta_y$	3,29 cm	2,62 cm
Ultimate displacement	$\delta_u$	3,72bcm	3,44 cm
Fundamental period	$T^*$	0,52	0,45
Displacement demand for LS limit state	$S_d(T^*)$	3,09 cm	2,64 cm

Table A.2: Risk index for the Life Safety limit state in both directions for EB-EX 3.

Displacement demand	$d_{max}$	4,0 cm
Displacement capacity	$d_c$	4,8 cm
Capacity/demand ratio	IS	1,20

Displacement demand	$d_{max}$	3,2 cm
Displacement capacity	$d_c$	4,2 cm
Capacity/demand ratio	IS	1,30

### Case 4 of the exoskeleton EB-EX 4

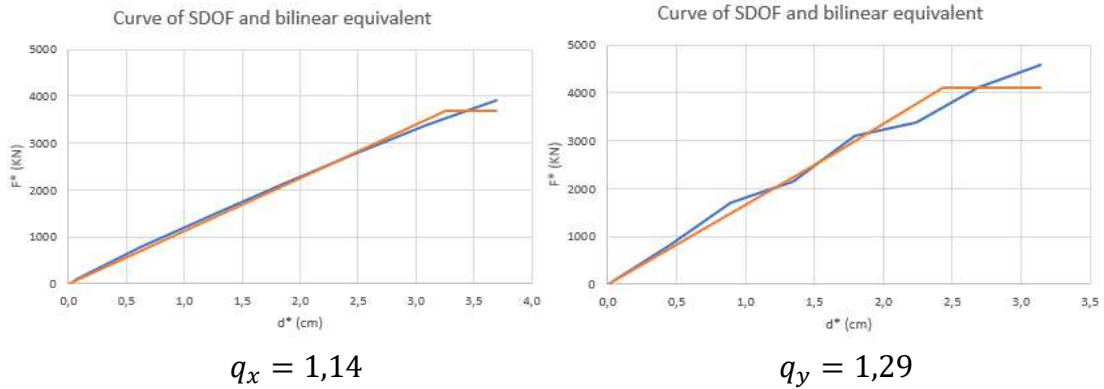


Figure A.3: Curve of the SDOF system and bilinear equivalent curve in both directions for EB-EX 4.

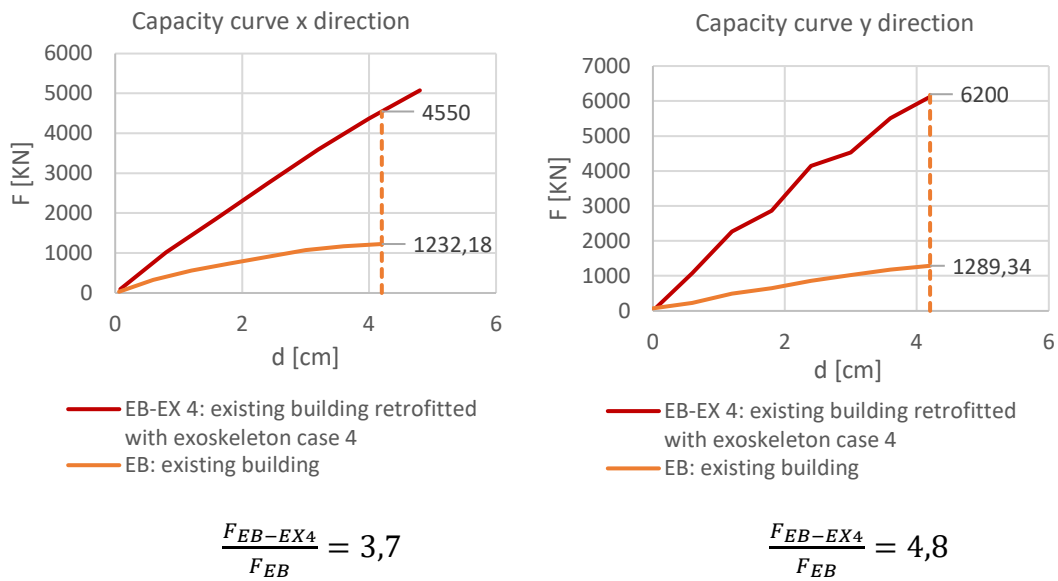


Figure A.4: Evaluation of the increased strength in both directions for EB-EX 4.

Table A.3: Parameters of the SDOF system in both directions for EB-EX 4.

Parameter	Symbol	Value	
		x direction	y direction
Mass	$m^*$	688201 kg	671846 kg
Partecipation factor	$\Gamma$	1,298	1,34
Yelding force	$F_y^*$	3699 KN	4109 KN
Yelding displacement	$\delta_y$	3,26 cm	2,44 cm
Ultimate displacement	$\delta_u$	3,70 cm	3,14 cm
Fundamental period	$T^*$	0,489	0,40
Displacement demand for LS limit state	$S_d(T^*)$	2,93 cm	2,08 cm

Table A.4: Risk index for the Life Safety limit state in both directions for EB-EX 4.

Displacement demand	$d_{max}$	3,8 cm
Displacement capacity	$d_c$	4,8 cm
Capacity/demand ratio	IS	1,26

Displacement demand	$d_{max}$	2,8 cm
Displacement capacity	$d_c$	4,2 cm
Capacity/demand ratio	IS	1,51

## Case 5 of the exoskeleton EB-EX 5

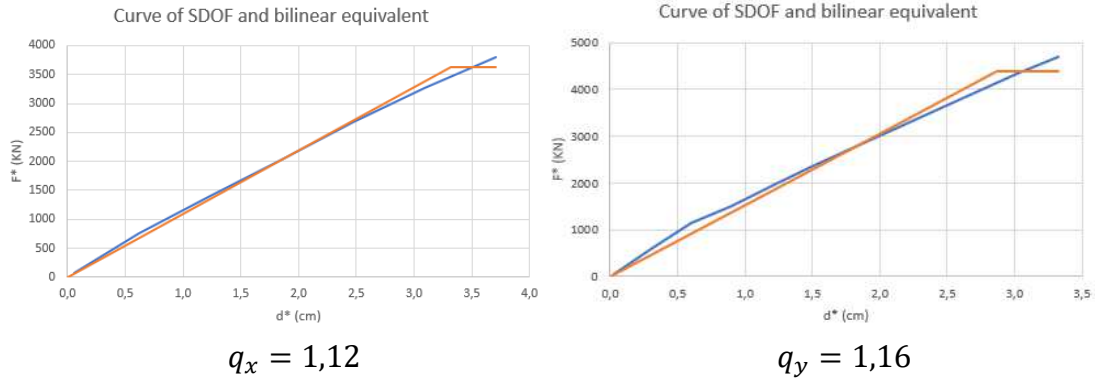


Figure A.5: Curve of the SDOF system and bilinear equivalent curve in both directions for EB-EX 5.

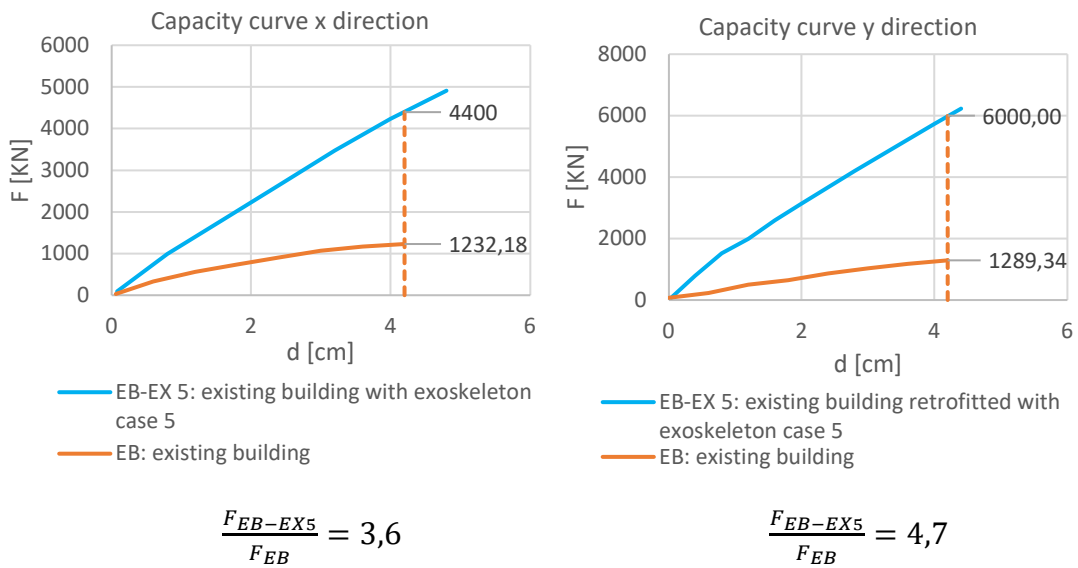


Figure A.6: Evaluation of the increased strength in both directions for EB-EX 5.

Table A.5: Parameters of the SDOF system in both directions for EB-EX 5.

Parameter	Symbol	Value	
		x direction	y direction
Mass	$m^*$	679815 kg	662820 kg
Partecipation factor	$\Gamma$	1,29	1,325
Yelding force	$F_y^*$	3631 KN	4376 KN
Yelding displacement	$\delta_y$	3,3 cm	2,87 cm
Ultimate displacement	$\delta_u$	3,7 cm	3,32 cm
Fundamental period	$T^*$	0,496	0,41
Displacement demand for LS limit state	$S_d(T^*)$	2,97 cm	2,27 cm

Table A.6: Risk index for the Life Safety limit state in both directions for EB-EX 5.

Displacement demand	$d_{max}$	3,8 cm
Displacement capacity	$d_c$	4,8 cm
Capacity/demand ratio	IS	1,25

Displacement demand	$d_{max}$	3,0 cm
Displacement capacity	$d_c$	4,4 cm
Capacity/demand ratio	IS	1,46

## Case 6 of the exoskeleton EB-EX 6

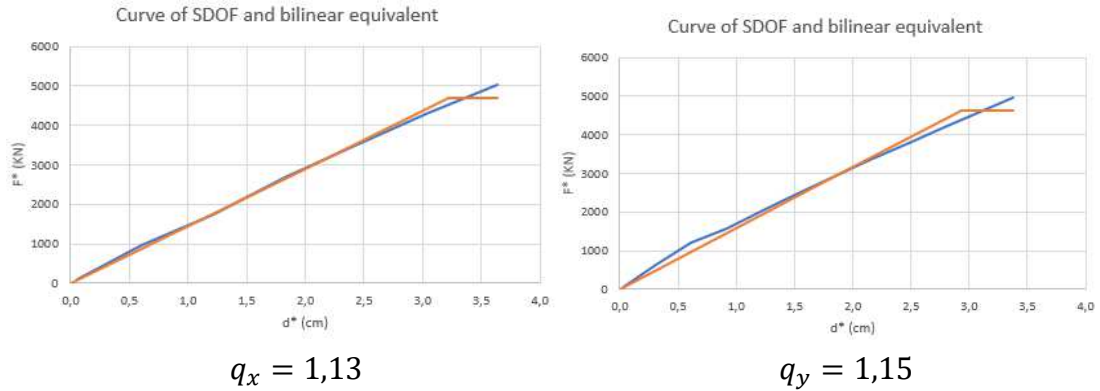


Figure A.7: Curve of the SDOF system and bilinear equivalent curve in both directions for EB-EX 6.

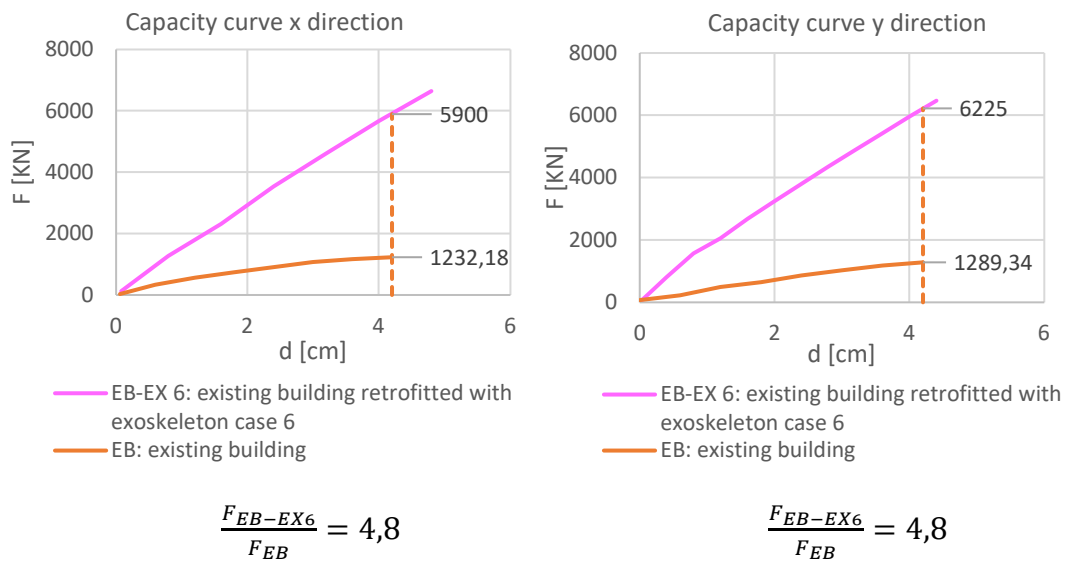


Figure A.8: Evaluation of the increased strength in both directions for EB-EX 6.

Table A.7: Parameters of the SDOF system in both directions for EB-EX 6.

Parameter	Symbol	Value	
		x direction	y direction
Mass	$m^*$	684745 kg	628751 kg
Partecipation factor	$\Gamma$	1,32	1,30
Yelding force	$F_y^*$	4704 KN	4641 KN
Yelding displacement	$\delta_y$	3,22 cm	2,94 cm
Ultimate displacement	$\delta_u$	3,64 cm	3,37 cm
Fundamental period	$T^*$	0,43	0,40
Displacement demand for LS limit state	$S_d(T^*)$	2,45 cm	2,1 cm

Table A.8: Risk index for the Life Safety limit state in both directions for EB-EX 6.

Displacement demand	$d_{max}$	3,2 cm
Displacement capacity	$d_c$	4,8 cm
Capacity/demand ratio	IS	1,49

Displacement demand	$d_{max}$	2,7 cm
Displacement capacity	$d_c$	4,4 cm
Capacity/demand ratio	IS	1,62



## Case 7 of the exoskeleton EB-EX 7

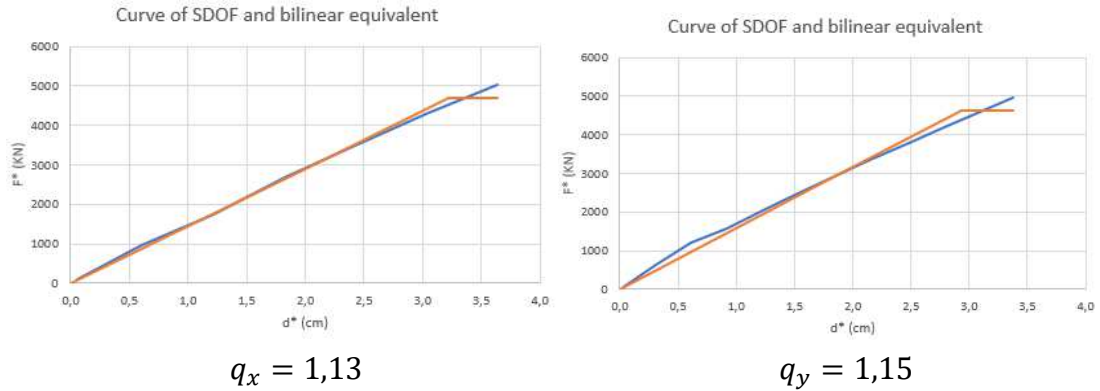


Figure A.9: Curve of the SDOF system and bilinear equivalent curve in both directions for EB-EX 7.

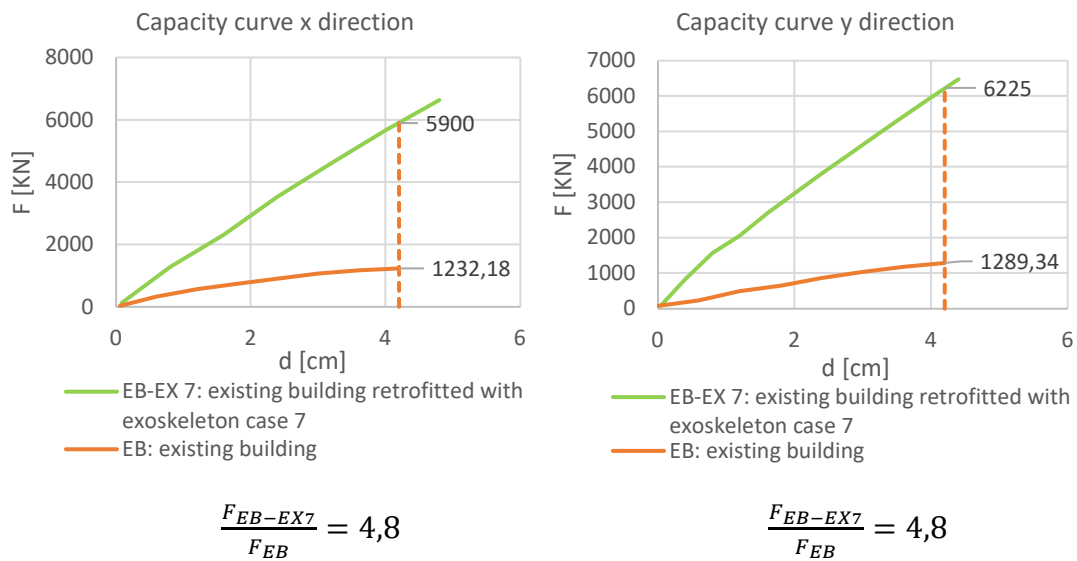


Figure A.10: Evaluation of the increased strength in both directions for EB-EX 7.

Table A.9: Parameters of the SDOF system in both directions for EB-EX 7.

Parameter	Symbol	Value	
		x direction	y direction
Mass	$m^*$	684745 kg	628751 kg
Partecipation factor	$\Gamma$	1,32	1,30
Yelding force	$F_y^*$	4704 KN	4641 KN
Yelding displacement	$\delta_y$	3,22 cm	2,94 cm
Ultimate displacement	$\delta_u$	3,64 cm	3,37 cm
Fundamental period	$T^*$	0,43	0,40
Displacement demand for LS limit state	$S_d(T^*)$	2,45 cm	2,1 cm

Table A.10: Risk index for the Life Safety limit state in both directions for EB-EX 7.

Displacement demand	$d_{max}$	3,2 cm
Displacement capacity	$d_c$	4,8 cm
Capacity/demand ratio	IS	1,49

Displacement demand	$d_{max}$	2,7 cm
Displacement capacity	$d_c$	4,4 cm
Capacity/demand ratio	IS	1,62

## Case 8 of the exoskeleton EB-EX 8

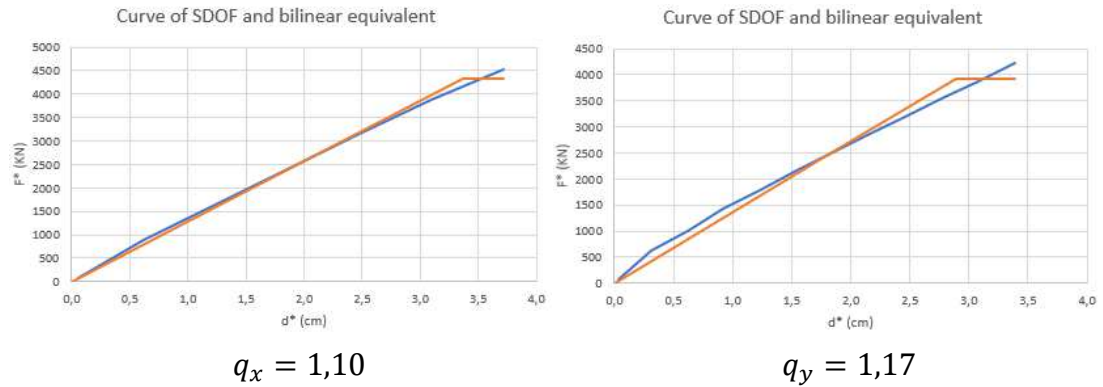


Figure A.11: Curve of the SDOF system and bilinear equivalent curve in both directions for EB-EX 8.

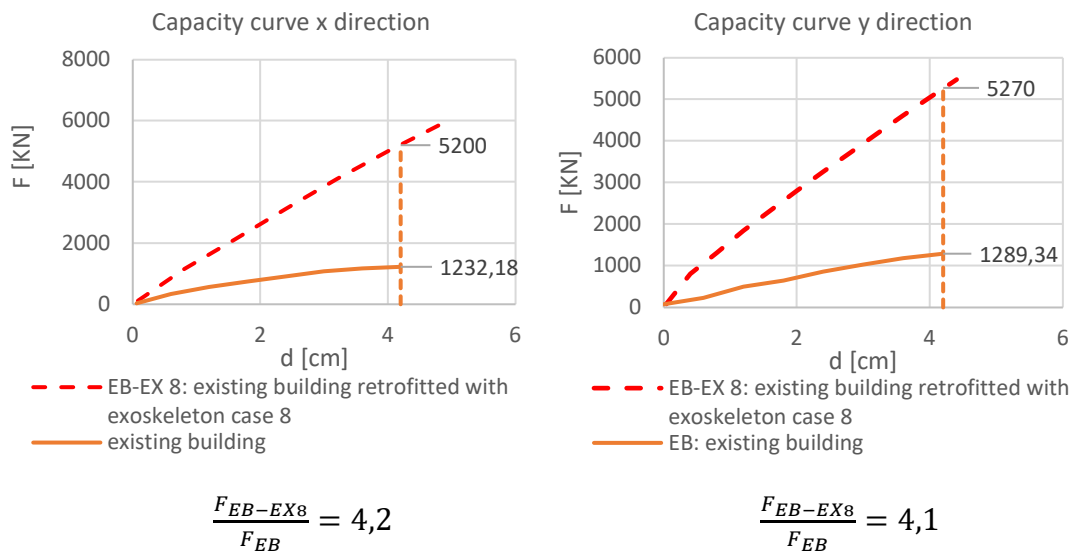


Figure A.12: Evaluation of the increased strength in both directions for EB-EX 8.

Table A.11: Parameters of the SDOF system in both directions for EB-EX 8.

Parameter	Symbol	Value	
		x direction	y direction
Mass	$m^*$	672686 kg	624371 kg
Partecipation factor	$\Gamma$	1,29	1,30
Yelding force	$F_y^*$	4335 KN	3927 KN
Yelding displacement	$\delta_y$	3,37 cm	2,89 cm
Ultimate displacement	$\delta_u$	3,72 cm	3,39 cm
Fundamental period	$T^*$	0,45	0,43
Displacement demand for LS limit state	$S_d(T^*)$	2,72 cm	2,4 cm

Table A.12: Risk index for the Life Safety limit state in both directions for EB-EX 8.

Displacement demand	$d_{max}$	3,5 cm
Displacement capacity	$d_c$	4,8 cm
Capacity/demand ratio	IS	1,37

Displacement demand	$d_{max}$	3,1 cm
Displacement capacity	$d_c$	4,4 cm
Capacity/demand ratio	IS	1,41

## Case 9 of the exoskeleton EB-EX 9

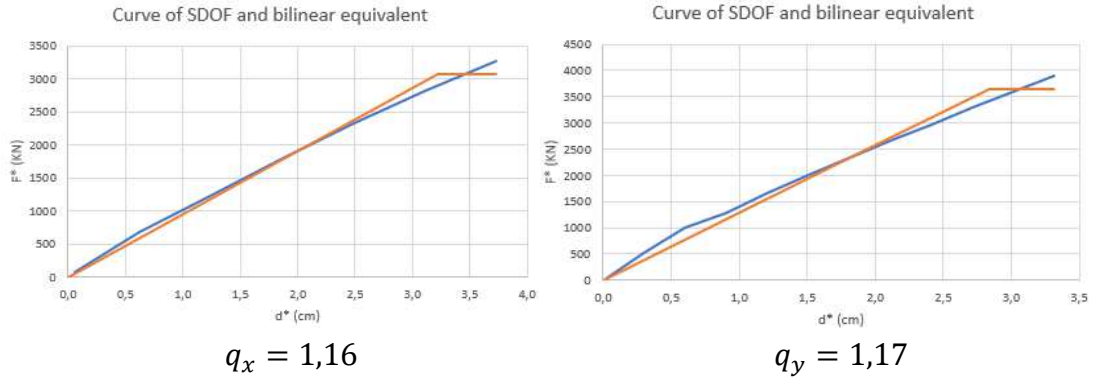


Figure A.13: Curve of the SDOF system and bilinear equivalent curve in both directions for EB-EX 9.

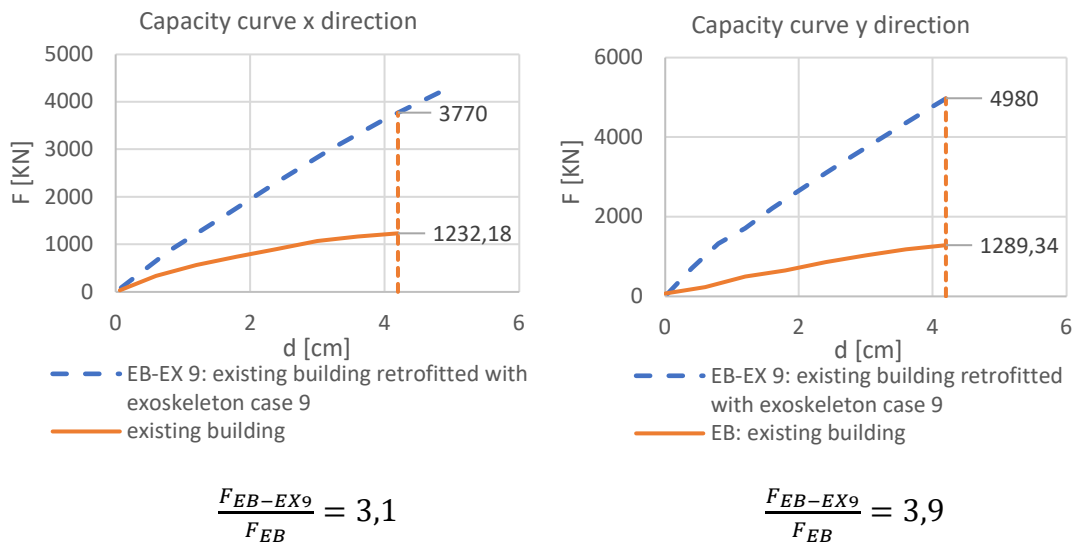


Figure A.14: Evaluation of the increased strength in both directions for EB-EX 9.

Table A.13: Parameters of the SDOF system in both directions for EB-EX 9.

Parameter	Symbol	Value	
		x direction	y direction
Mass	$m^*$	666115,7 kg	661616 kg
Partecipation factor	$\Gamma$	1,29	1,326
Yelding force	$F_y^*$	3069 KN	3657 KN
Yelding displacement	$\delta_y$	3,22 cm	2,84 cm
Ultimate displacement	$\delta_u$	3,73 cm	3,32 cm
Fundamental period	$T^*$	0,53	0,45
Displacement demand for LS limit state	$S_d(T^*)$	3,15 cm	2,7 cm

Table A.14: Risk index for the Life Safety limit state in both directions for EB-EX 9.

Displacement demand	$d_{max}$	4,1 cm
Displacement capacity	$d_c$	4,8 cm
Capacity/demand ratio	IS	1,19

Displacement demand	$d_{max}$	3,6 cm
Displacement capacity	$d_c$	4,4 cm
Capacity/demand ratio	IS	1,24